Effects of Activating K_{ATP} Channel Mutations on Neuronal Function

A Thesis submitted to the University of Oxford

for the degree of Doctor of Philosophy

James S. McTaggart

Magdalen College

Trinity 2011

Abstract

Effects of Activating K_{ATP} Channel Mutations on Neuronal Function

James S. McTaggart, Magdalen College, University of Oxford

Submitted for the degree of DPhil, Trinity 2011

Gain-of-function mutations in the ATP-sensitive potassium channel (K_{ATP} channel) cause a spectrum of disease in human beings. Some patients, with relatively severe mutations in the channel, present with diabetes mellitus in neonatal life along with neurological symptoms such as muscle hypotonia, balance problems, cognitive and motor developmental delay, and hyperactivity - a syndrome known as iDEND. The most common iDEND-causing mutation, the V59M mutation, has been modelled in a transgenic mouse, and the mutant channels may be expressed in specific cells of the body.

In this thesis, I used mice with V59M K_{ATP} channels expressed in all neurons (the n-V59M mouse), or in parvalbumin-expressing neurons alone (the p-V59M mouse). The electrical activity of cerebellar Purkinje cells was significantly inhibited in both of these mouse models. As cerebellar Purkinje cells provide the sole output from the cerebellar cortex, these results suggest that cerebellar dysfunction may be a feature of iDEND. Behavioural phenotyping of the p-V59M mouse revealed that it was weaker and more hyperactive on free-running wheels compared to controls. These phenotypes are reminiscent of the muscle hypotonia and hyperactivity of iDEND patients, which suggests that dysfunction of parvalbumin-expressing neurons may contribute to the symptoms of iDEND. Consistent with the notion that cerebellar dysfunction is a feature of iDEND, patients performed worse than controls on a cerebellar-dependent hand-eye coordination task, and showed impaired coordination of eye movements. Taken together, the results presented in this thesis indicate that the neurological symptoms of iDEND may be dissected using the V59M mouse model. The possibilities for translation of these experimental results to clinical practice are discussed.

Contents

Acknowledgements

My greatest thanks go to my supervisor, Professor Frances Ashcroft. She has been a wonderful source of ideas, enthusiasm and experience throughout my studies. I also thank my family for their ever-present support, advice and encouragement. Finally, I thank Michael Davies because without his love and understanding this thesis would not have been possible.

Thanks also to the Medical Research Council for their financial support during my DPhil studies.

Declaration

The work in this thesis is my own, with the following exceptions. Miss Michaela Iberl provided valuable technical assistance by genotyping most of the mice that were used in Chapters 3 and 4. Dr John-Stuart Brittain programmed the Matlab scripts that were used to analyse the patient tracking data in Chapter 5. Population data for controls on the 10-peg moving task, which were also presented in this chapter, were supplied by Dr Tom Scerri. RNA integrity for RT-qPCR experiments, which were presented in Chapters 3 and 6, was assessed by Ms Sheena Lee. Dr Chris Church and Ms Carolina Lahmann provided figures that are presented in the appendices.

List of publications arising from this work

Church, C., Lee, S.*, Bagg, E.A.L.*, McTaggart, J.S.*, Deacon, R., Gerken, T., Lee, A., Moir, L., Mecinovic, J., Quwailid, M.M., Schofield, C.J., Ashcroft, F.M., Cox, R.D., *A mouse model for the metabolic effects of the human fat mass and obesity associated FTO gene.* PLoS Genet, 2009. **5**(8): p. e1000599.

Clark, R.H., McTaggart, J.S.*, Webster, R.*, Mannikko, R.*, Iberl, M., Sim, X.L., Rorsman, P., Glitsch, M., Beeson, D., Ashcroft, F.M., M*uscle dysfunction caused by a KATP channel mutation in neonatal diabetes is neuronal in origin.* Science, 2010. **329**(5990): p. 458-461.

McTaggart, J.S., R.H. Clark, and F.M. Ashcroft, *The role of the KATP channel in glucose homeostasis in health and disease: more than meets the islet.* J Physiol (Lond), 2010. **588**(pt 17): p 3201-9.

* denotes equal contribution

Abbreviations

ADHD	Attention deficit hyperactivity disorder
AMPA	2-amino-3-(5-methyl-3-oxo-1,2- oxazol-4-yl)propanoic acid
ANOVA	Analysis of variance
ATP	adenosine 5'-triphosphate
BBB	blood-brain barrier
β-cell	pancreatic beta-cell
BMI	body mass index
BSA	bovine serum albumin
CCD	charge-coupled device
cDNA	complementary DNA
CHI	congenital hyperinsulinism
(a)CSF	(artificial) cerebrospinal fluid
CNQX	6-cyano-7-nitroquinoxaline-2,3-dione
DAB	3,3'-Diaminobenzidine
DAPI	4', 6-diamidino-2-phenylindole
DEND	developmental Delay, Epilepsy and Neonatal Diabetes syndrome
EGTA	ethylene glycol-bis-(β-aminoethyl ether) N, N, N', N'-tetra-acetic acid
ENU	N-ethyl-N-nitrosourea
FTO	fat mass and obesity-associated
GABA	Gamma-aminobutyric acid
GAD	Glutamic acid decarboxylase
(e)GFP	(enhanced) green fluorescent protein
GTP	guanosine 5'-triphosphate
GWA	genome-wide association
HEPES	N-(2-hydroxyethyl)piperazine-N'-(2-ethanesulfonic acid)
HRP	Horse radish peroxidase
HSC-70	Heat shock cognate 70kDa protein
IC_{50}	Half maximal inhibitory concentration
iDEND	intermediate DEND syndrome (no epilepsy is present)

IgG	Immunoglobulin G
I_H	Hyperpolarisation-activated current
IRES	internal ribosomal entry sequence
K_{ATP} channel	ATP-sensitive potassium channel
LacZ	β-galactosidase
MANOVA	Multivariate ANOVA
MC4R	Melanocortin 4 receptor
MPTP	1-methyl-4-phenyl-1,2,3,6-tetrahydropyridine
NDM	Neonatal diabetes mellitus
NeuN	Neuronal nuclear protein
PB	Phosphate buffer (no NaCl present)
PBS	phosphate buffered saline
PCR	Polymerase chain reaction
PIP_2	Phosphatidylinositol 4,5-bisphosphate
PNDM	Permanent neonatal diabetes mellitus
P_o	Single-channel open probability
POMC	Pro-opiomelanocortin
PVDF	polyvinylidene difluoride
RT-PCR	reverse transcription polymerase chain reaction
RT-qPCR	reverse transcription quantitative polymerase chain reaction
SDS	Sodium dodecyl sulphate
SNP	single nucleotide polymorphism
SUR	sulphonylurea receptor
TNDM	Transient neonatal diabetes mellitus
TBST	0.1% Tween 20 tris-buffered saline
T2DM	type 2 diabetes mellitus
Z/EG	LacZ/eGFP double reporter mouse

Chapter 1: Introduction

1.1 Genetic Susceptibility to Obesity and Diabetes

Obesity is a major cause of morbidity and mortality and is spreading rapidly across the world [1]. Obese individuals are defined as having a body mass index (BMI; in kg/m^2) of greater than 30. They have an increased risk of developing type 2 diabetes mellitus (T2DM), coronary heart disease, certain forms of cancer, and osteoarthritis of large and small joints [2, 3].

The increase in the prevalence of obesity over the last three decades appears to be driven by a changing environment, characterised by excessive calorie intake, lower physical activity and a variety of other 'obesogenic' factors [4, 5]. The current increase in the prevalence of T2DM is thought to stem from the increase in obesity [6], though other factors, such as age [7], are also important contributors to an individual's risk. However, even in the current environment some people do not become overweight or obese and some do not develop T2DM even when obese [8, 9]. These observations suggest that genetic differences may be an important factor in an individual's risk of developing these conditions.

It is well established that BMI is strongly heritable. For example, the concordance of BMI of monozygotic twins is high (≥0.7), but dizygotic twins are less similar (~0.3) [10, 11]. And studies of adopted twins who were reared apart show a strong relationship between the BMI of adopted children with their biological parents but none when compared with their adoptive parents [11, 12]. These and other studies have lead to the consensus that variation in BMI is largely due to heritable genetic differences [13, 14], with heritability estimated at approximately 55-85% for both adults and children [14].

The heritability of T2DM is less clear [9]. The disease tends to run in families as the siblings of a diabetic individual have a nearly 4-fold increased risk of developing T2DM compared with the general population [15]. In twin studies of T2DM, concordance rates have ranged from 0.29 to 1.00 in monozygotic twins, and 0.10 to 0.43 in dizygotic twins (the concordance of dizygotic twins is approximately half that of monozygotic twins) [16]. And concordance between monozygotic and dizygotic twins increases with the duration of the follow-up period [17]. These and other data suggest that genetic differences influence an individual's risk of T2DM [16].

1.1.1 Genetic influences on body weight and obesity

Before recent advances in our understanding of the human genome, the genetic variants underlying the heritability of obesity were identified by studying human beings and mouse models displaying severe, early-onset, rare forms of the disease. These cases were often aggregated in pedigrees and displayed Mendelian inheritance which, in concert with their conspicuous presentation, indicated that they were likely to be caused by the malfunction of a single gene. It was hoped that identification of the causal gene could shed light on the aetiology of the common form of the disease.

Some of the key genes involved in energy homeostasis were identified in this way; notably leptin via the ob/ob mouse [18] and the leptin receptor via the db/db mouse [19], and elements of the melanocortin system such as the melanocortin 4 receptor (MC4R) [20]. Although these genes were discovered in mouse models, mutations in homologous genes were rapidly identified in human beings with severe early-onset obesity [21-24]. Other genes that are important in energy homeostasis, such as proopiomelanocortin (*POMC*), were first discovered in severely obese human beings, and then knocked out in mice to confirm their function [25-27].

However, these monogenic forms of obesity are rare; severe, young-onset obesity has a monogenic cause in only approximately 7% of cases [28]. And these monogenic disorders result in extremely severe obesity; less than 0.01% of the general population is so severely obese [9]. Therefore, these coding mutations in single genes do not contribute to the risk of obesity in the general population.

Our ability to find the genetic variants that predispose to common, complex disease has greatly advanced in recent years. Firstly, the completion of the Human Genome Project [29] has enabled greater understanding of the genomic variation present in human beings. For example, the Human Haplotype Map Consortium has identified over 3.1 million single nucleotide polymorphisms (SNPs) across the euchromatic portion of the genome - approximately 25-35% of all the common SNPs [30]. Secondly, high-throughput genotyping technology has also advanced. Chips have been developed that capture ~60-80% of the common genetic variation reported in the HapMap [31]. Therefore, it is now possible to correlate disease states with common genetic differences, analysing results from tens of thousands of people in genome-wide association (GWA) studies. GWA is a hypothesis-free approach that does not rely on familial relatedness, so GWA studies can simply use large cohorts of cases and controls and thus be based on much larger sample sizes than typical family-based studies.

In a GWA study looking for genetic variants associated with T2DM, SNPs in the first intron of the *FTO* (fat mass and obesity-associated) gene region were identified [32]. These included the variants rs9939609, rs17817449, rs3751812, rs1421085 and rs9930506. When BMI was taken into account, however, the association was abolished, suggesting that the SNPs were associated with T2DM via their association with BMI. Approximately 16% of individuals of European descent were homozygous for the at-risk alleles, and had an ~1.67-fold increased risk of obesity, weighing on average ~3kg more than controls [32, 33]. These results were

corroborated in many other studies, and the association did not seem to be limited to individuals of a specific ethnic background [33-47].

At least 50 other BMI-associated loci have subsequently been identified through the GWA method [48]. These include SNPs that are downstream of the melanocortin-4 receptor (*MC4R*) [40, 49] and near pro-opiomelanocortin (*POMC*) [50] - genes that were previously identified in studies of monogenic obesity, and whose physiological role in energy homeostasis is relatively well understood [51].

1.1.2 Genes that predispose to T2DM

Some genetic variants associated with T2DM were identified before the advent of GWA, by candidate-gene studies. In contrast to GWA studies, candidate-gene studies focus on genetic analysis restricted to one or more specific genes. The genes are selected on the basis of a perceived match between their known or presumed functions and the biological characteristics of the disease state.

It was known that the ATP-sensitive potassium channel (K_{ATP} channel) was crucially involved in insulin secretion from pancreatic beta-cells (β-cells) (discussed in section 1.2.4) and that mutations in the *KCNJ11* and *ABCC8* genes, that encode the Kir6.2 and SUR1 subunits of the channel, caused congenital hyperinsulinism - a disease affecting glycaemic control [52-54]. Therefore focus fell on these two genes to see if common coding variants were associated with T2DM.

Although initial studies were controversial, a consensus developed and a common polymorphism in Kir6.2 (E23K) was identified that predisposed to T2DM [55]. Although the increase in disease risk is small (odds ratio, 1.2), the population risk is highly significant

because ~60% of people carry at least one K allele. The E23K polymorphism is found in strong linkage disequilibrium with another variant, S1369A, in the adjacent SUR1 gene (i.e. E23 was always found in conjunction with S1369, and K23 with A1369). Therefore either variant could have caused the increased disease risk. At least 30 other loci associated with risk of T2DM have since been identified through GWA studies [48].

1.1.3 The K_{ATP} channel and the FTO protein

There are a variety of methods that can be used to identify genetic variation that underlies common diseases such as T2DM and obesity. Although the identification of novel candidate genes or gene regions is an important step in our understanding of the aetiology of common disease, such associations need to be validated by physiological investigation.

If the associated SNP is exonic, as is the case for the E23K/S1369A variants, then the functional consequences of those changes need to be identified. Indeed, physiological studies of the E23K/S1369A variants have been carried out and are discussed in section 1.2.3.

But in GWA studies, the associated genetic variants are often *near* to the coding regions of genes, rather than in the exons themselves. The proximity of a SNP to a gene does not necessarily mean that the gene is the cause of variation in body mass; the function of that locus needs to be identified. For example, the SNP may be in a section of DNA that is close to a gene, but actually be involved in long-distance transcriptional regulation of a different gene [56]. Further difficulty arises when the associated SNP is near a gene or genes of unknown function. Both of these points are relevant when understanding how the SNPs near *FTO* influence body weight. When first associated with obesity, *FTO* was “a gene of unknown function in an unknown pathway” [32]. Subsequent studies have shown that the gene shares

a CpG island with the adjacent *RPGRIP1L* gene, suggesting that the two genes are coregulated [57]. And the obesity-associated SNPs have been linked with changes in expression levels of *RBL2* (another gene near *FTO*) rather than changes in expression of *FTO* itself [58]. Therefore, without physiological investigations it is impossible to suggest how, or even if, *FTO* function is linked to body mass.

Other obesity-associated SNPs are near genes, such as *MC4R* and *POMC*, that are known to be involved in energy homeostasis [51], but as the SNPs are not exonic, it remains to be seen how (or indeed if) they influence the function of these genes. It is worth reiterating that *MC4R* was first linked to obesity via a monogenic disorder. This illustrates how studies of rare, severe forms of disease may be useful in our understanding of common disease.

In summary, the genetic variants that predispose to common obesity and T2DM are becoming clear, but the way in which they alter physiological processes often remains unclear. Although some of the associated SNPs are in or near genes with a recognised functional importance in energy homeostasis or glucose homeostasis (e.g. the E23K/S1369A variant in the K_{ATP} channel), others are near genes of which little is known (e.g. *FTO*). In this thesis, I have explored the physiological functions of the K_{ATP} channel and the FTO protein, which are involved in the aetiology of T2DM and obesity.

1.2 The K_{ATP} Channel

In the mid-1980s, a novel potassium channel was identified in cardiac myocytes that closed in response to intracellular ATP concentrations in the millimolar range [59]. A similar channel was identified in pancreatic β- cells [60, 61]. This ATP-sensitive potassium channel (K_{ATP} channel) plays an important role in the physiology and pathophysiology of various

tissues, including the heart [59], skeletal and smooth muscle [62, 63], the pancreas [60, 61] and the central nervous system [64].

1.2.1 Structure of the K_{ATP} channel

The K_{ATP} channel is composed of 4 pore-forming Kir6.x subunits and four regulatory sulphonylurea receptor (SUR) subunits, forming a hetero-octameric complex [65, 66].

Kir6.x subunits form a potassium-selective inwardly rectifying channel [67, 68]. The rectification of the channel is due to a high-affinity block by endogenous intracellular polyamines and magnesium ions, which are forced into the channel at positive membrane potentials [69, 70]. ATP binding to the Kir6.x subunit causes K_{ATP} channel closure [71]. There are two isoforms of Kir6.x: Kir6.1 (encoded by *KCNJ8*) is expressed in vascular smooth muscle [69] and Kir6.2 (encoded by *KCNJ11*) is expressed more widely, in the pancreatic β-cell, cardiac and skeletal muscle and the brain [70] (Table 1.1).

The sulphonylurea receptor, a member of the ATP Binding Cassette superfamily [72], plays a regulatory role. It is necessary for the sensitivity of the K_{ATP} channel to stimulation by Mg-nucleotides, which is mediated via its two cytosolic nucleotide-binding domains [73, 74]. It is also necessary for the activating effects of potassium channel openers such as diazoxide, and inhibition by sulphonylurea drugs, such as tolbutamide and glibenclamide (see below) [72, 73]. There are three isoforms of the sulphonylurea receptor: SUR1 (encoded by *ABCC8*) is expressed in pancreatic β- cells and brain [69, 72], SUR2A in skeletal and cardiac muscle [75, 76] and SUR2B in smooth muscle and brain [77-80] (Table 1.1). SUR2A and SUR2B are splice variants of the same gene - *ABCC9* - and differ only in their C-terminal 42 amino acids [81].

Kir6.2 is unable to reach the membrane surface in the absence of SUR and vice versa [82]. This is because both subunits contain an endoplasmic reticulum retention motif (RKR) within their cytosolic domain that is masked only when the two subunits associate together. This ensures that only fully functional K_{ATP} channels are trafficked to the plasma membrane. The ER retention signal in Kir6.2 may be deleted by truncation of the C-terminus of the protein at residue 355 (Kir6.2ΔC), which permits independent surface expression of Kir6.2 [71, 82]. This allows the intrinsic properties of Kir6.2 to be assessed in the absence of SUR.

Table 1.1 K_{ATP} channel subunits by location

Location	Kir6.x subunit	SUR subunit
Brain (primarily neurons)	Kir6.1 or Kir6.2	SUR1 or SUR2B
Pancreatic β-cells	Kir6.2	SUR1
Skeletal and cardiac muscle	Kir6.2	SUR2A
Vascular smooth muscle	Kir6.1	SUR2B

1.2.2 Regulation of the K_{ATP} channel

The K_{ATP} channel is regulated by a number of different factors. As well as intracellular nucleotides [60, 83-85] and pH [86], cytosolic compounds such as lipids also interact with the channel. Phosphatidylinositol-4,5-bisphosphate (PIP_2) [87-89] and long-chain acyl CoAs, such as oleoyl CoA, stimulate channel activity and reduce ATP sensitivity [90, 91].

It is now clear that metabolic regulation of K_{ATP} channel activity is mediated by both Kir6.2 and SUR. The ATP-binding site responsible for channel closure is on Kir6.2 [71] whereas MgADP binding to SUR opens the channel [71, 73, 74]. MgATP can also stimulate K_{ATP} channel activity via SUR [91], but it must first be hydrolysed to MgADP [92]. SUR therefore

functions as a second metabolic sensor, and when combined with Kir6.2 creates a channel with exquisite sensitivity to changes in adenine nucleotide concentrations [93].

The different SUR isoforms have different pharmacology and therefore confer slightly different properties to K_{ATP} channels. Channels containing SUR1 are sensitive to block by the sulphonylurea drugs glibenclamide, tolbutamide and gliclazide [72, 94]. They are also activated by diazoxide [95]. Channels containing SUR2A have reduced sensitivity to gliclazide and tolbutamide, but are activated by the potassium channel openers pinacidil and cromakalin [88, 91, 94, 96-100]. SUR2B has a similar pharmacological specificity to SUR2A [101].

The choice of sulphonylurea receptor also determines the sensitivity of the K_{ATP} channel to metabolic inhibition. Channels containing SUR1 subunits open more easily when cell metabolism is inhibited [80, 102]. How this is achieved remains unclear as the IC_{50} for MgATP inhibition in excised patches is similar for all types of channel [102].

1.2.3 The K_{ATP} channel in insulin secretion

The best understood physiological role of the K_{ATP} channel is in stimulus-secretion coupling in pancreatic β-cells. The discovery of the K_{ATP} channel explained how changes in glucose levels resulted in changes in β-cell membrane potential [61, 103]. Indeed, it became apparent that the resting membrane potential of the β-cell was principally determined by K_{ATP} channel activity [83]. Thus, when K_{ATP} channels are shut, the resistance of the β-cell membrane is high and even small changes in currents across the membrane can induce relatively large changes in the membrane potential [104].

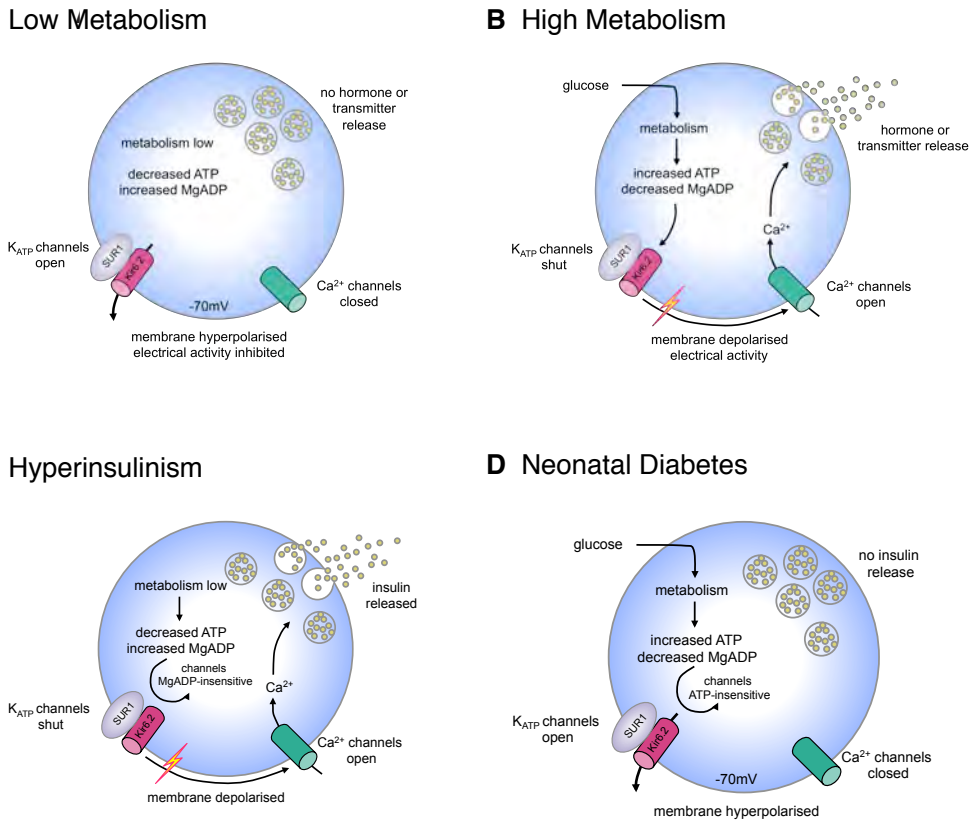

Figure 1.1 K_{ATP} channels couple membrane excitability to metabolism

(**A**) K_{ATP} channels are open when metabolism is low due to low ATP and relatively high MgADP concentrations. The open channels allow a potassium flux that hyperpolarises the membrane, preventing electrical activity. (**B**) When metabolism increases (e.g. due to increased blood glucose levels following a meal), ATP concentrations rise and MgADP concentrations fall, closing K_{ATP} channels. This triggers membrane depolarisation and electrical activity, which in turn stimulates cell functions such as muscle contraction, neuronal action potentials and hormone secretion. (**C**) Loss-of-function mutations in Kir6.2 or SUR1 lead to permanent K_{ATP} channel closure - independent of cell metabolism. Consequently, the β-cell membrane is always depolarised, producing continuous calcium influx and insulin secretion. (**D**) Gain-of-function mutations in Kir6.2 or SUR1 prevent K_{ATP} channel closure by adenine nucleotides. Consequently, the β-cell membrane remains hyperpolarised even when blood glucose levels are high, preventing insulin secretion and therefore resulting in diabetes. Figure adapted from McTaggart *et al.* (2010).

We now know that at substimulatory glucose concentrations the β-cell K_{ATP} channel is open. Hence the cell membrane is hyperpolarised and voltage-gated calcium channels are closed [83], so insulin secretion is not initiated (Figure 1.1). In response to an increase in the blood glucose concentration, glucose is transported into pancreatic β- cells and metabolised, thereby increasing intracellular ATP levels and lowering ADP levels. This closes the K_{ATP} channel, producing a membrane depolarisation that opens voltage-gated calcium channels. The influx of calcium into the β-cell triggers insulin exocytosis [93, 105].

In summary, K_{ATP} channels in the β-cell act as metabolic sensors, coupling the metabolism of a cell to its membrane potential and thus the cell's electrical excitability [106, 107]. This principle also applies in extra-pancreatic tissues, where closure of K_{ATP} channels allows the release of neurotransmitters, or initiation of muscle contraction.

1.2.4 The E23K/S1369A mutation

As the K_{ATP} channel plays a crucial role in insulin secretion, mutations in Kir6.2 or SUR1 can lead to significant difficulties in maintaining glucose homeostasis. As previously discussed, the E23K mutation in Kir6.2 and S1369A mutation in SUR1 are associated with risk of T2DM. While the genetics is clear, the functional effects of these variants both *in vivo* and *in vitro* are controversial. Both increases and decreases in the ATP sensitivity of Kir6.2/SUR1 channels have been reported when E23 in Kir6.2 is mutated to K23 [108-110]. Others have argued that it is not the K23 variant that is causal but the A1369 variant in SUR1 [111].

Considerable variability has also been reported for the effects of the E23K polymorphism on insulin secretion and insulin sensitivity in human beings but in larger studies plasma insulin concentrations are lower, insulin secretion is reduced and insulin sensitivity is enhanced [110, 112-114]. The reduced insulin concentration and secretion are consistent with

increased K_{ATP} currents in pancreatic β- cells. But the origin of the enhanced insulin sensitivity is unknown; it cannot be due to enhanced K_{ATP} channel activity in muscle as this would be expected to have the opposite effect [78]. Perhaps it is caused by a mechanism in the brain.

1.2.5 Loss-of-function mutations in the K_{ATP} channel and congenital hyperinsulinism

Although the physiological impact of the E23K/S1369A mutations are controversial, other coding mutations in the K_{ATP} channel cause more severe symptoms, which are easier to interpret. Congenital hyperinsulinism (CHI) is characterised by continuous, unregulated insulin secretion despite very low plasma glucose levels [115, 116]. Patients usually present shortly after birth with persistent hypoglycaemia that requires immediate treatment to avoid brain damage. Infants are also large for gestational age due to stimulation of foetal growth by the excess insulin. In general, CHI caused by mutations in the K_{ATP} channel genes is severe, being refractory to treatment with diazoxide [115, 117], so patients require subtotal pancreatectomy, which often results in pancreatic insufficiency and a high incidence of iatrogenic diabetes.

K_{ATP} channel mutations are the most common cause of CHI: >150 have been found in SUR1 and 24 in Kir6.2 [118]. In these patients, K_{ATP} channels are not present in the plasma membrane, or they are present but do not open because they are no longer activated by MgADP [119-123]. Most mutations are recessive, suggesting that 50% K_{ATP} channel function is sufficient to prevent hypersecretion of insulin. A few dominant mutations have been identified which are less severe and often responsive to diazoxide [124]. All mutations in K_{ATP} channel genes that cause CHI lead to a marked reduction in the whole-cell K_{ATP} current, even at low glucose. Consequently, the β- cell membrane is permanently depolarised, producing continuous calcium influx and insulin secretion (Figure 1.1).

CHI may also arise through mutation of the metabolic enzymes glucokinase [125, 126], glutamate dehydrogenase [127], and short-chain L-3-hydroxyacyl-CoA dehydrogenase [128]. In about half of patients the genetic basis of CHI has not yet been determined [104].

1.2.6 Gain-of-function mutations in the K_{ATP} channel and neonatal diabetes mellitus

Gain-of-function mutations in Kir6.2 or SUR1 cause neonatal diabetes mellitus (NDM). Patients normally, but not exclusively, present within the first 6 months of life with severe hyperglycaemia. In many people the diabetes is permanent (PNDM) but in others it follows a remitting relapsing time course and is therefore transient (TNDM) [129, 130]. The majority (~71%) of cases of TNDM are caused by abnormalities of an imprinted locus on chromosome 6q24 that results in the overexpression of a paternally expressed gene [118, 131], but it can also be caused by heterozygous mutations in Kir6.2 [132-134]. Around 20% of patients with PNDM also exhibit neurological/neuromuscular problems, including mental and motor developmental delay, muscle hypotonia, and (occasionally) epilepsy - a syndrome known as DEND (developmental Delay, Epilepsy, Neonatal Diabetes) or intermediate DEND (iDEND) if epilepsy is absent [134-136]. This spectrum of symptoms is a consequence of the widespread tissue distribution of K_{ATP} channels.

Over 40 different NDM mutations have been described in Kir6.2 and a similar number in SUR1 [118]. All Kir6.2 mutations cause dominant disease, but SUR1 mutations are genetically more heterogeneous, with homozygous, heterozygous and compound heterozygous mutations being described. PNDM is most commonly associated with Kir6.2 mutations and TNDM with SUR1 mutations. Fifteen Kir6.2 mutations (but only two in SUR1) cause neurological problems [118].

All Kir6.2 mutations causing NDM impair channel inhibition by ATP [93, 135]. Some act by increasing the intrinsic (unliganded) channel open probability (P_o), which indirectly reduces ATP block - it remains unclear if they influence gating directly or via changes in PIP_2 binding. Other mutations cluster around the putative ATP-binding site and are likely to impair ATP binding. Mutations may also alter ATP binding allosterically, or influence the mechanism by which occupancy of the ATP-binding site is transduced into changes in channel gating. There is also evidence that some Kir6.2 mutations enhance Mg-nucleotide activation (mediated via SUR1). Interestingly, the shifts in ATP sensitivity observed in Kir6.2-E23K mutations [110] (the variants linked with increased risk of T2DM) are similar to those found with some NDM mutations, raising the question of why KK carriers have only a small increase in diabetes risk and not NDM. Only a handful of SUR1 mutations have been studied in detail but their effects are equally complex, with some increasing MgATP activation and others increasing P_o.

The severity of the clinical phenotype correlates reasonably well with the ability of MgATP to inhibit channel activity in inside-out patches (Figure 1.2) [93, 137]. Mutations that have relatively little effect on ATP sensitivity, such as Kir6.2-R50Q and Kir6.2-R201H [135, 138] cause PNDM alone. Other mutations, such as Kir6.2-Q52R and Kir6.2-I296L cause DEND. The most common mutation causing iDEND is Kir6.2-V59M [135, 139, 140]. Because NDM mutations impair the ability of ATP to inhibit the channel, they all increase the whole-cell K_{ATP} current. Consequently, the β- cell remains hyperpolarised even in the presence of glucose, preventing insulin secretion and causing diabetes (Figure 1.1).

NDM patients were originally treated with insulin injections but the discovery of the causal role of K_{ATP} channels has enabled ~90% of patients (>400 to date) to switch to sulphonylurea therapy [139, 141-146]. This results in a significant improvement in their clinical condition: fluctuations in glucose homeostasis are reduced and HbA1C levels fall, reducing the risk of diabetic complications [141, 143].

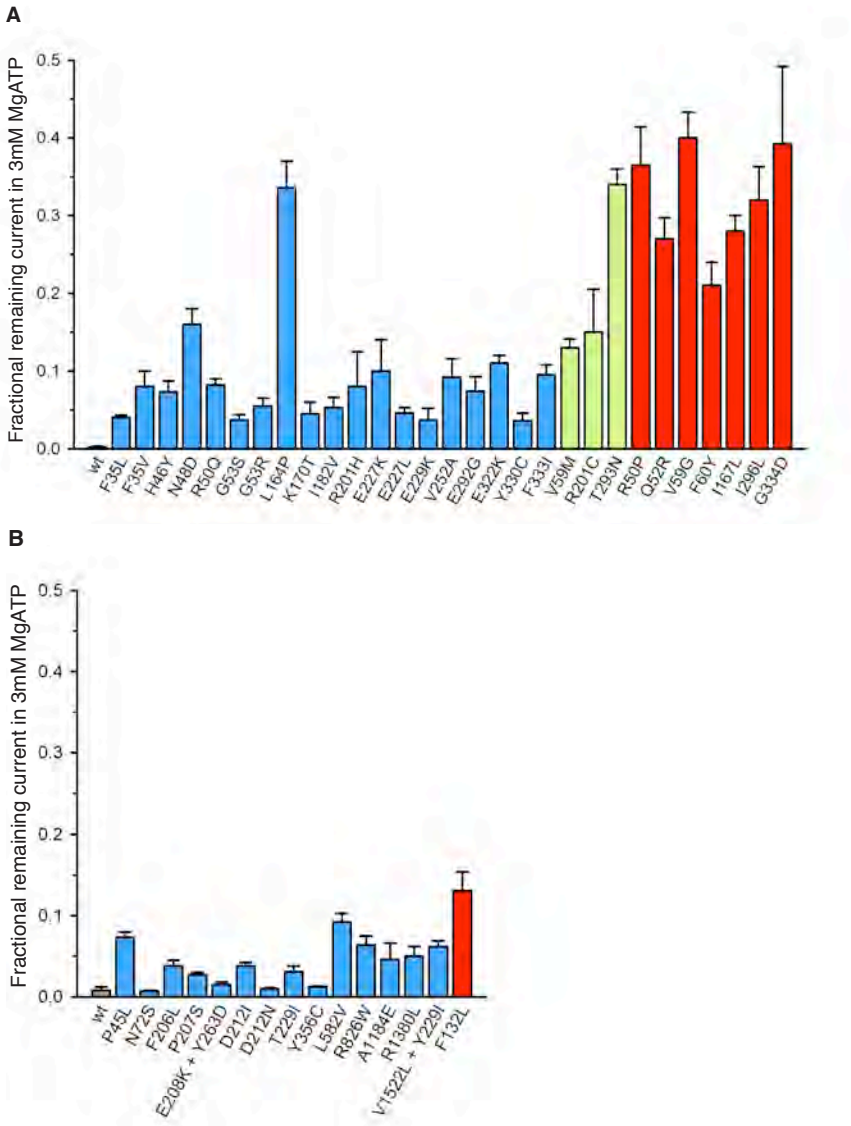

Figure 1.2 ATP sensitivity and disease severity

Disease severity correlates with the extent of unblocked K_{ATP} channel current measured from inside-out patches in 3mM MgATP. (**A**) ATP sensitivity of Kir6.2/SUR1 channels with wild-type (wt) or mutant Kir6.2, as indicated. 50% wild-type and 50% mutant Kir6.2 mRNAs were injected to simulate the heterozygous state of the patients. (**B**) ATP sensitivity of Kir6.2/SUR1 channels with wild-type (wt) or mutant SUR1, as indicated. Again, channels were heterozygous. Data are mean ± SEM. Blue bars = neonatal diabetes alone. Green bars = iDEND. Red bars = DEND. Figure adapted from McTaggart *et al.* (2010).

There is a good correlation between the efficacy of sulphonylureas at blocking whole-cell K_{ATP} currents and the ability of the patient with the same mutation to respond to sulphonylurea therapy (Figure 1.3). It should be noted that PNDM patients with Kir6.2 mutations need significantly higher doses of sulphonylureas to treat their diabetes than are typically used to treat T2DM [141]. This is likely to be because sulphonylurea block is less efficient when nucleotide inhibition on Kir6.2 is decreased [73, 147].

In some iDEND and DEND patients, the neurological/neuromuscular problems also improve with sulphonylurea therapy. Some patients become able to walk and stand unaided, with improvements in muscle tone [148-152]. Cognitive functions may also improve [149-152]. However, not all patients show such improvements [147, 148, 153].

The improvement in neuronal function with sulphonylurea therapy may also be accompanied by improvements in cerebral blood flow. Single-photon emission CT imaging of a patient with the Kir6.2-H46L mutation showed increased regional blood flow in the brain, particularly in the cerebellar region, following transition from insulin to glibenclamide therapy [152]. As cerebral blood flow is correlated with neuronal activity, the results of this case study suggest that systemic sulphonylurea treatment may increase neuronal activity. Clearly, further studies need to be carried out before firm conclusions can be drawn.

The heterogeneity of the neurological/neuromuscular improvement following sulphonylurea treatment is likely to be due to a number of factors. Firstly, the severity of the mutation and the dosage of sulphonylurea drug will clearly be important (Figure 1.3). Secondly, the blood-brain barrier (BBB) may prevent accumulation of therapeutic concentrations of sulphonylureas in the brain [148, 151]. Indeed, in rodents, tolbutamide is pumped out of the cerebrospinal fluid (CSF) and therefore accumulates at only low levels [154]. However, as the cognitive ability of some patients does improve, it is likely that sufficient sulphonylurea crosses the BBB to close the mutant K_{ATP} channels to some extent.

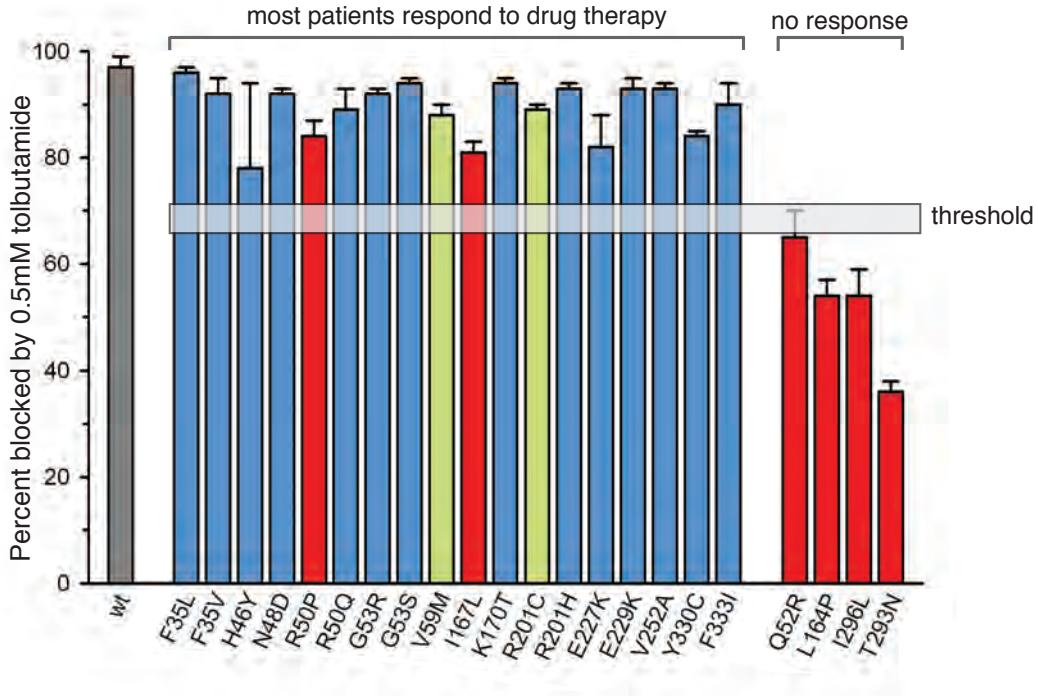

Figure 1.3 Tolbutamide sensitivity and clinical response

The tolbutamide sensitivity of recombinant K_{ATP} channels correlates with the ability of patients to transfer to sulphonylurea therapy. Bars show the percentage of K_{ATP} channel inhibition by 500μM tolbutamide in the presence of 3mM azide for wild-type channels (wt) and those with the Kir6.2 mutations, as indicated. Channels are composed of Kir6.2 with SUR1. Data are mean ± SEM. The transparent grey bar indicates the apparent threshold level for transfer (~70% block). Blue bars = neonatal diabetes alone. Green bars = iDEND. Red bars = DEND. Figure adapted from McTaggart *et al.* (2010).

Perhaps the relatively high doses of sulphonylureas administered to these patients [141] allow CSF concentrations to rise to a therapeutic level, despite the presence of efflux mechanisms.

Although gain-of-function K_{ATP} channel mutations are the most common cause of PNDM, and will be the focus of this thesis, the disease may also be caused by mutations in a number of other genes [134]. Homozygous and compound heterozygous mutations in glucokinase have also been reported to cause PNDM [155, 156]. These are thought to act indirectly by a reduced metabolic generation of ATP, which therefore impairs K_{ATP} channel closure. There are also several rare syndromes that feature PNDM including X-linked diabetes mellitus, Wolcott-Rallinson syndrome due to mutations in the *EIF2AK3* gene, pancreatic agenesis due to mutations in insulin promotor factor-1, and neonatal diabetes with cerebellar agenesis due to mutations in the *PTF1A* gene [157-160].

1.2.7 Mouse models of neonatal diabetes mellitus

It is very clear from mouse models of NDM that increased activity of K_{ATP} channels in β-cells alone is sufficient to produce diabetes. Truncation of the N-terminal 30 amino acids of Kir6.2 (Kir6.2-ΔN30) results in K_{ATP} channels with ~10-fold lower ATP sensitivity and reduced sulphonylurea sensitivity [161-164]. Expression of Kir6.2-ΔN30 in β- cells alone resulted in mice with severe hyperglycaemia concomitant with extremely low serum insulin levels; despite normal islet architecture, β-cell number and insulin content - indicating that reduced insulin secretion was the cause of the diabetes [165]. These mice developed ketoacidosis and typically died within 5 days.

Interestingly, mice that expressed the mutant gene at a lower level in the pancreas did not develop NDM, but instead had impaired glucose tolerance [166]. This indicates that both

mice and human beings are capable of developing a spectrum of diabetic phenotypes that correlate with the extent of K_{ATP} channel activity.

Subsequently, a mouse was generated with an additional mutation in the ATP-binding site of Kir6.2 (K185Q): Kir6.2-K185Q,ΔN30 mice. This transgene was targeted to β-cells using an inducible Cre line (injections of tamoxifen were needed for expression of the transgene) and these mice displayed a similar phenotype to the Kir6.2-ΔN30 model: they had severe glucose intolerance within 2 weeks of transgene induction, profound loss of β-cell mass, and reduction of total insulin content [167].

The Kir6.2-ΔN30 and Kir6.2-K185Q,ΔN30 models provide strong evidence that gain-of-function mutations in pancreatic K_{ATP} channels cause NDM. In both of these models, however, ATP-insensitivity in the channel was induced by synthetic mutations that do not occur in patients with NDM. Furthermore, neither of these models display impairment in neuromuscular function, implying that pancreatic β-cell dysfunction does not underlie those symptoms of iDEND (as might be expected).

Recently, a novel mouse model was created, called the ROSA mouse, in which the coding sequence for Kir6.2-V59M (the most common iDEND-causing mutation) was inserted into the ROSA locus [168], which possesses a ubiquitously expressed promotor [169]. A loxP-flanked transcriptional STOP sequence was included upstream of Kir6.2-V59M so that mutant Kir6.2 mRNA expression could be induced in adult life, and also restricted to specific tissues. Thus, when ROSA mice were crossed with mice expressing Cre under transcriptional control of the rat insulin promotor, producing β- V59M mice, Kir6.2-V59M expression was targeted to pancreatic β-cells.

β-V59M mice expressed comparable levels of wild-type and mutant Kir6.2 mRNA in pancreatic islets. This is important as all NDM patients with Kir6.2 mutations are

heterozygous [118] and thus are expected to express, on average, 50% wild-type and 50% mutant Kir6.2 subunits. β- V59M mice also mimicked the phenotype of the patients. They developed severe diabetes soon after birth and by 5 weeks of age blood glucose levels were greatly increased and insulin levels were undetectable. Islets isolated from these mice secreted less insulin and showed smaller increases in intracellular calcium concentrations in response to glucose stimulation compared to wild-type mice. This correlated with a decreased number of β-cells in the islets, abnormal islet morphology and lower total insulin content. Therefore, β- cell specific expression of K_{ATP} channels with an iDEND-causing mutation replicated the diabetic symptoms of iDEND.

1.2.8 A mouse model of iDEND

Although gain-of-function K_{ATP} channels in β-cells cause diabetes, hyperglycaemia is unlikely to cause the neurological/neuromuscular symptoms of iDEND because they persist even when the patients are treated with insulin. Indeed, untreated β-V59M mice perform the same as controls when tested on a panel of motor strength and coordination tests [170], so β-cell dysfunction alone is insufficient to cause neurological/neuromuscular impairment.

The cognitive symptoms of iDEND are likely to be caused by the expression of mutant K_{ATP} channels in neurons alone. However, dysfunction of several tissues that express K_{ATP} channels, such as the skeletal and cardiac muscles, and the brain, could plausibly account for the neuromuscular problems. For example, muscle hypotonia can result from a defect in the electrical properties of the muscle (as in paramyotonia congenita [171, 172]), or from a lack of transmitter release from motor nerves innervating the muscle (as in Lambert Eaton myaesthenic syndrome [173]). If the heart were compromised then the reduced oxygen carrying capacity could also impair neuromuscular function.

Three pieces of evidence suggest that mutant K_{ATP} channels in neurons, rather than muscle cells, are responsible for the hypotonia in iDEND. Firstly, treatment with gliclazide, an SUR1-specific sulphonylurea drug, successfully improved the neuromuscular symptoms of a patient with a Kir6.2 mutation causing iDEND [150]. Secondly, mutations in SUR1 can cause DEND [174]. As SUR1 is specific to neurons (and the pancreas), these pieces of evidence from case studies indirectly suggest that neuronal impairment causes the neuromuscular symptoms of iDEND.

In a recent study [102], the relative importance of the muscles and the brain for the neuromuscular symptoms of iDEND was assessed directly. The ROSA mouse was crossed with either muscle creatine kinase-Cre or nestin-Cre [175] mice, producing m-V59M and n-V59M mice, which expressed Kir6.2-V59M specifically in muscle or nerve tissue, respectively. As expected, neither of these mice developed diabetes. When assessed on tests of muscle strength and motor coordination n-V59M mice, but not m-V59M mice, were weaker and less coordinated than their littermate controls (Table 1.2). Similarly, n-V59M, but not m-V59M, mice showed greater spontaneous locomotor activity. This is consistent with previous reports that iDEND patients are hyperactive [151, 152]. So these experiments suggest that the dysfunction of neurons causes the neuromuscular symptoms of iDEND.

Heterologous expression studies in *Xenopus* oocytes were carried out to determine why n-V59M but not m-V59M mice were affected on these tests. When Kir6.2-V59M was expressed with SUR1 (Kir6.2-V59M/SUR1), which is present in many neurons, whole-cell K_{ATP} currents were higher compared to wild-type channels, consistent with previous reports [176]. But when Kir6.2-V59M was expressed with SUR2A (Kir6.2-V59M/SUR2A), which is present in skeletal muscle, whole-cell K_{ATP} currents were not different to wild-type. Thus, although mutant K_{ATP} channels were present in the skeletal muscle membrane of m-V59M mice, muscle function was not affected because the SUR2A subunit mitigated the effect of the Kir6.2-V59M mutation on K_{ATP} channel activity.

Table 1.2 Summary of symptomology of iDEND patients and mouse models

Organism	Location of mutant Kir6.2 expression	Diabetes	Motor impairments	Hyperactivity
iDEND patients	β-cells, skeletal muscle, cardiac muscle, neurons	Yes	Yes	Yes
β-V59M mouse	β-cells	Yes	No	No
n-V59M mouse	Neurons	No	Yes	Yes
m-V59M mouse	Skeletal muscle, cardiac muscle	No	No	No

1.3 Physiological Functions of K_{ATP} Channels in the Brain

1.3.1 Distribution of K_{ATP} channels in the brain

As previously mentioned, K_{ATP} channels in the brain may be composed of all of the combinations of Kir6.1 and Kir6.2 with SUR1 and SUR2B [177-180]. Different combinations confer different sensitivities to metabolic stress [80, 180]. Given the functional importance of the particular subunits expressed, several attempts have been made to map the expression pattern of K_{ATP} channel subunits in the brain.

Kir6.2 is widely distributed [181-185] and is predominantly expressed in neurons, with little or no labelling in glial cells [183, 185]. It is not limited to a particular functional class of neurons as it is found in cells that co-express a variety of other characteristic proteins, such as glutamic acid decarboxylase 65, neuropeptide Y and tyrosine hydroxylase [183].

In contrast to the widespread distribution of Kir6.2, Kir6.1 is relatively weakly expressed in neurons, although some regions, such as the striatum, hypothalamus and zona incerta show moderate levels [185]. Another contrast is the prominent expression of Kir6.1 in glia as it is found in astrocytes, tanycytes and Bergman glial cells in different areas of the brain [185].

Sulphonylurea receptor density in the brain is very low at birth but is rapidly upregulated in the first two weeks of life and continues to increase steadily until adult levels are reached [186, 187]. In adult animals, expression of SUR1 essentially overlaps with Kir6.2 [182, 184]. Some brain regions, however, such as the dorsal endopiriform nucleus and claustrum, have high SUR1 levels but low Kir6.2 [182]. In other regions, such as the subthalamic, oculomotor and lateral lemniscus nuclei, Kir6.2 levels are high but SUR1 levels are low. To my knowledge there are no studies that specifically map the expression of SUR2B in the brain, although channels containing this subunit have been identified in dopaminergic neurons of the substantia nigra by single cell PCR [80].

Functional studies corroborate the observation that K_{ATP} channels are widely expressed in the brain, as activity has been detected in neocortex [188], hippocampus [189-191], hypothalamus [192, 193], basal ganglia [180, 194] and brain stem [195].

1.3.2 K_{ATP} channels in neuroprotection

Neuronal death is often a consequence of excitotoxicity, as cellular depolarisation is associated with metabolic depletion and with detrimental Ca^{2+} influx [196, 197]. K_{ATP} channels may protect against this as they may render the electrical activity of neurons sensitive to changes in metabolism. Even brief (~2min) periods of hypoxia can cause intracellular ATP concentrations to fall to ~15% of normal values [198] so neuroprotection by

K_{ATP} channel activation may be of particular importance in stroke, respiratory failure, and seizure [181, 199, 200]. Consistent with this idea, when Kir6.2 knockout mice were given brief periods of hypoxia they experienced severe convulsions and died, whereas wild-type controls recovered with few ill effects [201]. Similarly, when hippocampal CA1 neurons were treated with glibenclamide, the post-hypoxic hyperpolarisation of these neurons was reduced compared to untreated cells [189].

It has been suggested that Kir6.2/SUR1 channels have the strongest neuroprotective effect [80, 200]. Interestingly, these channels are densely expressed in the hippocampus, neocortex and the cerebellum [183, 185] - brain areas that have a preponderance of spontaneously active neurons [202-205]. These neurons would rapidly succumb to a lack of oxygen if they were not inhibited during periods of metabolic stress, which may explain why Kir6.2/SUR1 levels are particularly high in these brain regions.

K_{ATP} channel-independent mechanisms of neuroprotection also exist [206, 207]. For example, activation of mitochondrial ATP-sensitive potassium channels, which are encoded by different genes to K_{ATP} channels [208], promote survival of cerebellar granule neurons during oxidative stress [209, 210].

1.3.3 Neuronal K_{ATP} channels in glucose homeostasis

Neuronal K_{ATP} channels also play an important role in glucose homeostasis [78, 137]. For example, hypothalamic K_{ATP} channels regulate hepatic glucose output as evidenced by the fact that stereotactic infusion of diazoxide into the hypothalamus inhibits hepatic glucose production and, conversely, that SUR1 knock-out mice show increased glucose production [211]. Furthermore, insulin suppresses hepatic glucose output by activating K_{ATP} channels in agouti-related-peptide-expressing neurons of the arcuate nucleus of the hypothalamus [212].

K_{ATP} channels render the electrical activity of many types of neuron sensitive to the ambient glucose level and thereby influence glucose homeostasis in a variety of ways. For example, reduced extracellular glucose causes opening of K_{ATP} channels in glucose-sensitive neurons of the ventromedial hypothalamus, triggering glucagon secretion and the counter-regulatory response to hypoglycaemia [193]. This is mediated via activation of the autonomic nervous system leading to release of catecholamines such as adrenaline, which is a powerful stimulator of glucagon secretion [213]. Similarly, K_{ATP} channel activation sufficient to abolish electrical activity of anorexigenic *POMC*-expressing neurons of the arcuate nucleus leads to hyperphagia, which influences blood glucose levels [214]. And partial activation of K_{ATP} channels in these cells, which reduces but does not abolish electrical activity, prevents glucose sensing and leads to impaired glucose tolerance [215].

Glucose-sensitive neurons expressing K_{ATP} channels have been found in many other brain regions, including the substantia nigra [216], neocortex [188], hippocampus [189, 217], which are not thought to participate in energy homeostasis. This may indicate that glucose-sensing is also an important factor in neuroprotection - acting to hyperpolarise neurons when glucose levels fall, which may precede the reduction in intracellular ATP.

1.4 The Fat Mass and Obesity-associated Protein (FTO)

1.4.1 Biochemistry of FTO

FTO is a 9-exon gene located on human chromosome 16 and mouse chromosome 8. The protein has homology with the AlkB family of DNA repair enzymes and *in vitro* biochemical studies show that it is a member of the Fe(II) and 2-oxoglutarate (2OG) dependent oxygenase superfamily [218-220]. In metazoans these enzymes are involved in diverse

processes including oxygen sensing, DNA repair, fatty acid metabolism and post-translational modifications [221]. *In vitro*, FTO is a DNA/RNA demethylase with a strong preference for 3-methylthymidine in single-stranded DNA or 3-methyluracil in single-stranded RNA [218-220], suggesting its physiological role involves nucleic acid modification. However, another study indicates that FTO is a transcriptional coactivator that enhances the transactivation potential of the CCAAT/enhancer binding proteins [222]. The possible role of FTO as a DNA/RNA demethylase, and/or as a transcriptional coactivator is consistent with its subcellular localisation in the nucleus [218, 223].

Structural studies show that the selectivity of FTO for single-stranded nucleotide substrates is conferred by a novel loop that covers the conserved 'jelly-roll' motif of the catalytic core [224]. Furthermore, *in vitro*, FTO dimerises, probably via its helical C-terminal domain, although it can exist in both monomeric and dimeric forms [225].

FTO is ubiquitously expressed in both the embryo and adult [32]. In the hypothalamus, expression is seen in the arcuate, paraventricular, dorsomedial and ventromedial nuclei [218] - sites that are critical for regulating energy balance [226]. The hypothalamic expression of *FTO* suggests a potential role in the control of food intake and/or whole body metabolism. However, *FTO* is expressed at high levels throughout the brain, including areas not associated with feeding, such as the cerebellum and hippocampus [218, 227, 228].

1.4.2 SNPs near *FTO* in human beings

As previously discussed, SNPs near *FTO* are associated with obesity. Many studies suggest that food intake is greater in human beings who carry at-risk *FTO* SNPs [36, 229-233]. However, other studies show no association [234-236]. Furthermore, some studies found no association of variants with energy expenditure measured by calorimetry in adults [229, 237].

On balance, there seems to be more evidence suggesting that SNPs in intron 1 of *FTO* are associated with increased energy intake, but these studies provide little mechanistic understanding of how these differences arise.

Primary transcripts containing the at-risk A allele at rs9939609 are more abundant than those with the T allele in blood and fibroblast cells from individuals within the normal weight range [57]. So it is possible that genetic variation leads to a shift in the allelic expression of *FTO.* Further support for this idea comes from the observation that obesity-associated loci near *FTO* may display haplotype-specific methylation patterns, which indicates that haplotypes may be differentially expressed [238]. However, these studies are indirect; they do not show that FTO protein is involved in energy homeostasis.

1.4.3 Exonic SNPs in *FTO*

Studies of human beings with exonic mutations in *FTO* (i.e. where the protein itself is affected) do not clarify matters. In a recent study, the *FTO* gene was sequenced in ~3000 individuals in order to determine the frequency of exonic mutations in the gene. Half of the participants were obese, and the other half had normal body weight. Fewer than 1% of individuals carried mutations (regardless of their body weight), and all were heterozygotes [239]. Mutations were found throughout the protein. Fourteen of these were tested in biochemical assays, and five mutations removed the catalytic activity of FTO, including two that altered absolutely conserved residues in the catalytic core - R316Q and R322Q. Most of the mutations, however, including several others that were in the catalytic core, had no effect on the activity of FTO. There was no clear relationship between BMI and FTO function; heterozygous loss-of-function mutations in FTO were found in both lean and obese individuals, and the prevalence of mutations was roughly equal in both groups. The results of this study suggest that heterozygous exonic mutations in FTO, which interfere with the

catalytic activity of the protein, do not affect body weight, so it is possible that the single unaffected copy of FTO prevents any deleterious effects [239].

Consistent with this position, human beings who are homozygous for the FTO-R316Q mutation die before 3 years of age, and have retarded growth with multiple malformations and functional impairments of the brain and peripheral tissues [240]. By contrast, heterozygous family members have no obvious phenotype. There are no reports of the BMI and adiposity of individuals homozygous for FTO-R316Q, but their growth retardation and general illness means that such measures are of little validity.

In summary, studies of human beings with exonic mutations in *FTO* suggest that the protein is crucial to multiple bodily processes, but its involvement in energy homeostasis remains unresolved. When only one copy is affected there is no clear effect on body weight. In the only individuals who have been identified with two mutant copies of FTO, the effects are very severe, which makes it difficult to identify a specific role in energy homeostasis.

1.4.4 Transgenic mouse models of FTO function

In contrast to the studies on human beings, mouse models of *FTO* function have provided strong and relatively consistent evidence that it is involved in energy homeostasis. The first mouse lacking *FTO* was not specifically engineered; it had a 1.6Mb deletion on chromosome 8 that eliminated 6 genes, including *FTO* [241-243]. Mice homozygous for this deletion died prenatally, but heterozygous mice were born and displayed multiple defects in brain patterning, and head and body morphogenesis. Indeed, the mouse was called “fused toes” due to its polydactyly. Body weight differences were not reported for these mice, although such a measure would be of questionable validity given the general deleterious effect of the mutation.

Subsequent mouse models were selective for *FTO*. Deletion of *FTO* had a generally deleterious effect; homozygous knockout mice had increased postnatal mortality, postnatal growth retardation, and decreased lean mass and adipose tissue [223]. Paradoxically, despite their reduced body mass, these mice were relatively hyperphagic and displayed reduced spontaneous locomotor activity, although their metabolic rate was higher than controls. These mice were also less likely to become obese when they were fed a high-fat diet. Heterozygous mice were phenotypically normal in most tests. This profile, especially the requirement for homozygosity and the growth and morphological phenotype, is reminiscent of the human beings with homozygous FTO-R316Q mutations, and of the fused toes mouse.

Interestingly, in a subsequent study, mice were constructed in which both copies of *FTO* were knocked out specifically in neurons and these animals showed a similar profile of growth and metabolic alterations as complete *FTO* knockout mice [244].

The three previous studies looked at the phenotype of mice lacking *FTO*. In another study, a mouse was found in an N-ethyl-N-nitrosourea (ENU) archive with a point mutation in exon 6 of *FTO* (FTO-I367F). This mutation reduced the catalytic activity of the protein and the mouse had lower levels of FTO protein in all tissues compared to controls - i.e. FTO function was reduced, rather than completely lost. The mouse had a lean phenotype with a specific reduction in fat mass, and increased metabolism [225]. There were no obvious deleterious effects in growth or body morphology. Interestingly, contrary to the examples discussed so far, the mutation had a dominant effect. As these mice were expected to express half wild-type and half mutant FTO subunits it was suggested that FTO-I367F was an antimorphic allele - the wild-type FTO subunits could be disrupted by formation of heterodimeric complexes. Thus, in summary, specific loss or reduction in FTO function is associated with a lean phenotype in three mouse models, which supports the notion that FTO is involved in energy homeostasis.

The food intake and metabolic profiles of the complete knockout mice and the ENU mutant mice were different. The phenotype of the knockout mouse was particularly complex, but as the mice failed to thrive, the differences in their activity and feeding behaviour may reflect compensation for their general malaise. By contrast, the mice with reduced FTO function did not experience increased postnatal morbidity, indicating that they were generally 'healthier' than the knockout mice. In terms of feeding and metabolic phenotypes, the only feature shared by both models was their increased metabolic rate, which suggests that this is an important factor in the leanness of these mice.

Recently, a mouse was constructed that expressed either one or two extra copies of *FTO*. Mice over-expressing *FTO* showed a dose-dependent increase in body weight, largely due to increased fat mass, and had no obvious growth defects or difference in viability [245]. Food intake was higher whether they were fed standard chow or a high fat diet. Although the effect on body weight and food intake was clear, the effects on other parameters were inconsistent. For example, spontaneous activity levels were higher in mice possessing two extra copies of *FTO* who were fed on standard chow, but the same effect was not seen when the mice were fed on a high fat diet. Furthermore, at 8 weeks of age, serum leptin levels were lower in mice over-expressing *FTO* compared to controls, despite their increased fat tissue (leptin mRNA levels were higher in the adipose tissue, as expected), but this effect was not seen at 20 weeks of age [245].

In summary, it would seem that loss of FTO function results in lower body fat and potential growth abnormality. Extra amounts of FTO result in increased body fat and no defects in growth. Therefore these studies provide strong evidence that FTO is involved in energy homeostasis, but it is likely to participate in other cellular processes as well.

Although the mechanisms that lead to the differences in body weight remain unclear, and the effects of manipulation of FTO levels in adulthood remain to be explored, it is possible that inhibition of FTO could reduce body weight. Therefore, pharmacological antagonists of FTO may be useful in the treatment of obesity.

1.4.5 Physiological functions of FTO

The studies of human beings and mice described above indicate that FTO is involved in a variety of different physiological processes. Although FTO is ubiquitously expressed, it remains to be seen if its function is universal or specific to particular tissues. Furthermore, many different factors may regulate *FTO* expression: in human beings, *FTO* mRNA levels are higher in skeletal muscles of males than females; and age may also be an important factor as *FTO* mRNA levels in skeletal muscle and adipose tissue are lower in older people [246].

Early physiological studies looked at the regulation of *FTO* expression based on nutritional status. The aim was to see if *FTO* expression levels were correlated with the increased hunger that is associated with fasting. Results were controversial. In mice, one study showed ~40 hour food deprivation correlated with decreased *FTO* mRNA in the arcuate nucleus of the hypothalamus of 7-week-old animals [218]. But in another report, there was no significant difference in *FTO* transcript levels in the hypothalamus of 4-week-old animals - there was only a trend towards lower levels after fasting [247]. In rats, one study showed ~40 hour food deprivation correlated with increased *FTO* mRNA levels in the hypothalamus of ~8-week-old animals [228] but long-term energy restriction was associated with decreased transcript levels in the hypothalamus of 8-week-old animals [248]. In the only study to look at the protein level, FTO was lower in 8-week-old rats subjected to long-term energy restriction [248]. Thus, the link between *FTO* expression levels and nutritional status is highly controversial.

Several studies suggest that increased levels of *FTO* are associated with increased body size or tissue mass, regardless of the intronic variant that the individual possesses. For example, higher levels of *FTO* mRNA in the placenta are correlated with greater neonatal mass and length [249], and levels of the transcript in adipose tissue are positively correlated with BMI [246, 250] (but see [251] for an exception).

The association between the obesity-associated SNPs and food intake has been examined in several different studies, but there are very few studies that have focussed on the influence of the SNPs on other physiological processes. Obesity-risk SNPs have been associated with decreased brain volume [252]. And adipocytes from people with the at-risk A-allele of the rs9939609 variant showed less spontaneous lipolysis than those from individuals with the T-allele [250]. Clearly, further studies need to be carried out to clarify the physiological impact of the obesity-associated SNPs near *FTO*.

In summary, little is known about the physiological function(s) of the FTO protein. Progress may be slow because FTO is ubiquitously expressed, and its function may depend on a variety of different factors. The transgenic mice described above [223, 245], which were developed with the Cre/lox system, may be useful in narrowing down the tissues that are most important. There are also question marks over the biochemical function of FTO. Although it is found in the nucleus, the rate at which it demethylates DNA is slow [220]. Thus, this may not be the primary function of the protein. Furthermore, it may have different functions in different tissues. Clearly, there are many fundamental questions that remain to be resolved.

1.5 Physiological Studies of Genes that Predispose to Type 2 Diabetes Mellitus and Obesity

The focus of this thesis will be the role of K_{ATP} channels, and the FTO protein, in the brain. As described above, it is known that K_{ATP} channels have an important physiological role in the brain, and it is known that gain-of-function mutations in the channel cause the neurological symptoms of iDEND. But the relative importance of different brain regions and circuits in the pathophysiology of iDEND is unknown. It is also known that the expression of *FTO* in the brain is critical for normal growth and body weight [244], but the bodily processes that affect *FTO* expression are unclear. In particular, the regulation of *FTO* expression by nutritional deprivation remains controversial.

In this thesis I will present data suggesting that cerebellar output is likely to be impaired in iDEND. Consistent with this conclusion, I show that iDEND patients (but not PNDM patients) perform worse than controls in hand-eye coordination tasks. Furthermore, I show that expression of V59M K_{ATP} channels in parvalbumin-expressing neurons alone recapitulates some of the motor symptoms of iDEND, suggesting that parvalbumin neuronal dysfunction may be important in the disease. I will also present data suggesting that FTO is expressed in neurons, but that its expression levels are not changed following nutritional deprivation.

Chapter 2: Methods

2.1 Mice

All experiments were conducted in accordance with the UK Animals (Scientific Procedures) Act (1986) and University of Oxford ethical guidelines.

2.1.1 Animal care

Mice were housed in same-sex littermate groups of 2-8 where possible. Occasionally mice were housed singly (for example if they were the only male or female in that litter). Animals were maintained in a temperature and humidity controlled room on a 12hr light-dark cycle (lights on at 7am). Regular chow food (Special Diets Services RM3) was freely available. Mice had *ad libitum* access to water at all times.

2.1.2 Generation of mutant mice

The construction of ROSA mice has been described previously [168]. Briefly, a point mutation was introduced in a construct containing the murine Kir6.2 coding sequence, such that a methionine residue would be included in position 59 instead of valine (Kir6.2-V59M). The Kir6.2-V59M sequence was preceded by a loxP-flanked stop codon and followed by a flippase recognition target (FRT)-flanked green fluorescent protein sequence whose translation was enabled by an internal ribosomal entry signal (IRES GFP). This construct was targeted to the ROSA26 locus to ensure that a single copy of the mutant gene was expressed, from a known location. The endogenous, ubiquitously expressed [169], ROSA promotor was used to prevent excess gene expression. The 'floxed' stop codon ensured that

the Kir6.2-V59M was not expressed unless Cre recombinase was also present. Therefore, by mating ROSA mice with other transgenic lines that express Cre driven by a tissue-specific promotor, double transgenic mice were produced that expressed Kir6.2-V59M in specific tissues.

To target the Kir6.2-V59M transgene specifically to neurons, ROSA mice were crossed with mice expressing Cre recombinase under the control of the nestin promotor (Nestin-Cre mice (Jackson Laboratory, stock name Tg(Nes-cre)1Kln/J #003771; [175]), resulting in the production of n-V59M mice. Due to the time course of Cre expression produced by the nestin-Cre mouse, the n-V59M mice were expected to express Kir6.2-V59M mRNA in neurons by embryonic day 11 [253, 254]. The litters from breeding pairs of nestin-Cre and ROSA mice were composed of wild-type, nestin-Cre, ROSA and n-V59M mice - i.e. there were three types of control mice.

Mice expressing the Kir6.2-V59M gene selectively in parvalbumin-expressing cells (p-V59M mice) were generated in a similar fashion; ROSA mice were crossed with Parvalbumin-Cre mice (Jackson Laboratory, stock name *Pvalb*$^{tm1(cre)Arbr}$/J #008069). Parvalbumin-Cre mice were supplied by Dennis Kaetzel and had been backcrossed to a C57BL/6J background until congenic. They were then intercrossed till homozygous for Cre; therefore these mice always passed on the parvalbumin-Cre transgene. Thus, the litters from breeding pairs of parvalbumin-Cre and ROSA mice were composed of p-V59M mice and parvalbumin-Cre mice - i.e. there was only one type of control mouse.

The construction of POMC-Z/EG (Proopiomelanocortin-Cre-LacZ-EGFP) mice has been described previously [255, 256]. POMC-Cre mice express Cre in loci where *POMC* is endogenously expressed. The Z/EG mouse is a double reporter strain that expresses β-galactosidase (*LacZ*) throughout embryonic development and adult stages. However, in the presence of Cre expression, the *lacZ* gene is removed, which activates the expression of

the second reporter - enhanced GFP. Mating POMC-Cre and Z/EG mice resulted in double transgenic progeny that expressed eGFP in *POMC*-expressing neurons (POMC-Z/EG mice). POMC-Z/EG mice were provided by Prof. Jens Bruning, Institute of Genetics, Cologne and were congenic on a C57BL/6 background. Z/EG mice were also crossed with nestin-Cre and parvalbumin-Cre mice producing Nes-Z/EG and Pv-Z/EG mice respectively. These mice were expected to express eGFP in all neurons or in neurons that express parvalbumin.

ROSA mice were backcrossed for at least 3 generations to a C57BL/6J background prior to breeding - they were originally on a mixed background with C57BL/6J and 129/sv heritage [168]. Nestin-Cre and parvalbumin-Cre mice were congenic on a C57BL/6J background. The original breeding pairs of n-V59M mice were produced by crossing ROSA mice, that had been backcrossed to C57BL/6J for 3 generations, with nestin-Cre mice. The colony was maintained by intercrossing the progeny of this original breeding pair. Therefore all n-V59M mice used in experiments presented in this thesis were likely to have a mixed C57BL/6J and 129/sv background. p-V59M mice were produced by crossing ROSA mice, that had been backcrossed for at least 4 generations to a C57BL/6J background, with parvalbumin-Cre mice. New breeding pairs were formed by mating parvalbumin-Cre mice from the stock that was congenic on C57BL/6J, with ROSA mice that had been further backcrossed onto C57BL/6J background. Therefore p-V59M mice were likely to have a greater C57BL/6J character than n-V59M mice.

2.1.3 Genotyping of mutant mice

Genotypes of mice were identified by PCR using DNA isolated from ear biopsies. Tissue samples (~5mm^2) were lysed, and DNA extracted, using the Promega Tissue DNA kit and Promega Maxwell machine. Transgenic sequences were amplified by PCR using specific primers (Table 2.1). Each reaction consisted of 15µl PCR Master Mix (Fermentas DreamTaq

Green PCR Master Mix), 0.5µl of 10µM primers (Sigma), and nuclease-free water (Sigma) to a final volume of 30µl. A positive control DNA sample, and a negative control sample (nuclease-free water) were included in each PCR run. All samples were run for 30-35min at 100V on a 2% agarose gel and visualised with ethidium bromide. A 100bp DNA ladder (Invitrogen) was run in at least one lane on each row of the gel.

Table 2.1 Genotyping PCR primer information

Primer	Sequence (5' to 3')	Amplicon size (bp)
Cre	fwd: ACGAGTGATGAGGTTCGCA rev: ATGTTTAGCTGGCCCAAATGT	~230
ROSA-Kir6.2-V59M	P1: AAAGTCGCTCTGAGTTGTTATC P2: GATATGAAGTACTGGGCTCTT P3: GCATCGCCTTCTATCGCCT	590 (ROSA-wt) 460 (ROSA-Kir6.2-V59M)
POMC-Cre	P1: TGGCTCAATGTCCTTCCTGG P2: CACATAAGCTGCATCGTTAAG P3: GAGATATCTTTAACCCTGATC	~1200 (POMC) (positive control) ~700 (Cre)
GFP	fwd: CTGGTCGAGCTGGACGGCGAC rev: CACGAACTCCAGCAGGACCAT	~600

2.1.4 Behavioural testing of mice

Muscle strength (3 tests) and motor coordination (2 tests) were assessed at 11-12 weeks of age. Testing was carried out over a maximum of 48 hours. Spontaneous locomotor activity (2 tests) was measured at 16-18 weeks of age. All behavioural experiments were performed blinded with respect to the genotype of the animal.

Muscle strength was assessed with the weight-lifting [257], inverted screen [258] and horizontal bar [259] tests [260]. For weight-lifting, mice were allowed to grasp a series of increasingly heavy weights that consisted of 1-7 links cut from a chain. Each weight was attached to a ball of tangled fine gauge stainless steel wire. The lightest weight was approximately 20g, with each subsequent one being 13g heavier. The mouse was picked up by its tail and suspended vertically downwards, above the weight. It was allowed to grasp the ball of tangled wire attached to the weight, and was then lifted vertically, while still gripping, such that the weight was suspended ~3cm above the bench surface. The mouse held each weight for up to 3s. When a weight was dropped before 3s had elapsed, the time was noted and the mouse was not tested with the heavier ones. The score was the total number of seconds the mouse completed during the test (i.e. a score of 14 was awarded to a mouse that held the first four weights for a full 3s and held the fifth weight for 2s).

For the inverted screen test, mice were placed in the centre of a 43x43cm^2 grid composed of 12mm squares of 1mm diameter wire, framed by a 4cm deep wooden beading. The frame was then inverted smoothly and held 30cm above a soft surface. The total time the mouse remained on the grid was noted, and was converted into a score, according to convention: 1 (110s or less before falling), 2 (110-250s), 3 (251-599s) or 4 (600s). As the scoring thresholds were not evenly spaced it was possible that the scoring system could mask differences within a scoring band. So the raw timings of the mice (how long they managed to hold onto the screen, in seconds) were also analysed.

The horizontal bar test comprised a 38cm-long, 2mm-thick brass bar, which was held 49cm above a padded bench surface by supporting columns at each end. The mouse was placed on the centre of the bar, hanging from its forepaws. It was left holding the bar for a maximum of 30s. The performance of the mice (how long they clung to the bar) was converted to a score: 1 (5s or less on the bar), 2 (6-10s), 3 (11-20s), 4 (21-29s), 5 (30s). Most mice

traversed the bar, rather than simply hanging on in the centre; if the mouse reached an end column it was removed from the apparatus and received a maximum score of 5.

Motor coordination was assessed with the static rods test [261] and an accelerating rotarod [262, 263]. For the static rods test, a cylindrical wooden rod, 600mm long and 35mm in diameter was fixed at one end above a drop of ~65cm. Padding was provided to cushion any falls. Each mouse was placed 20mm away from the protruding end of the rod, facing away from the bench. The time to turn around 180° (while remaining upright), and to translocate to the end of the rod was noted. If the mouse fell before it reached the end of the rod this was noted, as was the time at which it fell. The mice were tested on two further rods of 22mm and 9mm diameters. In the accelerating rotarod task, mice attempted to remain on top of a rod that rotated about its long axis. The rotarod (Ugo Basile, Italy, model 7650) was adjusted to have a start speed of 2.5 r.p.m. and an acceleration rate of 20 r.p.m./min. The rod was started and the mice were placed onto it, facing the direction of rotation, and allowed to run for 10s at 2.5 r.p.m. before the rod was accelerated. The time elapsed before the mouse fell was noted, up to a maximum of 120s.

Spontaneous locomotor activity was measured using activity monitoring enclosures and free-running wheels. The Threshold Activity System (Med Associates, St Albans VT) measured spontaneous activity over a 23hr period in an environment that was similar to the normal home cage of the mice [102]. Free-running wheel cages were also similar to the normal home cage environment of the mice, but they contained a running wheel (50cm circumference) equipped with a computer (Cateye Velo 8) that measured the duration of wheel use, distance covered and speed of the mice (average and maximum). The activity of mice was measured over a 23hr period [102].

2.1.5 Drinking behaviour

Mice were singly housed and the weight of their water bottle was measured at approximately 11am and then 10am the following day to give a measure of 23-hour water intake.

2.1.6 Brain slice electrophysiology

Mice were killed by cervical dislocation and the vermis of the cerebellum was rapidly dissected and immersed in ice-cold artificial cerebrospinal fluid (aCSF) containing (in mM): 125 NaCl, 21 $NaHCO_3$, 2.5 KCl, 1.2 NaH_2PO_4, 10 HEPES, 2 $CaCl_2$, 2 $MgCl_2$, 5 glucose, adjusted to pH 7.4 with NaOH. The vermis was transferred to the cutting chamber of a Leica VT1000S or Leica VT1200S vibratome and immersed in gassed ice-cold aCSF. 200µm thick parasagittal brain slices were cut and allowed to recover for at least 45min at 20-23°C in gassed aCSF.

Slices were then transferred to a recording chamber and continuously perfused at 2-4 ml/min with gassed aCSF. All experiments were carried out at 20-23°C. Pharmacological agents were bath-applied to slices and were therefore dissolved in aCSF. All pharmacological agents were stored as a 1000x stock, dissolved in dimethylsulphoxide. The concentrations of drugs differed depending on the experiment being performed, so these details are presented in the methods section of each chapter.

Neurons were visualised by infrared interference contrast video microscopy on an upright microscope (Zeiss Axioskop) fitted with a Hitachi KP-M1AP analogue monochrome charge-coupled device (CCD) camera, or a Hamamatsu system comprising a C7500-11 analogue monochrome CCD camera coupled to a C2741-62 camera controller. The output was displayed on a Panasonic monochrome analogue monitor. For whole-cell recordings, patch pipettes were filled with internal solution containing (in mM) 128 K-gluconate, 10 KCl,

10 HEPES, 1 EGTA, 2 $MgCl_2$, 0.3 Na-GTP and 3 K_2-ATP, pH 7.3 adjusted with KOH. For cell-attached recordings, pipettes were filled with aCSF solution. Pipettes were made from borosilicate glass (Clark GC150F) and pulled and polished using a DMZ universal puller. Pipettes had a tip resistance of 4-6MΩ. Recordings were acquired using an EPC-9 patch-clamp amplifier (HEKA). Data were filtered and sampled with Pulse software (Heka Electronik) and analysed with Pulsfit 8.67 (Heka Electronik).

2.1.7 Fixation and immunohistochemistry of mouse brain

Mice were terminally anaesthetised by intraperitoneal injection of 0.01mg pentobarbital sodium (Euthatal, Merial) and perfused intracardially with phosphate-buffered saline (PBS) followed by 4% paraformaldehyde (Taab) in 0.1M phosphate buffer pH7.4 (PB). The whole brain was removed from the skull and postfixed in 4% paraformaldehyde PB at 4°C for at least 24 hours. Brains were cryoprotected prior to sectioning on a freezing microtome (Leica SM2000R) by immersion in 30% sucrose in PB at 4°C for approximately 18hr. 40-50µm sections were cut and rinsed three times for 20min in 0.3% Triton X100 (Sigma) PBS (PBS-Triton) at room temperature.

For fluorescence immunohistochemistry, sections were blocked for 1-1.5hr at room temperature in PBS-Triton containing 5% bovine serum albumin (BSA, Sigma) and 5% goat serum (Sigma). Sections were then incubated with the appropriate concentration of primary antibody in PBS-Triton with 5% BSA, 5% goat serum for approximately 1hr at room temperature then transferred to 4°C for 18-36hrs. Details of the primary antibodies and working dilutions are given in Table 2.2. Sections were incubated with each subsequent antibody for 1hr, at room temperature. Sections were washed three times for 10min between each antibody incubation step. PBS was used for the first two washes and PBS-Triton for the final one. After completion of primary antibody incubation, sections were incubated with

biotinylated secondary antibodies (anti-rabbit IgG, Vector Labs BA-1000 or anti-mouse IgG, Vector Labs BA-9200, 1:200 dilution), followed by Texas-Red Avidin D (Vector Labs, A-2006, 1:100 dilution), then Biotinylated Anti-Avidin D (Vector Labs, BA-0300, 1:100 dilution) and finally Texas-Red Avidin D again. After completion of all antibody incubation steps, sections were washed once in PBS, followed by incubation for 20min in PBS with 2ug/ml DAPI (Sigma, D9542-5MG). After a further three 10min washes in PBS, sections were mounted on double-subbed slides, and coverslipped using Vectashield hardset mounting medium (Vector Labs, H-1400 or H-1500).

For horseradish peroxidase (HRP) immunohistochemistry, sections were processed according to the ABC method (Vector Labs). Sections were treated with 10ml methanol containing 100µl hydrogen peroxide (30% W/V; Sigma), followed by three 5min washes in PBS. Sections were then blocked for 1hr at room temperature in PBS-Triton with 3% goat serum followed by incubation with an appropriate concentration of primary antibody in PBS-Triton with 1% goat serum for 24-60hrs at 4°C. Following three 10min washes in PBS-Triton, sections were incubated with the manufacturer's recommended concentration of biotinylated secondary antibody for 1.5hr at room temperature in PBS-Triton with 3% goat serum. After two 10min washes in PBS, sections were then treated with the Vectastain Elite ABC kit (Vector Labs, PK6100) for 1-2hrs at room temperature. After completion of these antibody incubation steps, sections were washed a further three times for 10min in PBS and colour developed using a diaminobenzidine (DAB) kit with metal enhancer (Sigmafast D0426, Sigma). Following three final washes to remove traces of DAB, sections were mounted on double-subbed slides and left to air-dry overnight. Finally, sections were dehydrated and cleared by 5min incubations in rising concentrations of ethanol (30%, 50%, 70%, 100%) and two incubations in 100% xylene, before coverslipping in DePeX mounting medium (VWR International).

Table 2.2 Primary antibodies used in immunohistochemistry experiments

Target	Manufacturer and code	Dilution ratio
FTO	Courtesy of Chris Church	1:200
GFP	Invitrogen, A11122	1:250
NeuN	Millipore, MAB377X	1:200

2.1.8 Total protein extraction from mouse tissue

Mice were killed by cervical dislocation in the middle of the light cycle and tissues were rapidly dissected and snap-frozen in liquid nitrogen. Frozen tissues were ground into powder in a pestle and mortar and ice-cold RIPA lysis buffer was added. RIPA lysis buffer contained 150mM NaCl, 1% Nonidet P40, 0.5% Sodium Deoxycholate, 0.1% Sodium Dodecyl Sulphate (SDS), 50mM Tris pH 8.0 and complete protease inhibitors (according to the manufacturer's instructions; G-Biosciences Protecease-50 EDTA free). pH was adjusted to 7.4 with HCl. The volume of RIPA buffer varied by tissue: muscle 0.75-1.5ml, brain 1.5-5ml. Tissue lysates were transferred from the pestle and mortar to 1.5ml tubes and 10 units of Benzonase (Novagen) were added. Tubes were incubated on ice for 30min and agitated at regular intervals. Non-soluble material was pelleted at 20,000g in an Eppendorf 5417R centrifuge at 4°C for 20min. The supernatant was carefully removed and transferred to a fresh 1.5ml tube and immediately stored at -80°C before further processing.

Protein concentrations were quantified using the Bio-Rad DC Protein Assay - a colorimetric assay. Briefly, 5µl aliquots of each sample were loaded into a 96-well flat bottomed plate. 25µl alkaline copper tartrate solution containing SDS was added, followed by 200µl Folin Reagent. Colour was left to develop for ~15min. The absorbance of each sample at 750nm was then read using a microplate reader (Dynex Spectra MR). Protein concentrations were

determined by comparison with a standard curve: the absorbance values of samples of BSA in RIPA buffer at 0, 1.25, 2.50, 3.75. 5.00, 12.50 and 18.75 and 25.00mg/ml were measured and plotted against concentration using Microsoft Excel and fitted with a logarithmic curve. The absorbance at 0mg/ml was taken as ' background absorbance' and this value was subtracted from all samples. The gradient of the straight line was used to calculate the concentrations of the experimental samples using the following formula:

$$\text{Concentration} = e^{(\text{absorbance/gradient})}$$

If the sample was <3.5mg/ml it was concentrated using Millipore Centrifugal Filter Units (Ultracel - 3k), according to the manufacturer's instructions.

2.1.9 Western blots for immunological detection of proteins

35-50µg of total protein was loaded into 4-12% Bis-Tris SDS-PAGE gels (NuPAGE Novex, Invitrogen) and separated using MES running buffer (Invitrogen) in an X-Cell electrophoresis module at 180V for approximately 45min. Novex Sharp Pre-stained protein standards (Invitrogen) were run in each gel along with samples. Separated proteins were transferred for approximately 1.5hr at 30V to polyvinylidene difluoride (PVDF) membrane (Millipore) using 20% methanol NuPAGE transfer buffer (Invitrogen).

Membranes were blocked for approximately 18hr at 4°C with 5% skimmed milk in 0.1% Tween20 tris-buffered saline (TBST) (Sigma) and subsequently probed for 1hr at room temperature with antibodies specific for target and loading control proteins. Antibodies used in Western blot experiments are detailed in Table 2.3. After incubation with primary antibody, blots were rinsed three times for 5min in TBST then probed with an appropriate secondary antibody conjugated to horseradish peroxidase (HRP-anti-rabbit IgG, GE Healthcare, NA934; HRP-anti-mouse IgG, GE Healthcare, NA931). Blots were then rinsed five times for 5min in TBST and bands visualised with enhanced chemiluminescence reagent (SuperSignal West

Pico, Pierce). Bands were exposed to X-ray film and bands were developed using film developer and fixer solutions (Xograph).

Films from developed blots were acquired using an Epson Perfection 2450 flatbed scanner. The resulting images were analysed using the gel analysis function of ImageJ software (National Institutes of Health, USA, [264]). For each blot, the density of the target protein bands was quantified and expressed as a relative value (0-1). The same was done for loading control protein bands. The relative quantity of the target protein was normalised by dividing by the relative quantity of the loading control protein.

Table 2.3 Primary antibodies used for Western blots of mouse tissue protein

Protein target	Manufacturer and code	Dilution ratio
c-Fos	Abcam, ab7963	1:100
FTO	Courtesy of Chris Church	1:200
HSC-70	Abcam, ab19136	1:1000

2.1.10 RNA extraction and cDNA synthesis

Mice were killed by cervical dislocation in the middle of the light cycle and tissues were rapidly dissected, sectioned into small pieces, immersed in RNAlater solution (Qiagen), and stored at 4°C for 2-3 hours to allow complete permeation. Tissues were then stored at -80°C (still in RNAlater) until ready to process.

Total RNA was extracted, following the manufacturer's instructions, from 30mg of thawed tissue using the RNeasy Mini Kit (Qiagen). Tissue samples were lysed and homogenised in RLT buffer and β-mercaptoethanol using a rotor-stator homogeniser (Pro Scientific). Muscle

samples were treated with proteinase K (Qiagen) immediately after homogenisation to aid RNA extraction. All samples were treated with an on-column DNase digestion step to remove traces of genomic DNA. The concentration of purified total RNA was measured in triplicate (and the mean calculated) on a Nanodrop Spectrophotometer (Thermo Scientific) and its quality checked with an Agilent Bioanalyzer. Only samples with an RNA Integrity Number ≥6.5 were processed further. The majority of samples had an RNA Integrity Number >8.

1µg of total RNA was reverse transcribed in a 20µl final volume using the High Capacity complementary DNA (cDNA) Reverse Transcription kit with RNase inhibitor (Applied Biosystems). A separate microgram of total RNA was processed identically, but with no reverse transcriptase present (Non-RT control). The reaction cycle consisted of 10min at 25°C followed by 30min at 48°C. The resultant cDNA samples were subsequently diluted to the working concentration of 4ng/µl using nuclease-free water (Sigma) and stored at -80°C.

2.1.11 Reverse transcription quantitative PCR experiments

Reverse transcription quantitative PCR (RT-qPCR) was performed using an ABI Prism 7000 Sequence Detection System (Applied Biosystems) using SYBR green reagents (Power SYBR green, Applied Biosystems). All reactions were performed in triplicate in a final volume of 25µl containing: 12.5µl Power SYBR Green Master Mix, 300nM primers (forward and reverse), 20ng (5µl) of cDNA template and nuclease-free water up to final volume. The reaction cycle comprised an initial denaturation for 10 min at 95°C, followed by 40 cycles of 95°C/15sec; 60°C/60sec.

Primers were designed using Geneious Pro software (Biomatters Inc) using NCBI sequence information (Table 2.4). Primer specificity was checked *in silico* using BLAST and *in vitro* using gel electrophoresis and melt curve analysis. Primer efficiencies were calculated by

running serial dilutions of tissue cDNA: 100ng, 50ng, 25ng, 12.5ng, 12.25ng and 6.125ng (equivalent to dilution factors 1, 0.5, 0.25, 0.125, 0.0625. 0.03125). Threshold cycle values (Ct values) were measured using the ABI SDS 3000 software (Applied Biosystems). Baseline signal levels were calculated between cycles 3-14 and the threshold level was set to 0.3. Data were exported for analysis in Microsoft Excel. Each sample was run in triplicate, enabling calculation of an average Ct value. These values were plotted against log(dilution) and the efficiency of the reaction was calculated using the following equation: $10^{(-1/slope)}$ [265]. A value of 2 indicated that the reaction was optimal. Deviation from 2 indicated that there were factors that were interfering with reaction, such as off-target PCR products, or primer dimers. All primers used in experiments in this thesis had efficiency of 1.9-2.1, which indicated that there were no major complications (Table 2.4). Efficiency values were used in calculations of relative quantities of experimental samples.

Tissue samples used in experiments were also run in triplicate and average Ct values calculated. The Pfaffl method was used to transform Ct values into relative quantities. Relative quantities were calculated per primer pair - i.e. if experimental samples X, Y, Z were run with primers A, B, C, the relative quantities were calculated for A(X, Y, Z), B(X, Y, Z), C(X, Y, Z). The following equation was used:

$$\text{Relative quantity} = \text{efficiency}^{(\text{ct value most abundant - ct value sample})}$$

Thus relative quantities of all samples for a given primer pair ranged from 0-1. The relative quantities of the reference genes were imported into the genorm applet for Microsoft Excel, which was used to calculate the number of reference genes necessary for adequate normalisation, and the normalisation factor (the geometric mean) [266]. The normalisation factor was then applied to the gene(s) of interest. Genorm analysis was carried out on complete sets of tissue samples. From these analyses the mean quantity was calculated for each tissue and this was used for statistical analysis.

Table 2.4 RT-qPCR primer information

Short name	Accession number	Sequence (5' to 3')	Amplicon (bp)	Efficiency
ACTB	NM_007393	fwd: GCAGCTCCTTCGTTGCCGGT rev: TACAGCCCGGGGAGCATCGT	132	2.1
FTO	NM_011936	fwd: GGACATCGAGACACCAGGAT rev: AGGTGCCTGTTGAGCACTCT	158	2.0
HMBS	NM_001110251	fwd: GTGGCTGGCCTACAGCGCAT rev: TGGCTCGGACTTCCACGGCT	112	2.0
HPRT1	NM_013556	fwd: CCGGCAGCGTTTCTGAGCCA rev: GCTCGCGGCAAAAAGCGGTC	123	2.1
HSPA8	NM_031165	fwd: CAGCGCAGCTGGGCCTACAC rev: TAGCTTGGCGTGGTGCGGTT	152	1.9
KCNJ11	NM_010602	fwd: CGGGCGCATGGTGACAGAGG rev: CGATGGGCCTGGGCCGTTTT	126	2.0
RPL13A	NM_009438	fwd: CCTCCCGAGGCCCCTACCAC rev: CTTGAGGCGCTCCAGGGCAG	113	2.2
SUR1	NM_011510	fwd: ACAGCCTTCGCAGACCGCAC rev: GCCCGAGCCAGGCAGAACAG	106	1.9
SUR2	NM_005691	fwd: GCAATCAAAACCAATAAACAGG rev: CCCCATGAGAAGTATCCATT	132	1.9
UBC	NM_019639	fwd: GCAGCTGGAAGATGGCCGCA rev: GGGCTCGACGTCCAGGGTGA	142	2.1

2.1.12 Semi-quantitative RT-PCR reaction conditions

Mouse Kir6.2 transcripts were amplified by PCR from 100ng cDNA prepared from total tissue RNA. Primers used were (5' to 3'): forward: ATGCTGTCCCGAAAGGGCATT, reverse: GGCGATGAGCCACCAGACCAT. Each PCR reaction consisted of 20µl Mastermix (Fermentas DreamTaq Green PCR Master Mix), 0.5µl of 10µM primers, 2µl of 50ng/µl cDNA, 7µl nuclease-free water - total reaction volume was 30µl. After 40 cycles (95°C/30s; 60°C/30s; 72°C/1min), PCR products were digested with BtsCI restriction enzyme (New England Biolabs) for ~2h at 50°C. Reactions consisted of 10µl PCR product, 2µl Buffer 4, 0.5µl BtsCI, 7.5µl nuclease-free water. Digested PCR fragments were visualised on a 2% agarose gel with Ethidium Bromide. The V59M mutation in Kir6.2 removes the restriction sequence that BtsCI recognises. So in mice expressing only wild-type Kir6.2 mRNA, there were two bands in the final gel. In mice expressing both wild-type and mutant Kir6.2 mRNA there were three bands in the final gel - the highest molecular weight band corresponded to Kir6.2-V59M.

2.2 Microscopy

2.2.1 Epifluorescence and bright field microscopy

Slides were viewed with a Leica DMRB microscope fitted with Zeiss objectives and images were captured using a Nikon DXM1200 or Leica DFC500 camera. Samples were excited using a Prior HBO100 or Leica SFL7000 UV light source. A FITC 411 filter was used to visualise GFP fluorescence, and DAPI fluorescence was visualised using an A filter (bandpass filter 340-380nm) and a suppression filter (long pass 425nm). The same Leica DMRB microscope and objectives were used to visualise HRP-stained sections with bright-field microscopy.

2.2.2 Confocal laser scanning microscopy

An LSM 510 Meta confocal microscope (Carl Zeiss) was used with a Plan-Apochromat 63x/ 1.4 oil objective (Carl Zeiss). GFP and Alexa 488 were excited using the 488nm line of an Argon laser and emitted light was collected between 512 and 565nm in the Meta channel of the confocal system. Texas-red was excited using the 543nm line of a HeNe laser and emitted light collected between 597 and 629nm in the Meta channel. DAPI was excited in the two-photon mode with the 740nm line of a Chameleon laser and emitted light detected between 447 and 480nm in the Meta channel.

2.3 Human Beings

Studies were conducted in accordance with the Declaration of Helsinki. Ethical approval was obtained from the Diabetes Alliance for Research in England (DARE) and the University of Chicago Pritzker School of Medicine, USA. Informed, written consent was received from participants (or their parents/guardians, in the case of minors) before carrying out any experiments. Patients with activating mutations in the *KCNJ11* gene were recruited along with non-affected members of their family to act as controls.

Experiments were carried out in London, UK and Chicago, USA. In London, participants were tested in a relatively quiet space. Family members and other attendees of the meetings were present during completion of the tasks. There were no visual distractions in front of the participants as they carried out the three tasks, though noises from the surrounding meeting could be heard. In Chicago, participants were tested in a designated quiet room with minimal audible or visual distraction. Family members were occasionally present during testing.

2.3.1 Coordinated hand-eye tracking of a target

Participants used a custom-built joystick to control a cursor presented on the 17” screen of a laptop (Figure 2 A) [267]. The joystick had a built-in arm rest and target tracking only required movement of the wrist. All participants used their right hand to control the joystick. The target and cursor moved in a straight line, horizontally across the middle of the screen. Participants were requested to track the target as it moved from left to right and back again. Movement of the target was programmed, and movement of the cursor recorded, by a custom-made application for Microsoft Windows (2dtrack, courtesy of Tim Pragnell). Data were acquired via a USB data acquisition device (National Instruments USB-6008) and sampled at 50Hz.
Data were analysed using custom-built routines in Matlab (Mathworks), designed by Dr John-Stuart Brittain. Details of the analysis methods are provided in Chapter 5.

Three tasks were undertaken, each composed of 12 tracks in total - 6 rightward and 6 leftward. Each track was ~6s long and the target paused for 1s at either end of the tracking run before the next track commenced. The tasks were undertaken in sequential order. In the first task (task 1), the target moved at a constant speed from left to right and right to left. This was the most basic paradigm and enabled participants to become accustomed to the task. In task 2 the target moved in a sinusoidal manner - accelerating and decelerating at a constant rate. As the target moved with variable speed, this variant of the task was potentially more sensitive to deficits in velocity calibration. In task 3 the target moved at constant speed but the visual presentation of the target was switched off (it was blanked) during the middle third of each track. Participants were asked to continue “as if the target was still there”. Therefore they needed to rely on extra-visual, ‘memory-guided’ (predictive) movement.

A 2-D tracker

B Bead board

C Annett peg board

Figure 2 Equipment used in tests of hand-eye coordination

(**A**) Participants moved a joystick, which had little resistance to movement, to track a target that moved horizontally across the screen of a laptop computer. Participants were able to rest their arm in a comfortable position while carrying out the task. (**B**) The bead board, with five wells of decreasing diameter. Participants were timed while they transferred twenty 4mm beads (not shown) into the largest well of the board, and then sequentially into the smaller wells. (**C**) The Annett peg board. Participants used one hand to move the ten wooden pegs, one at a time, from one side of the board to the other. The other hand was then tested. Participants completed one trial with each hand.

2.3.2 Bead board

An aluminium board (30cm x 21cm, 2cm thick) was made with five wells, each ~1cm deep. The wells were of decreasing diameter - 52mm, 44mm, 36mm, 28mm, 20mm, each approximately 1cm deep (Figure 2 B) [268]. The time taken to transfer 20 spherical wooden beads (4mm diameter) from a circular plate (18cm diameter) to the 52mm diameter well of the bead board was measured. Following a break of ~1min participants were timed when transferring the beads, one at a time, using their preferred hand, from the 52mm diameter well to the 44mm diameter well. They were instructed to proceed immediately to transfer the beads individually from the 44mm diameter well to the 36mm well, then to the 28mm well and finally to the 20mm well.

2.3.3 Annett peg moving task

This task involved the transfer of 10 cylindrical wooden pegs (5cm long, 8mm diameter) from one side of a wooden frame (24cm x 38cm) to the other (Figure 2 C) [269, 270]. The pegs were held in the frame by 10 holes (1.3cm diameter, 1.8cm deep) spread equidistant (2.5cm apart) along each of the long arms of the frame. Participants were timed while moving the pegs as fast as possible, one at a time without dropping any pegs, using one hand. Following a break of ~2min participants repeated the task using the other hand. One trial was completed per hand.

2.3.4 Eye movement videos

Participants were filmed while carrying out prosaccade and smooth pursuit eye movements. In both cases participants sat ~1.5m in front of the investigator. For prosaccades the index

fingers of the right and left hand of the investigator were held out, roughly in line, and separated by ~1.5m. The participant was asked to move their eyes to look at the tip of a finger when it was moved. Fixation was maintained on that finger until the tip of the other finger was moved, at which point the participant made a prosaccade to fixate on that finger. For smooth pursuit, the participant was asked to follow the tip of the index finger of the investigator which was moved at constant speed from side to side. The distance moved was similar to the distance between the fingers for prosaccade movements.

2.4 Statistical Analysis and Figures

Figures were made with Sigmaplot 11 (Sysstat Software) and Pages '09 (Apple). All statistical analyses were performed with SPSS 19 (IBM). The details of the particular tests used are provided in the methods section of each chapter. Data sets were tested to see if their distributions satisfied the assumptions required by specific statistical tests. These assumptions are described below. Where assumptions were violated, the details of the violation, and the way in which it was handled, was reported in the methods section for that particular data set.

2.4.1 General assumptions for parametric statistical tests (ANOVA and post-hoc t-tests)

The skewness and kurtosis of each set of data was assessed to ensure that they were normally distributed. Data were considered to be significantly skewed, and therefore unsuitable for parametric analysis, if skewness was greater than 3 times the standard error of skewness, or kurtosis was greater than 3 times the standard error of kurtosis. The homogeneity of variances of each data set was also assessed, using Levene's test. For

Analysis of Variance (ANOVA), if variances were unequal then the alpha level was adjusted such that $p < 0.01$ was considered significant [271]. For independent samples t-tests, if variances were unequal then significance was established by referring to the p statistic derived from Welch's t-test. (Welch's test derives a similar p statistic to the independent samples t-test, but does not assume that variances are equal.)

2.4.2 Specific assumptions for multivariate and repeated measures ANOVAs

Box's test for equality of covariance matrices was used to confirm that data sets could be analysed with the MANOVA test. Data were considered to have violated the assumption of equality of covariance matrices if the p value from Box's test was ≤ 0.01. If this assumption was violated the alpha level was adjusted such that $p < 0.01$ was considered significant [271].

Mauchly's test of sphericity was used to confirm that data sets with repeated measures dependent variables could be analysed with mixed between-within ANOVAs. Data were considered to have violated the assumption of sphericity if the p value from this test was ≤ 0.05. If this assumption was violated then the alpha level was adjusted such that $p < 0.01$ was considered significant [271].

2.4.3 Corrections for multiple comparisons.

Where multiple comparisons were made within the same data set, a Bonferroni adjustment was made to the alpha level to guard against committing type I errors. Results were considered significant if the p value of the test was less than 0.05 divided by the number of comparisons [271] - i.e. when 3 comparisons were made, $p < 0.017$ was considered

statistically significant. The number of comparisons varied depending on the data set, so details of the Bonferroni adjusted p values are presented in the methods section of each chapter.

2.4.4 Reporting statistical significance

In the results section of each chapter, p values are used to indicate the outcome of each statistical test. The full details of the test statistics (e.g. F, t and U values) are given in Appendix 12.

Chapter 3: The Electrophysiology of Cerebellar Purkinje Cells in iDEND

3.1 Summary

1) The n-V59M mouse expressed approximately equal amounts of wild-type Kir6.2 and Kir6.2-V59M mRNAs. Kir6.2-V59M was likely to be expressed in all neurons of the brain, but could only form functional K_{ATP} channels in neurons that endogenously expressed SUR.

2) Total Kir6.2 mRNA levels from n-V59M mouse brain were higher than those from controls, but SUR1 levels were unchanged, so K_{ATP} channel density was unlikely to be affected. Therefore the n-V59M mouse was a reasonable model of iDEND.

3) Cerebellar Purkinje cells from n-V59M mice were hyperpolarised and fired fewer spontaneous action potentials than control cells. The addition of tolbutamide restored the membrane potential and firing rate of n-V59M Purkinje cells to the level of controls.

4) Despite the pronounced effect on Purkinje cell electrophysiology, whole-brain c-Fos mRNA and protein levels were unaffected.

5) In summary, cerebellar Purkinje cells of the n-V59M mouse were inhibited. As they are the sole output from the cerebellar cortex, cerebellar dysfunction may contribute to the neurological symptoms of iDEND.

3.2 Introduction

3.2.1 Some neurological symptoms of iDEND are attributable to cerebellar dysfunction

As discussed in Chapter 1, the neurological and neuromuscular symptoms of iDEND are likely to be caused by expression of mutant (gain-of-function) K_{ATP} channels in neurons alone. As K_{ATP} channels are widely expressed throughout the brain, it is likely that dysfunction of many systems contributes to the neurological symptoms of iDEND, but dysfunction of certain brain areas may cause specific symptoms.

Cerebellar dysfunction caused by trauma [272] or genetic mutations, such as in Joubert syndrome [273], causes a variety of motor impairments such as hypotonia, muscle weakness, intention tremor and ataxia [274]. Furthermore, cerebellar lesions and abnormalities are associated with hyperactivity [275-277]. Some of these symptoms, including hypotonia and hyperactivity, are also seen in iDEND.

K_{ATP} channels are densely expressed in the cerebellum, particularly in Purkinje cells, but are also found in cells of the molecular and granular layers [182, 185]. As Purkinje cells provide the sole output from the cerebellar cortex, it is possible that their dysfunction due to the presence of mutant K_{ATP} channels contributes to the neurological symptoms of iDEND.

3.2.2 Is cerebellar electrophysiology affected by the presence of mutant K_{ATP} channels?

In this chapter I have investigated the electrophysiological consequences of expression of mutant K_{ATP} channel subunits in cerebellar Purkinje cells, by using the n-V59M mouse model of iDEND [102] described in Chapter 1. This mouse model is expected to express

Kir6.2-V59M in >90% of neurons because nestin-Cre - an efficient, neuronal specific Cre line [175, 254, 278] - was used to target transgene expression. I verified this assumption by crossing nestin-Cre mice with the Z/EG reporter mouse [256], producing Nes Z/EG mice. The Z/EG reporter mouse expresses GFP, driven by the strong chicken β-actin promotor, in cells where Cre is present. Nes Z/EG mice were perfused and their brains sectioned so that the pattern of GFP expression (which corresponds to the pattern of nestin-Cre expression) could be visualised.

All patients with iDEND caused by mutations in Kir6.2 are heterozygous [118] so they are expected to express equal amounts of mutant and wild-type Kir6.2 transcripts. The n-V59M mouse possesses two copies of the wild-type Kir6.2 gene and a further copy of the Kir6.2-V59M gene, which was expressed via the ROSA promotor. To see if the mouse mimicked the heterozygous state of patients, I compared the gene dosage of Kir6.2 in the brain of n-V59M mice and their littermate controls by reverse transcription quantitative polymerase chain reaction (RT-qPCR). To distinguish between wild-type and mutant Kir6.2 transcripts I also quantified GFP mRNA levels - in the n-V59M mouse the Kir6.2-V59M transgene was linked to a GFP cassette, so quantification of GFP provided a more direct measurement of Kir6.2-V59M expression.

As discussed in Chapter 1, functional assembly of K_{ATP} channel complexes requires the presence of both Kir6.2 and SUR subunits. Thus, I also quantified SUR1 levels to see if channel density was altered in the brain of n-V59M mice. The levels of Kir6.2, GFP and SUR were also quantified in triceps muscle samples from these mice (SUR2 was quantified instead of SUR1) to confirm that transgene expression was limited to the brain.

To see if the presence of Kir6.2-V59M subunits affected the electrophysiology of the cerebellum, I recorded the electrical activity of single Purkinje cells from brain slices of n-V59M mice and littermate controls. Tolbutamide, an SUR1-specific K_{ATP} channel closer [72,

94, 279], was used in these experiments to confirm that differences were due to variability in K_{ATP} current magnitude. The intrinsic electrophysiology of the Purkinje cells was revealed by using blockers of synaptic transmission. This was done in order to determine if the long-term expression of Kir6.2-V59M had an effect on the gross electrophysiology of the Purkinje cells.

As mutant K_{ATP} channels allow potassium to flow out of the cell, neurons that express the channels should be inhibited. As K_{ATP} channels are expressed throughout the brain, Kir6.2-V59M expression might reduce brain activity globally. To test this idea, I quantified the transcript and protein levels of the immediate-early gene c-Fos from the whole-brain of n-V59M and control mice. Most neurons show a low basal level of c-Fos mRNA and protein expression, but the levels increase, transiently, within 30-35min of neuronal activation [280, 281]. Therefore, quantification of c-Fos provided another measure of the electrical activity of the brain.

3.3 Methods

Details of the transgenic mice (genetic background, breeding strategy etc) are given in Chapter 2.

3.3.1 Fluorescence microscopy and immunohistochemistry of Nes Z/EG brain sections

Two-week-old Nes Z/EG mice were perfused with fixative and mid-sagittal brain sections were cut as described in Chapter 2. Mice were perfused at this age so that the results from these studies could be compared to the results from the electrophysiological experiments, which were also carried out on two-week-old mice. Sections from each mouse were processed in two ways: intrinsic GFP was visualised by epifluorescence microscopy (nuclei

were stained with DAPI); a separate set of sections was probed with anti-GFP antibodies and stained with DAB (see Chapter 2 for details) for visualisation of GFP by bright-field microscopy.

3.3.2 Quantification of mRNA from n-V59M mice and controls

Details of tissue storage, RNA and cDNA preparation, and RT-qPCR data analysis are given in Chapter 2. The whole brain and triceps muscle were dissected from wild-type (WT), ROSA, nestin-Cre (Cre) and Nes-Cre ROSA (n-V59M) mice at 5-7 weeks of age. Samples were processed as 'sets' that were composed of one WT, one ROSA, one Cre, and one n-V59M mouse. Each set was composed of only one sex, with four sets from female and three sets from male mice.

RT-qPCR was used to determine the amount of Kir6.2, SUR1 (for brain samples), SUR2 (for muscle samples), and GFP mRNA expressed in the brain and triceps muscle of control and n-V59M mice. The raw RT-qPCR data was converted to relative values and normalised as described in Chapter 2. Before normalisation, GFP transcript levels were expressed relative to Kir6.2 levels. Thus, GFP and Kir6.2 levels could be compared directly. The normalisation factor was calculated from the geometric mean of the levels of the reference genes ACTB, HPRT1 and HSPA8. Levels of Kir6.2, SUR and GFP transcripts were quantified in the tissues from all seven sets of mice. c-Fos transcripts were quantified in the tissues from only five sets of mice - three sets from male mice and two sets from female mice.

The levels of Kir6.2, GFP and SUR transcripts were measured from 4 different types of mice. Therefore, these data were analysed using two-way ANOVAs - genotype and sex were the two independent variables. All assumptions (which are given in Chapter 2) were satisfied for the data for Kir6.2 and SUR2 levels in the triceps, and SUR1 and c-Fos levels in the brain.

Thus, when analysing those data sets, $p < 0.05$ was considered statistically significant. For brain Kir6.2 levels, Levene's test indicated unequal variances between the groups ($p = 0.008$), so $p < 0.01$ was considered significant for those data [271].

3.3.3 Whole-cell recordings of cerebellar Purkinje cells from n-V59M mice

The membrane potential and firing frequency of neurons was measured using the whole-cell patch-clamp technique. 3mM ATP was included in the pipette solution, which was high enough to close wild-type, but not Kir6.2-V59M, K_{ATP} channels - approximately 15% of current through Kir6.2-V59M K_{ATP} channels remains in the presence of 3mM ATP (Figure 1.2). Further details of the composition of the intracellular solution are given in Chapter 2, along with the composition of the extracellular solution and the method used to prepare cerebellar brain slices.

For whole-cell recordings, slices were prepared from n-V59M mice (n=5) and littermate controls (n=6; 3 Cre, 3 ROSA mice) at postnatal day 10 to 22 (overall mean age = 15 days, mean age of n-V59M mice = 15 days, mean age of control mice = 14 days).

Whole-cell patch-clamp experiments were carried out in a repeated measures design. Single Purkinje cells were patched in brain slices that were perifused with a constant flow of oxygenated solution. The slices were initially bathed in aCSF alone ('basal'), then in aCSF containing 200μM tolbutamide, and finally switched back to aCSF alone - washing out the tolbutamide. The slices were bathed in each solution for approximately 5min. The electrical activity of the Purkinje cells was recorded continuously throughout all of these changes - so recordings lasted ~15min. After completion of the recording the slice was discarded.

If the cell did not survive for the duration of the protocol (e.g. the patch ruptured), and if no tolbutamide had been infused, then another cell from the same slice was patched. If tolbutamide had been infused then the slice was discarded. Recordings were made from 2-5 slices from each mouse. At least one cell per mouse survived the duration of the recording protocol. Overall, 10-17 neurons were analysed in each drug-treatment condition.

When breaking in, the cell was considered to be damaged, and its electrical activity was not recorded, if the membrane potential was depolarised to above approximately -30mV. If the cell had a strongly hyperpolarised membrane potential and was not firing action potentials then it was depolarised to approximately -50mV by injection of current to confirm that action potentials could be elicited. If action potentials were seen then the injected current was removed and the cell's spontaneous electrical activity was recorded. If action potentials were not seen then the cell was considered to be damaged, and its electrical activity was not recorded.

For the measurements in control solution or in the presence of tolbutamide, the electrical activity of the Purkinje cells was measured from the 1min of recording prior to the addition or removal of tolbutamide. For the washout condition, a 1min period of the recording was measured after tolbutamide had been washed out for ~3min. In all cases, the firing rate and membrane potential of the neurons had stabilised by the time point at which measurements were made. The membrane potential of neurons was determined from slow time-scale recordings on which a clear basal line was evident. This baseline was taken as the membrane potential. Firing frequency was calculated using Pulsefit software - a threshold of -30mV was used to identify action potentials. An average membrane potential and firing rate for each condition was calculated for each mouse. These average values were then used in statistical analyses, which are described below.

3.3.4 Statistical analysis of whole-cell electrophysiological recordings

The unequal number and distribution of males and females in the control and n-V59M groups (control group, 4 male, 2 female; n-V59M group, 1 male, 4 females) meant that the impact of sex could not be assessed. As there were no significant differences in the K_{ATP} channel transcript levels of the three different types of control mouse, their results were pooled for these experiments. Thus, genotype was the only independent variable and it had two levels (control and n-V59M).

To assess the effect of tolbutamide on control and n-V59M Purkinje cells, three repeated measures t-tests were used to compare their membrane potentials in each of the treatment conditions in a pairwise manner (i.e. basal vs 200μM tolbutamide, basal vs washout, 200μM tolbutamide vs washout). The effect of tolbutamide on the firing rates of control and n-V59M Purkinje cells was assessed in the same manner.

To compare the membrane potentials of control and n-V59M Purkinje cells in the three different treatment conditions, three independent samples t-tests were carried out comparing each of the treatment conditions (i.e. basal control vs basal n-V59M, 200μM tolbutamide control vs 200μM n-V59M, washout control vs washout n-V59M). The firing rates of control and n-V59M Purkinje cells were compared in the same manner.

In some of the analyses described in this section, data sets were tested multiple times. However, because the sample sizes were relatively small (≤ 6 mice were tested in each condition), I decided that the risks of committing type I and type II errors were relatively balanced and therefore Bonferroni adjustments were not made. Thus, for each of the analyses described above, p values were two-tailed and $p < 0.05$ was considered statistically significant.

3.3.5 Cell-attached recordings of cerebellar Purkinje cells from n-V59M mice

The whole-cell patch-clamping method involves rupturing the cell membrane so that the electrical activity of the cell can be recorded. Due to the invasive nature of this method, certain factors, which are discussed in section 3.5.4, may confound the results. Thus, the electrical activity of the Purkinje cells of n-V59M and littermate control mice was also recorded in the cell-attached configuration, which causes minimal perturbation of the intracellular environment. For cell-attached recordings, slices were prepared from n-V59M mice (n=5) and littermate controls (n=10 ; 3 WT, 4 Nes-Cre, 3 ROSA) at postnatal day 12-24 (overall mean age = 16 days, mean age of n-V59M mice = 17 days, mean age of control mice = 16 days).

After cutting, brain slices were incubated in aCSF for 30-45min and then transferred to the recording chamber. Slices were recorded while immersed in aCSF alone ('basal'), or aCSF containing 500μM tolbutamide, or aCSF containing 500μM tolbutamide plus 10μM CNQX and 20μM bicuculline ('500μM tolbutamide and synaptic blockers').

Cerebellar Purkinje cells are spontaneously active [204, 205] and receive primarily glutamatergic and GABAergic innervation [282, 283], so the inclusion of CNQX and bicuculline, which are specific blockers of AMPA and $GABA_A$ receptors [284, 285], allows the assessment of the intrinsic electrophysiology of Purkinje cells. When the electrical activity of cerebellar Purkinje cells is recorded in sagittal brain slices, the vast majority of postsynaptic currents are GABAergic [282, 283]. However, CNQX was still included in these experiments so that potential differences in spontaneous presynaptic glutamate release were controlled for.

The electrical activity of each Purkinje cell was recorded for ~4min. 2-8 cells were recorded from each slice before it was discarded. Up to 3 slices were used from each mouse in each

treatment condition. Mean firing rates for each condition were calculated; 14-33 neurons were analysed in each treatment condition.

Five n-V59M mice were used in these experiments, and the firing rates of their Purkinje cells were recorded in all three treatment conditions. For some control mice, however, all three treatment conditions were not tested. Most of the mice that were not tested in all conditions were tested chronologically earlier, and during the recording sessions it took time to optimise the patch-clamping equipment for cell-attached rather than whole-cell experiments. Thus, during these recording sessions there was not enough time to gather data for each of the three different treatment conditions. In other cases, the pharmacological agents were not available during the recording session. Thus, the Purkinje cells of two control mice were recorded in the basal state alone, cells from four control mice were recorded in the basal state and in 500μM tolbutamide, and cells from three control mice were recorded in all three treatment conditions. The Purkinje cells of one further control mouse were recorded only in 500μM tolbutamide and synaptic blockers, so that the data set as a whole was more balanced.

The average firing rate of each cell was calculated by analysing three 10s sections of the continuous recording. The analysed sections were separated by 60s, so firing rates were measured at minute 1, 2 and 3 of the recording. The mean firing rates of the Purkinje cells in the three treatment conditions were used in statistical analyses, which are described below.

3.3.6 Statistical analysis of cell-attached electrophysiological recordings

Not all mice were tested in all three treatment conditions, so there was ‘missing data’ in this repeated measures experiment. Purkinje cells from all n-V59M mice were measured in all three treatment conditions, so three repeated measures t-tests were used to systematically

probe all of the pairwise comparisons for these mice (basal vs tolbutamide, tolbutamide vs tolbutamide and synaptic blockers, basal vs tolbutamide and synaptic blockers). In contrast, the number of conditions tested on each control mouse varied, so repeated measures t-tests could not be carried out. Thus, three independent samples t-tests were used to systematically probe all of the pairwise comparisons for these mice. To compare the firing activity of control and n-V59M mice in the three treatment conditions, three independent samples t-tests were carried out.

Sample sizes were relatively small (≤ 10 mice) so, as described in section 3.3.4, Bonferroni adjustments were not made when making multiple comparisons in the cell-attached electrophysiological data sets. Thus, $p < 0.05$ was considered statistically significant for each analysis and p values were two-tailed.

3.3.7 Comparison of firing rates recorded in the whole-cell and cell-attached configurations

An independent samples t-test was conducted to compare the mean basal firing rates of control Purkinje cells that were recorded in the whole-cell and cell-attached configurations. The same analysis was carried out on data from n-V59M Purkinje cells. $p < 0.05$ was considered significant for these analyses.

3.3.8 Quantification of c-Fos protein levels

Total protein was extracted from the whole brain of 15-week-old nestin-Cre and n-V59M mice (n=6, 3 pairs of males, 3 pairs of females). After the total protein was run on a gel and transferred to a PVDF membrane, it was probed with an anti-c-Fos antibody. The density of

the c-Fos protein band was quantified and the levels of c-Fos protein in control and n-V59M mice were compared using a two-way ANOVA. All assumptions, given in Chapter 2, were satisfied, so $p < 0.05$ was considered significant for this analysis. The methods for protein extraction, gel electrophoresis and Western blotting are given in Chapter 2.

3.4 Results

3.4.1 Cre expression in the nestin-Cre mouse

Nes Z/EG mouse brains were densely stained with DAB, indicating that GFP expression levels were high, and widespread throughout the brain. In the cerebellum, most Purkinje cells were labelled, as were cells in the granular and molecular layers (Figure 3.1 A, B; Appendix 1). GFP was seen in all brain areas, including the neocortex (Figure 3.1 C) and hippocampus (Figure 3.1 D). By contrast, identically processed brain sections from control littermates of Nes Z/EG mice were not fluorescent and were not stained with DAB (data not shown).

3.4.2 K_{ATP} channel transcript levels in the n-V59M mouse

Two-way ANOVAs were used to analyse the RT-qPCR data, with sex and genotype as the between-subjects factors. There were no interaction effects between sex and genotype for any of the data sets. There was only one significant difference based on sex - triceps Kir6.2 levels were significantly higher in females compared to males ($p = 0.013$). However, this result was not important in the current context because SUR2 levels were not significantly different between the sexes ($p = 0.828$), so channel density in the triceps muscle was unlikely to be different in male and female mice.

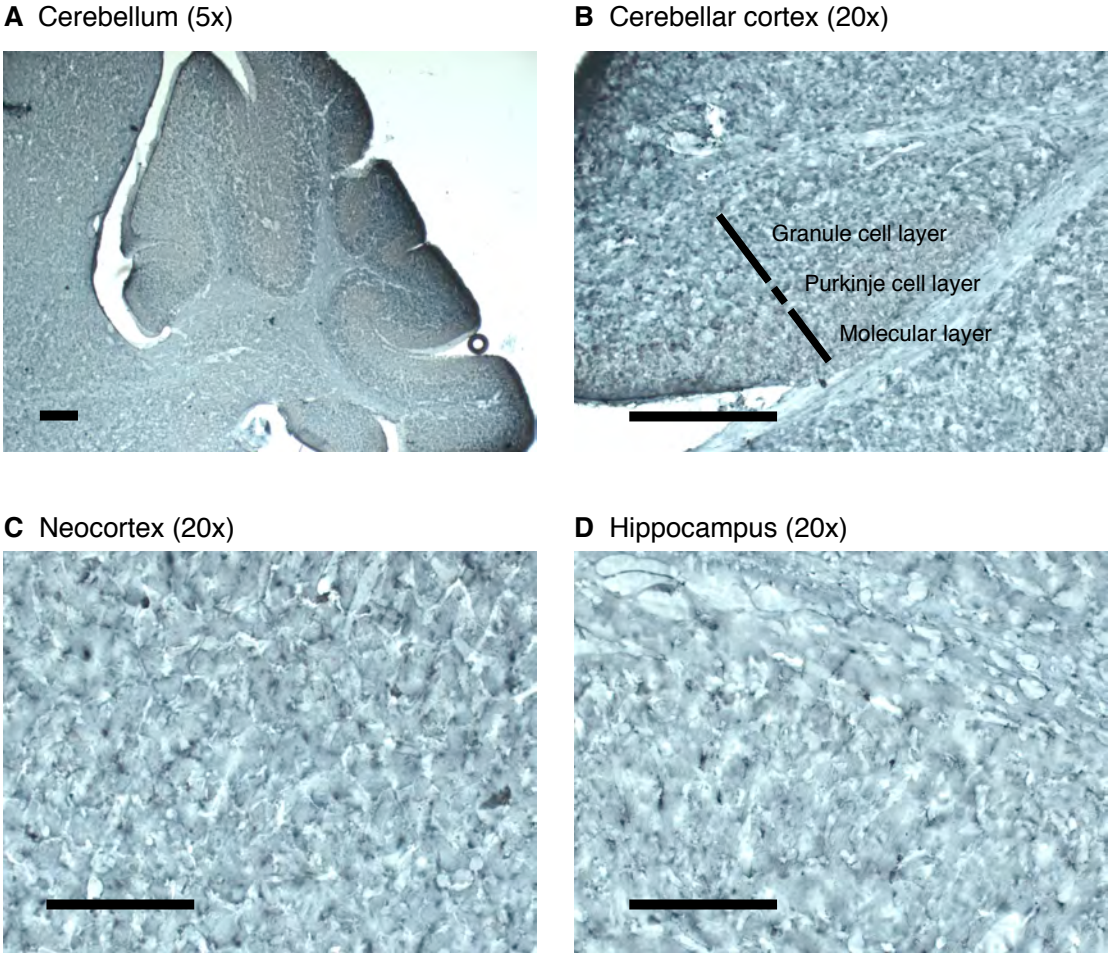

Figure 3.1 GFP in the brain of Nes Z/EG mice

Representative images of GFP expression from a 2-week old Nes Z/EG mouse. Black staining indicates the presence of GFP. Cerebellum at 5x magnification (**A**), and 20x magnification (**B**). GFP was seen in the cytoplasm and nucleus of cells throughout the cerebellum, including most Purkinje cells. The molecular and granule cell layers were also strongly stained. Staining was seen in all brain areas, including the neocortex (**C**), and hippocampus (**D**). Images are representative of 2 mice. Horizontal black bars indicate 200μm.

In the remainder of this section I only report the impact of genotype on levels of K_{ATP} channel transcripts. As there were no important sex-dependent differences, the data for male and female mice are shown pooled in all figures.

Brain Kir6.2 levels were ~2.5-fold higher in n-V59M mice compared to controls, but there were no significant differences between the four types of mice ($p = 0.024$; Figure 3.2 A). (Note that $p < 0.01$ was considered significant for these data, as explained above.) The data from the three types of control mice were pooled to increase statistical power, and this pooled mean level of Kir6.2 was compared to the mean from n-V59M mice (Figure 3.2 B). This analysis showed that Kir6.2 levels in the brain were significantly higher in n-V59M mice compared to controls ($p = 0.003$).

GFP levels were measured to provide an unambiguous quantification of Kir6.2-V59M levels. Appreciable levels of GFP mRNA were detected only in the brains of n-V59M mice. The level of GFP mRNA in n-V59M brain was similar to the level of Kir6.2 found in the brain of control mice. It was also approximately equal to the difference in Kir6.2 levels of control and n-V59M mouse brains (Figure 3.2 B). Thus, these data suggest that n-V59M mice express approximately equal levels of wild-type and mutant Kir6.2 mRNA in the brain.

Levels of Kir6.2 in the triceps of the four types of mice were not significantly different ($p = 0.515$, Figure 3.2 C). Similarly, there were no significant differences between the mice in brain SUR1 levels ($p = 0.754$, Figure 3.2 D) or triceps SUR2 levels ($p = 0.129$, Figure 3.2 E). The transcript levels of SUR2 in the brain were not measured.

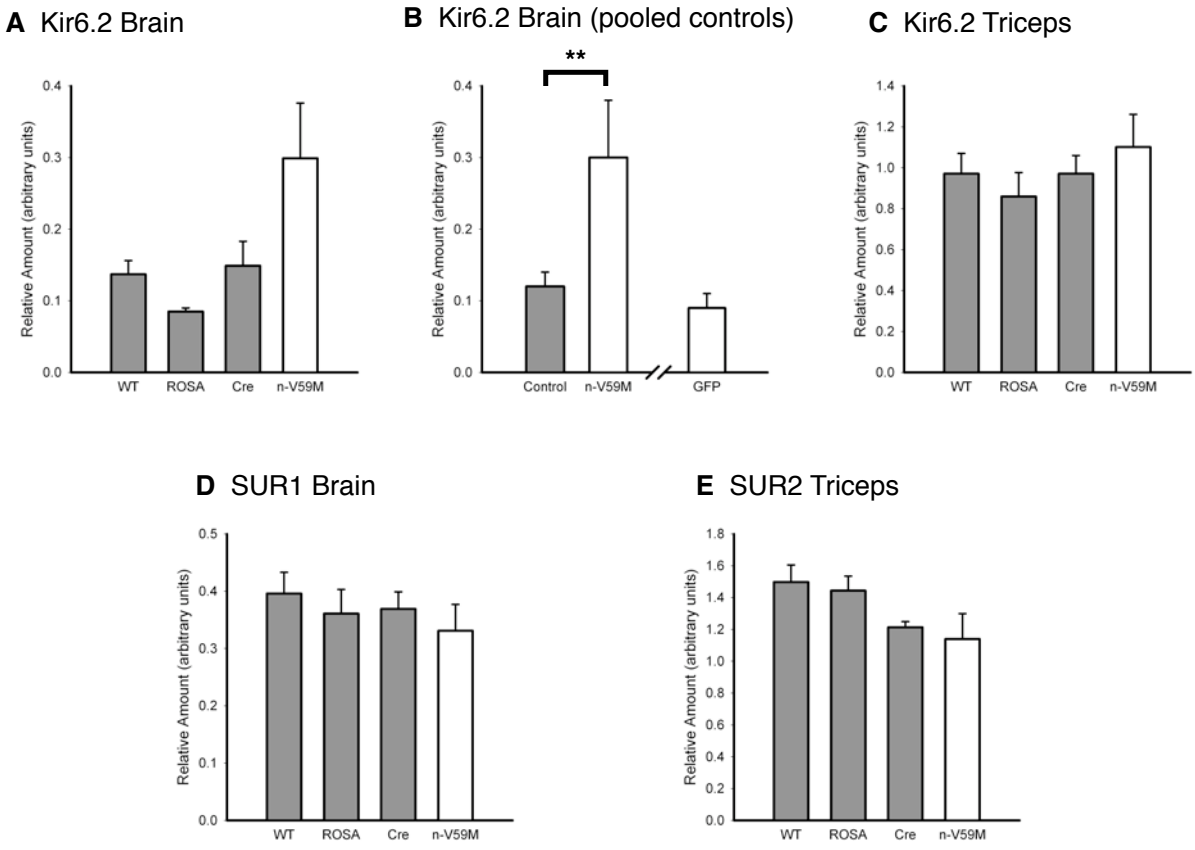

Figure 3.2 Kir6.2 and SUR expression in tissues from n-V59M mice

RT-qPCR was used to quantify transcript levels of Kir6.2, SUR and GFP in the brain and triceps muscle of n-V59M mice and their controls. (**A**) Kir6.2 levels in the brain of n-V59M mice (white bar, n=7) and their controls (grey bars, n=7). There were no significant differences in Kir6.2 levels from the brain of the four different genotypes of mice (two-way ANOVA). (**B**) The Kir6.2 levels from the three different types of control mice were pooled to increase statistical power (grey bar, n=21) and compared to levels from n-V59M mice (white bars, n=7). Kir6.2 levels were significantly higher in the brain of n-V59M mice compared to the pooled controls. **, $p < 0.001$, two-way ANOVA. GFP levels in the brain of control and n-V59M mice were also quantified to provide a specific quantification of the Kir6.2-V59M transgenic construct. GFP was quantified relative to Kir6.2 levels, so quantities of the two transcripts may be compared. As expected, GFP was only found in brain samples from n-V59M mice (white bar to the right of the break in the x-axis). The amount of GFP mRNA was similar to the additional amount of Kir6.2 mRNA found in the brain of n-V59M mice. Thus, the additional Kir6.2 mRNA found in the brain of n-V59M mice is likely to be Kir6.2-V59M. (**C**) Kir6.2 levels in the triceps muscle of control (grey bars, n=7) and n-V59M mice (white bar, n=7) were not significantly different (two-way ANOVA). SUR1 levels in the brain (**D**) and SUR2 levels in the triceps muscle (**E**) were also quantified. There were no statistically significant differences in the levels of SUR in brain and triceps from the different genotypes of mice (two-way ANOVAs). Data are mean ± SEM.

3.4.3 Membrane potentials of n-V59M Purkinje cells

In aCSF alone, there was a clear difference in the membrane potential and firing rate of n-V59M Purkinje cells compared to controls (Figure 3.3 A). n-V59M Purkinje cells were markedly hyperpolarised compared to wild-type cells and they fired fewer spontaneous action potentials. The addition of 200μM tolbutamide, did not obviously change the membrane potential and firing rate of control Purkinje cells. By contrast, n-V59M Purkinje cells were clearly depolarised when tolbutamide was added, and spontaneous action potentials were often fired more frequently.

Effects of tolbutamide treatment on control and n-V59M Purkinje cells:

The addition and subsequent washout of 200μM tolbutamide had no significant effect on the membrane potential of control Purkinje cells (Figure 3.4 A; Table 3.1; basal vs tolbutamide, $p = 0.052$; tolbutamide vs washout, $p = 0.487$). By contrast, the addition of 200μM tolbutamide significantly depolarised n-V59M Purkinje cells (Figure 3.4 A; $p = 0.013$). The subsequent washout of tolbutamide returned the membrane to a more hyperpolarised state, though this trend did not reach statistical significance ($p = 0.069$).

The membrane potential of control cells was more hyperpolarised after tolbutamide washout compared to the basal state ($p = 0.025$). By contrast, the membrane potential of n-V59M cells in the basal and washout conditions was not significantly different ($p = 0.763$). A potential explanation for why control Purkinje cells became more hyperpolarised during the recording session is provided in section 3.5.4.

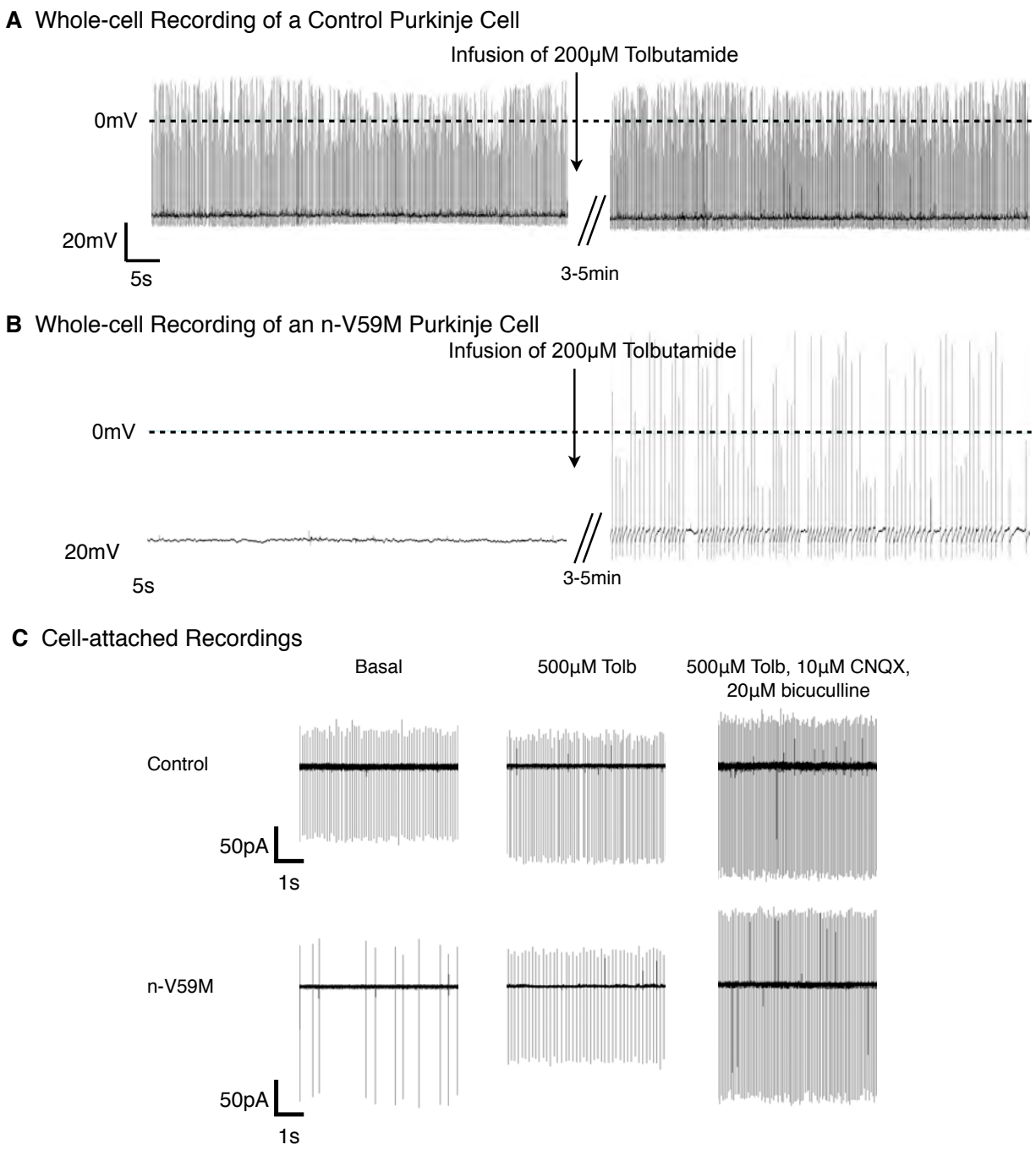

Figure 3.3 Electrical activity of cerebellar Purkinje cells of n-V59M mice

Representative whole-cell current-clamp recordings from cerebellar Purkinje cells of control (**A**) and n-V59M (**B**) mice. The traces show 60s sections of continuous recordings of the spontaneous activity of single Purkinje cells in the presence of aCSF alone (basal, left) and in aCSF with 200µM tolbutamide, which closes K_{ATP} channels (right). The traces show the activity of the same cell before and after administration of tolbutamide. The dotted lines indicate the 0mV level. Traces are representative of 6 control and 5 n-V59M mice. (**C**) Representative cell-attached recordings showing the spontaneous activity of cerebellar Purkinje cells from control (above) and n-V59M (below) mice. Traces show 6s sections of continuous recordings. Unlike whole-cell experiments, in cell-attached recordings, Purkinje cells were recorded in aCSF alone (basal, left), or aCSF with 500µM tolbutamide (middle), or aCSF with 500µM tolbutamide 10µM CNQX and 20µM bicuculline (right). Thus, each trace is from a different Purkinje cell. Traces are representative of 10 control and 5 n-V59M mice.

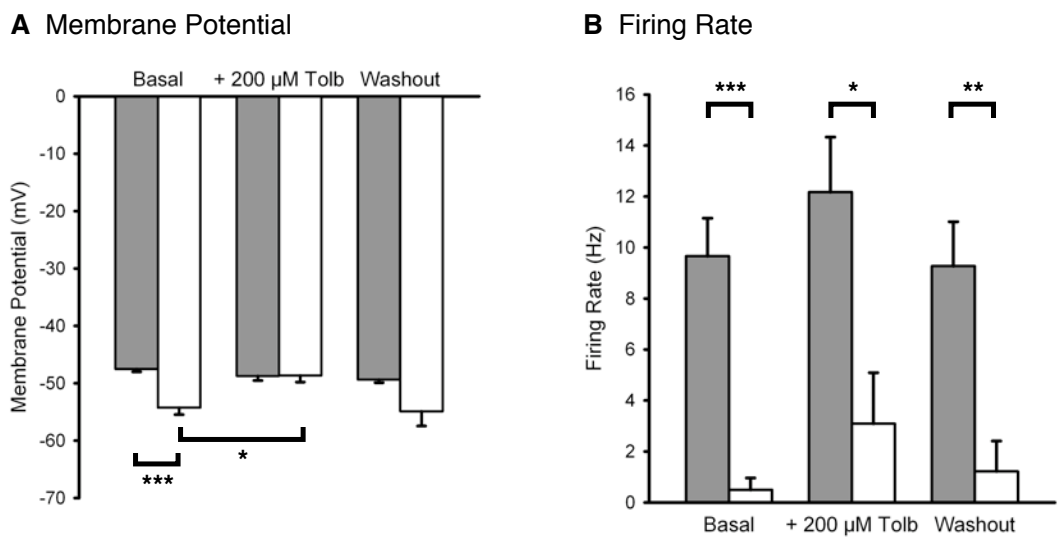

Figure 3.4 Electrical activity of cerebellar Purkinje cells from n-V59M mice, recorded in the whole-cell configuration

Spontaneous electrical activity of cerebellar Purkinje cells from control (grey bars, n=6) and n-V59M (white bars, n=5) mice recorded in the whole-cell configuration. (**A**) The membrane potential of Purkinje cells was measured when they were bathed in aCSF alone ('basal', left), in aCSF with 200µM tolbutamide (middle), and after subsequent 'washout' of tolbutamide (right). In the basal state, n-V59M Purkinje cells were significantly hyperpolarised compared to controls. ***, $p < 0.001$, independent samples t-test. The addition of tolbutamide had no significant effect on the membrane potential of control Purkinje cells. By contrast, n-V59M Purkinje cells were significantly depolarised, to the level of controls, by the addition of 200µM tolbutamide. *, $p < 0.017$, repeated measures t-test. After washing out tolbutamide, the membrane potential of n-V59M mice returned to a relatively hyperpolarised state. (**B**) The addition of tolbutamide had no significant effect on the firing rates of control Purkinje cells. The firing rates of n-V59M Purkinje cells were also not changed by the addition of tolbutamide. However, the firing rates of n-V59M Purkinje cells were significantly lower than those of controls in each of the three different treatment conditions. *, $p < 0.017$; **, $p < 0.01$; ***, $p < 0.001$; independent samples t-tests. Data are mean ± SEM.

Differences between control and n-V59M Purkinje cells:

In the basal state, n-V59M Purkinje cells were significantly hyperpolarised compared to controls ($p < 0.001$), but the two groups were not significantly different in the presence of 200μM tolbutamide ($p = 0.948$) or after tolbutamide had been washed out ($p = 0.099$; Figure 3.4 A; Table 3.1).

Table 3.1 Membrane potentials of control and n-V59M Purkinje cells

	Basal		200μM tolbutamide		Washout	
Genotype	Mean (mV)	SD	Mean (mV)	SD	Mean (mV)	SD
Control	-47.53	1.07	-48.73	1.95	-49.36	1.31
n-V59M	-54.26	2.70	-48.64	2.59	-54.89	5.77

3.4.4 Firing rates of n-V59M Purkinje cells, measured in the whole-cell configuration

The sampling frequency used to record the electrical activity of Purkinje cells in the whole-cell configuration was too slow (1.5kHz) to capture the full amplitude of cerebellar action potentials. This resulted in the truncation of some spikes (Figure 3.3 A). The impact of this problem is discussed in section 3.5.3.

Effects of tolbutamide treatment on control and n-V59M Purkinje cells:

The firing rates of control Purkinje cells were not significantly changed when 200μM tolbutamide was added ($p = 0.085$) or when it was washed out ($p = 0.109$). Indeed, the firing rate after tolbutamide washout was the same as in the basal state ($p = 0.746$; Figure 3.4 B; Table 3.2). The pattern was the same for the n-V59M Purkinje cells (basal vs 200μM

tolbutamide, p = 0.172; 200μM tolbutamide vs washout, p = 0.117; basal vs washout, p = 0.376).

Differences between control and n-V59M Purkinje cells:

The firing rates of n-V59M Purkinje cells were significantly lower than controls in each of the three treatment conditions (basal, $p < 0.001$; 200μM tolbutamide, p = 0.014; after tolbutamide washout, p = 0.005).

Table 3.2 Firing rates of control and n-V59M Purkinje cells from whole-cell recordings

	Basal		200μM tolbutamide		Washout	
Genotype	Mean (Hz)	SD	Mean (Hz)	SD	Mean (Hz)	SD
Control	9.66	3.64	12.17	5.29	9.27	4.27
n-V59M	0.50	1.02	3.09	4.46	1.22	2.66

3.4.5 Firing rates of n-V59M Purkinje cells, measured in the cell-attached configuration

A separate set of control and n-V59M mice was used to measure action potential firing frequency in the cell-attached mode. These recordings were acquired with a higher sampling frequency (14.1kHz, filtered at 2.9kHz) than the whole-cell recordings described above. In the cell-attached mode, the seal resistance during the recording influences the size of the recorded action potentials (recordings with tighter seals show action potentials with larger amplitudes). Therefore, in Figure 3.3 B, which shows sections of recordings from six separate cells, the amplitudes of action potentials are different in each panel. However, because the sampling frequency was sufficiently high, the action potentials within each panel are uniform in amplitude.

Effects of tolbutamide treatment on control and n-V59M Purkinje cells:

The firing rates of control Purkinje cells in the basal state and in the presence of tolbutamide were not significantly different (Figure 3.5; Table 3.3; $p = 0.663$). By contrast, n-V59M Purkinje cells had a significantly higher firing rate in tolbutamide than they did in the basal state ($p = 0.009$).

Both control and n-V59M Purkinje cells fired significantly faster than the basal state when tolbutamide and synaptic blockers were present (control, $p < 0.001$; n-V59M, $p = 0.008$). This is consistent with previous reports that Purkinje cells in this type of slice preparation experience tonic synaptic inhibition [282, 283].

Differences between control and n-V59M Purkinje cells:

In the basal state, the firing rate of n-V59M Purkinje cells was significantly lower than control cells (Figure 3.5; Table 3.4; $p = 0.002$). However, their firing rates in tolbutamide and in tolbutamide and synaptic blockers were not significantly different (tolbutamide, $p = 0.427$; tolbutamide and synaptic blockers, $p = 0.831$).

Table 3.3 Mean firing rates of control and n-V59M mice, obtained via on-cell recordings

	Basal		500µM tolbutamide		500µM tolbutamide and synaptic blockers	
Genotype	Mean (Hz)	SD	Mean (Hz)	SD	Mean (Hz)	SD
Control	9.54	2.80	10.15	2.68	18.17	1.47
n-V59M	3.52	2.39	8.71	3.37	17.39	6.83

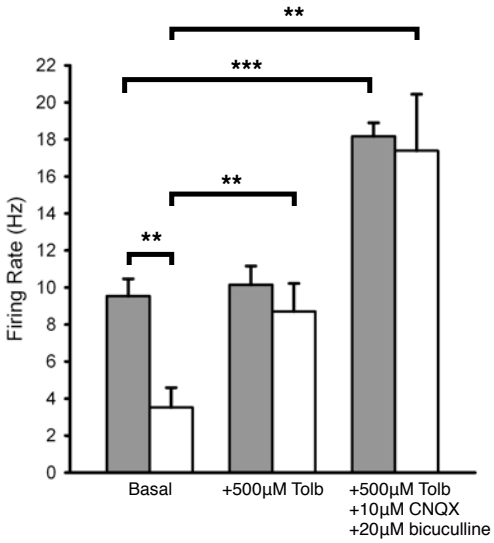

Figure 3.5 Electrical activity of cerebellar Purkinje cells from n-V59M mice, recorded in the cell-attached configuration

Mean action potential firing rates of control (grey bars, n=4-9) and n-V59M Purkinje cells (white bars, n=5) recorded in the cell-attached configuration. Action potentials were quantified from cells that were bathed in aCSF alone ('basal', left), in the presence of 500µM tolbutamide (middle), and in the presence of 500µM tolbutamide plus 10µM CNQX and 20µM bicuculline (right). Firing rates of n-V59M Purkinje cells were significantly lower than those of controls. **, $p < 0.01$, independent samples t-test. The firing rates of control Purkinje cells were not changed when tolbutamide was added. By contrast, n-V59M Purkinje cell firing rates were significantly increased, to the levels of controls, by the addition tolbutamide. **, $p < 0.01$, repeated measures t-test. The firing rates of control and n-V59M Purkinje cells were significantly higher, compared to their respective basal firing rates, when they were bathed in tolbutamide & synaptic blockers. ***, $p < 0.001$, independent samples t-test. **, $p < 0.01$, repeated measures t-test. In tolbutamide & synaptic blockers, the firing rates of Purkinje cells from the two types of mice were not significantly different.

3.4.6 Comparison of firing rates from whole-cell and cell-attached recordings

There was no significant difference in the mean basal firing rate of control Purkinje cells recorded in the whole-cell or on-cell configuration (Tables 3.2 and 3.3; $p = 0.940$). However, the basal firing rate of n-V59M Purkinje cells was significantly higher in the cell-attached than the whole-cell configuration ($p = 0.032$).

3.4.7 Whole-brain c-Fos levels in n-V59M mice

c-Fos transcript levels in the brain of control and n-V59M mice were not significantly different (Figure 3.6A; $p = 0.605$). c-Fos protein levels in the brain of Cre and n-V59M mice were also not significantly different (Figures 3.6 B, C; $p = 0.493$).

3.5 Discussion

3.5.1 Mutant K_{ATP} channels are expressed in all appropriate neurons in n-V59M mice

The GFP produced by the Z/EG reporter mouse is not targeted to any subcellular structures, so it is seen in the cytoplasm and nucleus of cells that express Cre [256]. Nestin-Cre mice were expected to induce GFP expression in >90% of neurons [175, 254, 278]. Consistent with these reports, GFP expression was widespread in the brain of Nes Z/EG mice. This was true whether the GFP was visualised directly by epifluorescence microscopy (Appendix 1) or if it was identified with a specific antibody and stained with DAB for visualisation by bright-field microscopy (Figure 3.1). Though the current experiments did not attempt to confirm the identity of GFP-expressing cells as neurons, it is reasonable to assume that this is the case.

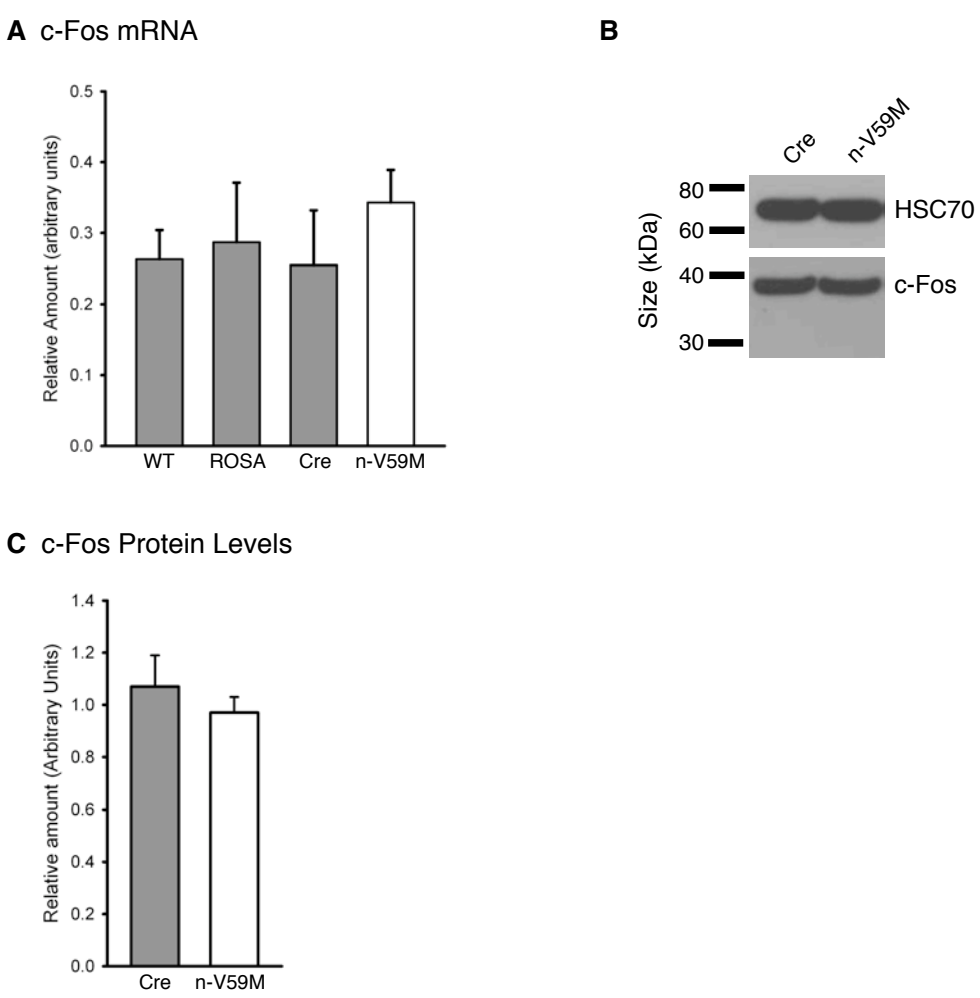

Figure 3.6 c-Fos expression in n-V59M mice

(**A**) RT-qPCR was used to quantify mRNA levels of the immediate early gene c-Fos in the brain of control (grey bars, n=5) and n-V59M mice (white bar, n=5). There were no significant dfferences in c-Fos transcript levels between the four different genotypes of mice (two-way ANOVA). (**B**) Representative Western blot showing protein levels of c-Fos in the brain of Cre (control) and n-V59M mice. Image is representative of 6 pairs of mice. (**C**) c-Fos protein levels in the brain of control (grey bars, n=6) and n-V59M (white bar, n=6) mice were measured. There was no significant difference in the c-Fos protein levels of Nes-Cre and n-V59M mice (two-way ANOVA). Data are mean ± SEM.

Although the sections were relatively homogenous in appearance, it was unlikely that this was due to background fluorescence or non-specific antibody binding because brain sections from littermate controls of Nes Z/EG mice were not fluorescent, and were not stained by DAB. Furthermore, in some brain regions of Nes Z/EG mice, such as the Purkinje cell layer of the cerebellum, GFP-labelled cell somata were visible (Appendix 1 B).

These experiments confirmed that the nestin-Cre mouse induced transgene expression throughout the brain. Thus, in n-V59M mice (which were made by crossing nestin-Cre and ROSA mice), it can be assumed that Kir6.2-V59M expression was induced in all neurons. However, the mutant Kir6.2 subunits will only form functional channels in neurons that normally express SUR because both subunits are required for appropriate trafficking of the K_{ATP} channel complex to the plasma membrane [71, 76, 82]. Therefore, in the n-V59M mouse, mutant K_{ATP} channels will only influence those neurons that normally express the channel.

3.5.2 The ratio of wild-type to mutant Kir6.2 in n-V59M mice is similar to iDEND patients

The ATP-insensitivity of V59M K_{ATP} channels is dependent upon the proportion of wild-type to mutant Kir6.2 present in the cell [176]. All patients with iDEND arising from mutations in Kir6.2 are heterozygous [118], therefore they are expected to express, on average, 50% wild-type and 50% mutant Kir6.2 mRNA.

Total Kir6.2 mRNA levels were ~2.5-fold higher in n-V59M mice compared to controls. If the additional levels of Kir6.2 are attributed to Kir6.2-V59M expression, then this measurement indicates that approximately 60% of the total Kir6.2 transcripts in the brain of n-V59M mouse

are from the mutant allele. The results from the quantification of GFP support this interpretation; GFP levels were approximately equal to the level of Kir6.2 found in the brain of control mice. Thus, the n-V59M mouse was hemizygous; approximately 50-60% of brain Kir6.2 mRNA in the mouse was the mutant Kir6.2-V59M transcript.

These experiments only provided an estimate of Kir6.2-V59M gene-dosage in the n-V59M mouse. As previously mentioned, Kir6.2-V59M was likely to be produced in all neurons, not just the subset that normally expressed Kir6.2. So the levels of Kir6.2-V59M that were detected by RT-qPCR probably overestimated the levels of mutant transcript that were found in single neurons that expressed K_{ATP} channels. Furthermore, the ROSA promotor is not expressed uniformly across the brain [286]. Thus, although approximately 50-60% of the total brain Kir6.2 is the mutant transcript, the gene-dosage in individual neurons is unclear.

If a true knock-in mouse was made, in which the V59M mutation was present in one of the endogenous copies of *KCNJ11*, it is likely that this mouse would more accurately mimic the gene-dosage of the patients. In lieu of this, however, the n-V59M mouse is a reasonable model of iDEND for three reasons: (1) it expresses a mixture of wild-type and mutant Kir6.2 mRNA, (2) mutant K_{ATP} channels will only be expressed in neurons that normally express the channel, and (3) SUR1 levels are not altered, so K_{ATP} channel density is unlikely to be affected.

3.5.3 Sampling frequency of whole-cell recordings

In the whole-cell configuration, electrical activity was sampled at 1.3kHz, which was too slow to capture the entire amplitude of cerebellar action potentials. This resulted in the truncation of some spikes (Figure 3.3 A). In on-cell recordings, which were sampled at a higher frequency (2.9kHz), the amplitude of action potentials of each cell was relatively constant

(Figure 3.3 B). This is consistent with the understanding that the amplitude of action potentials from individual neurons are relatively constant [287]. Although the action potentials recorded in whole-cell experiments were of variable amplitude, it is unlikely that any events were 'missed' as whole-cell and cell-attached firing rates of Purkinje cells from control mice in aCSF alone were not significantly different.

3.5.4 Whole-cell and cell-attached recordings

In the cell-attached configuration, recordings are made with the patch pipette sealed to the surface of the cell. Thus, intracellular molecules and processes are relatively unperturbed when neurons are recorded in this configuration [288]. By contrast, in the whole-cell configuration, the patch of membrane that is under the lumen of the sealed pipette is ruptured. Thus, the pipette solution is coextensive with the intracellular environment and intracellular constituents become diluted with whatever is in the pipette solution.

Purkinje cell electrical activity was recorded using both of these patch-clamping methods and their firing rates were higher when recorded in the cell-attached compared to the whole-cell configuration. There are many possible explanations for this result. For example, if Purkinje cell intracellular ATP concentrations were >3mM then formation of the whole-cell configuration (which were carried out using a pipette solution containing 3mM ATP) would effectively dilute intracellular ATP, and lead to opening of V59M (but not wild-type; Figure 1.2) K_{ATP} channels. This could cause a reduction in the firing rate of the cell.

A similar mechanism could account for the fact that control Purkinje cells were more hyperpolarised at the end of the recording session (after tolbutamide was washed out) than they were at the start (the 'basal ' state). In this case, it is possible that depletion of intracellular ATP lead to the gradual hyperpolarisation of these cells. Furthermore, as

described in section 1.2.2, numerous other intracellular constituents interact with K_{ATP} channels, so it is possible that the dilution of those factors lead to the gradual hyperpolarisation of the membrane.

n-V59M Purkinje cells recorded in the whole-cell configuration did not hyperpolarise during the recording session. Perhaps this is because the V59M K_{ATP} channels are less sensitive to changes in intracellular ATP concentrations (Proks et al, 2005), so depletion of intracellular ATP may not have a pronounced effect on these cells. Furthermore, they were already somewhat open, and the membrane potential was nearer to E_K, so any further opening of K_{ATP} channels may have a lesser effect on these cells than for the controls.

The confounding effects caused by the whole-cell configuration were unlikely to impact upon the conclusions drawn in this chapter. Firstly, the changes in the membrane potentials of the control Purkinje cells were small (see Table 3.1), and the hyperpolarisation was not associated with a significant change in the firing activity of the cells. Secondly, experiments were carried out on control and n-V59M Purkinje cells in the same way - the electrical activity of the two types of cells was compared when they had been ruptured for a similar amount of time. Finally, the conclusions in this chapter are primarily dependent upon the comparison of control and n-V59M Purkinje cells in the basal state. n-V59M Purkinje cells fired significantly fewer spontaneous action potentials than control cells when recorded in both the whole-cell and cell-attached configuration, so the method of electrophysiological recording did not have a material impact upon the conclusions drawn in this chapter.

3.5.5 K_{ATP} channels in control Purkinje cells

The membrane potential and firing rate of control Purkinje cells was unaffected by the addition of 200μM tolbutamide. This is consistent with previous reports that wild-type K_{ATP}

channels are largely closed under normal conditions [200]. This may be expected as K_{ATP} channels are involved in neuroprotection - opening during periods of metabolic stress, which hyperpolarises the neurons, reduces their energy demand and reduces Ca^{2+} influx. Such a mechanism would not be effective unless K_{ATP} channels were largely closed under normal conditions.

The intrinsic firing rate of Purkinje cells (i.e. the firing rate of the cell when synaptic inputs have been blocked) has been reported to be 40-70Hz [289-294]. However, in my experiments the intrinsic firing rate of control Purkinke cells was approximately 18Hz. The reason for this difference is unclear - mice were used in some of the studies cited above, so it is unlikely that it is due to the model used. Furthermore, the ionic constituents of the extracellular and intracellular solutions used in the cited studies were broadly similar to mine. One obvious difference, however, was the glucose concentration used. In the cited studies, recordings were made in high (10-25mM) glucose concentrations. By contrast, my experiments were conducted in 5mM glucose, which is similar to to the plasma glucose level (glucose levels in the CSF are somewhat lower [295, 296]). Thus, it is possible that Purkinje cells have a higher firing rate in high glucose.

In theory, high extracellular glucose concentrations might lead to increased intracellular ATP concentrations in the Purkinje cells, so their higher spontaneous activity could be attributed to increased K_{ATP} channel closure. However, this is unlikely to be the case because in my experiments the intrinsic activity of the cells was measured in the presence of tolbutamide. Furthermore, consistent with previous reports, my experiments show that K_{ATP} channels in Purkinje cells are largely closed in aCSF with 5mM glucose. Thus, the higher intrinsic firing rates of Purkinje cells that are observed in other studies are likely to be caused by a K_{ATP} channel-independent mechanism.

3.5.6 Cerebellar Purkinje cells are inhibited in iDEND

In heterologous expression experiments, K_{ATP} channels that incorporate Kir6.2-V59M subunits are relatively insensitive to metabolic inhibition and therefore 'overactive' - allowing excessive potassium flux [176]. This also seems to be the case in cerebellar Purkinje cells. When bathed in aCSF alone, Purkinje cells from n-V59M mice were significantly hyperpolarised compared to controls. The inhibition of these cells was likely to be due to the presence of mutant K_{ATP} channels as the addition of 200μM tolbutamide, which closes SUR1-containing K_{ATP} channels, caused a significant depolarisation of the n-V59M Purkinje cells. When the drug was washed out, the membrane potential of the cells returned to a more hyperpolarised state.

The basal firing rates of n-V59M Purkinje cells were also lower than controls. This was true whether the cells were recorded in the whole-cell or cell-attached configurations. This is consistent with the results discussed above, as the relative hyperpolarisation of the n-V59M cells would be expected to inhibit the initiation of action potential firing. In summary, these experiments indicate that cerebellar Purkinje cells are inhibited in iDEND.

3.5.7 The effect of tolbutamide on n-V59M Purkinje cells

In the whole-cell configuration, the firing rates of n-V59M Purkinje cells increased slightly when 200μM tolbutamide was added, but not significantly so. This was puzzling as the membrane potential of these cells was depolarised, to the level of controls, by the administration of 200μM tolbutamide. Thus, one might expect their firing rates to be similar. It is worth noting, however, that the membrane potential that was measured in these experiments was not the true resting potential. As the cells were firing action potentials

constantly (control Purkinje cells more so than n-V59M cells) the cell was never ‘ at rest’. Thus, the measurement of membrane potential was potentially more prone to inaccuracy than the measurement of action potential firing frequency (because action potentials are ‘all-or-nothing’).

Some experiments, carried out by Carolina Lahmann, suggested a possible explanation for the incomplete restoration of firing activity. Her dose-response curve for heterologously expressed V59M K_{ATP} channels suggested that 200μM tolbutamide could be insufficient to close V59M K_{ATP} channels (Appendix 2). Although the heterozygous channels (those produced by a 50:50 mixture of wild-type and mutant Kir6.2 mRNA) were closed by 200μM tolbutamide, significant residual current still flowed through homozygous-channels (which had only mutant Kir6.2 subunits). The RT-qPCR results I obtained from the whole-brain of n-V59M mice did not reveal the precise gene-dosage of wild-type to mutant Kir6.2 mRNA in n-V59M Purkinje cells (see discussion in section 3.5.2), but they suggested that roughly 50-60% of Kir6.2 mRNA in neurons was the Kir6.2-V59M transcript. Thus, it is possible that more than half of the Kir6.2 transcripts in n-V59M Purkinje cells were of the mutant variety, and thus 200μM tolbutamide did not fully close the mutant channels in these cells.

Even small amounts of residual K_{ATP} channel activity could be sufficient to inhibit the initiation of action potential firing. For example, if mutant K_{ATP} channels are present in the axon hillock, where voltage-gated sodium channels are at their highest density, then even small amounts of potassium conductance through unblocked mutant K_{ATP} channels could cause sufficient shunting inhibition to prevent the generation of an action potential. In support of this interpretation, immunohistochemistry studies suggest that Kir6.2 is most densely localised to the somata of neurons [185]. These small differences in membrane resistance may not be apparent in the membrane potential of the cell, but could reduce their action potential firing activity.

From the dose-response curve, it was clear that 500μM tolbutamide was sufficient to close even homozygous V59M K_{ATP} channels, so this concentration was used in the subsequent cell-attached patch-clamping experiments. The cell-attached method was used as it does not involve rupturing the cell membrane, so intracellular processes are less likely to be perturbed and the neurons are recorded in a more physiological state (as discussed in section 3.5.4). Thus, in the second set of experiments, the Purkinje cells were recorded using a technique that was less likely to interfere with cellular processes, and sufficient tolbutamide was used to close the mutant K_{ATP} channels, regardless of their composition.

In the cell-attached configuration, the firing rates of n-V59M cells were significantly higher in 500μM tolbutamide than they were in the basal state. Indeed, the firing rates of n-V59M and control Purkinje cells in tolbutamide were not significantly different. Therefore, these experiments indicated that the reduced firing rate of n-V59M Purkinje cells was due to the presence of mutant K_{ATP} channels. They also suggested that the expression of Kir6.2-V59M mRNA from prenatal development did not induce any gross compensatory changes in the electrophysiology of n-V59M Purkinje cells. This conclusion is discussed in more depth in section 3.5.8.

The electrophysiology data I have presented in this chapter do not reveal whether the difference in basal firing rate of n-V59M and control Purkinje cells is due to expression of mutant K_{ATP} channels in Purkinje cells themselves, or via altered synaptic input due to expression of mutant channels in, for example, interneurons or granule cells. Previous studies have shown that K_{ATP} channels are expressed in Purkinje cells [297, 298], so it is likely that at least part of the effect is due to direct expression in these cells. In the future this may be clarified by quantifying the frequency of synaptic inputs that n-V59M Purkinje cells receive. The importance of mutant K_{ATP} channels in the Purkinje cell itself can be confirmed by recording its activity while all synaptic currents are blocked (e.g. by infusion of tetrodotoxin, or CNQX and bicuculline). Although similar experiments were carried out by me,

and are discussed below, K_{ATP} channels had already been closed by tolbutamide before synaptic currents were blocked, so the effect of the mutant K_{ATP} channels on the Purkinje cell itself could not be determined.

In summary, the electrophysiological experiments presented in this chapter revealed that cerebellar Purkinje cells were inhibited in the n-V59M mouse. The inhibition was likely to be caused by mutant K_{ATP} channels because in the presence of tolbutamide, which closes K_{ATP} channels, the firing activity of n-V59M Purkinje cells was not significantly different to that of controls. These results confirm that Kir6.2-V59M transcripts produced by the ROSA cassette are processed appropriately and that these subunits are included in functional K_{ATP} channels, providing further validation that the n-V59M mouse is a reasonable model of iDEND. As cerebellar Purkinje cells provide the sole output from the cerebellar cortex, and they are inhibited in the n-V59M mouse, it is likely that cerebellar function is compromised in iDEND.

3.5.8 Does long-term expression of Kir6.2-V59M induce compensatory effects?

Prolonged neuronal depolarisation or hyperpolarisation can result in compensatory changes in the complement of ion channels that are expressed in the neuronal membrane [299-302] and anecdotal reports suggest that iDEND patients who are treated with sulphonylureas from early life have a better prognosis for their neurological symptoms. Thus, it is possible that some of the symptoms of iDEND are linked to developmental effects caused by the presence of mutant K_{ATP} channels in the brain.

The n-V59M mouse might be a useful model for understanding these developmental effects. Nestin expression occurs at embryonic day 10-11 [254] and SUR is expressed in the brain from approximately embryonic day 12 [303] (I could find no reports showing the developmental expression pattern of Kir6.2). Thus, functional mutant K_{ATP} channels should

be present in the brain of n-V59M mice during embryonic development. However, although SUR1 expression starts in embryonic development, K_{ATP} channel expression at birth is relatively low in most brain areas and expression levels rise rapidly in postnatal development [187]. Thus, the developmental effects of mutant K_{ATP} channel expression may predominantly occur postnatally, rather than prenatally.

In my electrophysiology experiments, when Purkinje cells were bathed in a concentration of tolbutamide that was sufficient to close all mutant channels, and recorded using a method that was minimally invasive, the firing rates of n-V59M and control Purkinje cells were not significantly different. This was also the case when synaptic inputs were blocked. In the latter condition, the firing activity of the Purkinje cells was determined by its intrinsic electrophysiology - the complement of ion channels that was present in its membrane. Thus, the presence of Kir6.2-V59M K_{ATP} channels in n-V59M Purkinje cells from early embryonic development did not seem to induce any gross compensatory changes in their electrophysiology.

Of course, these experiments do not rule out the possibility that other neurons are affected by developmental changes. Furthermore, although the gross intrinsic electrophysiology of the Purkinje cells did not seem to be affected, I did not assess the preservation of other aspects of their electrophysiology - such as synaptic plasticity, which is thought to be crucial for the function of the cerebellum [304]. Thus, it remains unclear if long-term expression of mutant K_{ATP} channels in neurons has developmental effects at the cellular level.

3.5.9 Whole-brain c-Fos levels were not altered in n-V59M mice

Protein and mRNA levels of the immediate-early gene c-Fos were not different in the brains of control and n-V59M mice. There are several reasons why this may be the case. Firstly, not

all neurons express K_{ATP} channels, so perhaps the level of inhibition caused by these mutant channels is too low on a whole-brain level to be detected. Secondly, the nature of the neurons that are inhibited is important. Inhibition of GABAergic neurons, such as cerebellar Purkinje cells, would be expected to lead to increased activity elsewhere. If the inhibition caused by mutant K_{ATP} channels affects both excitatory and inhibitory neurons, and if mechanisms of plasticity also come into play, then it is reasonable that c-Fos levels in the whole brain may not be different in n-V59M mice compared to controls. Thirdly, although it is clear that Purkinje cells are significantly hyperpolarised when they express Kir6.2-V59M K_{ATP} channels, other neurons may not be as severely affected. This may be because they have a lower dose of mutant Kir6.2 mRNA; indeed, as previously mentioned, the ROSA promotor is not uniformly expressed in the brain. But it could also be because different neurons express different types and quantities of ion channels [287]. These differences could mitigate the effects of the mutant K_{ATP} channels.

Indeed, it is perhaps surprising that n-V59M Purkinje cells were so strongly hyperpolarised. Previous reports have shown that Purkinje cells express hyperpolarisation-activated cation channels (I_H) [293]. These channels become activated at hyperpolarised membrane potentials and allow a cation flux, which acts to depolarise the membrane. The presence of this channel would counteract the hyperpolarising effect of the mutant K_{ATP} channels. I did not attempt to identify I_H in n-V59M Purkinje cells. However, if these channels are indeed activated in these cells, then perhaps the effect of mutant K_{ATP} channels is so significant as to negate their influence. In the future, I_H could be blocked using the pharmacological agent ZD7288 [305] to see if it influences the electrophysiology of n-V59M Purkinje cells.

3.5.10 Implications for our understanding and treatment of iDEND

As Purkinje cells provide the sole output from the cerebellar cortex, the results presented in this chapter indicate that cerebellar function is compromised in iDEND. As discussed in section 3.2.1, some of the neurological symptoms of iDEND, such as hypotonia and hyperactivity, are also seen in patients who have damage to the cerebellum. However, damage to other nervous tissue, such as the spinal cord, may also result in muscle hypotonia [306, 307], and hyperactivity may arise due to damage to the frontal lobe [308, 309]. Thus, although it is tempting to conclude that cerebellar dysfunction causes hypotonia and hyperactivity in iDEND, it is unlikely that the cerebellum alone is responsible.

The inhibition of neurons by mutant K_{ATP} channels would be expected to impair neuronal processing across the brain. If neuronal processing is impaired during critical periods of development, then treatment after this point will not allow the acquisition of that skill or ability. However, other skills and abilities are not acquired in critical periods and merely require normal neuronal functioning. Consequently, children who are developmentally delayed when they are treated with sulphonylureas can 'catch up' on some milestones [148]. The precise mechanisms underlying the developmental delay of iDEND patients are unclear, and it is difficult to predict how much an individual patient will improve when transferred to sulphonylureas. Indeed, the cognitive function of some patients does not improve [147, 148, 153]. However, anecdotal reports indicate that the earlier an iDEND patient is treated with sulphonylureas (rather than insulin) the better the prognosis for their neurological symptoms.

In individuals who transfer later in life, it is possible that their neurons will have undergone compensatory changes in response to their long-term hyperpolarisation. Such changes may affect the response of the patient to sulphonylurea therapy. For example, if the neurons have induced compensatory mechanisms that counteract inhibition, then closure of mutant K_{ATP} channels in these neurons may make them over-active. If this is true across the brain then it

is possible that treatment with sulphonylureas could induce seizures in individuals who have previously been seizure-free. Consistent with this hypothesis, treatment with sulphonylureas has been associated with the onset of seizures in one case [148]. However, these seizures may have been linked to damage caused by previous hypoglycaemic episodes, and there are no other similar reports.

Cerebellar Purkinje cells from n-V59M mice did not seem to have any gross electrophysiological differences compared to control cells, which indicated that the long-term expression of mutant K_{ATP} channels did not induce compensatory changes in these cells. The preservation of other important cellular mechanisms, such as synaptic plasticity, was not assessed. Thus, it remains unclear if compensatory mechanisms at a cellular level are an important consideration in the treatment of the neurological symptoms of iDEND patients. However, these experiments suggest that the function of cerebellar Purkinje cells may be restored in iDEND patients as long as high enough concentrations of sulphonylureas are present in their brain.

V59M K_{ATP} channels are only fully closed by high concentrations of sulphonylureas. Thus, it is important to know how much sulphonylurea reaches the brain of iDEND patients. Efflux mechanisms exist in the BBB that are capable of transporting tolbutamide [154], so it is likely that concentrations of sulphonylurea in the brain are lower than those recorded in the periphery. Anecdotal evidence suggests that this is indeed the case, as CSF that was sampled by lumbar puncture from one iDEND patient contained no sulphonylurea. It is likely, however, that in other patients at least some of the drug reaches the brain because their neurological symptoms improve when they transfer to sulphonylurea treatment [152, 310]. Indeed, cerebellar blood flow in an iDEND patient was increased after they transferred to sulphonylurea treatment [152]. As blood flow is a proxy measure of activity, these results support the notion that cerebellar activity is lower in iDEND, and that sulphonylureas can accumulate sufficiently in the brain to increase neuronal activity.

Future investigations are needed to better understand the penetrance of sulphonylureas into the brain. Potentially, such experiments could inform the development of new sulphonylureas that have greater BBB penetrance, or adjunct agents that increase the accumulation of sulphonylureas in the brain.

Chapter 4: Parvalbumin-expressing Neurons in iDEND

4.1 Summary

1) Parvalbumin-Cre and ROSA mice were crossed to produce p-V59M mice. These mice expressed Kir6.2-V59M in the brain, particularly in the cerebellum, and also in the triceps muscle. Control mice showed no expression of Kir6.2-V59M in the tissues that were tested.

2) Whole-cell patch-clamping of cerebellar Purkinje cells revealed a bistable pattern of firing, with clear 'up' and 'down' states in cells from both control and p-V59M mice. The duration of firing of p-V59M Purkinje cells from p-V59M mice was lower than control mice, but in the presence of 500μM tolbutamide there was no difference between the mice. Administration of CNQX and bicuculline, along with tolbutamide, abolished the 'down' states of control and p-V59M Purkinje cells, which indicated that they were driven by inhibitory presynaptic activity.

3) p-V59M Purkinje cells fired fewer spontaneous action potentials in a one minute period compared to control cells. However, when tolbutamide was present, or tolbutamide and synaptic blockers, the firing rates of p-V59M and control Purkinje cells were not significantly different. These results indicated that the electrical output from the cerebellum was impaired in p-V59M mice compared to controls. However, the expression of Kir6.2-V59M had a less pronounced effect on the electrophysiology of Purkinje cells from p-V59M compared to n-V59M mice. This was possibly due to differences in the genetic backgrounds of the mice.

4) Muscle strength tests were carried out on 12-week-old control and p-V59M mice. There was no significant difference between the mice on the horizontal bar and inverted screen tests. However, p-V59M mice were significantly impaired compared to controls on the weight-lifting task. Of the three tests, weight-lifting required the most strength, so performance on this task was likely to be the most sensitive to muscle weakness. Thus, p-V59M mice were significantly weaker than controls.

5) The multiple static rods and rotarod tests were used to assess the motor coordination of 12-week-old p-V59M and control mice. There were no significant differences between control and p-V59M mice on these two tests.

6) Spontaneous activity was measured using activity monitors and free-running wheels. The circadian rhythm of activity, the time to settle in a new environment, and total activity over 23 hours was not significantly different for control and p-V59M mice housed in enclosures fitted with activity monitors. By contrast, p-V59M mice showed greater usage of the free-running wheels, as they ran further and with a higher average speed. Therefore p-V59M mice were hyperactive in some, but not all, tests.

7) The results presented in this chapter indicate that expression of Kir6.2-V59M limited to parvalbumin-expressing inhibitory interneurons is sufficient to cause muscle weakness and hyperactivity (in some tests). Thus, dysfunction of these circuits may underlie some symptoms of iDEND. Further studies are needed to identify the relative importance of the parvalbumin-expressing neurons of the neocortex and cerebellum for the muscle weakness and hyperactivity phenotypes.

4.2 Introduction

The behavioural phenotype of the n-V59M mouse could have been caused by changes in the electrical activity of excitatory and/or inhibitory neurons. Because there is evidence that in some brain areas (e.g. the hippocampus) there is a greater density of K_{ATP} channels in inhibitory cells [217], I tested the effect of the V59M mutation in inhibitory cells.

GABA is the principle inhibitory neurotransmitter in the brain, and is produced by the enzyme glutamatic acid decarboxylase (GAD). In preliminary experiments (not shown) crossing ROSA mice with GAD-Cre mice did not result in any double transgenic offspring. Therefore, I used parvalbumin-Cre mice as paravalbumin is expressed in a subpopulation of inhibitory neurons [311-313].

4.2.1 Parvalbumin

Parvalbumin is a cytoplasmic, high-affinity calcium-binding protein that is expressed in the brain [314], and in skeletal [315] and cardiac muscles [316]. As previously mentioned, neurons in the brain that express parvalbumin are inhibitory, comprising approximately 20% of the total GABAergic population [311], and expression is found in a variety of brain regions, including the hippocampus [311], neocortex [312] and the cerebellar cortex [313]. In the cerebellar cortex, Purkinje, basket and stellate cells express parvalbumin [317-319]. Parvalbumin-positive interneurons are also present in the spinal cord [320, 321].

Parvalbumin is first expressed in the brain in postnatal life, and its expression is induced in different brain regions at different times [322-325]. For example, parvalbumin expression in the neocortex starts at approximately postnatal day 15 and increases until approximately postnatal day 21, at which point expression levels become relatively constant throughout

adult life [325]. By contrast, parvalbumin is found in the cerebellum from postnatal day 5 [326].

Interestingly, levels of K_{ATP} channels in the brain of rodents also rise during postnatal development [187]; although SUR expression begins at around embryonic day 12 [303], the density of channels in the neuronal membrane is relatively low at birth, and rises gradually until adult-like levels are reached at around 5-6 weeks of age [187].

Thus, the expression levels of both K_{ATP} channels and parvalbumin are correlated, in that both increase during the first few weeks of life. However, there are no studies that have systematically determined the degree of overlap of these two proteins. Some neurons, however, such as cerebellar Purkinje cells, are known to express both parvalbumin and K_{ATP} channels.

4.2.2 The p-V59M mouse

In the current chapter, I used the parvalbumin-Cre mouse [319, 327] to restrict the expression of Kir6.2-V59M mRNA to parvalbumin-expressing inhibitory neurons. By targeting a smaller population of neurons, the aim of these experiments was to narrow down the brain regions and circuits that might underlie the motor symptoms of iDEND.

I crossed parvalbumin-Cre and ROSA mice to create p-V59M mice, which were expected to express Kir6.2-V59M in parvalbumin-expressing neurons. I confirmed this expression pattern in two ways. Firstly, I used end-point reverse transcription PCR (RT-PCR) to identify Kir6.2-V59M transcripts in the cerebellum, brain (minus cerebellum), triceps muscle and heart of p-V59M mice. Secondly, to show where Kir6.2-V59M was likely to be expressed in the brain of p-V59M mice, I crossed parvalbumin-Cre and Z/EG mice to make Pv-Z/EG mice,

and performed immunohistochemistry experiments to show the pattern of GFP expression in their brains. (The Z/EG mouse is described in detail in Chapters 2 and 3.)

The electrical activity of p-V59M Purkinje cells was recorded to see if they were different to controls. Tolbutamide was used to see if those differences could be attributed to excessive K_{ATP} channel activity. The intrinsic electrical activity of these cells was also measured to see if there were any gross deleterious effects caused by the long-term expression of Kir6.2-V59M.

Behavioural tests were conducted to see if muscle strength, motor coordination, and the spontaneous activity level of p-V59M mice were altered compared to controls. The same tests had been used to characterise n-V59M mice [102]. Thus, the aim was to compare the electrophysiological and behavioural phenotypes of the n-V59M and p-V59M mouse models so that the relative importance of parvalbumin-expressing cells in iDEND could be determined.

4.3 Methods

Details of the transgenic mice (genetic background, breeding strategy etc) are given in Chapter 2. Although there are no reports that parvalbumin is expressed in pancreatic β-cells, I confirmed that p-V59M mice were not diabetic by checking the urine glucose levels of adult mice. I also measured the spontaneous 23-hour water intake levels of 12-week-old control and p-V59M mice. The water intake data were analysed using a two-way ANOVA, and $p < 0.05$ was considered significant.

4.3.1 End-point reverse transcript PCR, with subsequent digestion by BtsCI

RNA was extracted from the cerebellum, brain (minus cerebellum), triceps and heart of adult (~23-week-old) p-V59M and control mice. Kir6.2 mRNA was amplified by PCR, and wild-type and Kir6.2-V59M transcripts were distinguished by digesting the PCR products with BtsCI restriction enzyme. Details of all of these steps are given in Chapter 2.

4.3.2 Immunohistochemistry on Pv-Z/EG mice

Pv-Z/EG mice were perfused with paraformaldehyde at 2, 12 and 16 weeks of age, and brain sections were prepared as described in Chapter 2. These ages corresponded to the timings of the various tests carried out on p-V59M mice: electrophysiology at 2-weeks-old, strength and coordination testing at 12-weeks-old, and spontaneous activity testing at 16-weeks-old. The 2-week-old mice were perfused at postnatal day 18. Brain sections from each mouse were processed in two ways: intrinsic GFP was visualised by epifluorescence microscopy (nuclei were stained with DAPI); and a separate set of sections was probed with anti-GFP antibodies and stained with DAB (see Chapter 2 for details) for visualisation of GFP by bright-field microscopy. At least 2 mice were used at each age. Brains from control mice were processed in the same way but showed no GFP expression (data not shown).

4.3.3 Electrophysiology of cerebellar Purkinje cells of p-V59M mice

Whole-cell patch-clamping experiments were carried out to record the electrical activity of cerebellar Purkinje cells from p-V59M (n = 6, 5 males, 1 female; mean age = 16 days) and control (n = 8, 3 males, 5 females; mean age = 17 days) mice. The intracellular and

extracellular solutions were the same as those used in Chapter 3. The composition of the solutions, and the method used to make brain slices are given in Chapter 2.

Whole-cell recordings of Purkinje cell electrical activity were carried out in a similar way to those described in Chapter 3. Single Purkinje cells were recorded while the slice was first bathed in aCSF alone ('basal'), then in aCSF with 500μM tolbutamide, and finally in aCSF with 500μM tolbutamide plus 10μM CNQX and 20μM bicuculline (500μM tolbutamide and synaptic blockers). The reasons for using these pharmaceutical agents at these concentrations, are given in Chapter 3. The slice was bathed in these solutions for 3-5 minutes before the next solution was perfused. The electrical activity of p-V59M and control Purkinje cells was recorded using Pulsefit software (HEKA) and sampled at 2.9kHz.

The electrical activity of the Purkinje cells was measured from 1min sections of the continuous recording. The selection method for the 1min sections is described in Chapter 3. Control and p-V59M Purkinje cells showed a bistable phenotype with clear 'up ' states in which the membrane potential was relatively depolarised and action potentials were fired, and 'down' states in which the membrane potential was relatively hyperpolarised and devoid of action potentials (Figure 4.3 A). To measure this property, the percentage of time the cell spent in action potential activity during a 1min period was quantified. This measure was termed the "duration of firing". For cells that were constantly firing, with no 'down' states, the duration of firing was therefore 100%. Firing frequency was measured using Pulsefit software. Any potential deviation above 0mV was classified as an action potential. An average duration of firing and firing rate for each condition was calculated for each mouse. These average values were used in statistical analyses.

The membrane potential of the Purkinje cells during 'up' states was relatively stable and was measured according to the method described in Chapter 2. These data were analysed using an independent samples t-test, and $p < 0.05$ was considered significant. The membrane

potential in ‘down’ states fluctuated, and so could not be analysed in this way. For example, the membrane potential in the ‘down ’ states of the control cell shown in Figure 4.3 A, recorded in aCSF alone, ranged from -68mV at its lowest, to -58mV at its highest.

The statistical analyses that were used to analyse the duration of firing, and the firing rates of p-V59M Purkinje cells were similar to those described in section 3.3.4. For the duration of firing data, statistical analysis could not be performed on the data that was acquired when the cells were bathed in 500μM tolbutamide and synaptic blockers. This was because all control Purkinje cells were firing continuously in this condition; therefore there was no variance in their duration of firing. Similarly, all but one p-V59M Purkinje cell was firing continuously in this condition. The duration of firing of control Purkinje cells in aCSF alone and 500μM tolbutamide was compared using a repeated measures t-test. The duration of firing for p-V59M Purkinje cells was analysed in the same way. To compare the duration of firing of control and p-V59M Purkinje cells in aCSF alone and in 500μM tolbutamide, two independent samples t-tests were carried out.

For the firing frequency data, three repeated measures t-tests were used to compare the firing rates of control Purkinje cells that were bathed in aCSF alone, aCSF with 500μM tolbutamide, and aCSF with 500μM tolbutamide and synaptic blockers. The same tests were used to analyse the data from p-V59M Purkinje cells. In order to compare the firing frequency of control and p-V59M Purkinje cells in the three different treatment conditions, a separate set of three independent samples t-tests were carried out.

Although multiple pairwise comparisons were made, I did not make Bonferroni corrections to the alpha level for these analyses (reasons for this decision are given in section 3.3.4). Thus, $p < 0.05$ was considered statistically significant.

4.3.4 Behavioural testing of p-V59M mice

The body weight of mice can influence their performance on behavioural tests [328], thus the body weights of p-V59M and control mice were measured weekly from 8 to 16 weeks of age.

Motor strength was assessed by the horizontal bar, inverted screen and weight-lifting tests [328]. Motor coordination was assessed by the static rods and accelerating rotarod tests. Further details of these tests are given in Chapter 2. Control (n = 38, 20 males, 18 females) and p-V59M (n = 70, 31 males, 39 females) mice were tested at 12-13 weeks of age (mean = 12.0).

Spontaneous locomotor activity over a 23-hour period was measured using a home-cage activity monitoring system. Control (n = 33, 18 males, 15 females) and p-V59M (n = 55, 24 males, 31 females) mice were tested at 16-18 weeks of age (mean = 16.2).

Spontaneous locomotor activity was also assessed by housing the mice in a standard enclosure that was equipped with a free-running wheel. The usage of this wheel was recorded by a computer, which measured the total time spent running on the wheel, the distance covered, and the maximum and average speeds. Control (n = 42, 21 males, 21 females) and pV59M (n = 73, 31 males, 42 females) were tested at 16-21 weeks of age (mean = 16.7).

4.3.5 Statistical analysis of behavioural data

Several data sets from the behavioural experiments were significantly skewed. The criteria used to determine skewness are given in Chapter 2.

Body weight:

The body weight data were analysed using a mixed between-within ANOVA. Some data points were missing because the body weight of all mice was not measured at all time points. There was no systematic distribution of missing data points (i.e. a similar number of data points were missing for both control and p-V59M mice), thus they were handled by excluding cases list-wise from the ANOVA, and $p < 0.05$ was considered significant for this analysis.

Tests of strength:

The data for the horizontal bar and inverted screen tests were significantly skewed. Thus, both of these data were analysed using two separate Mann-Whitney U tests - one with genotype as the between-subjects factor and the other with sex. As the data sets were tested multiple times, Bonferroni adjustments were made, as discussed in Chapter 2, so $p < 0.025$ was considered statistically significant for these analyses. All p values were two-tailed. The data for the weight-lifting test satisfied all assumptions (Chapter 2) that are required for analysis by two-way ANOVA. Thus, $p < 0.05$ was considered significant for this analysis.

Tests of motor coordination:

The data for the orientation times of the mice on the static rods test were significantly skewed. Therefore these data were analysed using Mann-Whitney U tests, taking genotype and sex as between-subjects variables: $p < 0.025$ was considered significant for these analyses. The data for the transit times of the mice on the static rods test satisfied all assumptions (Chapter 2) required for analysis by mixed between-within ANOVA. Thus, $p < 0.05$ was considered significant for this analysis.

Results for the Rotarod were analysed using a two-way ANOVA, and $p < 0.05$ was considered significant.

Spontaneous activity in activity monitoring enclosures:

To see if there were any differences in the time it took p-V59M and control mice to settle into the activity monitoring enclosures, activity levels in the first four hours were analysed. Activity levels for each hour were considered to be separate dependent variables, and the data for each hour were significantly skewed. Thus, data from each hour were analysed, taking genotype and sex into account, by using two Mann-Whitney U tests: $p < 0.025$ was considered significant for each of the analyses. Two further Mann-Whitney U tests were used to see if activity levels were different between the first and second hours of the testing period depending on the sex or genotype of the mice: $p < 0.025$ was also considered significant for these analyses. The data for the spontaneous activity levels of p-V59M and control mice over the whole 23-hour measurement period satisfied all assumptions, given in Chapter 2, required for analysis by two-way ANOVA. Thus, $p < 0.05$ was considered significant for this analysis.

Spontaneous activity in the running-wheel enclosures:

The data for total time spent on the wheel, distance covered, and maximum speed were significantly skewed Thus, these data were analysed using Mann-Whitney U tests, examining the impact of genotype and sex separately: $p < 0.025$ was considered significant for each of the analyses. The data for the average speed of the mice in the free-running wheels satisfied all assumptions, given in Chapter 2, required for analysis by two-way ANOVA. Thus, $p < 0.05$ was considered significant for this analysis.

4.4 Results

Glucose was not detected in the urine of any p-V59M or control mice. The water intake of the two types of mouse was also not significantly different (Appendix 3, p = 0.440). Thus, p-V59M mice were not diabetic.

There were no significant differences in the body weights of p-V59M and control mice based on genotype (p = 0.766) and no significant interaction between genotype and sex (p = 0.224). However, as expected, male mice were significantly heavier than females (p = 0.045, Appendix 3).

In all two-way ANOVAs that are reported below, there were no interactions between sex and genotype. Furthermore, in all analyses there were very few differences based on sex - those that were found are reported below. Thus, unless otherwise stated, the statistical significances reported below are confined to comparisons based on genotype. Male and female data have been pooled in all the figures presented.

4.4.1 Semi-quantitative RT-PCR of Kir6.2-V59M in p-V59M mice

Kir6.2 mRNA amplification was seen in all RT+ cDNA samples, but no RT- controls (Figure 4.1 A, B). Thus the original RNA samples were free of significant amounts of contaminating genomic DNA. When the RT+ samples were digested with BtsCI, only two bands were seen in all of the samples from control mice (Figure 4.1 C), which confirmed that only wild-type Kir6.2 was present. By contrast, digestion of cDNA samples from p-V59M mice resulted in the presence of three clear bands in samples from the cerebellum and triceps muscle (Figure 4.1 D). A faint third band was also seen in the cDNA sample from the brain minus the cerebellum. There were only two bands in p-V59M heart cDNA samples.

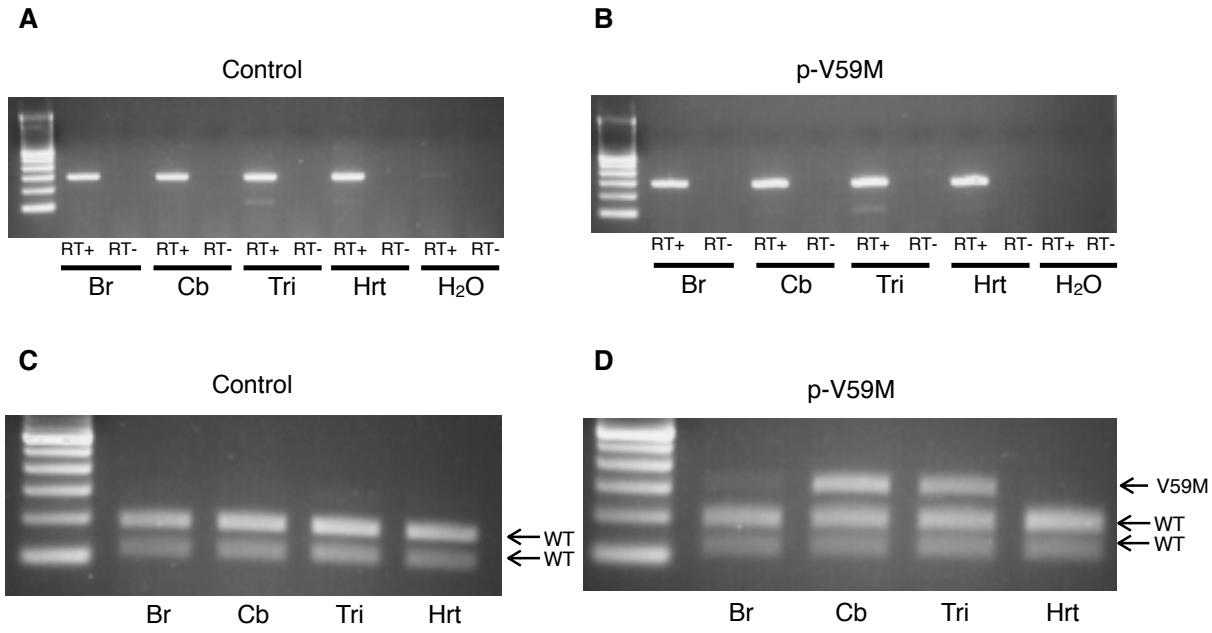

Figure 4.1 Kir6.2 expression in the p-V59M mouse

Kir6.2 expression in tissues isolated from adult (21 to 23 weeks-old) control and p-V59M mice. (**A, B**) Identical RNA aliquots for each tissue were processed in a reverse transcription reaction with reverse transcriptase included (RT+) or omitted (RT-). Amplification of the Kir6.2 transcript was only seen in RT+ samples. Therefore there was little genomic DNA contaminating the RNA samples. (**C, D**) RT+ cDNA samples were digested with BtsCI, which cuts wild-type (WT) but not mutant (V59M) Kir6.2 cDNA. Thus, the presence of two bands indicated the presence of only wild-type Kir6.2 and three bands indicated wild-type Kir6.2 plus Kir6.2-V59M expression. Br, brain minus cerebellum; Cb, cerebellum; Tri, triceps; Hrt, heart. Images are representative of experiments on 4 control and 4 p-V59M mice.

Thus, although parvalbumin expression has been seen in the heart, the parvalbumin-Cre mouse did not induce measurable transgene expression in this tissue. In summary, these data indicate that Kir6.2-V59M is expressed relatively strongly in the cerebellum and triceps muscle of p-V59M mice, and it is present, but at a lower level, in extra-cerebellar brain regions.

4.4.2 Expression pattern of Cre in Pv-Z/EG mice

At 2 weeks of age GFP expression in Pv-Z/EG mice was seen predominantly in the cerebellum (Figure 4.2 A, B). Many, but not all, Purkinje cells were labelled. Cells in the granular and molecular layer were also labelled. These were likely to be stellate and basket cells [319]. Expression in the neocortex and hippocampus was extremely sparse - very few neurons were labelled (Figure 4.2 C, D). At 12 and 16 weeks of age, the expression pattern in the cerebellum was largely the same as at 2 weeks of age (Figure 4.2 A, B), but neocortical expression was markedly increased (Figure 4.2 C). Hippocampal expression was higher at 12 and 16 weeks compared to 2 weeks of age, but even in adulthood very few neurons were stained with GFP. Some GFP-expressing cells were also seen in other regions, such as the thalamus and basal ganglia (data not shown). Overall, it seemed that the general pattern of Cre expression from parvalbumin-Cre mice matched published data on the location of parvalbumin expression. However, GFP-expressing cells were less widespread than might have been expected from these reports, suggesting that only a proportion of all parvalbumin-expressing neurons expressed Cre.

The low number of GFP-expressing cells in the neocortex of 2-week-old mice, compared to that seen in 12- and 16-week-old mice, is consistent with the developmental pattern of parvalbumin expression, which is described in section 4.2.1.

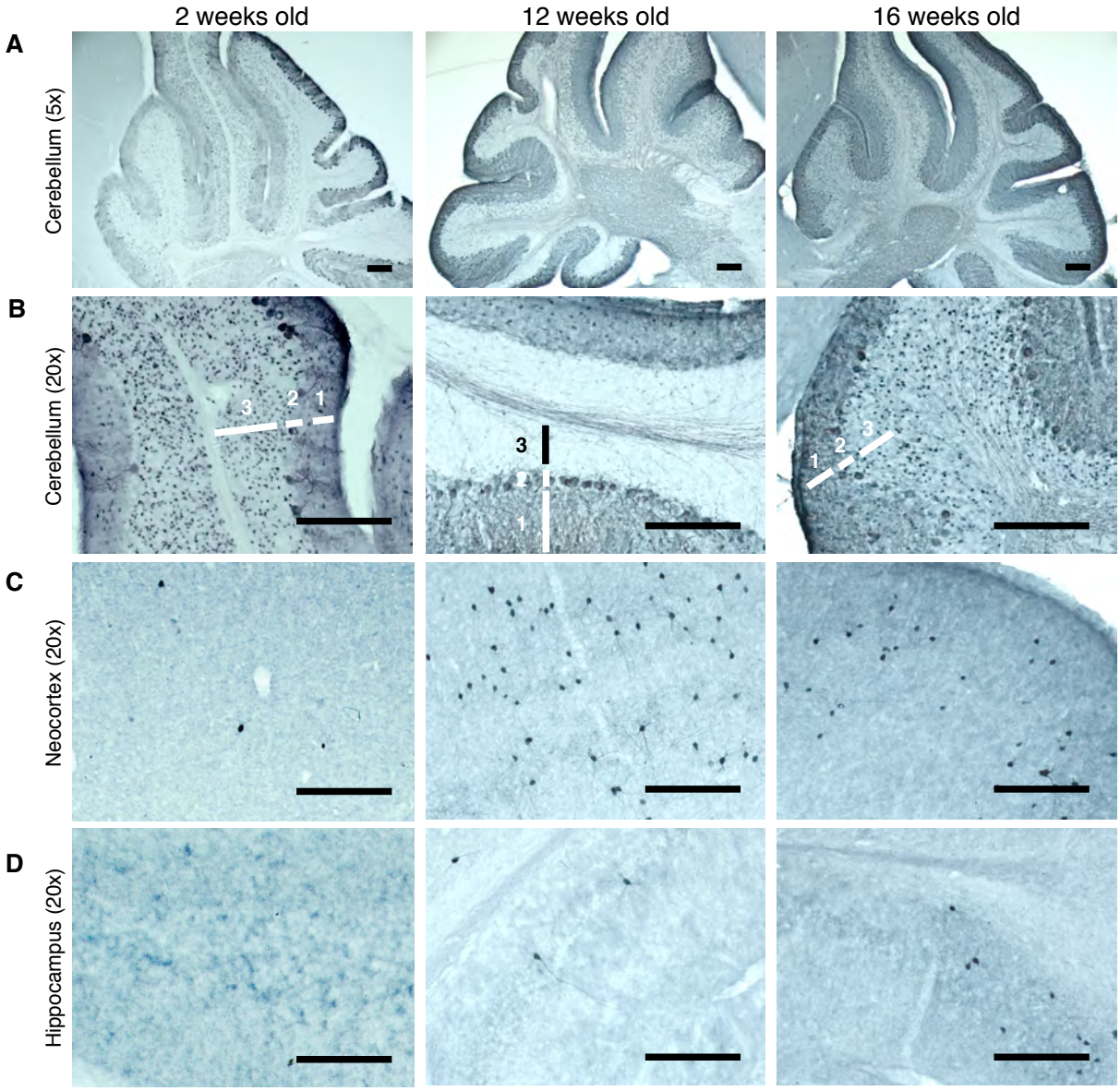

Figure 4.2 Pattern of Cre expression in Pv-Z/EG mice via expression of GFP as a reporter

GFP expression in the brain of 2-week old (left), 12-week old (middle) and 16-week old (right) Pv-Z/EG mice. GFP was stained by the ABC method and thus appears black. GFP expression was induced by the presence of Cre, which was targeted to specific neurons by the parvalbumin-Cre transgene. As parvalbumin-Cre mice were used to make p-V59M mice, the pattern of GFP staining also indicates where Kir6.2-V59M will be expressed in p-V59M mice. Images are representative of 2-3 Pv-Z/EG mice at each age. Horizontal black bars in the lower right corner represent 200µm.

(**A, B**) GFP was expressed in many Purkinje cells. Neurons in the granular and molecular layers were also stained. These were likely to be stellate and basket cells. (**B**) 1 = molecular layer, 2 = Purkinje cell layer, 3 = granular layer. **(C**) Very few cells in the neocortex of 2-week old Pv-Z/EG mice expressed GFP. A greater number of neocortical cells expressed GFP in 12-week old and 16-week old Pv-Z/EG mice. Thus, neocortical expression of GFP, which was driven by parvalbumin-Cre expression, was developmentally regulated postnatally. Stained neocortical cells were sparsely distributed. (**D**) Very few hippocampal neurons expressed GFP at 2-, 12- and 16-weeks old.

These immunohistochemistry results complement the RT-PCR results described is section 4.4.1. In adult mice, many cells in the cerebellum expressed GFP, which correlates with the high levels of Kir6.2-V59M seen in the RT-PCR experiments. By contrast, relatively few neurons in the rest of the brain expressed GFP, which explains why the third band in the RT-PCR analysis of the 'brain-minus-cerebellum' sample was relatively weak.

4.4.3 The proportion of bistable control and p-V59M Purkinje cells

Control cells

Some Purkinje cells from control mice showed a bistable profile of firing activity, with clear 'up' states in which action potentials were fired and 'down' states that were devoid of action potentials (Figure 4.3 A). Other cells from these mice showed constant firing behaviour, with no 'down' states.

In the basal state, 50% of control cells were bistable (Table 4.1). The addition of 500µM tolbutamide did not cause an obvious alteration in the proportion of control cells that were bistable.

However, in 500µM tolbutamide and synaptic blockers, no control Purkinje cells were bistable - all of them showed constant firing behaviour in this condition. This indicates that the 'down' states of the bistable activity are initiated or regulated by synaptic innervation of the Purkinje cells.

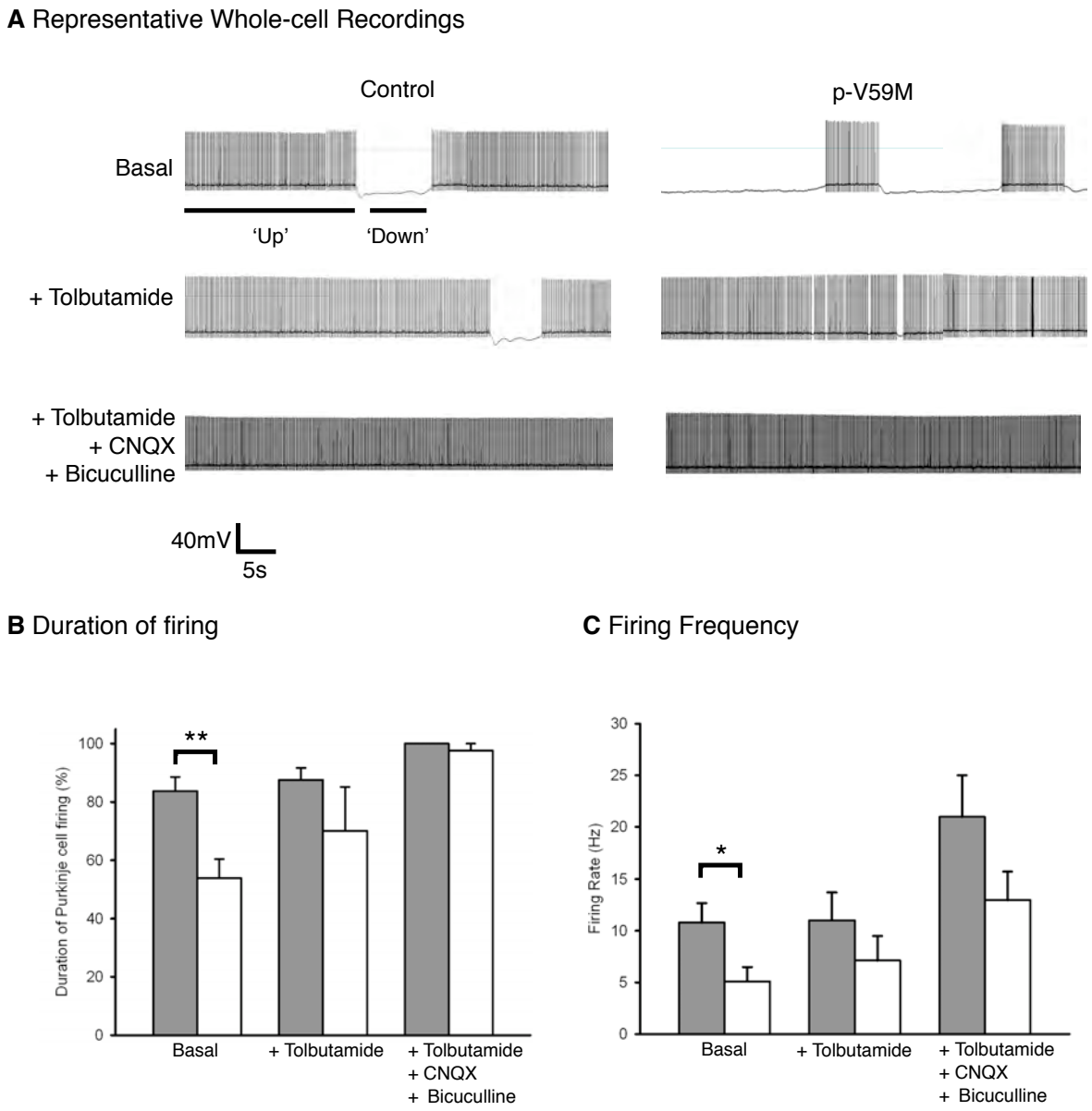

Figure 4.3 K_{ATP} channel activity in cerebellar Purkinje cells of p-V59M mice

(**A**) Representative whole-cell recordings from control (left panels) and p-V59M (right panels) mice. For each mouse, traces show the basal activity of a cell (top row), then activity of the same cell in the presence of 500µM tolbutamide (middle row), and subsequently the same cell in the presence of 500µM tolbutamide + 10µM CNQX + 20µM bicuculline (bottom row). 50% of control, and 80% of p-V59M Purkinje cells exhibited a bistable phenotype with clearly discernible 'up' and 'down' states, which are labelled in the basal trace from the control Purkinje cell. (**B**) Duration of firing of control (grey bars) and p-V59M (white bars) Purkinje cells. Basal (left), 500µM tolbutamide (middle), and 500µM tolbutamide + 10µM CNQX + 20µM bicuculline (right). The duration of firing was expressed as a percentage of time over a one minute period. **, $p < 0.01$, independent samples t-test. (**C**) Firing frequency of control (grey bars) and p-V59M (white bars) Purkinje cells. Basal (left), 500µM tolbutamide (middle), and 500µM tolbutamide + 10µM CNQX + 20µM bicuculline (right). *, $p < 0.05$, independent samples t-test. The total number of action potentials in a one minute period was quantified to determine the firing frequency of the cell. (**B, C**) Control: n = 8 mice, mean age 17 days, 21 neurons. p-V59M: n = 6 mice, mean age 16 days, 20 neurons. Data are mean ± SEM of n mice.

p-V59M cells

Compared to controls, a greater proportion of p-V59M Purkinje cells (80%) were bistable (Table 4.1). In 500µM tolbutamide, the proportion of bistable p-V59M Purkinje cells was reduced to a level similar to control Purkinje cells. These results indicate that the increased K_{ATP} current in p-V59M Purkinje cells promotes a bistable profile of firing.

Consistent with the results from the control cells, almost all p-V59M Purkinje cells showed constant firing behaviour when 500µM tolbutamide and synaptic blockers were present.

Table 4.1 Percentage of cells that showed a bistable profile of activity

Condition	Control	p-V59M
Basal	50% (11 of 22)	80% (16 of 20)
500µM tolbutamide	47% (9 of 19)	56% (9 of 16)
500µM tolbutamide and synaptic blockers	0% (0 of 18)	8% (1 of 12)

4.4.4 The duration of firing of control and p-V59M Purkinje cells

The effect of tolbutamide: the within-subjects factor

The duration of firing of control Purkinje cells did not change when they were treated with tolbutamide (Figure 4.3 B, p = 0.406). The duration of firing of p-V59M Purkinje cells also did not change when tolbutamide was added (p = 0.315).

Comparing control and p-V59M Purkinje cells: the between-subjects factor

In the basal state, the duration of firing of p-V59M cells was significantly lower than controls (p = 0.003). However, in 500µM tolbutamide the mean duration of firing was not significantly different for the two types of mouse (p = 0.227). These results indicate that the duration of

firing of the Purkinje cells in the basal state was dependent upon the genotype of the animal. In the presence of 500μM tolbutamide, however, the duration of firing was not different between the mice. Thus, it is likely that expression of mutant K_{ATP} channels in p-V59M Purkinje cells predisposes them to be in 'down' states of activity - i.e. to be hyperpolarised and not firing action potentials.

4.4.5 Membrane potential of p-V59M Purkinje cells

Because the membrane potentials of control and p-V59M Purkinje cells fluctuated between 'up' and 'down' states, it was impossible to measure an overall mean membrane potential for these cells. However, the average membrane potential of 'up' states of p-V59M Purkinje cells were not significantly different from those of control cells ($p = 0.239$; data not shown).

4.4.6 The firing frequency of control and p-V59M Purkinje cells

The effects of tolbutamide and synaptic blockers: the within-subjects factors

The firing rates of control Purkinje cells were not significantly changed when tolbutamide was added (Figure 4.3 C, $p = 0.809$), which is consistent with the notion that wild-type K_{ATP} channels in Purkinje cells are largely closed under normal conditions (Chapter 3). However, when synaptic blockers were added along with tolbutamide, the firing rates of control Purkinje cells were significantly increased ($p = 0.001$ compared to the firing rate in tolbutamide alone, $p = 0.005$ compared to the firing rate in the basal state). These data indicate that control Purkinje cells experience tonic inhibition. The removal of that inhibition causes an increase in firing activity, and is the intrinsic activity of the Purkinje cell.

The firing rates of p-V59M Purkinje cells were increased by the addition of tolbutamide, but this trend did not reach statistical significance ($p = 0.203$). This result is discussed in more detail in section 4.5.5. However, consistent with the results from the control Purkinje cells, when synaptic blockers were added along with tolbutamide, the firing rates of p-V59M Purkinje cells were significantly increased ($p = 0.015$ compared to the firing rate in tolbutamide alone, $p = 0.020$ compared to the firing rate in the basal state).

Comparing control and p-V59M Purkinje cells: the between-subjects factor

The firing rates of p-V59M Purkinje cells were lower than controls in the basal state ($p = 0.042$). However, in the presence of 500μM tolbutamide there was no significant difference in the firing rates of Purkinje cells from the two types of mice ($p = 0.318$). This indicates that the additional K_{ATP} current in p-V59M Purkinje cells causes their basal firing rates to be significantly lower compared to controls.

In the presence of 500μM tolbutamide and synaptic blockers, the firing rates of control and p-V59M Purkinje cells were not significantly different ($p = 0.153$). Thus, when K_{ATP} currents and synaptic inputs were blocked, the intrinsic firing rate of Purkinje cells did not seem to be different. This suggests that there were no major developmental changes that occurred in these cells in mice expressing mutant gain-of-function K_{ATP} channels.

4.4.7 Tests of muscle strength in p-V59M mice

The scores of p-V59M and control mice on the horizontal bar test were not significantly different (Figure 4.4 A, $p = 0.187$). However, the scores for both types of mice were significantly negatively skewed due to a ceiling effect - 89% of control and 96% of p-V59M mice achieved the maximum score (5).

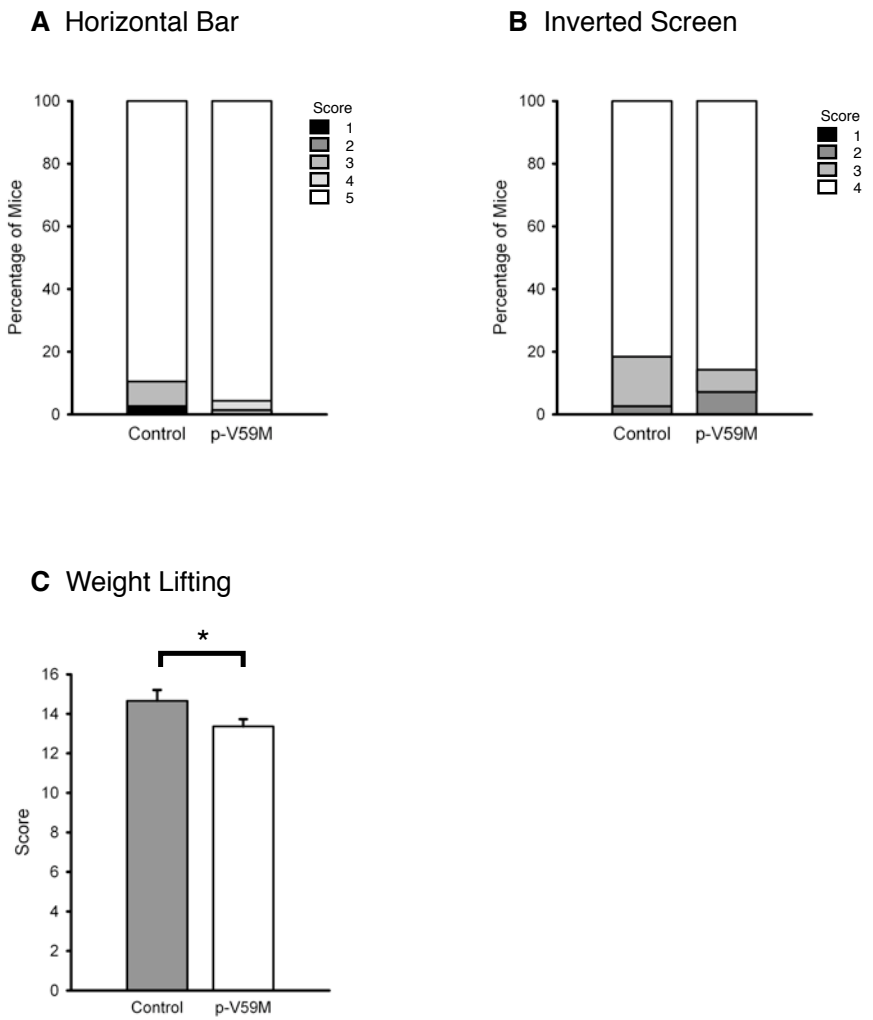

Figure 4.4 Behavioural phenotyping: Muscle strength tests at 12 weeks of age

Performance of 12-week old control (n=38, mean age = 12.0 weeks) and p-V59M (n=70, mean age = 12.0 weeks) mice on three tests of muscle strength. Percentage of control (left bars) and p-V59M (right bars) mice achieving the indicated score on the horizontal bar (**A**) and inverted screen (**B**) tests. There were no significant differences between control and p-V59M mice on either test. (**C**) Mean scores ± SEM for control (grey bar) and p-V59M (white bar) mice on the weight lifting test. *, $p < 0.05$, two-way ANOVA.

Similarly, the scores of p-V59M and control mice on the inverted screen test were not significantly different (Figure 4.4 B, p = 0.666). Again, however, the scores of the two types of mice were significantly skewed due to a ceiling effect - 82% of control and 86% of p-V59M mice achieved the maximum score. There was also no significant difference in the time that the mice managed to stay on the inverted screen (p = 0.732, data not shown) - thus, the scoring system had not masked any differences.

In contrast, scores on the weight-lifting test were normally distributed and p-V59M mice scored significantly lower than controls, indicating that they were weaker (Figure 4.4 C, p = 0.048).

In summary, the weight-lifting test indicated that p-V59M mice were weaker than controls. However, the performance of the two types of mice were not significantly different on the horizontal bar and inverted screen tests, which were also reliant on muscle strength. Possible explanations for these results are presented in section 4.5.7.

4.4.8 Tests of motor coordination in p-V59M mice

Very few mice fell from the static rods: 5% of control mice (2 of 38) fell from the 9mm rod, but none fell from any of the others, and no p-V59M mice fell from any of the rods.

There was no significant difference in the orientation times of p-V59M and control mice on the three different rods (Figure 4.5 A; widest rod, p = 0.740; middle rod, p = 0.631; thinnest rod, p = 0.547). Similarly, the transit times of p-V59M and control mice were not significantly different (p = 0.754). Thus, the performance of p-V59M and control mice on the static rods test was not significantly different.

A Multiple Static Rods

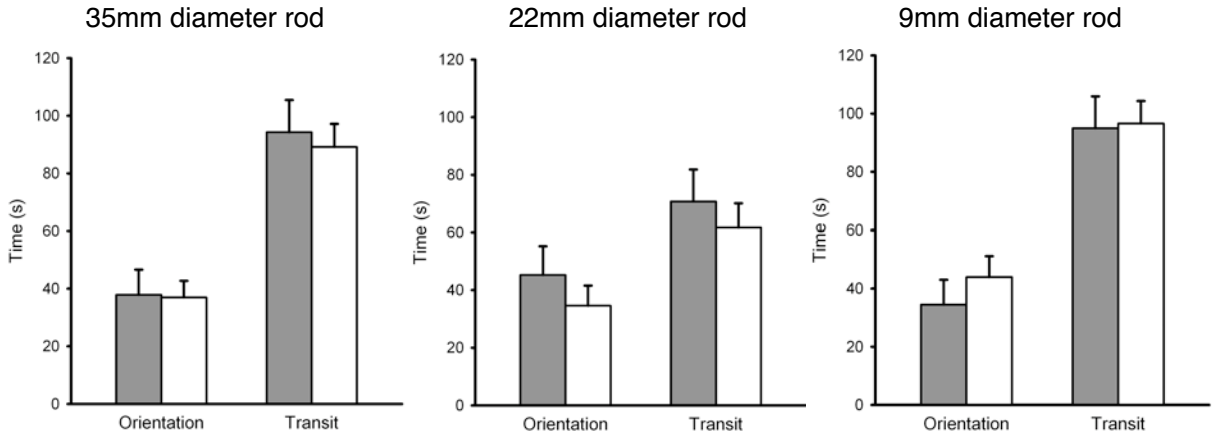

B Rotarod

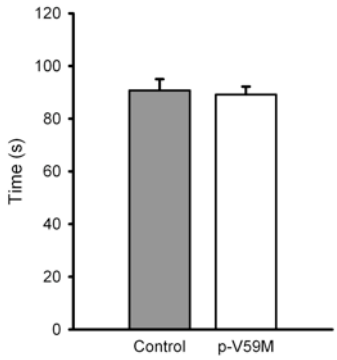

Figure 4.5 Behavioural phenotyping: Motor coordination tests at 12 weeks of age

Motor coordination tests carried out on 12-week old control (grey bars, n=38) and p-V59M (white bars, n=70) mice. (**A**) Orientation and transit times of mice on three static rods of various diameters, as indicated. Mean transit time on the 22mm rod was lower, regardless of sex or genotype, than the mean transit time on the 35mm or the 9mm rod (mixed between-within ANOVA). There were no other statistically significant differences between the mice. Note that although mean orientation times are plotted above, the data are significantly skewed. Thus, they were analysed using Mann-Whitney U tests. Transit times were analysed using two-way ANOVAs. (**B**) Time before falling from the accelerating rotarod for control (grey bar) and p-V59M (white bar) mice. There was no difference based on genotype (two-way ANOVA). Female mice managed to stay on the rotarod longer than males, but approximately equal numbers of male and female control and p-V59M mice were tested. Therefore data are presented with sexes pooled. Data are mean ± SEM.

However, the performance of the mice, regardless of genotype or sex, was not the same on the three different sizes of rod ($p < 0.001$). The mean transit time on the 22mm diameter rod was significantly lower than on the other two rods. The littermate controls of n-V59M mice also showed this pattern of performance on the three static rods [170].

The reason for this difference is unclear, but it is likely that performance improved on the 22mm rod compared to the 35mm rod because the mice had practiced and were comfortable with the demands of the task. It is likely that their performance was then worse on the 9mm rod because, unlike the 35mm and 22mm rod, the mice cannot stand on top of this rod and thus it is the most difficult and would also induce the greatest anxiety out of the three.

The performance of p-V59M and control mice on the rotarod was not significantly different (Figure 4.5 B, $p = 0.633$). However, on average, female mice managed to stay on the rotarod longer than males ($p = 0.045$), perhaps because they were smaller.

4.4.9 Spontaneous locomotor activity

When p-V59M and control mice were housed in a home-cage-like environment equipped with activity monitoring sensors, their activity levels in the first four hours after transfer were not significantly different (Figure 4.6 A; hour 1, $p = 0.289$; hour 2, $p = 0.143$; hour 3, $p = 0.966$; hour 4, $p = 0.270$). However, the activity of both types of mice was significantly higher in hour 1 compared to hour 2 ($p < 0.001$). These results indicated that both p-V59M and control mice settled into the new enclosure by the end of one hour; after this, their activity levels were constant for the following three hours.

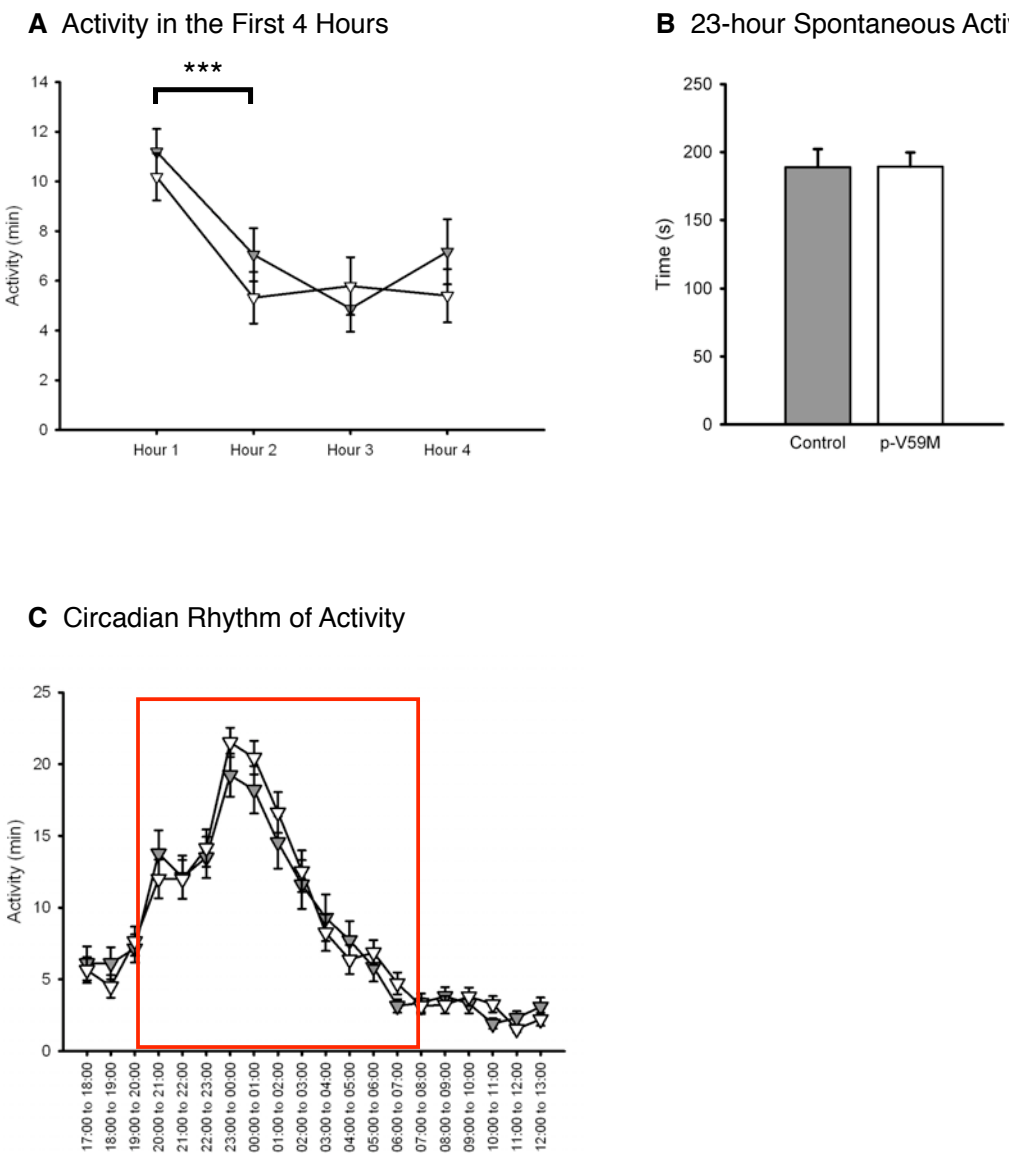

Figure 4.6 Spontaneous locomotor activity: Activity monitors at 16 weeks of age

Spontaneous locomotor activity measurements for 16-week old (mean age = 16.2 weeks) control (grey triangles or grey bars, n=33) and p-V59M (white triangles or white bars, n=55) mice. (**A**) Activity in the first 4 hours of housing in the sensor-equipped home cage. There were no significant differences based on sex or genotype at each time point (Mann-Whitney U tests). However, activity in the first hour was significantly higher than at hour 2 for both types of mouse. ***, $p < 0.001$, Mann-Whitney U test. (**B**) Total amount of spontaneous locomotor activity over a 23-hour period. There was no significant difference based on genotype (two-way ANOVA). Female mice were more active than males, but approximately equal numbers of male and female control and p-V59M mice were tested. Therefore data are presented with sexes pooled. (**C**) Spontaneous activity per-hour over a 20-hour period after the mice had settled into the sensor-equipped home cage for at least 1 hour. The red box indicates the duration of lights off in the animal house. There were no obvious differences in the circadian pattern of activity of control and p-V59M mice. Data are mean ± SEM.

There was no difference in the activity of p-V59M and control mice over a 23-hour period (Figure 4.6 B, $p = 0.834$). However, female mice (regardless of genotype) were more spontaneously active over a 23-hour period than males ($p = 0.032$). This is consistent with reports that female mice show greater spontaneous activity than males in a variety of tasks [329-331].

There was also no obvious difference in the circadian pattern of the spontaneous activity of p-V59M and control mice (Figure 4.6 C).

4.4.10 Spontaneous use of free-running wheels

Differences based on genotype

p-V59M mice tended to spend more time on the free-running wheel than controls (Figure 4.7 A), but this trend did not reach statistical significance ($p = 0.054$). However, p-V59M mice ran almost twice as far, on average, as controls (Figure 4.7 B, $p = 0.015$), and ran at a higher average speed than controls (Figure 4.7 C, $p = 0.007$). These results indicate that p-V59M mice are hyperactive compared to controls.

The maximum speeds recorded by p-V59M and control mice were not significantly different (Figure 4.7 D, $p = 0.322$), which indicated that expression of Kir6.2-V59M in parvalbumin-expressing cells did not impair the ability of the mouse to run at speed.

Differences based on sex

Female mice spent more time on the wheel than males ($p = 0.001$). In addition, female mice ran further than males ($p < 0.001$), and with higher average speed ($p = 0.001$). Although the average speeds of males and females differed, their maximum speeds were not significantly different ($p = 0.446$).

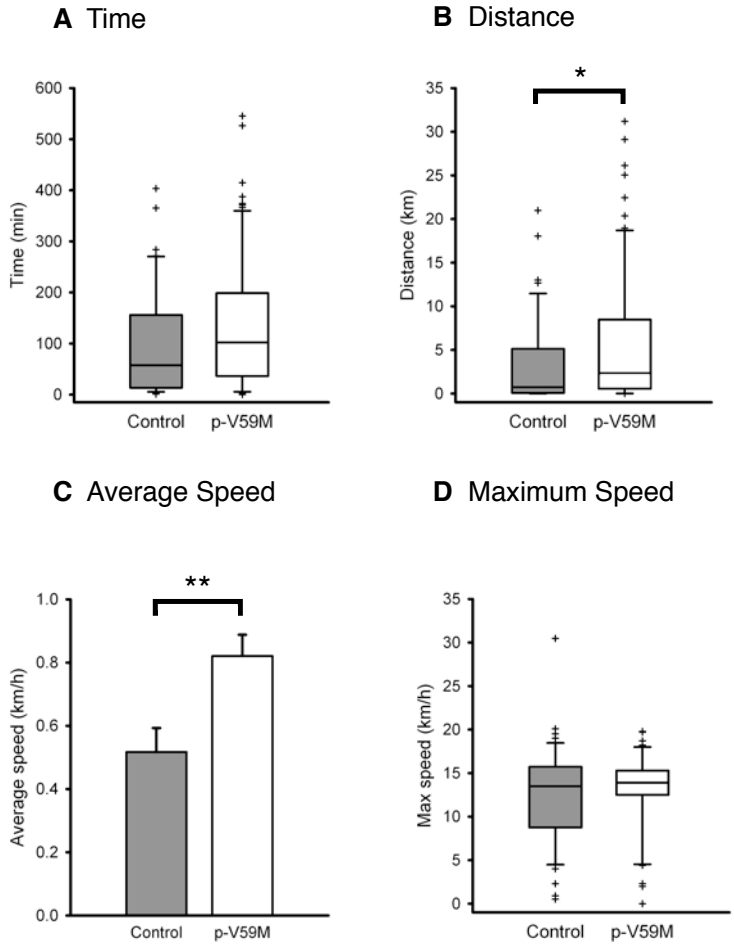

Figure 4.7 Spontaneous locomotor activity: Free-running wheels 16 weeks of age

The spontaneous locomotor activity of 16-week old (mean age = 16.7) control (grey bars, n = 42) and p-V59M (white bars, n = 73) mice was recorded over a 23-hour period while the mice were housed in enclosures that were equipped with running wheels. (**A**) Total time spent on the running wheel. There were no significant differences between the mice, though p-V59M mice tended to run for longer than control mice ($p = 0.054$, Mann-Whitney U test). (**B**) Total distance covered on the running wheel. p-V59M mice ran further than controls. *, $p < 0.05$, Mann-Whitney U test. (**C**) Average speed on the running wheel. p-V59M mice ran with a faster average speed than control mice. **, $p < 0.01$. (**D**) Maximum speed on the running wheel. There were no significant differences between control and p-V59M mice (Mann-Whitney U tests). In figures A, B and C, female mice scored higher than males. Approximately equal numbers of male and female control and p-V59M mice were tested, therefore data are presented with sexes pooled. For box plots, the box is bounded by the 25th and 75th percentile and is bisected by the median. Whiskers extend to the 10th and 90th percentile and outliers, which lie beyond the whiskers, are indicated by a cross. Figure C shows mean ± SEM.

These results are consistent with previous reports that female mice are more active than males on free-running wheels [331]. They are also consistent with the results from section 4.4.9 above.

4.5 Discussion

4.5.1 Differences in genetic backgrounds

The aim of the experiments presented in this chapter was to identify the importance of parvalbumin-expressing neurons in iDEND. To do this, I carried out a series of behavioural experiments on the p-V59M mouse model, which expressed Kir6.2-V59M mRNA in parvalbumin-expressing cells. These experiments had also been carried out on n-V59M mice, which expressed Kir6.2-V59M in all neurons. Thus, by comparing the results from p-V59M and n-V59M mice, the relative importance of parvalbumin-expressing neurons might be revealed.

p-V59M mice and n-V59M mice were created by crossing parvalbumin-Cre and nestin-Cre mice, respectively, with ROSA mice. Parvalbumin-Cre and nestin-Cre mice were congenic on a C57BL/6 background. ROSA mice initially had a mixed 129/SV and C57BL/6 background, and were backcrossed to a C57BL/6 background for at least 3 generations before mating. However, in order to be considered fully congenic, a strain must be backcrossed for at least 10 generations (Jax bulletin #4, 2000), so it is possible that non-C57BL/6 alleles were present in ROSA mice. Therefore, by crossing congenic parvalbumin-Cre and nestin-Cre mice with ROSA mice on a mixed background, although the progeny of these breeding pairs were likely to be largely C57BL/6 in character, they may have received some non-C57BL/6 alleles.

Mice with different genetic backgrounds may have differences in gene expression [332] and these differences may affect the electrophysiology of their neurons [333] and their behavioural characteristics [334]. Thus, it is possible that genetic background differences between the progeny of nestin-Cre/ROSA breeding pairs, and parvalbumin-Cre/ROSA breeding pairs may have influenced the results of the electrophysiological and behavioural experiments in which they were used. This could complicate comparison of the results.

In addition, nestin-Cre mice exhibit mild hypopituitarism, reduced body weight and length, and are less tolerant to glucose challenge, compared to their wild-type littermates [102, 335, 336]. This could indicate that expression of Cre in neurons alters brain function. Alternatively, the insertion of the nestin-Cre transgene may have disrupted the function of neighbouring loci [335]. The phenotype of the nestin-Cre mouse does not impact upon the results that are presented in Clark *et al.* (2010), because n-V59M mice were compared with nestin-Cre mice, so the effects of the nestin-Cre transgene were controlled for. However, the effects of the nestin-Cre transgene may complicate comparison of the results from nestin-Cre and parvalbumin-Cre mice.

I have collated the results from experiments that were carried out on the Cre-expressing littermate controls of n-V59M and p-V59M mice. I have also included, where possible, the results from experiments that were carried out on the Cre-expressing littermate controls of m-V59M mice, which had a mixed C57BL/6-129/SV background and expressed Cre in muscle tissue alone [102]. Finally, I have also included, where possible, the results from experiments that were carried out on ROSA littermate controls of n-V59M mice, which possessed the Kir6.2-V59M transgene alone; note that these mice did not express mutant K_{ATP} channels as they did not express Cre. These data are shown in Tables 4.2 and 4.3. Data for nestin-Cre, ROSA and Mck-Cre mice were taken from Clark *et al.* (2010). The aim of

this comparison was to see if there were any obvious differences in the phenotypes of the four types of control mice.

Electrophysiology

Purkinje cells from parvalbumin-Cre mice often showed a bistable mode of firing; the membrane potentials of these cells fluctuated, with easily identifiable sections of depolarisation and hyperpolarisation (Figure 4.3 A). Spikes were only fired during the depolarised sections. This pattern of activity was not seen in Purkinje cells from nestin-Cre or ROSA mice (Chapter 3, and Table 4.2).

The composition of the extracellular and intracellular solutions used for both sets of experiments were the same, so this could not have influenced the result. Electrophysiological studies of the rat cerebellum have shown that Purkinje cell bistability can be induced by blocking hyperpolarisation-activated non-specific cation channels (I_H) with the pharmacological agent ZD7288 [293]. However, I did not use ZD7288 in my experiments, so blockage of I_H is unlikely to be the reason why parvalbumin-Cre Purkinje cells were bistable.

Purkinje cells may also exhibit a *tri*-modal pattern of firing, which is characterised by periods of constant spiking, followed by brief periods of high-frequency spiking (a 'burst'), and finally a period of electrical silence, in which action potentials are not fired [337]. In my experiments, however, I did not observe 'burst' firing prior to the periods of electrical silence (Figure 4.3 A). Thus, Parvalbumin-Cre Purkinje cells were not firing according to a trimodal pattern.

Although the mechanism that lead to bistability of parvalbumin-Cre Purkinje cells is unclear, the firing rates of nestin-Cre, ROSA and parvalbumin-Cre Purkinje cells in the basal state were very similar (Table 4.2). Furthermore, the intrinsic firing rates were also similar. Thus, although it is possible that differences in the expression pattern of Cre, and/or differences in

the genetic backgrounds of the mice, caused parvalbumin-Cre Purkinje cells to fire in a bistable manner, these differences were not critical in determining the action potential firing frequency of the cells.

Body weight

All mice were fed the same diet. However, at 12 weeks of age, ROSA littermates of **n**-V59M mice were somewhat heavier than nestin-Cre, parvalbumin-Cre and Mck-Cre mice, which were similar in body weight (Table 4.3). Although this difference may suggest that the expression of Cre (in brain or muscle tissue) causes reduced body weight, this is unlikely to be the case because ROSA littermates of **m**-V59M mice were approximately the same weight as nestin-Cre, parvalbumin-Cre and Mck-Cre mice (data not shown, [102]). Thus, the body weights of the different control mice may be different from each other, but the reason for this difference is unclear.

Tests of muscle strength

The performance of the four types of control mice was broadly similar on the three tests of muscle strength (Table 4.3), although the average score of parvalbumin-Cre mice on the weight-lifting test was somewhat higher than nestin-Cre, Mck-Cre and ROSA mice.

Tests of motor coordination

The performance of parvalbumin-Cre mice on the motor coordination tests was quite different from that of nestin-Cre, ROSA and Mck-Cre mice (Table 4.3). Parvalbumin-Cre mice fell from the rotarod earlier than nestin-Cre, ROSA and Mck-Cre mice, which fell after approximately the same amount of time. On the static rods, the transit times of ROSA and Mck-Cre mice were broadly similar. Nestin-Cre mice completed the task somewhat faster than the other controls, and parvalbumin-Cre mice took longer to complete the task. Also, a lower proportion of parvalbumin-Cre mice fell from the 9mm static rod compared to nestin-Cre, ROSA and Mck-Cre mice. These results indicate that parvalbumin-Cre mice performed

somewhat differently compared to nestin-Cre, ROSA and Mck-Cre mice on the tests of motor coordination.

23-hour spontaneous locomotor activity

Nestin-Cre and parvalbumin-Cre showed similar levels of total spontaneous locomotor activity over a 23-hour period. The activity levels of ROSA mice were some lower than the two Cre-expressing control mice. Thus, it is possible that Cre expression in the brain, even in a subset of neurons, could have induced higher spontaneous locomotor activity.

Spontaneous usage of the free-running wheels

Nestin-Cre and parvalbumin-Cre mice showed clear differences in their usage of the free-running wheel. Nestin-Cre mice used the free-running wheel almost four times longer than parvalbumin-Cre mice, and they also ran three times as far and with three times the average speed. ROSA mice performed in a similar way to nestin-Cre mice on the free-running wheels. Thus, in this case the unequal performance of parvalbumin-Cre and nestin-Cre mice may be due to genetic background differences.

In summary, the nestin-Cre and parvalbumin-Cre littermate controls of n-V59M and p-V59M mice were likely to have differences in their genetic backgrounds, and also expressed Cre in different neurons, which might have influenced their phenotypes. Indeed, there were some obvious differences between the mice. Although parvalbumin-Cre Purkinje cells often showed a bistable firing profile, which was never seen in nestin-Cre Purkinje cells, the mean basal and intrinsic firing rates of the Purkinje cells from these two types of mice were not obviously different. Therefore, the firing rates of n-V59M and p-V59M Purkinje cells may be compared. The most conspicuous difference between the mice was in the usage of the free-running wheels: nestin-Cre mice ran longer, further, and with greater average speed than parvalbumin-Cre mice.

Table 4.2 Comparison of Purkinje cell electrophysiology of control mice

All values are rounded to the nearest integer and the SEM is provided where possible.

Characteristic	Nestin-Cre	Parvalbumin-Cre	ROSA (controls of n-V59M mice)
Bistability of Purkinje cells in the basal state	No bistable cells	50% bistable cells	No bistable cells
Mean firing rate of Purkinje cells in aCSF alone	10 ± 3 Hz (n=3)	11 ± 2 Hz (n=8)	10 ± 1 Hz (n=3)
Mean firing rate of Purkinje cells in aCSF, tolbutamide and synaptic blockers[1]	19 Hz (n=2)	21 ± 4 Hz (n=8)	17 Hz (n=1)

[1] Firing rates of Purkinje cells in aCSF, tolbutamide and synaptic blockers were collected by cell-attached patch-clamping for nestin-Cre and ROSA mice, and by whole-cell patch-clamping for parvalbumin-Cre mice.

Table 4.3 Comparison of the performance of control mice on behavioural tests.

SEM is provided where applicable.

Characteristic	Nestin-Cre	Parvalbumin-Cre	Mck-Cre	ROSA (littermates of n-V59M mice)
Mean body weight at 12 weeks old	Males: 29 ± 1g, Females: 22 ± 1g	Males: 31 ± 1g, Females: 24 ± 1g	Males: 30 ± 1g, Females: 24 ± 1g	Males: 35 ± 1g, Females: 27 ± 1g
Percentage of mice with maximum score on the horizontal bar test	95%	90%	90%	85%
Percentage of mice with maximum score on the inverted screen test	70%	80%	70%	75%
Mean score on the weight-lifting test	13 ± 0.2	14.5 ± 0.5	12.5 ± 0.3	13 ± 0.2
Mean time before falling from rotarod	113 ± 2 s	91 ± 4 s	113 ± 3 s	106 ± 3 s
Mean transit time on 9mm diameter static rod	40 ± 6 s	95 ± 11 s	52 ± 11 s	57 ± 8 s
Percentage of mice that fell from the 9mm static rod	10%	5%	15%	20%
Mean 23-hour spontaneous activity	183 ± 15 min	190 ± 13 min	n/a	153 ± 12 min
Time spent on free-running wheels[2]	200 ± 22 min	58 min	n/a	183 ± 19 min
Distance run on free-running wheels[2]	3.8 km	1.2 km	n/a	4.2 km
Average speed on free-running wheels	1.3 ± 0.1 km/hr	0.5 ± 0.1 km/hr	n/a	1.3 km/hr

[2] Data for the distance run on the free-running wheels for all mice were significantly skewed. Furthermore, time spent on the running wheel for parvalbumin-Cre mice, and average speed on the running wheel for ROSA mice, were also significantly skewed. Thus, for these data median values are provided. Other values are averages.

Similarly, the performance of parvalbumin-Cre and nestin-Cre mice was somewhat different on the tests of motor coordination. Thus, comparisons between n-V59M and p-V59M mice on these tasks should be made with caution.

4.5.2 The p-V59M mouse expressed Kir6.2-V59M in a restricted population of neurons

Immunohistochemistry experiments have shown that parvalbumin expression is expressed throughout the cortex, hippocampus and cerebellum [313]. However, Cre expression from parvalbumin-Cre mice was not so widespread. Semi-quantitative RT-PCR of p-V59M mouse brain RNA samples showed a clear Kir6.2-V59M band in cerebellar samples, but only a faint signal for the rest of the brain.

This pattern was also seen in Pv-Z/EG mouse brains. There was strong GFP expression in the cerebellum but only sparse expression in the cortex and very little in the hippocampus. The majority of cerebellar Purkinje cells were labelled. Thus, the results from these two different methods were in good agreement, and indicated that neurons expressing the Kir6.2-V59M transgene in p-V59M brain were most densely present in the cerebellum and sparse elsewhere.

Although Kir6.2-V59M expression was seen in the triceps of p-V59M mice, this is unlikely to influence the results of the behavioural tests because the expression of V59M K_{ATP} channels in muscle does not impair their function [102].

Kir6.2-V59M mRNA levels in the brains of p-V59M mice were not quantified. As these mice only expressed the transgene in a small subset of neurons, quantification of Kir6.2 mRNA levels should largely reflect expression of the wild-type gene. Thus, such experiments would not reveal the relative expression levels of wild-type and mutant Kir6.2 mRNA. A similar

problem was encountered when trying to ascertain the gene-dosage of the n-V59M mouse. In both n-V59M and p-V59M mouse models, it would be possible to determine the gene-dosage of Purkinje cells alone by collecting them using laser-capture microdissection. This pure sample of cells could then be analysed using RT-qPCR. Although these experiments could be used to compare gene-dosage in Purkinje cells, it is unlikely that the results would be applicable to other affected neurons because the ROSA promotor is not expressed uniformly across the brain [286]. Thus, the amount of information that would be gained would be limited, and these experiments were not attempted.

4.5.3 Mosaicism of Kir6.2-V59M expression in p-V59M mice

Parvalbumin-Cre mice induced Cre expression in a mosaic pattern. In Pv-Z/EG mice, GFP was seen in most, but not all Purkinje cells. By contrast, all Purkinje cells expressed GFP in Nes-Z/EG mice. Thus, parvalbumin-Cre mice targeted transgene expression to Purkinje cells less efficiently that nestin-Cre mice. Furthermore, the Cre expression pattern in Pv-Z/EG mice was variable from mouse to mouse, with the greatest variability in expression patterns being in the neocortex and hippocampus.

Mosaicism is common for Cre lines because, when they are made, founders are selected based on the low incidence of false-positive cells - i.e. all parvalbumin cells are not labelled with Cre, but all cells expressing Cre also express parvalbumin (Monyer, personal communication). The mosaicism and variability between mice could have influenced the results of the experiments presented in this chapter. Firstly, because not all parvalbumin neurons expressed Kir6.2-V59M, any possible phenotype would have been more subtle; the unaffected parvalbumin neurons may have compensated for the affected population. Secondly, in the electrophysiology experiments, which were completed with small samples of mice, the results were liable to be influenced by the heterogeneity of Cre expression between

mice. Although several cells were recorded from each mouse, the data sets are likely to include recordings from at least some Purkinje cells that did not express Kir6.2-V59M. Thus, the apparent effect of Kir6.2-V59M expression would have been diminished. Indeed, as the mean value for each mouse was composed of recordings from 2-5 cells there is a possibility that the inclusion of even a single wild-type neuron could significantly alter the mean data obtained from an individual mouse.

In summary, due to the mosaicism of Cre expression in this model, experiments on the p-V59M mouse are likely to underestimate the effect, at both the behavioural and electrophysiological level, of Kir6.2-V59M expression in parvalbumin-expressing neurons.

4.5.4 Mutant K_{ATP} channels promote a bistable mode of firing in p-V59M Purkinje cells

The electrophysiological experiments reported in this chapter were carried out to confirm that Kir6.2-V59M expression in the p-V59M mouse resulted in altered electrical activity of their Purkinje cells, which would indicate the presence of mutant K_{ATP} channels. Indeed, this was the case as, in the basal state, more p-V59M Purkinje cells were bistable (rather than firing continuously) than control cells, and p-V59M Purkinje cells spent more time in a hyperpolarised 'down ' state. When p-V59M and control Purkinje cells were exposed to 500µM tolbutamide, the proportion of bursting cells and the proportion of time that they were 'up' was not significantly different. Thus, the presence of mutant K_{ATP} channels appeared to promote bursting activity in p-V59M Purkinje cells.

When synaptic innervation was blocked, virtually all neurons fired continuously. As it was the hyperpolarised 'down' states that were removed, it was most likely that the bursting activity was driven by inhibitory GABAergic activity. This interpretation is supported by the

observation that Purkinje cells in sagittal slices receive primarily GABAergic innervation [283].

The mechanisms that drove the bursting characteristic were not further elucidated, as they were not material to the conclusions of this chapter. However, it seems reasonable to postulate that hyperpolarising K_{ATP} channel conductance through the mutant K_{ATP} channels counteracted depolarising mechanisms that lead to 'up' states. Thus, p-V59M Purkinje cells remained in the hyperpolarised state for longer than control Purkinje cells.

Cells in the molecular and granular cell layers of the cerebellum of Pv-Z/EG mice were labelled with GFP. According to previous reports, the labelled cells in the molecular and granular layers were likely to be stellate and basket cells [319], both of which synapse onto Purkinje cells [204]. Thus, it is possible that in p-V59M mice, the electrical activity of these cells were also influenced by the presence of Kir6.2-V59M and thus they could have contributed to the phenotype of the p-V59M Purkinje cells.

However, this is unlikely to be the case because stellate and basket cells are inhibitory, and inhibition of these cells would be expected to disinhibit Purkinje cells. This is in fact what you see when you remove synaptic inputs (Figure 4.3 C). In the future, the influence of Kir6.2-V59M on inhibitory stellate and basket cells could measured directly by recording their electrical activity, or indirectly by quantifying the frequency of inhibitory synaptic inputs onto p-V59M and control Purkinje cells.

In summary, mutant K_{ATP} channels significantly altered the electrical activity of p-V59M Purkinje cells compared to controls. Thus, functional mutant K_{ATP} channels were produced in Purkinje neurons of p-V59M mice, and their cerebellar output is likely to be significantly impaired compared to controls.

4.5.5 p-V59M Purkinje cells had lower firing rates than controls

In the basal state, p-V59M Purkinje cells had lower firing rates than controls. Thus, cerebellar output is likely to be impaired in p-V59M mice compared to controls. However, the firing rates of control and p-V59M Purkinje cells were not significantly different in the presence of 500μM tolbutamide, so it is likely that p-V59M Purkinje cells fired fewer spontaneous action potentials due to the presence of additional K_{ATP} channel flux.

When recorded in the whole-cell configuration, the mean basal firing rate of p-V59M Purkinje cells (~5Hz, Figure 4.3 C) was higher than that of n-V59M Purkinje cells (~0.5Hz, Figure 3.4 B). There are at least two explanations for this result. Firstly, as mentioned in section 4.5.3, the mosaicism of Cre expression produced by the parvalbumin-Cre transgene is likely to lead to an underestimation of the effects of Kir6.2-V59M expression in p-V59M Purkinje cells. Secondly, it is possible that n-V59M Purkinje cells received a higher dosage of Kir6.2-V59M mRNA than p-V59M Purkinje cells, which may be due to differences in the genetic backgrounds of the mice.

Although the analysis of Purkinje cell electrical activity showed that genotype (the between-subjects factor) was important for their basal activity, there were no significant within-subjects effects - i.e. the addition of tolbutamide did not alter the firing rates of control Purkinje cells or p-V59M Purkinje cells. The lack of effect of tolbutamide on control Purkinje cells indicates that wild-type K_{ATP} channels are largely closed under normal conditions, which is consistent with the results from Chapter 3. However, the lack of effect of tolbutamide on p-V59M Purkinje cells is more surprising. In 500μM tolbutamide, the firing rates of p-V59M Purkinje cells tended to be higher than in the basal state, but this trend did not reach statistical significance. This was also the case for n-V59M Purkinje cells recorded in the whole-cell configuration (Chapter 3). Therefore, it is possible that greater statistical power is required to resolve the within-subjects effect than the between-subjects effect.

In the future this hypothesis could be tested by measuring the firing activity of p-V59M Purkinje cells in the cell-attached configuration. Because this technique is less technically demanding than the whole-cell method, more cells can be recorded from each mouse, which improves the reliability of the data. Furthermore, cell-attached recordings also cause minimal perturbation of the intracellular environment (section 3.5.4), so these future experiments could also control for any detrimental influences of the whole-cell recording method on the electrical activity of the cells.

Although tolbutamide administration did not have a significant effect on the firing rate of p-V59M Purkinje cells, this was not material to the conclusions of this chapter. The most important comparisons were made between control and p-V59M Purkinje cells in the basal and 500μM tolbutamide conditions (i.e. the between-subjects factor of genotype was the most important factor).

In summary, because p-V59M Purkinje cells had a lower firing rate than controls in the basal state, it is likely that cerebellar output is impaired in p-V59M mice due to the presence of mutant K_{ATP} channels. The firing rates of p-V59M Purkinje cells were higher than those of n-V59M Purkinje cells, which indicated that cerebellar output in p-V59M mice was less severely affected by the presence of Kir6.2-V59M mRNA.

4.5.6 Developmental regulation of Kir6.2-V59M expression in p-V59M mice

The immunohistochemistry experiments carried out on Pv-Z/EG mouse brains indicated that, consistent with the developmental pattern of parvalbumin expression, Kir6.2-V59M was likely to be produced in different brain areas at different times. By 2 weeks of age, cerebellar GFP expression was similar to that seen in adult (12- and 16-week-old) mice. Thus,

parvalbumin-Cre expression in the cerebellum had stabilised by the time the electrophysiological experiments were carried out.

Although there was relatively little GFP expression in the neocortex at 2 weeks of age, the pattern of GFP expression in Pv-Z/EG mice at 12 and 16 weeks of age was consistent. Thus, by the time the behavioural tests were carried out, the expression of parvalbumin-Cre in the neocortex had also stabilised. In fact, because parvalbumin expression in the neocortex stabilises by around 3-4 weeks of age [325], it is likely that the pattern of parvalbumin-Cre expression in the neocortex also stabilises around this time.

As previously mentioned (in section 3.5.8), expression levels of K_{ATP} channels are relatively low at birth and rise over the first few postnatal weeks [187]. Thus, although parvalbumin-Cre expression levels (which determine Kir6.2-V59M expression) undergo postnatal maturation, this may not impair the ability of the p-V59M mouse to model the potential developmental complications of Kir6.2-V59M expression in parvalbumin-expressing neurons.

The long-term expression of V59M Kir6.2 subunits in p-V59M Purkinje cells did not seem to affect their gross electrophysiology. When the intrinsic firing rates of the cells were recorded (by blocking K_{ATP} channels with tolbutamide, and blocking synaptic transmission with CNQX and bicuculline), the firing rates of p-V59M Purkinje cells were not significantly different compared to controls. This result is consistent with that from n-V59M Purkinje cells (section 3.5.8).

4.5.7 p-V59M mice are weaker than controls

Three tests of muscle strength were used to compare p-V59M and control mice. p-V59M mice were only significantly weaker than controls on the weight-lifting test. Of the three tests,

weight-lifting is the most specific to muscle strength as it requires little coordination (unlike the horizontal bar test) and little stamina (unlike the inverted screen test) [328]. It is also likely to be the most sensitive to muscle weakness. In the horizontal bar and inverted screen tests the mouse has to support its own body mass, but in the weight-lifting test the lightest weight was 20g and each subsequent one was 13g heavier. As male mice weighed ~31g and female mice ~24g at the time of testing, they were expected to hold weights greater than their body weight from the second increment onwards.

This interpretation is supported by my data. The vast majority of p-V59M and control mice achieved the highest score in the horizontal bar and inverted screen tests (i.e. there was an obvious ceiling effect), but data from the weight-lifting task were normally distributed - the average score for controls was approximately 14.5, but the maximum score was 21. Thus, the weight-lifting test had the greatest headroom, which made it more sensitive than the other two tests.

Therefore, these data provide evidence that expression of Kir6.2-V59M in parvalbumin-expressing neurons alone is sufficient to produce muscle weakness.

4.5.8 p-V59M mice do not display motor malcoordination

Even though p-V59M Purkinje cells were significantly less electrically active than controls, p-V59M mice showed no impairments on the two tests of motor coordination. This result was somewhat surprising as it is well known that the cerebellum is involved in balance and motor coordination.

There are several possible explanations for this observation. Firstly, although p-V59M Purkinje cells were significantly impaired compared to littermate controls, the

electrophysiology of their Purkinje cells was less severely affected than in n-V59M mice (as discussed in section 4.5.5). Secondly, some p-V59M Purkinje cells did not express Kir6.2-V59M mRNA. This could mean that the severity of cerebellar impairment was low because unaffected Purkinje cells were able to compensate for the impaired population. Thirdly, it is possible that the motor coordination tests were not sensitive enough to detect the severity of cerebellar impairment displayed by p-V59M mice, or that performance on these tasks was not indicative of cerebellar function. Indeed, the rotarod is a non-specific locomotor coordination task [338], and other transgenic mice with mutations that specifically affect the electrophysiology of Purkinje cells are unimpaired on this task [339]. Finally, it is possible that motor coordination *per se* was indeed unaffected in p-V59M mice, but that motor learning (another cerebellar-dependent function) was impaired.

In the future, these different hypotheses could be tested by assessing the performance of the mice on a new piece of equipment, the Erasmus ladder [340], which is more sensitive than the rotarod in identifying cerebellar dysfunction in mice [341]. It consists of two open-ended black boxes that are equipped with a bright white light and connected by a ladder consisting of 37 double rungs. These rungs may be raised or lowered so that mice have to perform an alternating stepping pattern as they traverse the ladder. The accuracy and speed of the mouse's movement can be measured and indicates motor coordination, and the improvement in their performance over several learning trials can also be measured.

In summary, p-V59M mice were not significantly different from controls on two tests of motor coordination. It is possible that these tests were not sensitive enough, or specific enough, to detect the severity of cerebellar impairment that was present in the p-V59M mouse. Other mouse models with impaired Purkinje cell electrophysiology have also shown intact motor coordination; but in these other mice, motor learning, which is another cerebellar-dependent function, was impaired. Thus, in the future it would be interesting to see if motor learning is impaired in the p-V59M mouse.

4.5.9 p-V59M mice are hyperactive in some contexts

When housed in a new enclosure, p-V59M mice 'settled' as quickly as controls and the two types of mice showed the same levels of spontaneous activity throughout the day. Indeed, the total activity levels of p-V59M and control mice over 23-hours were not significantly different. By contrast, p-V59M mice showed greater spontaneous use of the free-running wheels: they ran further than controls and at a higher average speed. Therefore, p-V59M mice were hyperactive compared to controls in some contexts.

Although the activity monitoring system and the free-running wheels both gave a measure of spontaneous locomotor activity, usage of the free-running wheels is also dependent upon several other aspects of mouse behaviour. Rodents may use free-running wheels more if they have increased novelty seeking behaviour [342, 343] or increased stress levels [344]. Furthermore, the act of running may be rewarding [345, 346], and addictive [347]. Anxiety levels may also be altered after running on a wheel, although this is controversial as some studies suggest that exercise is anxiolytic [348, 349] but others suggest that it is anxiogenic [350, 351]. In summary, the use of free-running wheels is dependent upon many more factors than spontaneous activity levels alone. A dissociation between spontaneous locomotor activity in threshold monitors and free-running wheels, which is what was seen with the p-V59M mice, has been seen in at least one other study [350].

p-V59M mice ran further and with greater average speed than their controls. By contrast, n-V59M mice ran for longer and further than their controls, but with the same average speed. These results indicate that both of these mouse models of iDEND were hyperactive compared to their controls. Although the pattern of their behaviour on the free-running wheels was different (e.g. p-V59M mice ran with higher average speed than their controls, but n-V59M ran with the same average speed), conclusions cannot be drawn suggesting that this may be a specific effect of expression of Kir6.2-V59M in parvalbumin-expressing

neurons. As shown in Table 4.3, the activity of parvalbumin-Cre and nestin-Cre mice (the littermate controls of p-V59M and n-V59M mice) were also different for the free-running wheel task. Therefore, the results of n-V59M and p-V59M mice cannot be compared directly for this task.

These experiments showed that p-V59M mice were hyperactive in some contexts. In the future, it would be interesting to identify the psychological traits that underlie the hyperactivity of p-V59M mice on the free-running wheel because the same traits might underlie the hyperactivity of iDEND patients as well.

4.5.10 Implications for therapy

Sex was included as a factor when analysing several sets of data in this chapter. Although there were some sex-dependent differences there were no interactions between sex and genotype. Thus, in my experiments, the impact of the V59M mutation was never dependent upon the sex of the mouse. This is consistent with what is seen in human beings - both male and female patients with PNDM and iDEND have been identified, and just over half of the patients with these diseases are male [132], which indicates that the symptoms are independent of the sex of the individual.

The data presented in this chapter suggest that impairment of parvalbumin-expressing neurons results in muscle weakness and hyperactivity. As cerebellar Purkinje cells were impaired, it is possible that cerebellar dysfunction contributed to the phenotype of the p-V59M mouse. However, neurons outside of the cerebellum also expressed Kir6.2-V59M mRNA so the relative importance of the cerebellum compared to those other brain areas remains unclear. This could be elucidated in the future by restricting Kir6.2-V59M expression specifically to Purkinje cells by using the Purkinje cell protein 2-Cre mouse [352] mouse line.

It is interesting that p-V59M mice did not not show greater spontaneous activity in threshold monitors but were hyperactive on the running wheels. Mice with high levels of wheel-running behaviour have been used as models for attention-deficit hyperactivity disorder (ADHD) in other studies [353], and Ritalin, which is commonly used to treat ADHD in human beings [354], reduced wheel usage in those mice [355]. Some patients with iDEND have been prescribed Ritalin to help their hyperactivity symptoms (anecdotal), which suggests that hyperactivity on the running wheel might be a good model for hyperactivity in iDEND patients. Thus, it is possible that the identification of the psychological traits that lead to the hyperactivity of the p-V59M mice on the running wheel could lead to better management strategies for the hyperactivity of iDEND patients.

Chapter 5: Cerebellar Impairment in Patients with iDEND

5.1 Summary

1) Patients with gain-of-function mutations in Kir6.2 causing PNDM and iDEND were recruited. Unaffected family members were also recruited, where possible, to act as controls in all experiments.

2) Patients with iDEND, but not with PNDM alone, were impaired compared to age-matched controls on a coordinated hand-eye tracking task, which is dependent upon normal cerebellar function. Simple visual tracking of a target moving at a constant velocity was not significantly impaired. However, significant impairment was observed when the visual target moved sinusoidally, or if the visual presentation of the target was removed.

3) The performance of PNDM patients was not significantly different from age-matched controls on two tests of manual dexterity and motor coordination - the Annett peg moving task and the bead board. Patients with iDEND syndrome showed a trend towards longer times in both tasks but only two patients were tested, precluding statistical analysis.

4) Patients with iDEND, but not with PNDM alone, displayed aberrant prosaccadic and smooth pursuit eye movements. One individual displayed clear hypermetric saccades, which are characteristic of fastigial oculomotor region impairment, and 'cogwheel' tracking during smooth pursuit.

5) Therefore cerebellar function is likely to be impaired in iDEND, but not in PNDM, and disordered eye movements may be a previously overlooked symptom of iDEND.

5.2 Introduction

In the previous two chapters I have presented data that suggest cerebellar function is likely to be impaired in iDEND. If this is the case, then patients should exhibit additional symptoms that are characteristic of cerebellar impairment. Such symptoms may persist even when patients are treated with sulphonylureas as the penetrance of these drugs across the blood-brain barrier is relatively low (as discussed in Chapter 1).

5.2.1 Cerebellar dysfunction and eye movements

There are many different types of eye movement. Saccades are fast conjugate movements (the eyes move together) that centre the foveae of the eyes on a new point of interest. If we want to maintain foveation on a moving object, we initiate smooth pursuit eye movements, which are also conjugate. Many more types of eye movement exist, and have been described elsewhere [356].

Saccades and smooth pursuit eye movements are controlled by some circuits that are specific to each movement, and some common neural circuits. For example, saccades are crucially dependent on the caudal superior colliculus, but lesions to this area do not impair smooth pursuit eye movements [357, 358]. Similarly, smooth pursuit eye movements are impaired by lesions to the frontal pursuit area, but saccades are not affected [359]. By contrast, lesions to the cerebellum may impair both saccades and smooth pursuit eye movements [356, 360].

There are three cerebellar regions that are involved in eye movements: the floccular region, the nodulus and uvula, and the oculomotor vermis and fastigial nucleus [356, 360]. Lesions to each of these regions, e.g. due to stroke or trauma, have characteristic effects on eye

movements. For example, lesions to the floccular region impair smooth pursuit and gaze holding [361], whereas lesions to the oculomotor vermis and fastigial nucleus impair performance in saccades and smooth pursuit eye movements [362, 363].

Some eye movement disorders are specific to the cerebellum. For example, lesions to the oculomotor vermis, or unilateral lesions to the fastigial nucleus result in a characteristic 'cogwheel' pursuit deficit, in which horizontal smooth pursuit movements become superimposed with microsaccades [356, 360, 362, 364-366]. Another hallmark of cerebellar dysfunction is saccadic pulse dysmetria, especially hypermetria [356]. This is where the eyes move too far (hypermetria) or not far enough (hypometria) when attempting to make a saccade to a new target.

5.2.2 Hand-eye tracking of moving objects

The role of the cerebellum in oculomotor function is a part of its general role in the coordination and timing of movement. It seems to be most active during the coordinated movement of multiple parts of the body, such as the eye and hand [367-369].

The hand-eye coordination of human beings can be assessed by asking them to track a moving target with a cursor that they control with a joystick [267, 369]. When different parameters are adjusted, such as the velocity of the target and the predictability of its movement, the level of cerebellar activity, and the location of activity within the cerebellum also seems to change. When a target moves from side to side in a predictable manner at constant velocity (linear movement), the vermis of the cerebellum is activated [365, 370-372]. This is also true when the target smoothly and predictably accelerates and decelerates (sinusoidal tracking).

If the visual presentation of the target is removed (it is blanked) and participants are asked to continue tracking as if the target was still there, then greater cerebellar activation is seen [373]. In this situation, participants are required to rely on an internal, extra-visual representation of the movement. So the increased activation of the cerebellum might reflect its theorised role in developing internal, feed-forward models [374-377]. However, increased cortical activity (especially from the frontal eye fields [378]) is also observed when tracking blanked targets. This could indicate that the task is generally more difficult.

5.2.3 Manual dexterity and the cerebellum

The cerebellum also participates in the coordination of finger movements. Lesions to the cerebellum in human beings and monkeys impair the precision of finger movements [268, 272, 379]. Furthermore, cerebellar neurons are more active when monkeys and human beings perform tasks that involve reaching and grasping, or require coordinated finger movements [380-382].

Finger coordination in human beings may be assessed using the bead board task [268]. This involves transferring twenty small spherical beads, individually, into sequential wells of descending diameter (Figure 2 B). Lesions to the cerebellum impair performance on this task.

Hand and finger skill may also be tested with the Annett peg board [269]. In this task, participants transfer ten wooden pegs as quickly as possible from one side of a frame to the other, using a single hand (Figure 2 C). Performance on this task correlates with hand preference - e.g. individuals who express a strong preference for the right hand complete the task more quickly with the right than the left hand. Furthermore, dyslexic individuals who

have abnormal cerebellar morphology perform worse than controls on the task [270, 383], so the task may be sensitive to cerebellar impairment.

5.2.4 The cerebellum in iDEND

Cerebellar impairment would be expected to impair manual dexterity and performance on hand-eye tracking tasks. Thus, in the current chapter I compare the ability of patients with PNDM and iDEND to accurately track a moving target with that of non-diabetic controls. Although PNDM patients do not experience neurological symptoms (by definition), it remains possible that they show subtle differences in their neurological function. Thus, both iDEND and PNDM patients were tested to see if either patient group experiences difficulties in hand-eye tracking.

I employed a tracking task [267] that requires little motor strength (there is no resistance to work against), so that the the patients' hypotonia is unlikely to be a major confounding variable. Furthermore, as the movement required is a relatively simple wrist action, the task may be used to test young participants who may not have the basic coordination or cognitive ability necessary for a more complicated task (e.g. independent movement of the eyes and hand).

Hand and finger coordination was also assessed by use of the Annett peg moving task [269] and bead board task [268]. Oculomotor function was qualitatively assessed by filming patients while they made prosaccadic and smooth pursuit eye movements.

5.3 Methods

5.3.1 Participants

All patients with PNDM and iDEND were being treated with sulphonylurea drugs at the time of testing, although the dosage and agent differed between individuals. Furthermore, the age at which the patients had been transferred to oral therapy, and the duration of their treatment differed, and some patients had been hospitalised for hypoglycaemic attacks at some point in their life. None of these factors were taken into account during the following analyses.

For data analysis of visual tracking tasks, PNDM and iDEND patients were matched with a non-diabetic individual of a similar age and, where possible, the same sex (Tables 5.1 and 5.2). (The iDEND patient from pair 4 did not complete task 3.) Three patients with iDEND were unable to carry out the tasks as they showed high levels of attention deficit. All were male, had V59M mutations, and were aged 5, 6, and 9 years old. Other children, of a similar age, who did not have K_{ATP} channel mutations were able to complete the task. All of the individuals listed in Table 5.2 showed strong attentional control when carrying out the task. They did not look away from the screen, they did not talk and they sat still. Indeed, many of them said that they enjoyed carrying out the task.

Table 5.1 Controls vs PNDM for hand-eye tracking tasks

Pair	Group	Mutation	Age (years)	Sex
1	Control	wt	9	F
	PNDM	R201H	9	F
2	Control	wt	10	M
	PNDM	R201H	9	M
3	Control	wt	7	F
	PNDM	R201H	7	F
4	Control	wt	28	M
	PNDM	R201H	29	M
5	Control	wt	24	M
	PNDM	R201H	18	M
6	Control	wt	25	F
	PNDM	R201H	20	F
7	Control	wt	6	M
	PNDM	E322K	7	M
Pooled	Control		$\overline{x} = 16$	4M, 3F
	PNDM		$\overline{x} = 14$	4M, 3F

Table 5.2 Controls vs iDEND for hand-eye tracking tasks

Pair	Group	Mutation	Age (years)	Sex
1	Control	wt	25	F
	iDEND	V59M	13	F
2	Control	wt	27	F
	iDEND	V59M	20	F
3	Control	wt	15	M
	iDEND	V59M	17	F
4 *	Control	wt	8	F
	iDEND	V59M	9	M
5	Control	wt	10	M
	iDEND	R201C	9	F
6	Control	wt	30	F
	iDEND	R201C	33	F
7	Control	wt	35	F
	iDEND	R201S	36	M
Pooled	Control		$\overline{x} = 21$	2M, 5F
	iDEND		$\overline{x} = 20$	2M, 5F
* Patient with iDEND only completed tasks 1 and 2.				

For the analysis of the manual dexterity tasks, PNDM patients were matched with a non-diabetic individual of a similar age and, where possible, the same sex (Tables 5.3 and 5.4). Only the iDEND patients from pair 3 and 5 of the hand-eye tracking experiments were tested on the manual dexterity tasks. As only two individuals were tested, no statistical analysis was carried out on the data from iDEND patients.

Table 5.3 Controls vs PNDM for the bead board task

Pair	Group	Mutation	Age (years)	Sex
1	Control	wt	8	F
	PNDM	R201H	9	F
2	Control	wt	10	M
	PNDM	R201H	9	M
3	Control	wt	6	M
	PNDM	R201H	7	F
4	Control	wt	26	F
	PNDM	R201H	29	M
5	Control	wt	15	M
	PNDM	R201H	18	M
6	Control	wt	25	M
	PNDM	R201H	20	F
7	Control	wt	11	M
	PNDM	E322K	7	M
Pooled	Control		$\overline{x} = 14$	3M, 5F
	PNDM		$\overline{x} = 14$	3M, 5F

Table 5.4 Controls vs PNDM for the Annett peg board task

Pair	Group	Mutation	Age (years)	Sex
1	Control	wt	9	F
	PNDM	R201H	9	F
2	Control	wt	9	M
	PNDM	R201H	9	M
3	Control	wt	7	F
	PNDM	R201H	7	F
4	Control	wt	4	F
	PNDM	R201H	4	F
5	Control	wt	29	M
	PNDM	R201H	28	M
6	Control	wt	18	M
	PNDM	R201H	18	M
7	Control	wt	20	F
	PNDM	R201H	20	F
8	Control	wt	7	F
	PNDM	E322K	7	F
Pooled	Control		$\overline{x} = 13$	3M, 5F
	PNDM		$\overline{x} = 13$	3M, 5F

5.3.2 Coordinated hand-eye tracking of a moving target

The equipment is listed in Chapter 2, along with detailed descriptions of the tasks. Three tracking tasks were implemented. In the first task (task 1), the target moved at constant velocity. In task 2 the target accelerated and decelerated during each sweep at a predictable rate. In task 3 the target moved at constant velocity, but it was blanked in the middle third of

each sweep. In each task the target moved in a straight line, horizontally across the middle of the computer screen. The tasks are graphically represented in Figure 5.1.

The first sweep of each task was omitted from analysis because the target was not visible when the task began, so participants were often in the wrong starting position. The final sweep was also removed so that the number of leftward and rightward sweeps were equal. Thus, ten sweeps (5 leftward, 5 rightward) were analysed for each participant. Both controls and patients tended to perform better on rightward sweeps (data not shown). The reason for this difference is unclear, but may be due to differences in the hand-eye coordination for flexion versus extension of the wrist.

The following parameters were analysed:

(i) Discrepancy error: The difference between the position of the target and the cursor was calculated for each sampled point. The standard deviation of these differences was called the discrepancy error. Appendices 7, 9 and 10, show the results of a representative pair of participants from the iDEND versus control group on tasks 1, 2 and 3. In the appendices, discrepancy errors for each participant are plotted as box plots. In order to generate these figures the discrepancy error was calculated on a sweep-by-sweep basis, therefore the box plot is composed of 10 values per person. In Figures 5.2 A, 5.3 A and 5.4 A, the discrepancy error was calculated for the entire ten sweeps, producing a single (averaged) error value for each participant, which was used in the statistical analyses.

(ii) Velocity error: Discrepancy errors may arise due to a constant lag behind the target, or an inability to maintain a constant velocity, resulting in overshooting and undershooting. To give a measure of the smoothness of movement, a velocity error was calculated. The difference between successive points in the target track, and successive points in the cursor track was calculated. These differences were differentiated and the standard deviation of these

differentiated errors was called the velocity error. For example, in task 1, where the target moved at constant speed, the target moved the same distance between each sampled point. However, the cursor may have moved a different amount depending on the velocity of the participant's movements. If the participant had moved the cursor at the same rate as the target then their differentiated error would equal 1 for all points, and the standard deviation (the velocity error) would be zero. Appendices 7, 9 and 10, show the results of a representative pair of participants from the iDEND versus control group on tasks 1, 2 and 3. In the appendices, velocity errors for each participant are displayed in box plots. In order to generate these figures the velocity error was calculated on a sweep-by-sweep basis, therefore the box plot is composed of 10 values per person. In Figures 5.2 B, 5.3 B and 5.4 B the velocity error was calculated for the entire ten sweeps, producing a single (averaged) error value for each participant, which was used in the statistical analyses.

(iii) Direction error: As mentioned above, discrepancies between target and cursor positions may arise through velocity errors, resulting in overshooting or undershooting. In order to quantify this, I calculated the percentage of time each participant moved in the appropriate direction during the task. Successive points in the cursor track were subtracted. If the cursor was moving in the appropriate direction, then when moving left to right the cursor position should increase in value, and when moving right to left it should decrease in value. Therefore all differences ≥ 0 are 'correct' for rightward sweeps and differences ≤ 0 are 'correct' for leftward sweeps. This analysis is presented graphically on a sweep-by-sweep basis in Appendices 7, 9 and 10. In Figures 5.2C, 5.3C and 5.4C the overall percentage of movement in the correction direction (pooling rightward and leftward sweeps) was used for the statistical analyses.

Relatively few individuals were tested, and the patients had different mutations. Therefore, the Kruskall-Wallis ANOVA based on ranks (a non-parametric statistical test) was used to assess the significance of the results. Each analysis looked for differences between the four

groups: PNDM patients, iDEND patients, and the two groups of matched controls. Where significant differences were found, pairwise comparisons were carried out, using the Mann-Whitney U-test, to identify which groups were different. An appropriate Bonferroni adjustment to the alpha level was made, as previously described (Chapter 2). Although there were four groups, only three pairwise comparisons were made: PNDM versus their controls, iDEND versus their controls, and finally the two control groups were compared to each other.

5.3.3 Manual dexterity tests

The protocols for the Annett peg moving task and bead board are given in Chapter 2. For analyses, PNDM patients were matched with non-diabetic individuals for age and sex, where possible (Tables 5.3 and 5.4). Additional control data for the Annett peg moving task was obtained from Dr. Tom Scerri (Wellcome Trust Centre for Human Genetics) that encompassed a large range of ages for both sexes. Performance of PNDM patients and their controls were compared using the nonparametric Mann-Whitney U test.

5.3.4 Eye movement videos

Details of the protocol are given in Chapter 2. The eye movements of 3 controls, 9 patients with PNDM and 2 patients with iDEND were recorded.

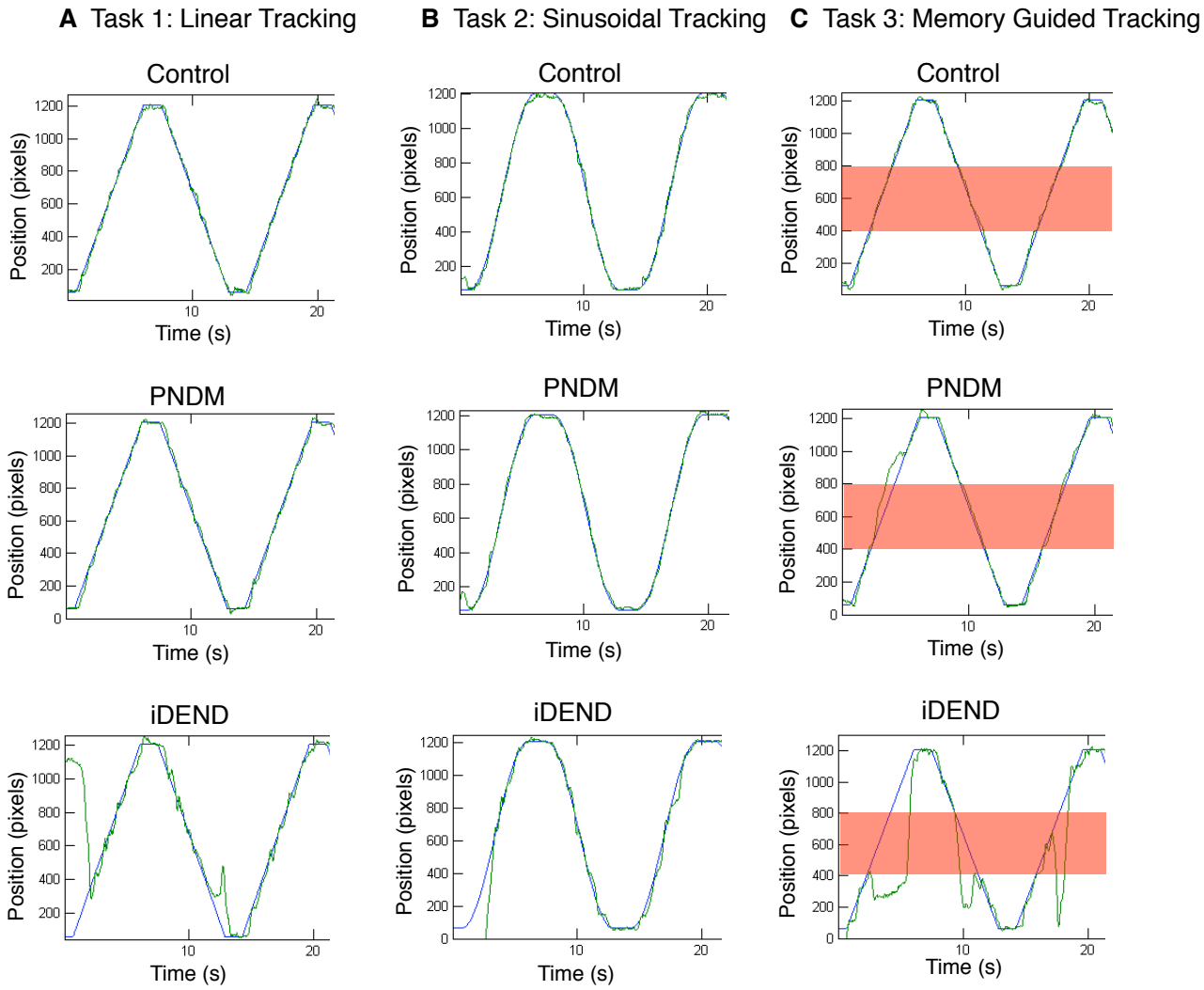

Figure 5.1 Representative traces of visual tracking in PNDM and iDEND

Blue lines indicate the movement of the target. Green lines indicate the movement of the cursor, which was controlled by the participant. Top row shows traces from a control participant in each of three tasks. Middle row and bottom row show traces for the same tasks performed by patients with PNDM and iDEND, respectively. Control, 15 years old, male; PNDM, 18 years old, male, R201H; iDEND, 17 years old, female, V59M. For all traces, a positive slope indicates a rightward movement of the target or cursor, and a negative slope indicates a leftward movement - i.e. figures show two rightward sweeps and one leftward sweep. Participants completed 12 sweeps in total (6 rightward, 6 leftward). (**A**) Target moved at constant velocity throughout - linear tracking. (**B**) Target accelerated and decelerated in a sinusoidal manner during the sweep. (**C**) Target moved at constant velocity throughout, but the visual presentation of the target was switched off (it was blanked) during the middle third of each sweep, as indicated by the red box. When the target is blanked participants must rely on memory-guided, predictive tracking.

5.4 Results

5.4.1 Linear tracking was not impaired in PNDM or iDEND

Representative results for task 1 are presented in Appendix 7. On task 1, the median discrepancy error of PNDM and iDEND patients was higher than the median of their matched controls (Figure 5.2 A) and the variability of the error values was highest in the iDEND group. However, the Kruskal-Wallis test revealed no significant differences in the error scores of the four groups ($p = 0.058$). The same pattern was seen for the velocity errors ($p = 0.068$) (Figure 5.2 B). Similarly, the median value for the direction error was lower for PNDM and iDEND patients compared to their respective controls (which indicated that they were moving in the correct direction for a lower proportion of the time) but this difference did not reach significance ($p = 0.333$). Therefore, patients with PNDM and iDEND were not significantly impaired compared to matched controls on the linear tracking task, though they tended to track less accurately.

As participants completed ten sweeps over the course of approximately 90 seconds, it was possible that their performance changed during the course of the task. For example, their performance might improve if they learnt to carry out the task in a more coordinated manner, and their performance might decline if their attention waned. The latter might be important as iDEND patients have been reported to show attentional deficits (discussed in Chapter 1). In order to assess if within-task effects were present, the discrepancy error value for the first and last five sweeps of the task were calculated separately for each participant (Appendix 8). There was no clear difference: roughly 50% of participants in each group improved (3 of 7 PNDM patients and 4 of 7 of their controls; 5 of 7 iDEND patients and 4 of 7 of their controls). The error from the last five sweeps was expressed as a percentage of the error from the first five sweeps, and these values were compared using the Kruskal-Wallis test, which revealed no significant differences between the groups ($p = 0.299$).

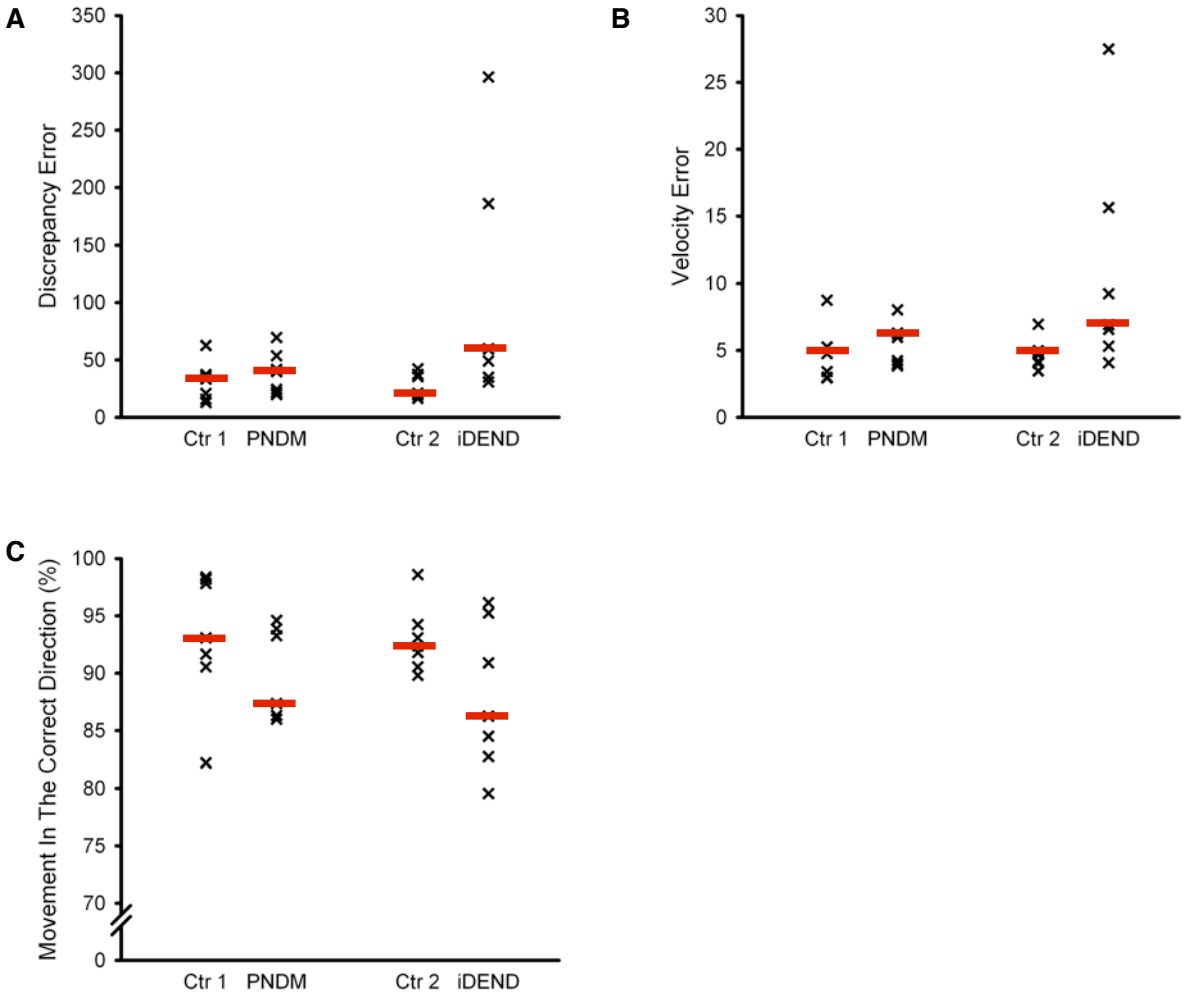

Figure 5.2 Visual tracking in PNDM and iDEND: Linear movement

Scatter plots showing errors when tracking a target moving at constant velocity (linear tracking). Data for PNDM (n=7) and iDEND (n=7) patients are plotted against matched controls, as indicated. The red bars indicate the median error. (**A**) Discrepancy errors of PNDM and iDEND patients and their matched controls. (**B**) Velocity errors of PNDM and iDEND patients and their matched controls. (**C**) Direction errors of PNDM and iDEND patients and their matched controls. There were no significant differences between the groups on any of the tasks (Kruskal-Wallis tests).

So error rates appear to be reasonably constant throughout the task, suggesting attention and learning do not influence the results.

5.4.2 Sinusoidal tracking is impaired in iDEND, but not in PNDM

Representative results for task 2 are presented in Appendix 9. On task 2, the median discrepancy error of PNDM and iDEND patients was higher than that of matched controls and the variability was highest in the iDEND group (Figure 5.3 A). The Kruskal-Wallis test revealed a statistically significant difference in discrepancy errors across the four groups ($p = 0.027$). Pairwise comparisons showed that there were no significant differences between the two control groups ($p = 0.902$) or between controls and PNDM patients ($p = 0.535$), but the discrepancy errors of iDEND patients were significantly higher than controls ($p = 0.002$).

The median velocity error of PNDM and iDEND patients was higher than that of their matched controls (Figure 5.3 B), but the difference was not statistically significant ($p = 0.251$). Similarly, there was no significant difference in the direction error of the groups ($p = 0.237$), even though both patient groups tended to move in the wrong direction more than their respective controls. Analysis of early versus late sweeps again indicated no significant differences ($p = 0.561$).

In summary, patients with iDEND track less accurately than controls when the speed of the target varies. However, the velocity and general direction of the patients' movement is not different to controls.

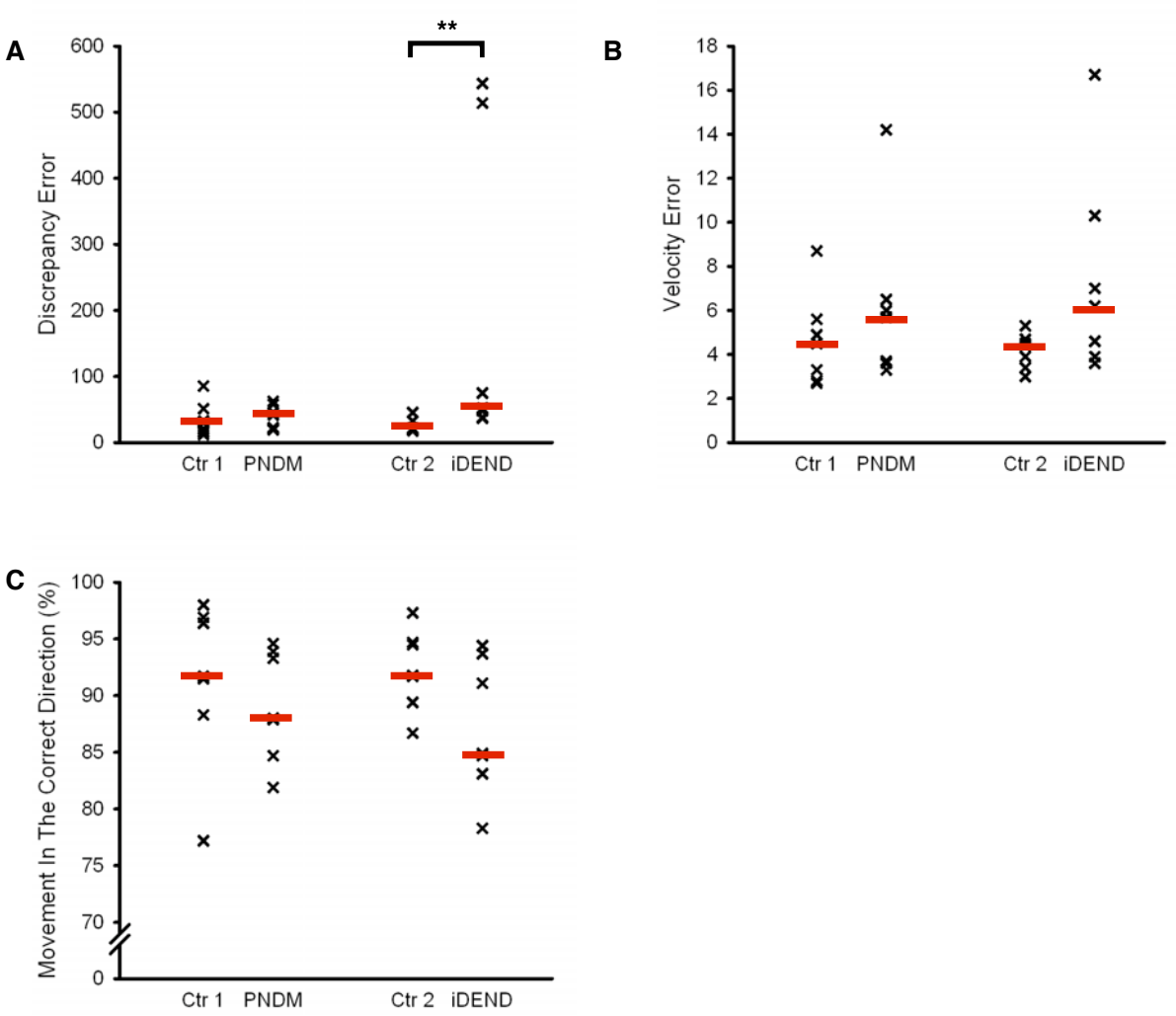

Figure 5.3 Visual tracking in PNDM and iDEND: Sinusoidal movement

Scatter plots showing errors when tracking a target moving with variable velocity (sinusoidal tracking). Data for PNDM (n=7) and iDEND (n=7) patients are plotted against matched controls, as indicated. The red bars indicate the median error. (**A**) Discrepancy errors of PNDM and iDEND patients and their matched controls. Patients with iDEND were significantly less accurate than controls, but PNDM patients were not affected. **, $p < 0.01$, post-hoc Mann-Whitney U-test. (**B**) Velocity errors of PNDM and iDEND patients and their matched controls. There were no significant differences between the groups (Kruskal-Wallis test). (**C**) Direction errors of PNDM and iDEND patients and their matched controls. There were no significant differences between the groups (Kruskal-Wallis test).

5.4.3 Linear tracking with a memory-guided section is impaired in iDEND, but not in PNDM

Representative results for task 3 are presented in Appendix 10. On task 3, the median discrepancy error of PNDM patients and their controls was similar. By contrast, the median discrepancy error of iDEND patients was higher than the median of their matched controls. The variability of error values across the four groups was highest in the iDEND patients (Figure 5.4 A). The Kruskal-Wallis test revealed a statistically significant difference in discrepancy errors across the four groups ($p = 0.021$). Post-hoc pairwise comparisons showed that there was no significant difference between the two control groups ($p = 0.731$) or between PNDM patients and their controls ($p = 0.805$), but the discrepancy errors of iDEND patients were significantly higher than their controls ($p = 0.009$).

The Kruskal-Wallis test indicated that the velocity errors of the groups were also significantly different ($p = 0.042$) (Figure 5.4 B). Post-hoc pairwise comparisons showed that there was no significant difference between the two control groups ($p = 0.534$) or between PNDM patients and their controls ($p = 0.383$), but the discrepancy errors of iDEND patients were significantly higher than controls ($p = 0.009$).

The direction errors of PNDM and iDEND patients and their controls were not significantly different ($p = 0.068$), though both patient groups tended to move in the wrong direction more than controls. Analysis of early versus late sweeps again indicated no significant within-task differences ($p = 0.146$).

In summary, patients with iDEND track less accurately than controls when they have to follow moving targets with extra-visual guidance. The velocity of their tracking is also impaired. However, they move in the correct direction for a similar proportion of time as controls.

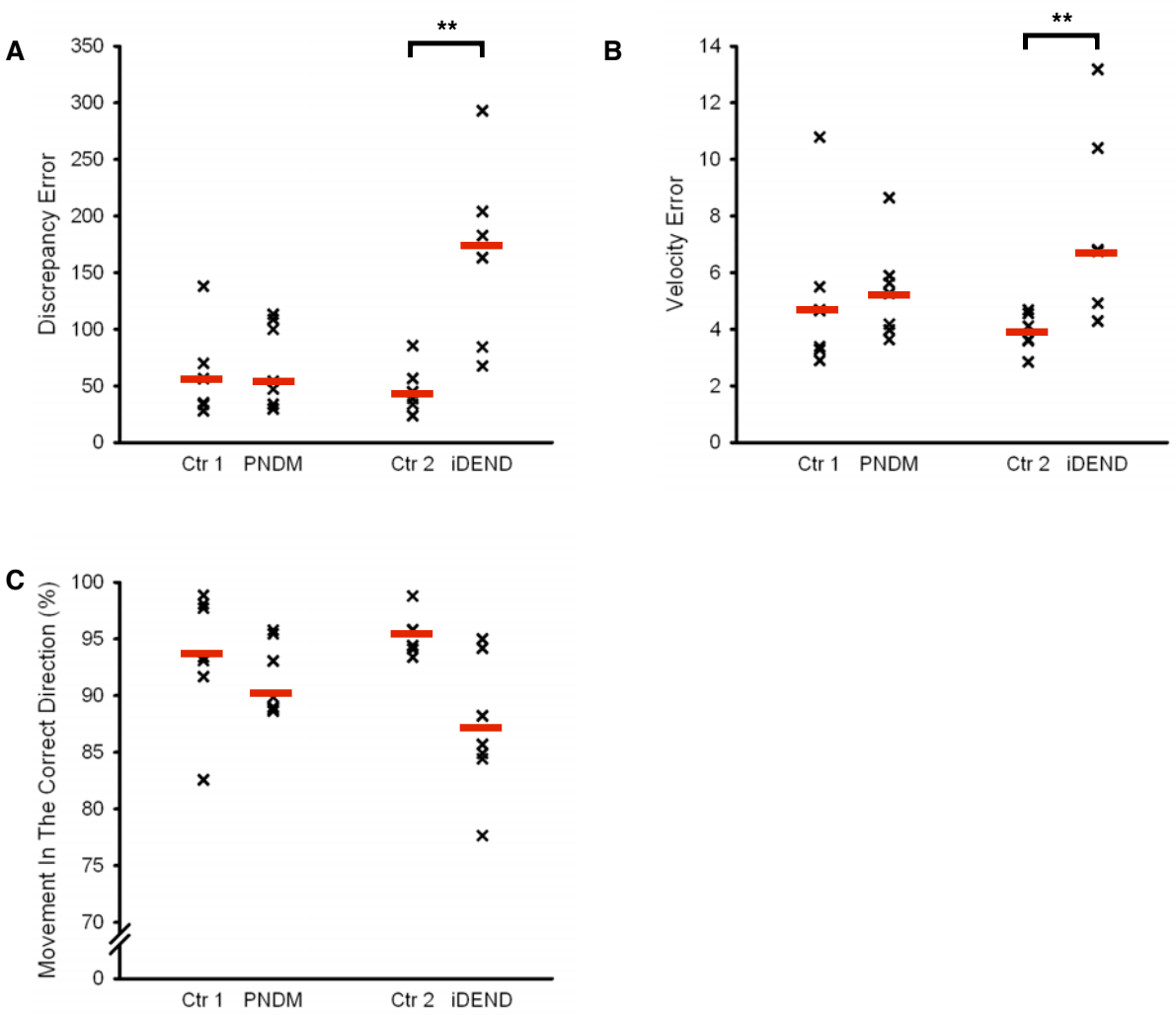

Figure 5.4 Visual tracking in PNDM and iDEND: Linear movement with memory-guided tracking

Scatter plots showing errors when tracking a target moving at constant velocity. The target was blanked during the middle third of each sweep. Data for PNDM (n=7) and iDEND (n=6) patients are plotted against matched controls, as indicated. The red bars indicate the median error. (**A**) Discrepancy errors of PNDM and iDEND patients and their matched controls. Patients with iDEND were significantly less accurate than controls, but PNDM patients were not affected. **, $p < 0.01$, post-hoc Mann-Whitney U-test. (**B**) Velocity errors of PNDM and iDEND patients and their matched controls. The velocity of the movements of iDEND patients were significantly less accurate than controls. **, $p < 0.01$, post-hoc Mann-Whitney U-test. (**C**) Direction errors of PNDM and iDEND patients and their matched controls. There were no significant differences between the groups (Kruskal-Wallis test).

Table 5.5 Discrepancy errors of iDEND patients

Mutation	Age	Task 1	Task 2	Task 3
V59M	13	185.9	543.7	292.9
V59M	9	296.4	513.9	n/a
V59M	20	59.9	48.2	84.4
V59M	17	59.5	75.0	182.7
R201C	9	49.1	51.7	204.0
R201C	33	34.9	37.2	67.6
R201S	36	30.8	38.6	163.3

5.4.4 Memory-guided tracking, but not visually guided tracking are impaired in iDEND, but not in PNDM

Task 3 may be decomposed into visually-guided tracking (the first and last third of each sweep; segments 1 and 3, respectively) and memory-guided tracking (segment 2, the middle third of the sweep). In order to determine if the significant difference found between patients and controls in task 3 was due to a difference in memory-guided tracking, the three segments of task 3 were analysed separately. Only the discrepancy error was calculated for each segment as this error appeared to be the most sensitive to gain-of-function mutations in the K_{ATP} channel.

In segment 1, the median discrepancy error of PNDM and iDEND patients was not significantly different than that of their matched controls (Figure 5.5 A, B, left, $p = 0.226$). This is consistent with the result from task 1.

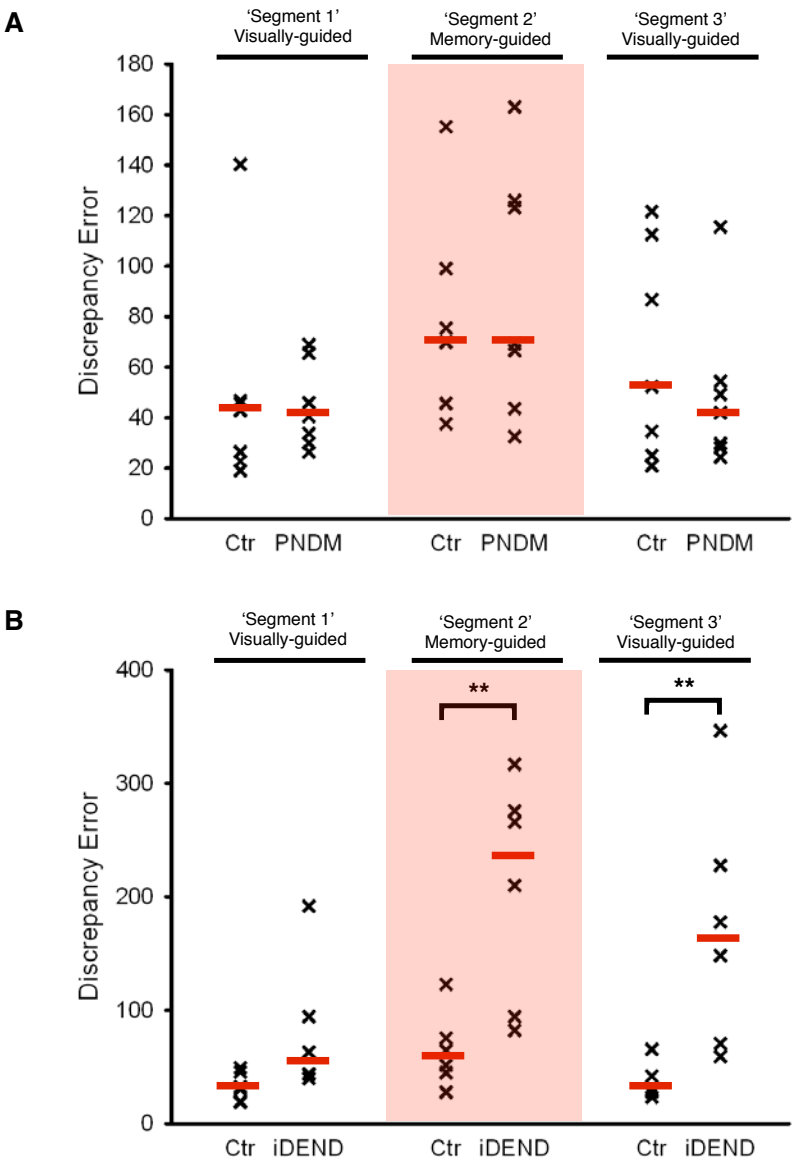

Figure 5.5 Comparison of visually-guided and memory-guided tracking in PNDM and iDEND

Scatter plots showing discrepancy errors of PNDM (n=7) and iDEND (n=6) patients and their matched controls, as indicated, on task 3. Task 3 was decomposed into three 'segments'. In segment 1 the target was visible, in segment 2 it was blanked, in segment three it was made visible again. The segments were analysed separately. Note the difference in the scale of y-axis on the two plots. The red bars indicate the median error. (**A**) Discrepancy errors of PNDM patients and their matched controls on segments 1-3 of task 3, as indicated. There were no significant differences (Kruskal-Wallis test). Note that the error rates of controls and PNDM patients increased when the target was blanked, which is consistent with the increased difficulty. (**B**) Discrepancy errors of iDEND patients and their matched controls on segments 1-3 of task 3, as indicated. Patients with iDEND were not significantly different from controls in segment 1. However, when the target was blanked in segment 2, and the participants were required to track the moving target by memory (in a predictive manner), the patients with iDEND were much less accurate than controls. This inaccuracy persisted when the target was turned back on in segment 3, though this may be because they did not have enough time to correct their position. **, $p < 0.01$ post-hoc Mann-Whitney U-test.

In segment 2, the median discrepancy error of PNDM and iDEND patients was higher than the median of their matched controls (Figure 5.5 A, B, middle). The variability of error values increased dramatically in the iDEND group, but remained relatively constant for the other three groups. The Kruskal-Wallis test indicated that the error values of the different groups were significantly different ($p = 0.026$). The post-hoc pairwise comparisons showed that there was no significant difference between the two control groups ($p = 0.628$) or between controls and PNDM patients ($p = 0.902$), but the discrepancy errors of iDEND patients were significantly higher than controls ($p = 0.009$).

In segment 3, the Kruskal-Wallis test indicated that the error values of the different groups were significantly different ($p = 0.014$). The post-hoc pairwise comparisons showed that there was no significant difference between the two control groups ($p = 0.366$) or PNDM patients and their controls ($p = 0.710$), but the discrepancy errors of iDEND patients were significantly higher than controls ($p = 0.004$).

As participants completed tasks 1-3 sequentially, it was possible that order effects could influence the result. In a similar way to that described for early versus late sweeps, it is possible that fatigue or waning concentration could diminish performance, or that performance might improve on the later tasks due to the practice. The intervening sinusoidal tracking task (task 2) could also interfere with an individual's ability to subsequently perform linear tracking. In order to assess the impact of these factors, discrepancy errors for segment 1 of task 3 were compared with discrepancy errors from task 1 for each group using a Kruskal-Wallis test. There was no significant difference for any of the four groups (PNDM patients, $p = 0.482$; controls for PNDM patients, $p = 0.277$; iDEND patients, $p = 0.522$; controls for iDEND patients, $p = 0.423$). Therefore performance in visually-guided linear tracking in task 3 did not seem to be influenced by prior practice.

5.4.5 Manual dexterity may be impaired in iDEND

Mann Whitney U-tests revealed no significant difference in the time taken to transfer twenty beads into the bead board ($p = 0.749$; Figure 5.6 A), or to complete the overall bead board task ($p = 0.848$; Figure 5.6 B), between controls and patients with PNDM. The mean score for the two iDEND patients was slightly higher than the mean for controls and PNDM patients, but the significance of this observation could not be assessed due to the low numbers tested.

The vast majority of individuals expressed a preference for using the right hand (data not shown). Consistent with this, the mean time to complete the Annett peg moving task was lower for the right hand than the left hand for each group tested (Figure 5.7 A, B). Mann Whitney U-tests revealed no significant differences between controls and PNDM patients in the time taken to complete the Annett peg board task whether carried out with the right hand ($p = 0.316$) or the left hand ($p = 0.382$). The mean score of the the two iDEND patients was again somewhat higher than the mean for controls and PNDM patients, but the significance of this observation could not be assessed due to the low numbers tested.

The performance of PNDM and iDEND patients on the Annett peg moving task was compared qualitatively to the performance of a population of controls (Figures 5.7 C, D). Using the right hand, the scores for all patients with PNDM lay within one standard deviation of the mean. One individual with iDEND (R201C mutation) scored within one standard deviation of the mean, but the other individual (V59M mutation) scored poorly - well outside two standard deviations of the mean. A similar pattern was seen for the left hand, although two PNDM patients now scored outside of one standard deviation of the mean. The patients with iDEND showed the same pattern as with the right hand.

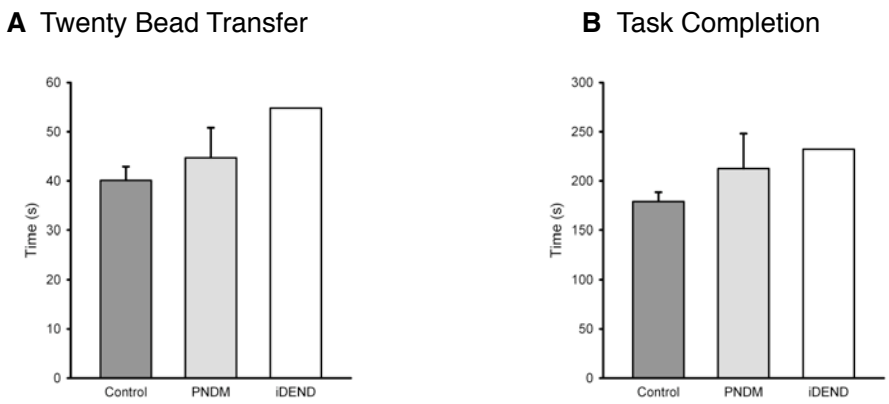

Figure 5.6 Bead Board task in PNDM and iDEND

Bar charts showing the performance of PNDM and iDEND patients and their matched controls on the bead board task. Control (dark grey bars, n=7, matched to the PNDM patients), PNDM (light grey bars, n=7) and iDEND (white bars, n=2). Data are mean ± SEM. (**A**) Time taken to transfer twenty 4mm wooden beads from a plate to the 52mm well of the bead board. (**B**) Time taken to transfer the beads sequentially into each of the five wells on the bead board. There were no significant differences between controls and PNDM patients (Mann-Whitney U tests).

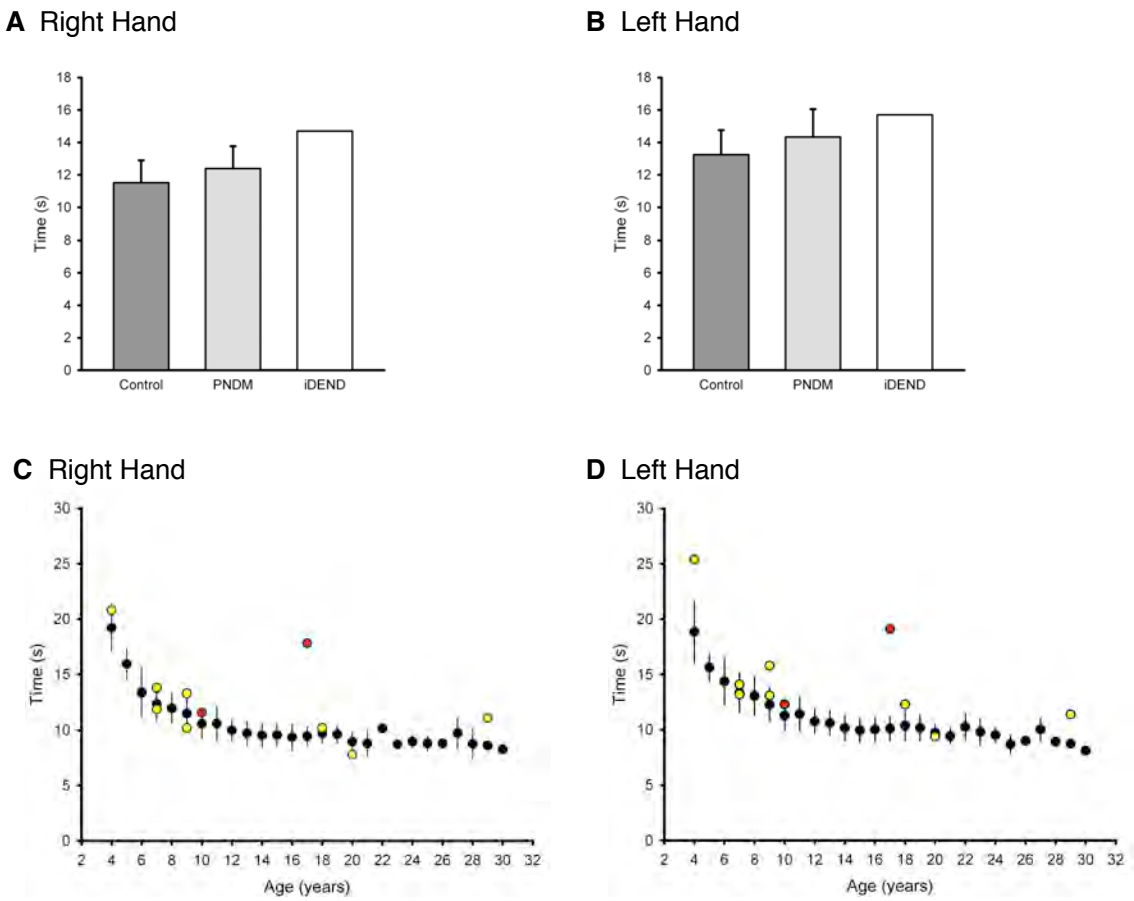

Figure 5.7 Annett peg moving task in PNDM and iDEND

The Annett peg moving task was used to assess manual dexterity of PNDM and iDEND patients and matched controls. (**A**, **B**) Time taken to transfer ten pegs from one side of the apparatus to the other, using only the right hand or the left hand, as indicated, for controls (dark grey bars, n=8, matched with the PNDM patients), PNDM (light grey bars, n=8) and iDEND (white bars, n=2) individuals. Data are mean ± SEM. There were no significant differences based on group or sex (Mann-Whitney U tests). (**C**, **D**) Time taken to transfer 10 pegs using the right or left hand, as indicated, for control (black), PNDM (yellow) and iDEND (red) individuals. The individual times for PNDM and iDEND patients are plotted. Control data, provided by Dr. Tom Scerri, are mean ± standard deviation, therefore the error bars encompass ~68% of the control population. The number of observations varied from 1-82 (n = 1 for ages 26, 29 and 30). Error bars were only plotted when there were 3 or more observations for that age.

5.4.6 Saccadic and smooth pursuit eye movements are impaired in iDEND

The eye movements of two iDEND patients were recorded. Both showed clear disorders of saccadic and smooth pursuit eye movements (Videos 1-4). By contrast, no controls and no PNDM patients showed impairments on either task. A representative example of a control participant performing saccadic and smooth pursuit eye movements is provided in Videos 5 and 6.

The impairments of the patients were not identical. In the individual with the R201C mutation, prosaccades were hypermetric. Her smooth pursuit eye movements were jerky, proceeding in a 'cogwheel' manner, with increased gain, and saccades back to the target position. This is in contrast to reports in the literature for patients with known cerebellar trauma that describe cogwheel tracking with reduced gain superimposed with catch-up saccades.

In the individual with the V59M mutation, prosaccades and smooth pursuit appeared to be grossly malcoordinated. She showed a strong tendency towards upward movements of the eyes when attempting to direct gaze from side to side. However, a systematic appraisal was complicated as her eye movements were usually associated with significant movements of the head. The individual was encouraged to move only her eyes, but head movements persisted.

5.5 Discussion

5.5.1 Performance on tracking tasks is consistent

The performance of individual participants was consistent within tasks and between tasks. Consistency within tasks was assessed by comparing errors from the first five sweeps with the last five sweeps. As errors were no different, possible learning or attention deficits do not seem to contribute significantly to performance. Furthermore, as visually-guided errors from task 1 and task 3 (segment 1 of task 3) were not different, it would seem that exposure to the intervening task did not interfere with subsequent performance.

The consistency of error values also suggested that attention did not vary within and between the tasks. Although attention did not seem to change during the testing period, it is possible that deficits in attention could still contribute to the higher levels of errors of iDEND patients. Indeed, as mentioned in the methods section, some younger iDEND patients with V59M mutations were not able to carry out the task - they stood up and walked away, or they repeatedly looked away from the screen and initiated conversations instead of completing the task. Although all of the iDEND patients included in these analyses did not show overt inattention, with these studies it is not possible to determine the impact of attentional deficit on task performance.

It is also worth pointing out that two of the iDEND patients who completed the visual tracking tasks also had their eye movements recorded. They were clearly able to understand the verbal instructions and carry out the protocol, which was of a similar duration and nature to the tracking tasks. Furthermore, the clear disturbance in their oculomotor coordination correlates well with the impairments in their tracking ability. It is likely, therefore, that the oculomotor malcoordination, not inattention, is the underlying cause of the tracking impairments.

5.5.2 Tracking is impaired in iDEND but not PNDM

Patients with PNDM were not impaired compared to matched controls on any of the three types of tracking task administered. Although their median errors were often higher than controls, the differences were not significant. This finding is consistent with the fact that neurological problems have not been reported in PNDM patients.

By contrast, patients with iDEND performed significantly worse than controls on tasks 2 and 3. Furthermore, although there were no significant differences between the groups on task 1, the trend neared significance ($p = 0.058$). So it is possible that recruitment of more patients (thus increasing the power of the statistical analysis) would reveal impairment on this task also. In general, the error scores of individuals with the V59M mutation were higher than those of patients with other iDEND mutations (Table 5.5).

Patients with iDEND were impaired on task 2, but not task 1, even though both tasks required visually-guided tracking. A greater impairment on task 2 might be expected, because the target was constantly changing velocity, making this task more difficult. However, velocity errors on task 2 (and task 1) were not significantly different to controls. An impairment in discrepancy, but not velocity, indicates that the patients generally track at the correct rate, but that the accuracy of tracking is impaired - it suggests that they tend to lag behind or stay in front of the target as it moves.

Task 3 appeared to be the most sensitive at discriminating impairments of iDEND patients. Discrepancy errors and velocity errors were significantly higher in iDEND patients than controls. Detailed analysis revealed this was primarily due to the impaired performance when the cursor vanished and participants were required to track by extra-visual means (segment 2 of task 3). Discrepancy errors in segment 3 were also significantly higher than controls, but

this is likely to be because tracking was already off-target when the target was turned back on and therefore errors from segment 2 will influence the error score from segment 3.

Tracking moving targets with coordinated movements of the eye and hand relies on intact cerebellar processing. As patients with iDEND perform worse than controls when tracking visible targets and targets that have been blanked, it is likely that the cerebellum is impaired in iDEND. The level of impairment on the tasks correlated with the 'load' that was placed on the cerebellum. There was no significant impairment on the easiest task (task 1), though the difference neared significance. Patients were impaired on task 2, which was harder. And in the task that placed the greatest processing load on the cerebellum, when the target was blanked, patients with iDEND were clearly impaired compared to controls. Therefore these results suggest that the cerebellum is impaired in iDEND.

The greatest and most specific demand on the cerebellum in coordinated tracking tasks comes when the eyes and hand are expected to move independently, i.e. the eyes must track a different target to the hand [369]. Therefore it would be interesting to examine the performance of patients with iDEND on this more complex, and cerebellar-specific version of the task.

5.5.3 Manual dexterity may be impaired in iDEND

No significant differences were found between controls and PNDM patients on either test of manual dexterity, in accord with the lack of neurological features in PNDM. Only two patients with iDEND were tested. The mean scores of both iDEND patients were higher than that of controls or PNDM patients, but when the individual's scores on the Annett peg board were compared to the performance of a population of controls, it would appear that patients with iDEND may not necessarily score significantly worse than controls, as the individual with the

R201C mutation scored within one standard deviation of the mean. In contrast, the score for the individual with the V59M mutation was beyond two standard deviations. More patients with iDEND need to be tested before firm conclusions can be drawn, but it is possible that manual dexterity might be impaired by some iDEND mutations.

5.5.4 Oculomotor malcoordination and iDEND

Only two patients with iDEND were available for eye movement recordings, so more individuals need to be assessed before firm conclusions can be drawn. However, both iDEND patients showed aberrant eye movements whereas those of controls and PNDM patients were unimpaired.

The individual with an R201C mutation in Kir6.2 displayed clear hypermetric saccades. Smooth pursuit was also impaired, and appeared to occur in a cogwheel manner, but with increased gain and saccades back to the target, rather than decreased gain with catch-up saccades, which is the pattern presented in literature reports (I could find no reports of increased gain with saccades back to the target). As discussed above, these features are characteristic of impairment of the oculomotor vermis and the fastigial oculomotor region of the cerebellum. (The fastigial oculomotor region receives its input from the oculomotor vermis.) Kir6.2 is expressed in the fastigial nucleus [183], and Purkinje cells of the vermis are inhibited in iDEND (Chapters 3 and 4). Therefore, it is reasonable to speculate that these impaired eye movements may be due to the presence of mutant K_{ATP} channels in the cerebellum.

The combination of saccadic and smooth pursuit impairments in this individual is interesting in the context of the literature. Unilateral lesions of the oculomotor vermis cause hypometric ipsilateral and hypermetric contralateral saccades [360] whereas unilateral lesions of the

fastigial oculomotor region lead to hypometric contralateral and hypermetric ipsilateral saccades. Bilateral oculomotor vermis lesions lead to hypometric saccades, and bilateral fastigial oculomotor lesions lead to hypermetric saccades. As this patient shows hypermetric saccades when moving the eyes both leftward and rightward, this would suggest that the fastigial oculomotor region was bilaterally impaired. The bilateral nature of the impairment is expected as Kir6.2-R201C will be produced throughout the cerebellum. However, bilateral fastigial oculomotor region lesions are not associated with impairments in smooth pursuit - it is thought that the lesions on either side cancel each other out, resulting in no net deleterious functional effects [365]. Therefore, as this individual shows both saccadic and smooth pursuit impairment it is unlikely that the fastigial oculomotor region alone is impaired. Perhaps impairments in other brain regions contribute to the unusual presentation of her cogwheel tracking.

The individual with a V59M mutation in Kir6.2 displayed grossly malcoordinated eye movements, with a predisposition towards upward movements of the eyes when attempting to gaze directly to the left or right. She also showed a strong tendency to move her head when making eye movements. It is possible that these head movements are a compensatory response to the impaired eye movements. If this is correct, and is a general compensatory mechanism seen in other individuals with iDEND, then this observation may impact upon the results from the hand-eye tracking task. It was assumed that the task would be sensitive to impairment of movements of the hand and/or the eyes, but if compensatory head movements are present that reduce the impact of the eye movement disorder then the results from the tracking tasks are likely to be an underestimate of the impairment in eye movement *per se*. However, the results will be a reflection of the success of these compensatory mechanisms, as complete compensation would result in no significant differences between patients with iDEND and controls. As errors were significantly different between the groups, then it can be assumed that compensatory mechanisms have not mitigated the deleterious effects of the K_{ATP} channel mutations on hand-eye tracking.

5.5.5 Implications for therapy

The results presented in this chapter provide strong evidence that the cerebellum is dysfunctional in iDEND. These results complement anecdotal observations that patients with iDEND are clumsy and have difficulty in walking in a straight line; and that young children with iDEND fall over more often than their peers. Furthermore, a previously overlooked symptom of iDEND may have been revealed: disordered eye movement. It remains to be seen if this impairment is universal to all iDEND patients but if so, it may be potentially useful in the diagnosis and/or treatment of iDEND.

Firstly, malcoordinated eye movements have been implicated in visual dyslexia [384]. Anecdotal reports suggest that patients with iDEND have difficulty in reading, though they also experience cognitive developmental delay. Nevertheless, it is possible that disordered eye movements could contribute to their difficulties. The eye movements and reading ability of dyslexics have been improved by the use of spectacles that filter specific wavelengths of light [385], but the mechanism underlying this improvement remains unclear. It would be interesting to see if the eye movements and reading ability of patients with iDEND are improved by use of these glasses.

Secondly, the experiments described in Chapters 3 and 4 indicate that no major developmental effects occur at the level of cerebellar Purkinje cells when Kir6.2-V59M is expressed. Therefore it is possible that the impairment in eye movements will remit given sufficient sulphonlyurea treatment. If this is so, then the measurement of eye movements may be a useful, quantitative clinical tool for determining the level of alleviation of the neurological symptoms of iDEND.

Chapter 6: Regulation of FTO Expression in the Brain

6.1 Summary

1) In previous studies, FTO mRNA levels were measured in rodents following prolonged (40-48 hour) periods of fasting. Fasting for this duration has been shown to cause significant metabolic and psychological stress. Therefore, alteration of FTO mRNA levels may have reflected these pathophysiological processes. In the experiments presented in this chapter, mice were fasted overnight.

2) FTO mRNA and protein levels in the brain and two types of skeletal muscle were not altered following an overnight fast.

3) The number of POMC neurons (which regulate anorexigenic behaviour) that expressed FTO protein did not change following an overnight fast.

4) FTO protein was found in the nuclei of cells throughout the brain. FTO expression was not restricted to specific brain regions. Areas of high neuronal density, such as the cerebellum and hippocampus, were conspicuous. Fasting did not alter the uniform distribution of FTO expression in the brain.

5) FTO protein was expressed in neurons almost exclusively. There were some non-neuronal cells that expressed FTO, but these were few.

6) I found no evidence that FTO levels were altered by fasting. Perhaps the physiological function of FTO will be better understood by knocking-out or over-expressing the protein in specific tissues.

6.2 Introduction

There is little physiological understanding of how FTO influences body weight, as discussed in Chapter 1. In particular, it remains unclear if nutritional status (e.g. fasting) alters FTO levels. The heterogeneity of the data reported in the literature is unlikely to be due to differences in the models used as differences between studies remain even when results from rats [228, 248] and mice [218, 247] are considered separately.

Human beings with intronic variants near *FTO* show increased food intake, and feeding behaviour is altered in mice that lack or over-express *FTO* (as discussed in Chapter 1). These data suggest that FTO influences obesity and fat mass via changes in food intake, which suggests a possible role for FTO in the brain. Since starvation induces a compensatory increase in food intake when food is reintroduced [386], it is possible that this behaviour reflects a change in the expression level or activity of FTO. Here, I set out to examine if changes in expression are involved.

6.2.1 Physiological validity of fasting

When investigating the influence of nutritional status on FTO levels, the duration of food deprivation has been highly variable. Some studies have imposed 40-48 hours of fasting, variously resulting in downregulation of FTO mRNA levels in the arcuate nucleus of the hypothalamus [218], upregulation of levels in the hypothalamus [228], and no significant changes in the hypothalamus [247]. Others have imposed long-term nutritional restriction [248], which results in decreased FTO mRNA levels in the hypothalamus.

Fasting mice for 16-24 hours leads to significant weight loss and depletion of hepatic glycogen stores [387-389], which is exacerbated by an additional day of fasting [389].

Indeed, ~60% of fat stores in mice are consumed during a 24 hour fast [390] and most of the mobilizable fat may be used up within two days of fasting [391]. Fasting mice for longer than 48 hours leads to increased mortality [391, 392]. As rodents are omnivorous, eating a wide variety of grains, plants and (when necessary) animal tissues [393], it is unlikely that they will normally experience food deprivation approaching 40-48 hours. Thus, fasting for >24 hours may result in pathophysiological responses in rodents.

Fasting leads to changes in plasma concentrations of enzymes and substances relating to carbohydrate and lipid metabolism [389], but there is little difference in these changes whether rodents are fasted for 24 hours or 48 hours. The preservation of circulating nutritional status during lengthy fasting may come at the price of metabolic health [394]. For example, glucocorticoid levels are markedly elevated in rats following 48 hours of food deprivation (higher than that seen following 24 hours of fasting [395, 396]), and the circadian rhythmicity of their release deteriorates [397].

Therefore long durations (40-48 hours) of fasting are not desirable when attempting to understand systems that respond to nutritional status. Indeed, long durations are not necessary. Fasting for as little as 5 hours results in similar insulin and re-feeding responses to overnight fasting (~16 hours), as well as similar downstream phosphorylation events related to insulin signalling [387]. Therefore, in summary, animals will be hungry after fasting for up to 24 hours, and their plasma biochemistry for carbohydrate and lipid metabolism will reflect their altered nutritional status. However, metabolic stress will be low. Therefore, if the physiological function of the FTO protein is to be deciphered, rather than its responses to pathophysiological conditions, then shorter periods of fasting should be studied.

6.2.2 Where should we look?

When searching for the physiological function of FTO in the brain, and how FTO might influence body weight, the majority of studies have looked solely within the hypothalamus. Specific neuronal groups within the hypothalamus regulate feeding behaviour [226]. For example, stimulation of the lateral hypothalamus results in voracious feeding behaviour [398], and ablation of the paraventricular nucleus dramatically increases feeding - indicating that the neurons in this region are anorexigenic [399]. Therefore, it is understandable that studies have focused on this brain area. However, high FTO mRNA levels have also been identified in the cerebellum and indeed throughout the brain [227, 228], so it would be interesting to see if its expression is differentially regulated in different brain regions.

6.2.3 Nutritional regulation of FTO expression

In this chapter I assessed the expression of *FTO* following overnight fasting. The relative amounts of FTO mRNA and protein were quantified in three different brain regions ('rostral brain', cerebellum and hypothalamus) and two different types of skeletal muscle (gastrocnemius and extensor digitorum longus). The three brain regions were selected for their different functional roles. As discussed above, normal hypothalamic function is crucial for feeding behaviour. (By looking at the whole hypothalamus, the FTO levels of the different neuronal groups - anorexigenic and orexigenic - were pooled.) By contrast, the cerebellum is crucial for motor coordination and timing (see Chapters 3-5) and is not considered to have an important role in feeding, though it may influence appetite through its connections with the hypothalamus [400]. Similarly, brain regions rostral of the hypothalamus are primarily composed of neocortex and deal primarily with a variety of cognitive, sensory and mnemonic functions [401]. The two types of skeletal muscle are both largely composed of fast twitch fibres [315, 402] and were included to see if any possible effects were limited to the brain.

To see if FTO levels changed in a specific population of contextually relevant neurons, I counted the number of *POMC*-expressing neurons of the arcuate nucleus of the hypothalamus that expressed FTO in the fed and fasted state. Activation of *POMC*-expressing neurons reduces food intake [403], therefore in the fasted state POMC neuronal activity was expected to be low. Immunohistochemistry was also used to qualitatively assess the pattern of *FTO* expression across the brain in the free-fed and fasted states.

A previous study had indicated that FTO mRNA was absent from the vast majority of glia [228]. No studies had shown directly that *FTO* is expressed in neurons, and it was also unclear if *FTO* was expressed in all neurons or in a subset. To address these questions, brain sections were double labelled with primary antibodies that were specific to neurons (anti-NeuN) and FTO, and the number of double stained cells were counted. This was done on brain sections from fed and fasted animals.

6.3 Methods

6.3.1 Nutritional regulation of FTO mRNA levels

C57BL/6J mice were killed by cervical dislocation in the middle of the light cycle (approximately 10am). Mice were either fed *ad libitum* ('free-fed') or were fasted for ~18 hours prior to tissue harvesting. Five tissue samples were collected: ' rostral brain', cerebellum, hypothalamus, gastrocnemius muscle, and extensor digitorum longus muscle. Rostral brain samples included all brain regions rostral of approximately Bregma +1.10mm - corresponding to regions "I" and "II" from Fredriksson et al, 2008 [228].

For RT-qPCR experiments 4 pairs of each sex of 7-week-old (mean age 52 ± 1.3 days old) C57BL/6J mice were used. Tissues were rapidly dissected and RNA was extracted and processed as described in Chapter 2. The three brain samples and two muscle samples from each mouse were probed for transcripts of the reference genes ACTB, HMBS, HPRT1, HSPA8, RPL13A and UBC (see Chapter 2 for further details) along with FTO. The relative quantity of FTO mRNA in each tissue was determined using the geNorm method [266]. Levels of FTO mRNA were normalised to the geometric mean of the levels of HSPA8, RPL13A and HMBS reference genes. The most stable reference gene was HSPA8.

The normalised relative quantities of FTO were compared by two-way ANOVA, assessing the impact of nutritional status (free-fed, fasted) and sex on levels of FTO mRNA for each tissue separately. The data for the rostral brain and hypothalamus satisfied all assumptions for analysis by ANOVA, as outlined in Chapter 2, therefore $p < 0.05$ was considered significant for these tissues. Levene's test showed that variances were not equal for data from the cerebellum, gastrocnemius muscle and extensor digitorum longus muscle. Therefore $p < 0.01$ was considered significant for these tissues [271].

To compare transcript levels between tissues a one-way ANOVA was conducted to assess the impact of tissue type (rostral brain, cerebellum, hypothalamus, gastrocnemius muscle, extensor digitorum longus muscle) on levels of FTO mRNA. Levene's test revealed that error variances were significantly different between the data sets therefore $p < 0.01$ was considered significant [271]. For the post-hoc pairwise comparisons, a Bonferroni adjustment was made to the alpha level, so $p < 0.005$ was considered significant.

In the geNorm analysis described above, which followed the standard protocol [266], only data from reference genes was included so that the most stable ones could be identified. To compare the stability of FTO to the stability of the reference genes a subsequent geNorm

analysis was performed that included all data (reference genes and FTO). The brain samples were assessed separately from the muscle samples in this analysis.

6.3.2 Nutritional regulation of FTO protein levels

For protein blotting experiments, 4 pairs of each sex of 8-week-old (mean age 57 ± 2.3 days old) C57BL/6J mice were used. Tissues were rapidly dissected and snap-frozen in liquid nitrogen before proteins were extracted and processed as described in Chapter 2. Separated proteins were probed for FTO using an antibody raised against the full-length recombinant murine FTO protein, which is described below. The same protein samples were also probed for HSC70, which is the protein product of the HSPA8 gene - the most stable reference gene identified during the RT-qPCR experiments. Therefore HSC70 acted as a stably expressed loading control.

Murine FTO was predicted to be 58kDa in weight [225], and the anti-FTO antibody used in these experiments detected a single band at approximately 60kDa in total protein samples from mouse tissues (Appendix 11). Furthermore, the antibody produced no signal in total protein samples isolated from an FTO knockout mouse (Appendix 11; the knockout mouse protein blot was kindly supplied by Chris Church). Finally, the antibody labelled cell nuclei when it was used in immunohistochemistry experiments (described in later sections). This is consistent with previous reports that FTO localises to the nucleus [218, 223]. In summary, these experiments indicate that the antibody was selective for FTO.

The quantities of FTO and HSC70 were determined by densitometry as described in Chapter 2. These values were then converted into relative quantities (all values were expressed relative to the highest from that blot), and the relative quantities of FTO were normalised to the relative quantities of HSC70.

The normalised, relative quantities of FTO for each tissue were compared using two-way ANOVAs, to assess the impact of nutritional status (free-fed, fasted) and sex. The data for the rostral brain, cerebellum, gastrocnemius muscle and extensor digitorum longus muscle satisfied all assumptions for analysis by ANOVA, as outlined in Chapter 2, therefore $p < 0.05$ was considered significant for these tissues. Levene's test indicated inequality of variances for the data from the hypothalamus, therefore $p < 0.01$ was considered significant for this tissue [271].

To compare protein levels between tissues (rostral brain, cerebellum, hypothalamus, gastrocnemius muscle, extensor digitorum longus muscle) a one-way ANOVA was conducted. All assumptions were satisfied (see Chapter 2) so $p < 0.05$ was considered significant. A Bonferroni adjustment was made to the alpha level for the post-hoc pairwise comparisons, so $p < 0.005$ was considered significant.

In a subsequent analysis the results for the three different brain regions were pooled, and the results for the two different muscle samples were pooled, to increase statistical power. These pooled results were then compared using a one-way ANOVA, to assess the impact of nutritional status (free-fed, fasted) on FTO protein levels in the brain and the muscles. All assumptions were satisfied, so $p < 0.05$ was considered significant.

6.3.3 FTO expression in POMC cells

For quantification of the proportion of POMC neurons expressing GFP, 7-week-old (mean age 50 ± 1.1 days) POMC Z/EG mice were perfused with a 4% paraformaldehyde solution and brains sectioned as described in Chapter 2. Neurons expressing *POMC* were efficiently

labelled in POMC Z/EG mice - more than 90% of neurons that express α-MSH (a peptide product of the *POMC* gene) express GFP in this mouse [255].

All subsequent steps were carried out blinded to the feeding status of the mice. Brain sections were probed with anti-FTO antibody, a biotinylated anti-rabbit IgG secondary antibody, and visualised with Texas-Red conjugated secondary antibodies using an Avidin-Biotin amplification protocol (Vector Labs). Sections were also treated with DAPI, which stains the nuclei of all cells.

Images from stained and mounted sections were acquired using confocal laser scanning microscopy at 63x magnification. At least 5 images were acquired for each mouse, and each condition. POMC neurons were identified in the acquired images by their intrinsic GFP fluorescence (Figure 6.2). As GFP in POMC neurons was expressed throughout the cytoplasm and nucleus, the identification of these cells was facilitated by looking at the DAPI staining (which is restricted to the nucleus). The number of FTO-positive (red) nuclei of POMC neurons were counted and expressed as a percentage of the total number of POMC neurons. An arbitrary, mental threshold was used to determine if a nucleus was FTO-positive or not. The feeding status of the animals was revealed after the percentage of FTO-positive POMC neurons was calculated.

The mean percentage of FTO-positive POMC cells in the free-fed and fasted states was compared using a two-way ANOVA to assess the impact of nutritional status and sex. All assumptions, as described in Chapter 2, were satisfied, so $p < 0.05$ was considered significant.

6.3.4 FTO expression throughout the brain

For other immunohistochemistry experiments, C57BL/6J mice (at least 3 males and 3 females) were perfused with a 4% paraformaldehyde solution at 7 weeks of age (49 days old). Brains were sectioned, probed with antibodies, and images acquired as described in Chapter 2.

Sections were processed in one of two ways. Some sections were probed with anti-FTO antibody alone, which was visualised with DAB, as described in Chapter 2. Separate sections were processed for fluorescence imaging. In these sections, FTO was labelled as previously described, and they were also probed with an anti-NeuN antibody, which labels neuronal nuclei. The manufacturer states that virtually all neurons are labelled by this antibody. However, they also state (and I confirmed) that Purkinje cells of the cerebellum are not. The anti-NeuN antibody was conjugated to Alexa 488 but this fluorescence signal proved too weak to identify neurons with confidence. Therefore the fluorescence signal was increased by probing with an anti-mouse IgG secondary antibody, which was conjugated to Alexa 477. As anti-FTO and anti-NeuN antibodies were raised in different species (rabbit and mouse, respectively), the secondary antibodies used to detect these primary antibodies were unlikely to cross react. This assumption was tested and there was no detectable fluorescence when anti-FTO was probed with anti-mouse IgG antibodies, and none when anti-NeuN was probed with anti-rabbit IgG antibodies (data not shown). Therefore cross-reactivity was minimal. Sections processed for fluorescence microscopy were also treated with DAPI, which stains nuclei of all cells. The proportion of FTO-positive neurons was calculated in a similar way to that described in section 6.3.3.

6.4 Results

There were no significant differences based on sex in any of the analyses. Therefore, only the results based on feeding status are reported below. In all figures, data from male and female animals are shown pooled.

6.4.1 FTO expression levels are unaltered following an 18-hour fast

There were no significant differences in FTO mRNA levels between free-fed and fasted animals (Figure 6.1 A): for rostral brain, $p = 0.797$; cerebellum, $p = 0.799$; hypothalamus, $p = 0.507$; gastrocnemius muscle, $p = 0.440$; and extensor digitorum longus muscle, $p = 0.912$. Therefore, FTO mRNA levels in all tissues were not significantly altered by fasting.

Looking at the pairwise comparisons of the data from free-fed animals, FTO mRNA levels from the three different brain regions were not significantly different. Similarly, levels from the two different types of muscle were not significantly different. However, the pairwise comparison for each brain sample versus each muscle sample was highly significant ($p < 0.001$ in each case). Therefore, FTO mRNA levels in the brain were significantly higher than in muscle. This is different to what has been reported previously, where FTO mRNA levels in skeletal muscle were found to be similar, or greater, than those in brain [228, 248]. However, neither study stated which muscles were analysed, so it is possible that FTO levels are higher in skeletal muscles other than gastrocnemius and extensor digitorum longus.

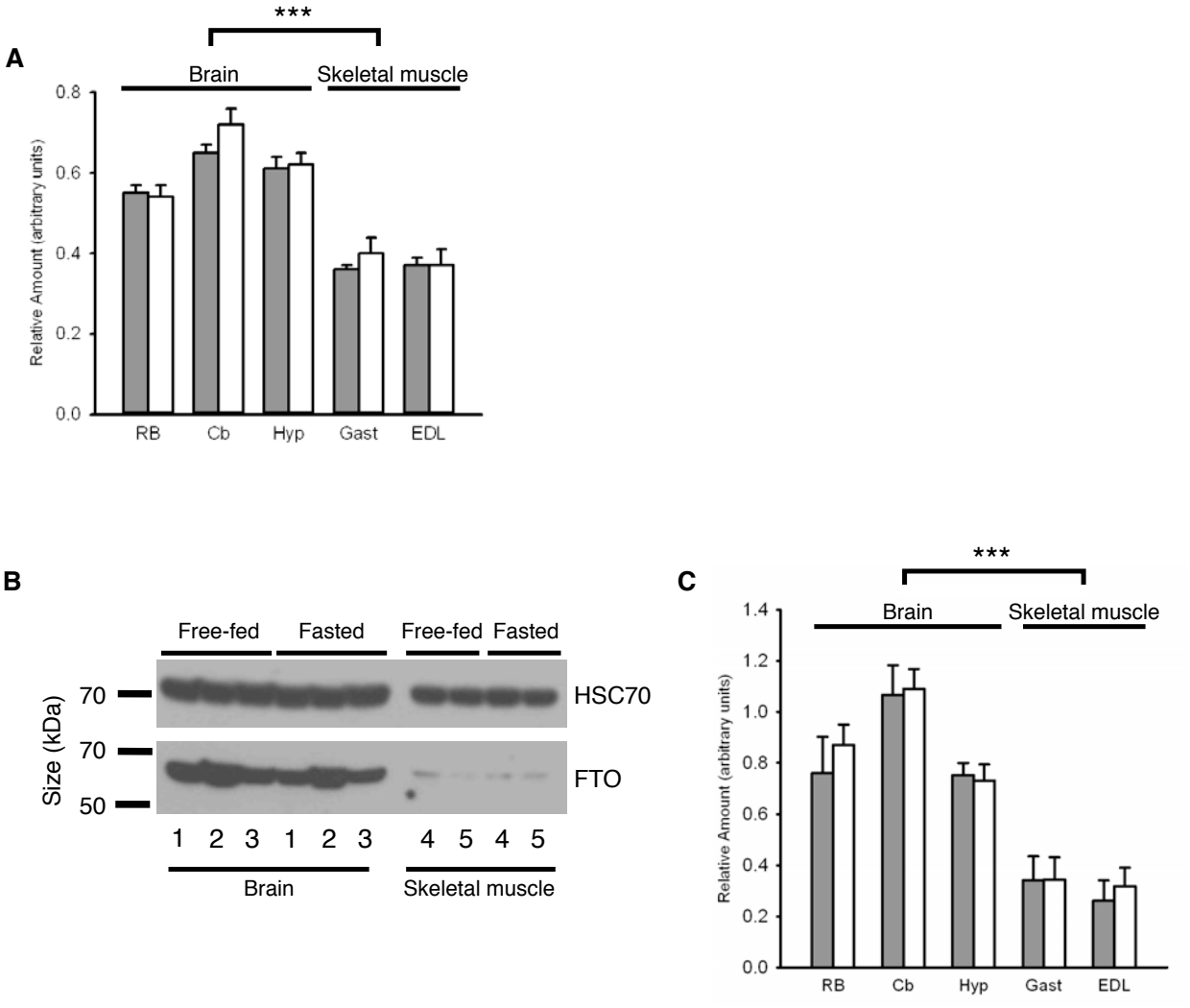

Figure 6.1 FTO mRNA and protein levels are not altered after ~18 hours of fasting

(**A**) RT-qPCR quantification of FTO transcript levels from free-fed (grey bars, n=8) and fasted (white bars, n=8) 7-week-old C57BL/6J wild-type mice. RB = rostral brain, Cb = cerebellum, Hyp = hypothalamus, Gast = gastrocnemius muscle, EDL = Extensor Digitorum Longus muscle. Data are mean ± SEM. There were no significant differences between brain samples, or between muscle samples, based on nutritional status (two-way ANOVAs). In free-fed mice, the level of FTO mRNA in each brain region was higher than in either of the two types of muscle (one-way ANOVA with post-hoc pairwise comparisons). ***, $p < 0.001$. (**B**) Representative Western blots of proteins from free-fed and fasted male C57BL/6J mice probed for murine FTO (58kDa) and heat shock cognate 70 protein (HSC70, 70kDa), which acted as a loading control. Lanes were loaded with total protein from rostral brain (1), cerebellum (2), hypothalamus (3), gastrocnemius muscle (4), extensor digitorum longus muscle (5). (**C**) Levels of FTO protein, normalised to HSC70, in tissues from free-fed (grey bars, n=8) and fasted (white bars, n=8) 8 week-old C57BL/6 wild-type mice. Data are mean ± SEM. There were no significant differences between brain samples, or between muscle samples, based on nutritional status (two-way ANOVAs). In free-fed mice, the pooled mean of the three brain samples was significantly higher than the pooled mean of the two muscle samples (one-way ANOVA). ***, $p < 0.001$.

A similar pattern of results was seen for FTO protein levels; there were no significant differences based on nutritional status (Figure 6.1 B, C) for rostral brain, $p = 0.526$; cerebellum, $p = 0.963$; hypothalamus, $p = 0.789$; gastrocnemius muscle, $p = 0.985$; or extensor digitorum longus muscle, $p = 0.870$. Therefore, FTO protein levels in all tissues were not significantly altered by fasting.

Looking at the data from free-fed animals, FTO protein levels from the three different brain regions were not significantly different. Similarly, levels from the two different types of muscle were not significantly different. However, FTO protein levels were significantly higher in the cerebellum than in either the gastrocnemius ($p < 0.001$) or the extensor digitorum longus ($p < 0.001$) muscle. Although FTO protein levels were not significantly different between the rostral brain and the muscles, or between the hypothalamus and the muscles, the comparisons neared significance. As the variability of these results were higher than from the mRNA experiments, it was possible that statistical power prevented these results from achieving significance. Consistent with this interpretation, when the results from the three brain samples were pooled and compared with the pooled results from the two muscle samples, FTO protein levels were significantly higher in brain than muscle ($p < 0.001$).

6.4.2 FTO transcript levels are often more stable than 'reference' genes

In the RT-qPCR experiments FTO levels were normalised relative to the geometric mean of three internal reference genes. The assumption is that the levels of the reference genes are not altered by fasting, which therefore provides a way of correcting for small errors in loading. However, by including FTO in the geNorm analysis it would seem that the validity of this assumption is dubious. FTO is among the three most stable genes in 5 of the 8 sets of brain samples, and is the fourth most stable in the other sets (Table 6.1). For the muscle samples, FTO is the most stable gene in 5 of the 8 sets, and is among the three most stable genes in

the other sets (Table 6.2). Therefore, FTO itself is one of the most stably expressed genes in these tissues, particularly in skeletal muscle. So normalising the quantity of FTO relative to these other (sometimes less stable) reference genes may be of questionable value. That said, when the raw relative values of FTO were plotted, the pattern was the same as that reported above, and there were still no significant differences based on feeding status (data not shown). So normalising the levels of FTO by the levels of these less stable reference genes did not alter the pattern of these results.

Table 6.1 Stability of reference genes and FTO in brain samples

	Most stable	2nd	3rd	4th
Pair 1	RPL13A	UBC	FTO	ACTB
Pair 2	UBC	FTO	HSPA8	ACTB
Pair 3	UBC	RPL13A	FTO	HMBS
Pair 4	UBC	FTO	HMBS	ACTB
Pair 5	HSPA8	UBC	RPL13A	FTO
Pair 6	UBC	HSPA8	FTO	RPL13A
Pair 7	RPL13A	UBC	HSPA8	FTO
Pair 8	HSPA8	RPL13A	UBC	FTO

Table 6.2 Stability of reference genes and FTO in muscle samples

	Most stable	2nd	3rd	4th
Pair 1	FTO	RPL13A	HMBS	HSPA8
Pair 2	FTO	HSPA8	HMBS	RPL13A
Pair 3	FTO	HMBS	HSPA8	RPL13A
Pair 4	HSPA8	HMBS	FTO	RPL13A
Pair 5	FTO	HSPA8	HPRT1	HMBS
Pair 6	FTO	HSPA8	HMBS	RPL13A
Pair 7	HPRT1	HSPA8	FTO	RPL13A
Pair 8	HPRT1	FTO	HMBS	HSPA8

6.4.3 The proportion of FTO-positive POMC neurons in the hypothalamus is not altered by fasting

Approximately 65% of POMC neurons were labelled with the anti-FTO antibody in sections from free-fed mice. This is consistent with previous reports that FTO is present in only some POMC neurons [223]. The proportion of FTO-positive POMC cells was not altered after 18 hours of fasting ($p = 0.541$) (Figure 6.2 A, B).

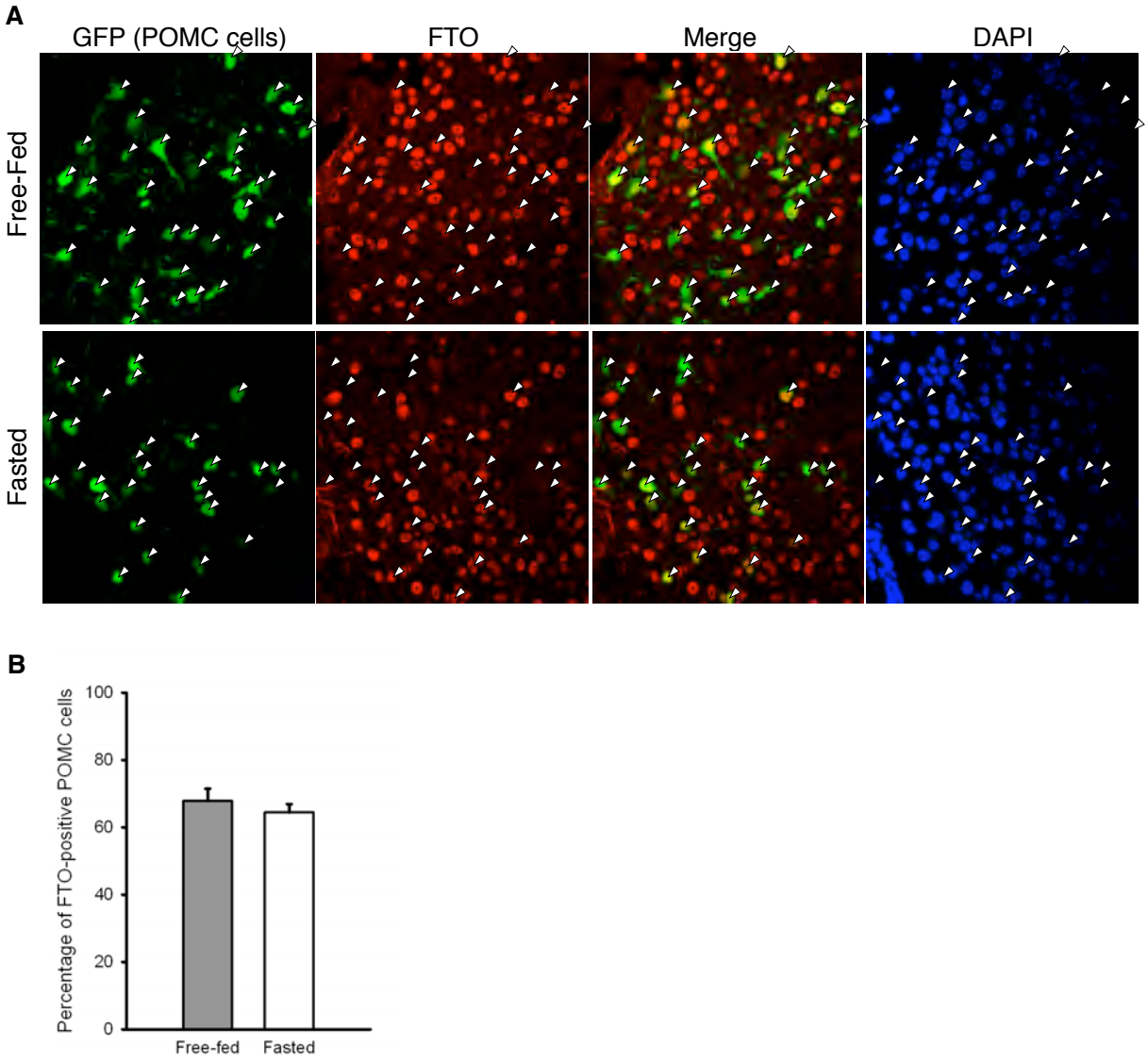

Figure 6.2 The proportion of POMC cells expressing FTO is not altered by fasting

(**A**) Representative confocal images of hypothalamic brain sections from free-fed (upper panels) and ~18hr fasted (lower panels) 7-week-old male POMC-Z/EG mice, which express GFP in appetite-suppressing POMC-expressing neurons (green). POMC cells are identified with white triangles in all images. Sections were probed with anti-FTO antibody (red) and nuclei were stained with DAPI (blue). Images are representative of 5 mice in each case. (**B**) Proportion of POMC cells expressing FTO in free-fed (grey bar, n = 5) and fasted (white bar, n = 5) 7-week-old POMC Z/EG mice. Data are mean ± SEM. There was no significant difference in FTO-positive POMC cells between the free-fed and fasted state (two-way ANOVA).

6.4.4 FTO protein is expressed uniformly in the brain

FTO expression levels were uniform in the three brain areas, as assessed by RT-qPCR and Western blotting. Consistent with these results, immunohistochemical experiments revealed FTO protein was expressed throughout the brain, including the hypothalamus (Figure 6.3a A), hippocampus and neocortex (Figure 6.3a B), and the cerebellum (Figure 6.3b A). In the cerebellum, cells were stained in the molecular, granular and Purkinje cell layers, as well as in the deep cerebellar nuclei (Figure 6.3b B). In all brain areas, FTO expression was restricted to the cell nucleus, consistent with previous reports [218, 223]. Fasting did not alter the nuclear localisation of FTO.

FTO protein expression was not limited to particular nuclei or brain structures in free-fed or fasted animals. However, regions with high neuronal density, such as the cerebellum and hippocampus, were conspicuous. This was consistent with the Western blot experiments as FTO protein levels were slightly enriched in the cerebellum compared to rostral brain and hypothalamus, though this difference did not reach statistical significance.

6.4.5 FTO is expressed in neurons

The immunohistochemistry experiments on POMC Z/EG mice described above showed that FTO was expressed in at least some neurons. To see if this was a general pattern, brain sections were double labelled with anti-FTO and anti-NeuN antibodies. These experiments revealed that FTO is expressed almost exclusively in neurons. The selective expression of FTO in neurons was seen throughout the brain, including the hypothalamus (Figure 6.4a A), cerebellum (Figure 6.4a B), neocortex (Figure 6.4b A) and hippocampus (Figure 6.4b B).

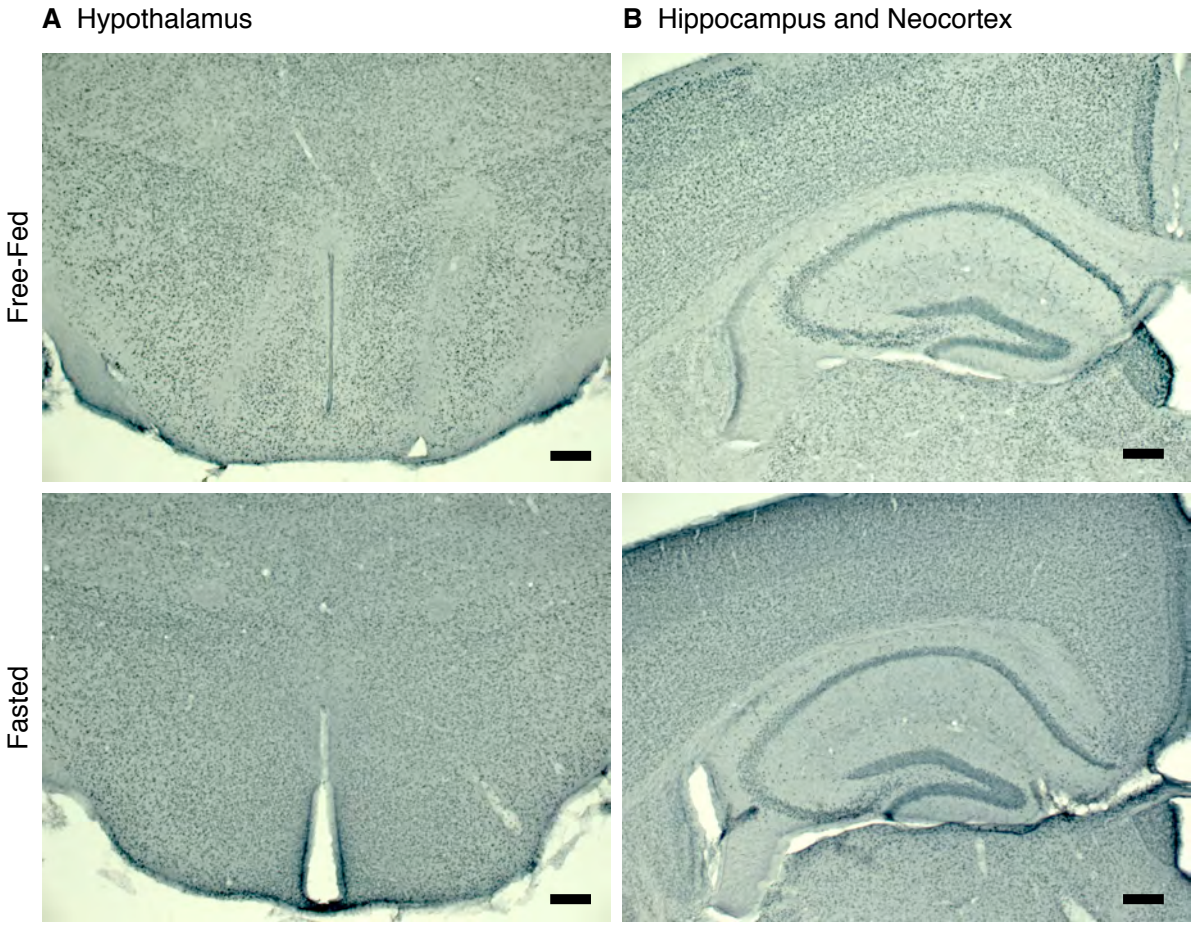

Figure 6.3a FTO protein is widely expressed in the brain

Representative images of sections from the hypothalamus (**A**), and the hippocampus and neocortex (**B**) of free-fed and fasted 7-week old female C57BL/6J mice. Sections were probed for FTO protein, which was stained with DAB (black). Regions with high neuronal density, such as the hippocampus, are conspicuous. But expression is widespread with FTO-positive nuclei seen throughout the brain. There were no obvious differences in either brain area based on nutritional status. Horizontal black bars indicates 200µm.

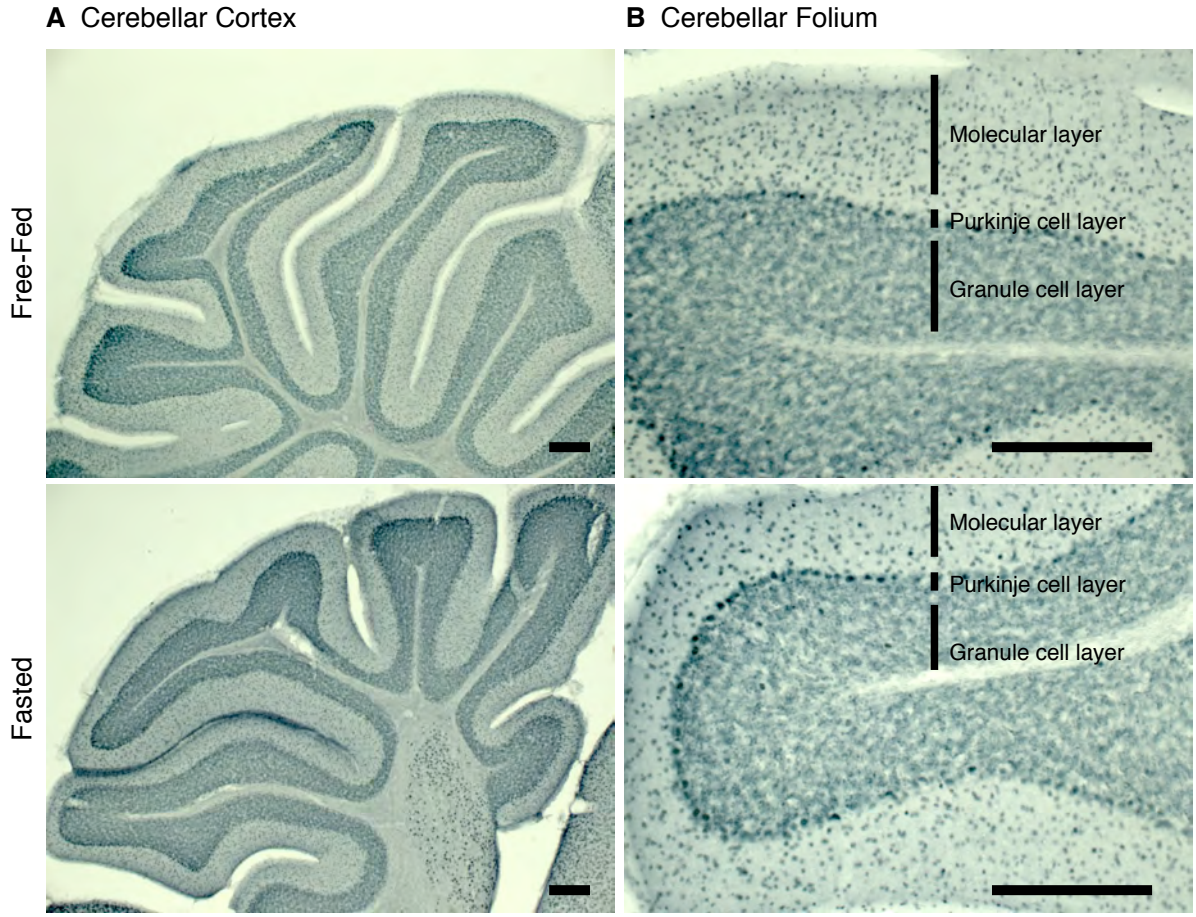

Figure 6.3b FTO protein is widely expressed in the brain

Representative images of sections from the cerebellum of free-fed and fasted 7-week old female C57BL/6J mice. Sections were probed for FTO protein, which was stained with DAB (black). (**A**) Low power images of the cerebellum reveal FTO-positive nuclei throughout the cerebellar cortex. (**B**) Higher magnification reveals FTO expression throughout the molecular and granular layer, and conspicuous expression in Purkinje cells. There were no obvious differences in either brain area based on nutritional status. Horizontal black bars indicate 200µm.

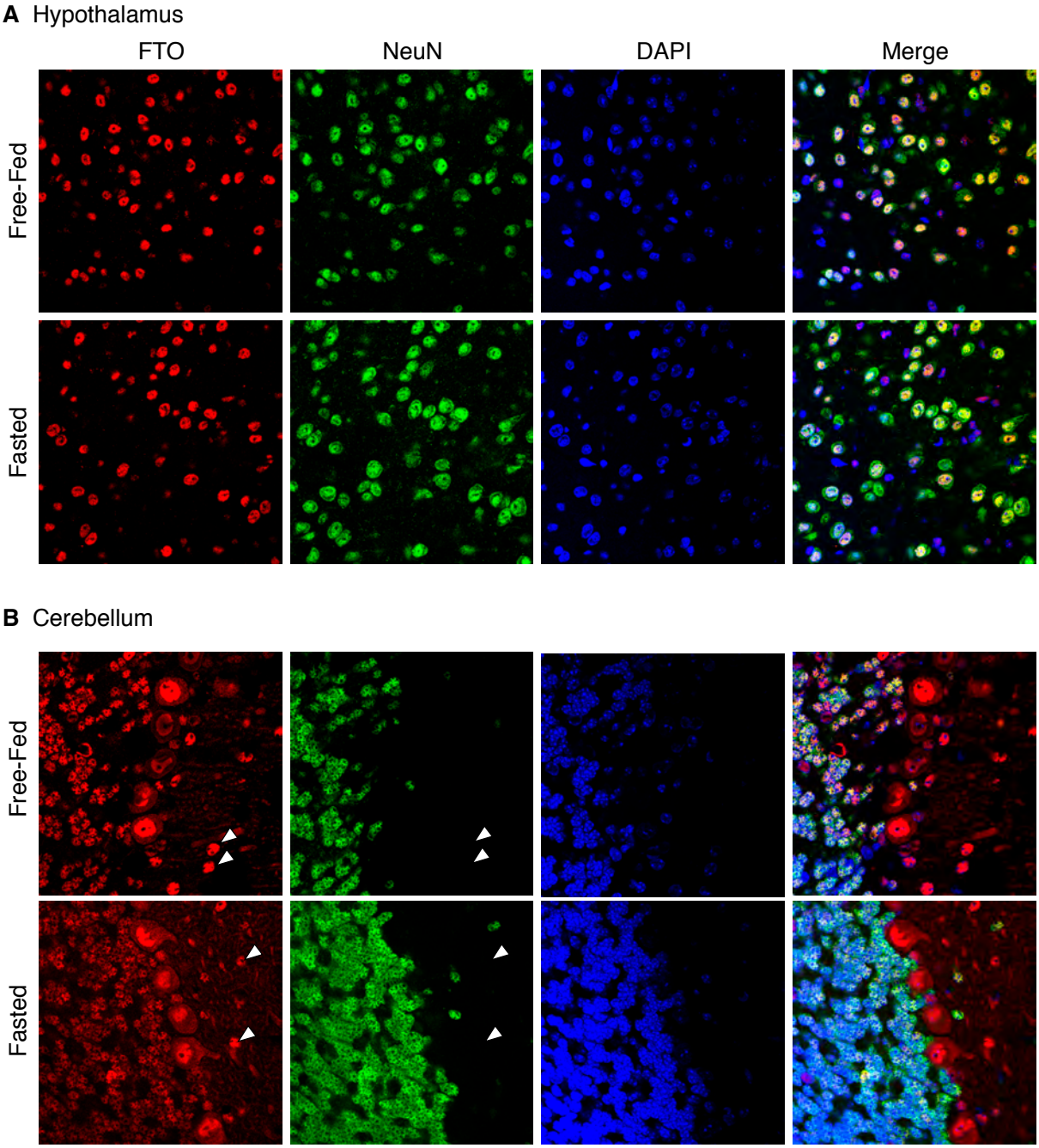

Figure 6.4a FTO is expressed primarily in neurons

Representative images of sections from the hypothalamus (**A**) and cerebellum (**B**) of free-fed (upper panels) and fasted (lower panels) 7 week-old male C57BL6/J mice. Sections were probed for FTO protein (red) and the Neuronal nuclear protein (NeuN, green). DAPI was used to stain all nuclei (blue). (**A**) The vast majority of NeuN-positive cells in the hypothalamus were also labelled with FTO. (**B**) The majority of NeuN-positive cells in the cerebellum were also labelled with FTO, but it was difficult to quantify this observation due to the high density of cells in this brain region. However, due to the highly organised structure of the cerebellum, it was relatively easy to identify some cells that were labelled with anti-FTO, but not anti-NeuN antibodies (examples are indicated with white triangles). These cells are possibly glia, but may be neurons that are not labelled with anti-NeuN. FTO-positive glia were also seen in other brain regions, but they were always very few. Images are representative of 5 mice. There were no obvious differences in the hypothalamus or cerebellum based on nutritional status.

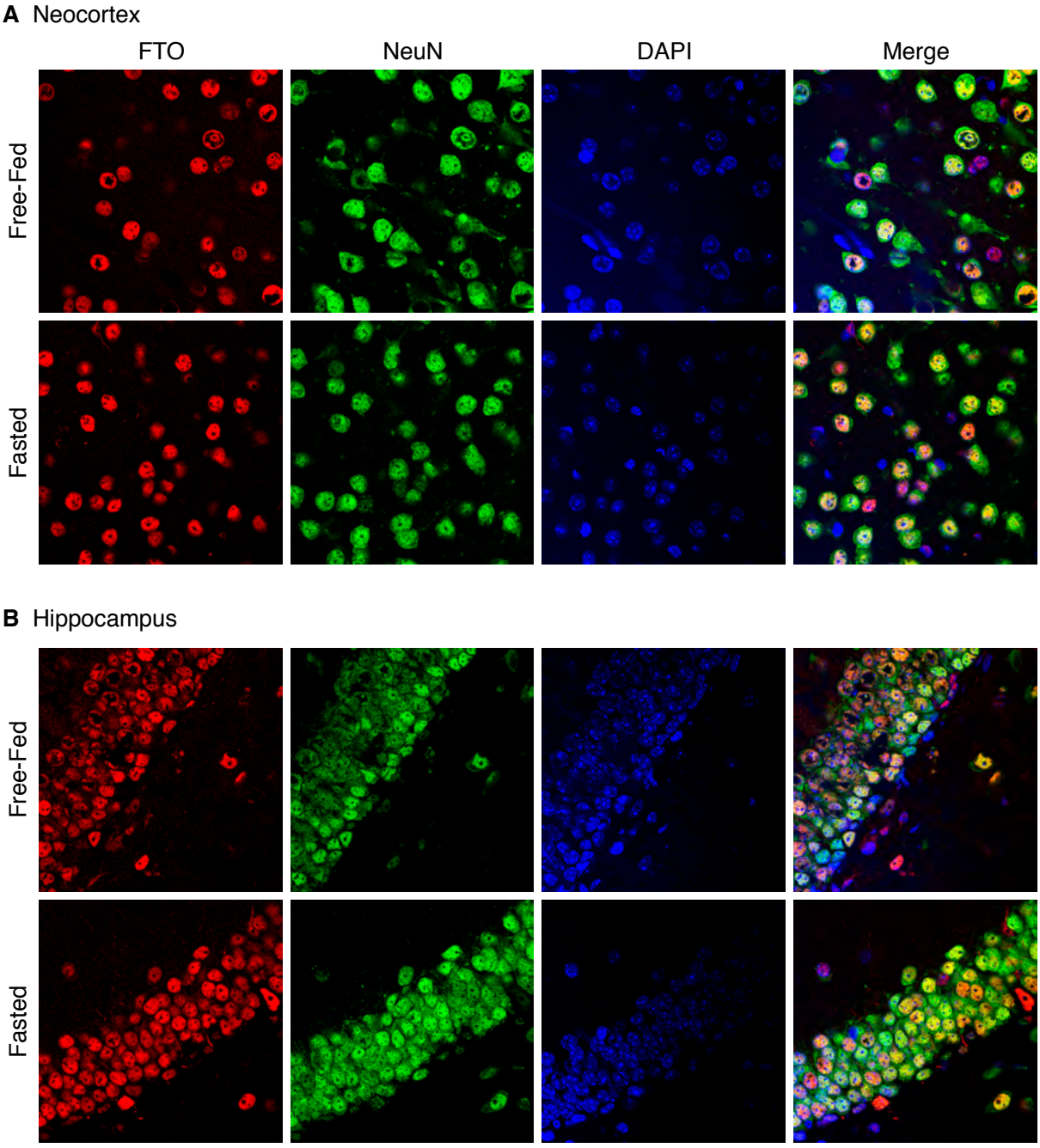

Figure 6.4b FTO is expressed primarily in neurons

Representative images of sections from the neocortex (**A**) and hippocampus (**B**) of free-fed (upper panels) and fasted (lower panels) 7-week-old male C57BL6/J mice. Sections were probed for FTO protein (red) and the Neuronal nuclear protein (NeuN, green). DAPI was used to stain all nuclei (blue). (**A**) The vast majority (>90%) of cells labelled with NeuN were also labelled with FTO. This analysis could not be carried out on the images from the hippocampus as the cell density was too high to accurate discern individual neurons. Images are representative of 5 mice. There were no obvious differences in either brain area based on nutritional status.

However, some cells were labelled with anti-FTO and not anti-NeuN. The laminar structure of the cerebellar cortex, with its highly ordered distribution of neurons, facilitated identification of these cells (Figure 6.4a B), but non-FTO-expressing NeuN-positive cells were also seen in other brain regions. These cells may be non-neuronal cells that express FTO. But it is also possible that they are neurons that are not labelled with anti-NeuN (indeed, as previously mentioned, cerebellar Purkinje cells are neurons but are not labelled with the antibody).

More than 90% of cells in the hypothalamus and neocortex that were labelled with NeuN were also labelled with FTO (Figures 6.4b A, B). This was the case whether the mouse was free-fed or fasted. Neuronal density was too high in the cerebellum and hippocampus to allow for accurate quantification.

6.5 Discussion

6.5.1 FTO expression is not altered by nutritional status

In the literature, focus has been placed on the nutritional regulation of FTO expression in the hypothalamus. However, in my experiments no significant differences were found in the hypothalamus or indeed any other brain region.

It is possible that the significant differences reported for other studies were due to the severity of fasting that was imposed on the mice. But, as discussed above, the physiological validity of extended periods of fasting is questionable, and the pathophysiological processes related to extended fasting may have resulted in secondary changes in FTO expression.

However, this conclusion may not be valid. After the experiments in this chapter were undertaken, a study was reported in which FTO mRNA levels in the hypothalamus of male

mice were upregulated following an overnight (~18 hour) fast [404]. These results were consistent with the previous report from this group in which they fasted rats for 48 hours [228]. Thus, the difference between my data and studies from this group do not appear to be due merely to the duration of fasting.

There are few obvious sources of difference between my studies and theirs. In their most recent report, they used male C57BL/6J mice. I used male and female C57BL/6J mice, but found no differences based on sex. We both killed the mice and harvested tissues at around 10am, and both sets of mice were housed with a similar lighting schedule. It is possible that age and diet are important. They used 12-week-old animals, whereas I used 7-week-old mice, and they fed their mice a different chow to mine. However, in their previous study they used rats, which were fed a diet that was different to my mice and their mice, and the results were concordant with their latest study.

It is difficult to determine if differences in analysis methods contribute to the variability in results presented in the literature as key details of the methods are missing. For example, Olszewski and colleagues [404] wrote that six reference genes were used to calculate the normalisation factor using the geNorm method (the same method that I used) but there do not appear to be six pairs of reference gene primers listed in the supplementary material. The geNorm method was used in two other studies [228, 247] but their results were not concordant. In the other study that imposed short-term fasting, only one reference gene was used to normalise FTO levels [218], but there are no other studies that took this approach, so the results cannot be compared. In my experiments, FTO itself was one of the most stable genes. Therefore my results suggest that FTO mRNA levels are unchanged by physiological durations of fasting.

The regulation of FTO protein levels following acute fasting has not been previously examined. In my experiments, I also assessed levels of FTO protein in the free-fed and

fasted states. Western blotting and immunohistochemistry experiments, including immunohistochemistry experiments on neurons that are involved in feeding behaviour, revealed no changes in FTO protein levels following an overnight fast. Therefore these experiments support the conclusion that *FTO* expression is not altered by nutritional status.

I conclude that FTO levels are not altered by feeding. As there are no changes in FTO expression, this is unlikely to be the mechanism by which FTO regulates food intake and thereby fat mass. However, it is possible that food restriction alters the *activity* levels of FTO, or its substrate selectivity. Perhaps future experiments could evaluate these possibilities.

By contrast, feeding behaviour may be changed by altering levels of FTO [223, 245]. Therefore transgenic mouse models that over- and under-express *FTO* may be more useful in furthering our understanding of the physiology of *FTO*.

These mice may also be useful for understanding whether *FTO* is involved in the development of neuronal circuits involved in feeding. Thus far, *FTO* has been knocked out or over-expressed in mice from early embryonic development, but all of the FTO transgenic mice reported so far have been made with the Cre/lox system, so future studies could knock out or over-express FTO in adulthood by using tamoxifen-induced Cre mouse lines.

6.5.2 Neuronal localisation of FTO

FTO was seen almost exclusively in neurons. In double immunohistochemistry experiments, more than 90% of neurons (identified by NeuN staining) were also labelled with FTO. However, in POMC Z/EG mice, only ~65% of GFP-positive (*POMC*-expressing) neurons were FTO-positive. The reason for this difference is unclear. POMC Z/EG mice are expected to express GFP in >90% of *POMC*-expressing neurons [255], so it is unlikely that many

POMC neurons were 'missed'. Also, FTO was stained in the same way for all experiments, so it is unlikely that technical problems contributed significantly to this difference. However, to rule out this possibility, brain sections should be double labelled with anti-FTO antibody and a POMC neuron-specific antibody, such as anti-melanocyte stimulating hormone antibody.

Although the same proportion of neurons were FTO-positive in the free-fed and fasted state it remains unclear if FTO is dynamically expressed. Perhaps levels in individual neurons fluctuate, but the overall proportion of FTO-positive cells remains the same. It is also possible that some non-neuronal cells express FTO. If this is confirmed, then it would be interesting to determine why certain neurons and glia express FTO and others do not. Perhaps they are undergoing different metabolic, transcriptional or electrical processes.

6.5.3 Future directions

In order to understand the role of FTO in obesity, it will be important to determine whether the SNPs in intron 1 of FTO alter its function. However, studies of the regulatory mechanisms governing FTO expression, and studies of transgenic mice that lack and over-express FTO may be useful in identifying the role of the protein in energy homeostasis.

In my experiments, FTO expression levels were not altered by fasting. In the future, it would be interesting to see if FTO protein *activity* is dependent upon nutritional status. Before this hypothesis is tested, however, it will be important to more fully characterise the cellular function of the FTO protein.

FTO demethylates 3-methylthymine *in vitro*, which suggests that it is involved in DNA repair [218]. The rate at which FTO demethylates DNA, however, is relatively low [220], so it is possible that this is not its primary function. Indeed, other studies indicate that FTO is a

transcriptional coactivator that enhances the transactivation potential of the CCAAT/enhancer binding proteins [222]. However, the factors that affect the transcriptional function of FTO have not be elucidated.

The relative importance of the catalytic and transcriptional functions of FTO remains unclear, but its demethylation activity seems to be important, because homozygous mutations in *FTO* that prevent 2-oxoglutarate turnover cause a severe syndrome in human beings that results in early death [240]. Heterozygous carriers of the same or similar mutations, however, are unaffected, so it is possible that the wild-type allele can compensate for the presence of the mutant gene [239]. The phenotype of FTO knock out mice is reminiscent of the human beings with homozygous catalytic mutations [240]. However, in these mice both the catalytic and transcriptional functions of FTO will be lost, so we cannot be sure which impairment causes its phenotype.

In the future, it would be interesting to see if there are any mutations in *FTO* that selectively interfere with each function. The study by Meyre *et al.* (2010) provides a list of coding mutations in *FTO* that are found in lean and obese individuals, so perhaps this could be a starting point. If mutations are found that interfere with the two functions separately, then these mutations could be modelled in mice in order to determine their relative importance.

As FTO overexpressor mice are hyperphagic, they are likely to have some alterations in brain function (either directly or via hormonal signals). Thus, it may also be useful to perform microarray experiments on these mice, looking at the transcriptome of the brain and adipose tissue. These experiments are on-going and the results will be available soon.

Chapter 7: Discussion

The aim of my project was to study the neuronal symptoms of iDEND, and the physiological role of FTO in the brain. These two strands of work were linked by the fact that common variants in or near the genes that encode for both the K_{ATP} channel and FTO are associated with the development of diabetes and obesity, respectively. However, during the course of my studies, I became more focused on iDEND.

Although my studies of FTO bore relatively little fruit, they did provide some insights into the neurophysiology of the protein. My interpretations of these studies, and suggestions for future experiments, are discussed in Chapter 6. In this chapter, I will confine the discussion to my studies of gain-of-function K_{ATP} channels in the brain.

7.1 Mouse studies of the neurological symptoms of iDEND

Patients with iDEND exhibit a variety of neurological symptoms, which are described in Chapter 1. As K_{ATP} channels are expressed throughout the brain, it is likely that dysfunction of many different regions contributes to their symptoms. In this thesis, I focussed on the motor symptoms of iDEND: muscle hypotonia, malcoordination and hyperactivity, and my aim was to identify brain regions or circuits whose dysfunction could be responsible for these symptoms. To do this, I used mouse models that expressed the most common iDEND-causing mutation (the Kir6.2-V59M mutation) in specific populations of neurons.

I used a mouse model, the n-V59M mouse, that had Kir6.2-V59M expression targeted to all neurons. Behavioural experiments showed that these mice were weaker, less coordinated, and more spontaneously active than controls [102]. Thus, the behavioural phenotype of this mouse mimicked the symptoms of the patients. In Chapter 3, I recorded the electrical activity

of cerebellar Purkinje cells from n-V59M mice. These experiments showed that, in the basal state, n-V59M Purkinje cells fired fewer spontaneous action potentials compared to controls, so transmitter release from these cells was likely to be inhibited. As Purkinje cells provide the sole output from the cerebellar cortex, these experiments suggest that cerebellar function is impaired in iDEND.

The behavioural phenotype of the n-V59M mouse could have been caused by changes in the electrical activity of excitatory and/or inhibitory neurons. Thus, I created a new mouse model, the p-V59M mouse, that had Kir6.2-V59M expression targeted to parvalbumin-expressing inhibitory neurons, which are present most densely in the neocortex, hippocampus and cerebellum. The behavioural experiments carried out on this mouse model, which are described in Chapter 4, suggested that the impairment of parvalbumin-expressing neurons alone was sufficient to cause muscle weakness, and hyperactivity (in some contexts), but coordination seemed to be unaffected.

These experiments indicate that the symptoms of iDEND may be dissected - I have shown that restriction of Kir6.2-V59M to only a subset of neurons is sufficient to recapitulate some, but not all of the motor phenotypes of the n-V59M mouse. If these experiments are continued in the future, using Cre lines that induce Kir6.2-V59M expression in different brain regions and circuits, then a clearer picture may emerge of which neurons are responsible for the different symptoms of iDEND. This improved knowledge may then translate to better therapy for the patients.

7.1.1 Dissecting the symptoms of iDEND

There are many commercially available mouse Cre lines that target specific neuronal populations, which can be used to identify neuronal circuits that are dysfunctional and cause

motor symptoms in iDEND. For example, the dopamine transporter Cre mouse [405] could be used to determine if the basal ganglia are involved. Indeed, if Cre was delivered using a viral vector, then it may be possible to induce Kir6.2-V59M expression in any brain area, even those for which there is no existing Cre mouse line.

In the future, it will be interesting to determine the specific importance of the cerebellum to the motor symptoms of iDEND. Cerebellar impairments due to lesions or congenital malformations are associated with many symptoms, including muscle hypotonia, malcoordination and hyperactivity. My electrophysiological experiments showed that cerebellar output was likely to be impaired in iDEND. Therefore, it is possible that these motor symptoms of iDEND are, at least partially, due to cerebellar dysfunction.

The specific importance of the cerebellum cannot be identified from my experiments on n-V59M and p-V59M mice because mutant K_{ATP} channels were not restricted to cerebellar cells alone. It is interesting to note, however, that the p-V59M mouse, which expressed Kir6.2-V59M in a subpopulation of neurons that included the cerebellar Purkinje cells, was weaker than its controls, and also more spontaneously hyperactive on the free-running wheels. However, the presence of V59M K_{ATP} channels in the neocortex, and other brain regions, of this mouse may have contributed to its phenotype. Therefore, in the future it would be interesting to restrict V59M K_{ATP} channels to Purkinje cells alone by using the Purkinje cell protein 2-Cre mouse [406], and assess the motor phenotype of these pcp-V59M mice.

Although expression of mutant K_{ATP} channels in parvalbumin cells recapitulated some of the motor impairments of the n-V59M mouse, it was interesting that p-V59M mice were not significantly malcoordinated compared to controls on the rotarod and static rods tests. This was somewhat surprising because the cerebellum is crucially important for motor coordination, and my electrophysiological studies showed that cerebellar output from the

p-V59M mouse was likely to be impaired. There are several explanations for the lack of malcoordination in p-V59M mice, and these are discussed in detail in Chapter 4. The most likely explanation is that the p-V59M mouse did not express sufficient levels of Kir6.2-V59M mRNA in a sufficiently high population of Purkinje cells, therefore the severity of cerebellar impairment was insufficient to affect performance on these tasks.

It is also possible, however, that performance on the rotarod and static rods is not dependent upon the function of the cerebellum. The performance of mice on the Erasmus ladder [340], is dependent upon cerebellar function, and is more sensitive than the rotarod in identifying cerebellar dysfunction in mice [341]. The accuracy and speed of the mouse's movement on this apparatus can be measured and indicates motor coordination, and the improvement in their performance over several learning trials can also be measured. Thus, it may be beneficial to test n-V59M, p-V59M and pcp-V59M mice on this equipment so that the relative importance of cerebellar dysfunction to the symptoms of iDEND can be assessed.

7.1.2 Other iDEND-causing mutations

As discussed in Chapter 1, many other gain-of-function mutations in Kir6.2 have been identified, and they cause a spectrum of disease. The severity of the patient's symptoms correlates with the severity of impairment in ATP-sensitivity that is caused by the mutation (Figure 1.2). The Kir6.2-V59M mutation is the most common cause of iDEND, and is present in n-V59M and p-V59M mice. The ATP-sensitivities of three other iDEND-causing mutations (H46L, R201C, T292N) have been studied. These mutations impair the ATP-sensitivity of the K_{ATP} channel to the same level, or greater, than V59M. Furthermore, all of the DEND-causing mutations in Kir6.2 have a more severe effect on ATP-sensitivity.

It is reasonable to assume that more severe mutations in the channel will lead to greater impairment of neuronal electrophysiology, because they are likely to produce a larger hyperpolarising potassium current and thus decrease neuronal firing frequency. Therefore, the results obtained from the n-V59M and p-V59M mouse (and indeed any future mice that express Kir6.2-V59M) are likely to be applicable to all patients with iDEND and DEND. In the future, this hypothesis can be tested by making a mouse model with a more severe, DEND-causing Kir6.2 mutation.

7.1.3 Blood-brain barrier penetrance

Most patients with iDEND are now treated with sulphonylureas. This ameliorates their neurological symptoms to variable extents. In many cases, although diabetes is well controlled, neurological problems are not abolished but merely reduced. Why this might be the case is still unclear. It might reflect developmental changes or long-term damage, which is discussed in more detail in section 7.1.4, but it could also reflect poor blood-brain barrier (BBB) penetrance.

We do not know the extent to which sulphonylurea drugs penetrate the BBB and accumulate in the brain. It is possible that some sulphonylureas penetrate or accumulate better than others. Sulphonylureas are lipid soluble, so they should cross the BBB. However, they are pumped out by proteins such as P-glycoprotein [407] and also by non-P-glycoprotein pathways [154].

The n-V59M and p-V59M mouse models might be used to characterise the penetrance of different sulphonylureas across the BBB, and the concentrations that they reach in the brain. This could be done directly, by sampling CSF from wild-type mice that have been given systemic treatment of sulphonylureas. However, the low volumes of CSF that can be

obtained from mice may hinder this plan. The penetrance of sulphonylureas into the brain could also be assessed indirectly, by measuring, for example, the muscle strength of n-V59M mice before and after sulphonylurea treatment.

It is possible that sulphonylurea treatment could improve some symptoms of iDEND more than others and the n-V59M mouse might be useful in identifying which symptoms are most treatable. The highest CSF concentrations of sulphonylurea, and thus maximal closure of mutant K_{ATP} channels, are likely to be reached by directly administering the drug into the brain, which can be done in the n-V59M mouse. Thus, if their strength, coordination and activity levels are measured before and after sulphonylureas are administered, then it may be possible to identify which iDEND symptoms are most improved by sulphonylurea treatment, and the 'best-treated' symptoms could then be used as a benchmark to determine how well the neurological symptoms of the patients are being managed.

7.1.4 Developmental effects of Kir6.2-V59M expression

There is anecdotal evidence that patients with iDEND might have a better prognosis for their neurological symptoms if they are treated with sulphonylureas early in life, rather than in adulthood. This implies that long-term expression of mutant K_{ATP} channels may have lasting effects on neuronal function.

There are many mechanisms that might be involved. Firstly, long-term inhibition of a neuron due to the expression of mutant K_{ATP} channels may induce alterations in its complement of ion channels. To see if this was the case in cerebellar Purkinje cells, I measured their intrinsic spontaneous activity while K_{ATP} channels and all synaptic inputs were blocked (Chapters 3 and 4). The intrinsic activity of Purkinje cells from n-V59M and p-V59M mice was not significantly impaired compared to their controls. Therefore, these data suggest that the

long-term expression of Kir6.2-V59M does not induce developmental changes in the gross electrophysiology of cerebellar Purkinje cells. More studies are required, however, to determine if intracellular mechanisms, such as synaptic plasticity, are altered in these cells. Furthermore, other cells in the cerebellar cortex and other parts of the brain might be affected by developmental changes. It is also possible that I did not see developmental alterations in Purkinje cell electrophysiology because I performed my experiments on 2-week-old mice. The effects may be more severe in later life.

Secondly, although K_{ATP} channels are thought to play a neuroprotective role in many neurons, long-term expression of gain-of-function K_{ATP} channels may make certain neurons more sensitive to cell death. For example, dopaminergic neurons in the substantia nigra of mice are protected from cell death caused by administration of 1-methyl-4-phenyl-1,2,3,6-tetrahydropyridine (MPTP) when Kir6.2 is knocked out [180]. If the K_{ATP} channels render the neurons more sensitive to the effects of MPTP due to their potassium flux, then the presence of mutant K_{ATP} channels may make them even more susceptible.

Thirdly, some of the developmental impairments in iDEND patients are also likely to be due to the presence of neuronal impairment during critical periods of development. Even if sulphonylurea treatment rectifies the developmental impairments at the neuronal level, it is unlikely that the skills that would have been accrued during critical periods could subsequently be acquired.

The developmental impact of mutant K_{ATP} channel expression in the brain could be assessed using the n-V59M mouse model. Sulphonylureas could be administered directly into the brains of these mice, using osmotic minipumps, at different ages and their cognitive and motor behaviour could be tested in adulthood.

7.1.5 Turning on Kir6.2-V59M expression in adulthood

During ischaemic events such as stroke, K_{ATP} channels open in many types of neuron in order to protect them against damage. However, neuronal death often still occurs, which may lead to brain dysfunction and subsequent compensatory mechanisms that restore some lost functions. By using tamoxifen-induced Cre lines to turn on mutant K_{ATP} channel expression in adulthood, it might be possible to characterise the mechanisms by which the brain compensates for neuronal dysfunction in maturity. Currently, mice are given artificial strokes, or specific brain lesions, in order to characterise these compensatory mechanisms. However, the V59M mouse model may provide novel insights compared to these traditional models, because the effects of the mutant K_{ATP} channels can be reversed by administering sulphonylureas centrally.

7.1.6 Cognitive problems in iDEND

I have focussed on motor problems in iDEND, but the cognitive problems of the patients might be addressed in a similar way. The learning and memory functions of n-V59M mice are impaired compared to controls, and they also show alterations in their affective behaviours, such as anxiety and novelty seeking [170].

It is possible that hippocampal dysfunction is important for the memory impairments, and neocortical dysfunction could underlie the affective alterations. In order to test these hypotheses, mice could be made with Kir6.2-V59M targeted to the neocortex and hippocampus by using the Fzd9-Cre mouse line [408] and their memory and affective phenotypes could be assessed.

7.1.7 A new mouse model of iDEND

Models of iDEND that are produced by mating ROSA mice with Cre lines have several limitations. As described in Chapter 3, the expression pattern of the ROSA promotor is variable through development, and across the brain, so gene dosage may not be accurately modelled. Furthermore, different Cre lines induce transgene expression at different stages of development (as discussed in Chapter 4), so the developmental effects of Kir6.2-V59M expression (if any) may not be modelled with fidelity. Indeed, the severity of the developmental effects might be variable for each Cre-ROSA mouse that is produced, because the time course of Cre expression in each particular mouse may be different.

A further problem arises if Kir6.2 and SUR1 expression are not confined to exactly the same cells. The ROSA promotor activates Kir6.2-V59M expression in all neurons, but it will only make K_{ATP} channels in cells that express SUR. I have made the assumption that all cells that express SUR also express Kir6.2 and thus K_{ATP} channels. However, if some neurons express SUR but not Kir6.2, this could lead to homozygous mutant K_{ATP} channels in cells that normally do not express K_{ATP} channels. It is possible that this is the case, because SUR1 may also have a second role in coupling to a non-selective cation channel, which plays a role in neuronal damage caused by stroke [409]. Which cells are involved, however, and if they also express Kir6.2, is unclear.

These problems could be circumvented by generating a true knock-in mouse - i.e. a mouse with the V59M mutation present in one of the endogenous copies of *KCNJ11*. However, if it is desired to restrict Kir6.2-V59M expression to neurons, this mouse would also need to be conditional (constructed using the Cre/lox system). This is not a simple matter. Furthermore, the timing of Kir6.2-V59M expression in this mouse model would still be dependent upon the timing of Cre expression.

7.2 Human studies of the neurological symptoms of iDEND

The experiments carried out on the n-V59M and p-V59M mouse models indicated that the electrophysiological output from the cerebellum was likely to be impaired in iDEND. This raised the possibility that iDEND patients could have cerebellar-dependent symptoms that had been previously overlooked. In Chapter 5, I showed that coordinated movements of the hand and eye of iDEND patients, but not PNDM patients, were impaired compared to matched controls.

I also recorded the eye movements of two iDEND patients as they performed prosaccades and smooth pursuit tasks. Both of these individuals had oculomotor malcoordination, which is indicative of cerebellar impairment. Indeed, one of these two individuals showed clear 'cogwheel' tracking, which is considered to be a hallmark of cerebellar dysfunction. Further studies are needed to determine if this observation can be generalised to all iDEND patients.

7.2.1 Implications for therapy

These discoveries may influence the medical treatment of iDEND patients. As the cerebellum appears to be impaired in patients with iDEND, it is possible that targeted physical therapy, which is used on people with traumatic injuries of the cerebellum, might improve the symptoms of the patients. Muscle hypotonia, for example, may be treated in this way. However, such interventions may not be successful in iDEND patients because the whole cerebellum, rather than just a region of it, is likely to be impaired.

The identification of impaired eye movements may be of greater clinical significance. Impaired eye movements due to cerebellar dysfunction have been implicated in some forms of dyslexia [410]. Several iDEND patients experience difficulty in reading (unpublished

observations). Although it is a controversial idea, it is possible that cerebellar dysfunction in iDEND patients leads to a phenotype similar to dyslexia, which may contribute to their general learning impairments. Dyslexia due to impaired eye movements may be improved by using glasses with coloured lenses [385]. Thus, it would be interesting to see if the reading ability of iDEND patients also improves by using these glasses.

If oculomotor malcoordination is a hallmark of iDEND, then it could be useful in guiding the treatment of the neurological symptoms of the disease. Assessment of eye movements in human beings is relatively quick and easy, so they can be checked (and quantified if possible) when a patient transfers to sulphonylurea therapy, and the dosage could be adjusted until eye movements are maximally improved. However, it is interesting to note that both of the iDEND patients that provided eye movement recordings were being treated with sulphonylureas. This may mean that their oculomotor malcoordination is insensitive to sulphonylurea treatment. However, it is also possible that the patients were being treated with sufficient sulphonylureas to control their blood glucose levels, but not maximally treat their neurological condition.

Eye movements can also be assessed in mice (e.g. [339, 411]), so the mouse models of iDEND may be useful in resolving this issue. If the eye movements of the n-V59M mouse are impaired, then the sensitivity of this symptom to sulphonylurea therapy could be assessed. Because sulphonylureas can be administered systemically or centrally in these mice, these experiments could be used to see if oculomotor malcoordination is sensitive to sulphonylurea treatment *per se*, and also to see if the lack of BBB penetrance is the reason why the iDEND patients are still affected, despite being treated with sulphonylureas.

7.3 A bright future for studies of iDEND?

In this thesis, I presented data derived from studies of mouse models of a human disease, and also data from the patients themselves. Such synergistic studies of patients and mice are extremely powerful - things learned in the patients can be tested in the mice and vice versa. Indeed, in my experiments on the n-V59M and p-V59M mice, I showed that cerebellar output was likely to be impaired in iDEND, and this lead me to look for cerebellar-dependent symptoms in the patients. Equally, once I found evidence of impaired eye movements in the patients, this suggested that a similar phenotype may be present in the mouse. This reciprocity of discovery is likely to lead to more rapid translation of results from bench to bedside.

In the past, the treatment of iDEND and PNDM has been revolutionised by this type of approach. Experiments on *Xenopus* oocytes indicated that neonatal diabetes caused by gain-of-function mutations in K_{ATP} channels could be treated with sulphonylureas [135]. Indeed, the glycaemic control of the patients was often better following transfer to the oral drugs compared to insulin injections. In the future, it may be possible to improve the treatment of the neurological symptoms of iDEND in a similar way.

It is clear that there are many discoveries to be made about which brain areas are responsible for the symptoms of iDEND, and how best these symptoms might be treated. These advancements will require intense, painstaking work. However, there is reason to be optimistic and, as Aristotle said, “Patience is bitter, but its fruit is sweet.”

References

1. WHO (2011) *Obesity and overweight. Fact Sheet No 311.* Retrieved from http://www.who.int/mediacentre/factsheets/fs311/en/index.html.
2. Willett, W.C., W.H. Dietz, and G.A. Colditz, *Guidelines for healthy weight.* N Engl J Med, 1999. **341**(6): p. 427-34.
3. Kopelman, P.G., *Obesity as a medical problem.* Nature, 2000. **404**(6778): p. 635-43.
4. Abelson, P. and D. Kennedy, *The obesity epidemic.* Science, 2004. **304**(5676): p. 1413.
5. Keith, S.W., et al., *Putative contributors to the secular increase in obesity: exploring the roads less traveled.* International journal of obesity (2005), 2006. **30**(11): p. 1585-94.
6. Gloyn, A.L. and M.I. McCarthy, *Genetics: how the UKPDS contributed to determining the genetic landscape of Type 2 diabetes.* Diabet Med, 2008. **25 Suppl 2**: p. 35-40.
7. Wilson, P.W., K.M. Anderson, and W.B. Kannel, *Epidemiology of diabetes mellitus in the elderly. The Framingham Study.* Am J Med, 1986. **80**(5A): p. 3-9.
8. Loos, R.J. and C. Bouchard, *FTO: the first gene contributing to common forms of human obesity.* Obesity reviews : an official journal of the International Association for the Study of Obesity, 2008. **9**(3): p. 246-50.
9. Frayling, T.M., *Genome-wide association studies provide new insights into type 2 diabetes aetiology.* Nat Rev Genet, 2007. **8**(9): p. 657-62.
10. Stunkard, A.J., T.T. Foch, and Z. Hrubec, *A twin study of human obesity.* JAMA, 1986. **256**(1): p. 51-4.
11. Stunkard, A.J., et al., *The body-mass index of twins who have been reared apart.* N Engl J Med, 1990. **322**(21): p. 1483-7.
12. Stunkard, A.J., et al., *An adoption study of human obesity.* N Engl J Med, 1986. **314**(4): p. 193-8.
13. Maes, H.H., M.C. Neale, and L.J. Eaves, *Genetic and environmental factors in relative body weight and human adiposity.* Behav Genet, 1997. **27**(4): p. 325-51.
14. Wardle, J., et al., *Evidence for a strong genetic influence on childhood adiposity despite the force of the obesogenic environment.* Am J Clin Nutr, 2008. **87**(2): p. 398-404.
15. Meigs, J.B., L.A. Cupples, and P.W. Wilson, *Parental transmission of type 2 diabetes: the Framingham Offspring Study.* Diabetes, 2000. **49**(12): p. 2201-7.
16. Das, S.K. and S.C. Elbein, *The Genetic Basis of Type 2 Diabetes.* Cellscience, 2006. **2**(4): p. 100-131.

17. Medici, F., et al., *Concordance rate for type II diabetes mellitus in monozygotic twins: actuarial analysis.* Diabetologia, 1999. **42**(2): p. 146-50.
18. Zhang, Y., et al., *Positional cloning of the mouse obese gene and its human homologue.* Nature, 1994. **372**(6505): p. 425-32.
19. Tartaglia, L.A., et al., *Identification and expression cloning of a leptin receptor, OB-R.* Cell, 1995. **83**(7): p. 1263-71.
20. Huszar, D., et al., *Targeted disruption of the melanocortin-4 receptor results in obesity in mice.* Cell, 1997. **88**(1): p. 131-41.
21. Montague, C.T., et al., *Congenital leptin deficiency is associated with severe early-onset obesity in humans.* Nature, 1997. **387**(6636): p. 903-8.
22. Clément, K., et al., *A mutation in the human leptin receptor gene causes obesity and pituitary dysfunction.* Nature, 1998. **392**(6674): p. 398-401.
23. Vaisse, C., et al., *A frameshift mutation in human MC4R is associated with a dominant form of obesity.* Nat Genet, 1998. **20**(2): p. 113-4.
24. Yeo, G.S., et al., *A frameshift mutation in MC4R associated with dominantly inherited human obesity.* Nat Genet, 1998. **20**(2): p. 111-2.
25. Krude, H., et al., *Severe early-onset obesity, adrenal insufficiency and red hair pigmentation caused by POMC mutations in humans.* Nat Genet, 1998. **19**(2): p. 155-7.
26. Yaswen, L., et al., *Obesity in the mouse model of pro-opiomelanocortin deficiency responds to peripheral melanocortin.* Nat Med, 1999. **5**(9): p. 1066-70.
27. Challis, B.G., et al., *A missense mutation disrupting a dibasic prohormone processing site in pro-opiomelanocortin (POMC) increases susceptibility to early-onset obesity through a novel molecular mechanism.* Hum Mol Genet, 2002. **11**(17): p. 1997-2004.
28. Farooqi, S. and S. O'Rahilly, *Genetics of obesity in humans.* Endocr Rev, 2006. **27**(7): p. 710-18.
29. Lander, E.S., et al., *Initial sequencing and analysis of the human genome.* Nature, 2001. **409**(6822): p. 860-921.
30. Consortium, I.H., et al., *A second generation human haplotype map of over 3.1 million SNPs.* Nature, 2007. **449**(7164): p. 851-61.
31. Mägi, R., et al., *Evaluating the performance of commercial whole-genome marker sets for capturing common genetic variation.* BMC Genomics, 2007. **8**: p. 159.
32. Frayling, T.M., et al., *A common variant in the FTO gene is associated with body mass index and predisposes to childhood and adult obesity.* Science, 2007. **316**(5826): p. 889-94.
33. Dina, C., et al., *Variation in FTO contributes to childhood obesity and severe adult obesity.* Nat Genet, 2007. **39**(6): p. 724-6.

34. Scuteri, A., et al., *Genome-wide association scan shows genetic variants in the FTO gene are associated with obesity-related traits.* PLoS Genet, 2007. **3**(7): p. e115.
35. Hinney, A., et al., *Genome wide association (GWA) study for early onset extreme obesity supports the role of fat mass and obesity associated gene (FTO) variants.* PLoS ONE, 2007. **2**(12): p. e1361.
36. Cecil, J.E., et al., *An obesity-associated FTO gene variant and increased energy intake in children.* N Engl J Med, 2008. **359**(24): p. 2558-66.
37. Ohashi, J., et al., *FTO polymorphisms in oceanic populations.* J Hum Genet, 2007. **52**(12): p. 1031-5.
38. Andreasen, C.H., et al., *Low physical activity accentuates the effect of the FTO rs9939609 polymorphism on body fat accumulation.* Diabetes, 2008. **57**(1): p. 95-101.
39. Peeters, A., et al., *Variants in the FTO gene are associated with common obesity in the Belgian population.* Mol Genet Metab, 2008. **93**(4): p. 481-4.
40. Loos, R.J., et al., *Common variants near MC4R are associated with fat mass, weight and risk of obesity.* Nat Genet, 2008.
41. Hunt, S.C., et al., *Association of the FTO gene with BMI.* Obesity (Silver Spring), 2008. **16**(4): p. 902-4.
42. Chang, Y.C., et al., *Common variation in the fat mass and obesity-associated (FTO) gene confers risk of obesity and modulates BMI in the Chinese population.* Diabetes, 2008. **57**(8): p. 2245-52.
43. Price, R.A., W.D. Li, and H. Zhao, *FTO gene SNPs associated with extreme obesity in cases, controls and extremely discordant sister pairs.* BMC Med Genet, 2008. **9**: p. 4.
44. Hotta, K., et al., *Variations in the FTO gene are associated with severe obesity in the Japanese.* J Hum Genet, 2008. **53**(6): p. 546-53.
45. Villalobos-Comparán, M., et al., *The FTO gene is associated with adulthood obesity in the Mexican population.* Obesity (Silver Spring), 2008. **16**(10): p. 2296-301.
46. Grant, S.F., et al., *Association analysis of the FTO gene with obesity in children of Caucasian and African ancestry reveals a common tagging SNP.* PLoS ONE, 2008. **3**(3): p. e1746.
47. Wing, M.R., et al., *Analysis of FTO gene variants with measures of obesity and glucose homeostasis in the IRAS Family Study.* Hum Genet, 2009. **125**(5-6): p. 615-26.
48. McCarthy, M.I., *Genomics, type 2 diabetes, and obesity.* N Engl J Med, 2010. **363**(24): p. 2339-50.
49. Chambers, J.C., et al., *Common genetic variation near MC4R is associated with waist circumference and insulin resistance.* Nat Genet, 2008. **40**(6): p. 716-8.

50. Speliotes, E.K., et al., *Association analyses of 249,796 individuals reveal 18 new loci associated with body mass index.* Nat Genet, 2010. **42**(11): p. 937-48.
51. Cone, R.D., *Anatomy and regulation of the central melanocortin system.* Nat Neurosci, 2005. **8**(5): p. 571-8.
52. Thomas, P.M., et al., *Inactivation of the first nucleotide-binding fold of the sulfonylurea receptor, and familial persistent hyperinsulinemic hypoglycemia of infancy.* Am J Hum Genet, 1996. **59**(3): p. 510-8.
53. Thomas, P., Y. Ye, and E. Lightner, *Mutation of the pancreatic islet inward rectifier Kir6.2 also leads to familial persistent hyperinsulinemic hypoglycemia of infancy.* Hum Mol Genet, 1996. **5**(11): p. 1809-12.
54. Inoue, H., et al., *Sequence variants in the sulfonylurea receptor (SUR) gene are associated with NIDDM in Caucasians.* Diabetes, 1996. **45**(6): p. 825-31.
55. Gloyn, A.L., et al., *Large-scale association studies of variants in genes encoding the pancreatic beta-cell KATP channel subunits Kir6.2 (KCNJ11) and SUR1 (ABCC8) confirm that the KCNJ11 E23K variant is associated with type 2 diabetes.* Diabetes, 2003. **52**(2): p. 568-72.
56. Kleinjan, D.A. and V. van Heyningen, *Long-range control of gene expression: emerging mechanisms and disruption in disease.* Am J Hum Genet, 2005. **76**(1): p. 8-32.
57. Berulava, T. and B. Horsthemke, *The obesity-associated SNPs in intron 1 of the FTO gene affect primary transcript levels.* Eur J Hum Genet, 2010. **18**(9): p. 1054-6.
58. Jowett, J.B., et al., *Genetic variation at the FTO locus influences RBL2 gene expression.* Diabetes, 2010. **59**(3): p. 726-32.
59. Noma, A., *ATP-regulated K+ channels in cardiac muscle.* Nature, 1983. **305**(5930): p. 147-8.
60. Cook, D.L. and C.N. Hales, *Intracellular ATP directly blocks K+ channels in pancreatic B-cells.* Nature, 1984. **311**(5983): p. 271-3.
61. Ashcroft, F.M., D.E. Harrison, and S.J. Ashcroft, *Glucose induces closure of single potassium channels in isolated rat pancreatic beta-cells.* Nature, 1984. **312**(5993): p. 446-8.
62. Spruce, A.E., N.B. Standen, and P.R. Stanfield, *Voltage-dependent ATP-sensitive potassium channels of skeletal muscle membrane.* Nature, 1985. **316**(6030): p. 736-8.
63. Standen, N.B., et al., *Hyperpolarizing vasodilators activate ATP-sensitive K+ channels in arterial smooth muscle.* Science, 1989. **245**(4914): p. 177-80.
64. Ashford, M.L., et al., *Adenosine-5'-triphosphate-sensitive ion channels in neonatal rat cultured central neurones.* Pflugers Arch, 1988. **412**(3): p. 297-304.

65. Shyng, S. and C.G. Nichols, *Octameric stoichiometry of the KATP channel complex.* J Gen Physiol, 1997. **110**(6): p. 655-64.
66. Clement, J.P., et al., *Association and stoichiometry of K(ATP) channel subunits.* Neuron, 1997. **18**(5): p. 827-38.
67. Kakei, M. and A. Noma, *Adenosine-5'-triphosphate-sensitive single potassium channel in the atrioventricular node cell of the rabbit heart.* J Physiol (Lond), 1984. **352**: p. 265-84.
68. Ashcroft, F.M., S.J. Ashcroft, and D.E. Harrison, *Effects of 2-ketoisocaproate on insulin release and single potassium channel activity in dispersed rat pancreatic beta-cells.* J Physiol (Lond), 1987. **385**: p. 517-29.
69. Inagaki, N., et al., *Reconstitution of IKATP: an inward rectifier subunit plus the sulfonylurea receptor.* Science, 1995. **270**(5239): p. 1166-70.
70. Sakura, H., et al., *Cloning and functional expression of the cDNA encoding a novel ATP-sensitive potassium channel subunit expressed in pancreatic beta-cells, brain, heart and skeletal muscle.* FEBS Lett, 1995. **377**(3): p. 338-44.
71. Tucker, S.J., et al., *Truncation of Kir6.2 produces ATP-sensitive K+ channels in the absence of the sulphonylurea receptor.* Nature, 1997. **387**(6629): p. 179-83.
72. Aguilar-Bryan, L., et al., *Cloning of the beta cell high-affinity sulfonylurea receptor: a regulator of insulin secretion.* Science, 1995. **268**(5209): p. 423-6.
73. Gribble, F.M., et al., *Properties of cloned ATP-sensitive K+ currents expressed in Xenopus oocytes.* J Physiol (Lond), 1997. **498 (Pt 1)**: p. 87-98.
74. Nichols, C.G., et al., *Adenosine diphosphate as an intracellular regulator of insulin secretion.* Science, 1996. **272**(5269): p. 1785-7.
75. Chutkow, W.A., et al., *Cloning, tissue expression, and chromosomal localization of SUR2, the putative drug-binding subunit of cardiac, skeletal muscle, and vascular KATP channels.* Diabetes, 1996. **45**(10): p. 1439-45.
76. Inagaki, N., et al., *A family of sulfonylurea receptors determines the pharmacological properties of ATP-sensitive K+ channels.* Neuron, 1996. **16**(5): p. 1011-7.
77. Shi, N.Q., B. Ye, and J.C. Makielski, *Function and distribution of the SUR isoforms and splice variants.* Journal of molecular and cellular cardiology, 2005. **39**(1): p. 51-60.
78. Miki, T. and S. Seino, *Roles of KATP channels as metabolic sensors in acute metabolic changes.* Journal of molecular and cellular cardiology, 2005. **38**(6): p. 917-25.
79. Isomoto, S., et al., *A novel sulfonylurea receptor forms with BIR (Kir6.2) a smooth muscle type ATP-sensitive K+ channel.* J Biol Chem, 1996. **271**(40): p. 24321-4.

80. Liss, B., R. Bruns, and J. Roeper, *Alternative sulfonylurea receptor expression defines metabolic sensitivity of K-ATP channels in dopaminergic midbrain neurons.* EMBO J, 1999. **18**(4): p. 833-46.
81. de Wet, H., et al., *The ATPase activities of sulfonylurea receptor 2A and sulfonylurea receptor 2B are influenced by the C-terminal 42 amino acids.* FEBS J, 2010. **277**(12): p. 2654-62.
82. Zerangue, N., et al., *A new ER trafficking signal regulates the subunit stoichiometry of plasma membrane K(ATP) channels.* Neuron, 1999. **22**(3): p. 537-48.
83. Ashcroft, F.M. and P. Rorsman, *Electrophysiology of the pancreatic beta-cell.* Prog Biophys Mol Biol, 1989. **54**(2): p. 87-143.
84. Dunne, M.J. and O.H. Petersen, *Intracellular ADP activates K+ channels that are inhibited by ATP in an insulin-secreting cell line.* FEBS Lett, 1986. **208**(1): p. 59-62.
85. Kakei, M., et al., *The ATP-sensitivity of K+ channels in rat pancreatic B-cells is modulated by ADP.* FEBS Lett, 1986. **208**(1): p. 63-6.
86. Proks, P., M. Takano, and F.M. Ashcroft, *Effects of intracellular pH on ATP-sensitive K + channels in mouse pancreatic beta-cells.* J Physiol (Lond), 1994. **475**(1): p. 33-44.
87. Baukrowitz, T. and B. Fakler, *KATP channels gated by intracellular nucleotides and phospholipids.* Eur J Biochem, 2000. **267**(19): p. 5842-8.
88. Fan, Z. and J.C. Makielski, *Anionic phospholipids activate ATP-sensitive potassium channels.* J Biol Chem, 1997. **272**(9): p. 5388-95.
89. Shyng, S.L. and C.G. Nichols, *Membrane phospholipid control of nucleotide sensitivity of KATP channels.* Science, 1998. **282**(5391): p. 1138-41.
90. Larsson, O., et al., *Activation of the ATP-sensitive K+ channel by long chain acyl-CoA. A role in modulation of pancreatic beta-cell glucose sensitivity.* J Biol Chem, 1996. **271**(18): p. 10623-6.
91. Gribble, F.M., et al., *Mechanism of cloned ATP-sensitive potassium channel activation by oleoyl-CoA.* J Biol Chem, 1998. **273**(41): p. 26383-7.
92. Zingman, L.V., et al., *Signaling in channel/enzyme multimers: ATPase transitions in SUR module gate ATP-sensitive K+ conductance.* Neuron, 2001. **31**(2): p. 233-45.
93. Ashcroft, F.M., *The Walter B. Cannon Physiology in Perspective Lecture, 2007. ATP-sensitive K+ channels and disease: from molecule to malady.* Am J Physiol Endocrinol Metab, 2007. **293**(4): p. E880-9.
94. Gribble, F.M. and F.M. Ashcroft, *Differential sensitivity of beta-cell and extrapancreatic K(ATP) channels to gliclazide.* Diabetologia, 1999. **42**(7): p. 845-8.
95. Nichols, C.G., *KATP channels as molecular sensors of cellular metabolism.* Nature, 2006. **440**(7083): p. 470-6.

96. Castle, N.A. and D.G. Haylett, *Effect of channel blockers on potassium efflux from metabolically exhausted frog skeletal muscle.* J Physiol (Lond), 1987. **383**: p. 31-43.
97. Wolleben, C.D., M.C. Sanguinetti, and P.K. Siegl, *Influence of ATP-sensitive potassium channel modulators on ischemia-induced fibrillation in isolated rat hearts.* Journal of molecular and cellular cardiology, 1989. **21**(8): p. 783-8.
98. Quasthoff, S., et al., *K+ channel openers suppress myotonic activity of human skeletal muscle in vitro.* European Journal of Pharmacology, 1990. **186**(1): p. 125-8.
99. Sauviat, M.P., et al., *Activation of ATP-sensitive K channels by a K channel opener (SR 44866) and the effect upon electrical and mechanical activity of frog skeletal muscle.* Pflugers Arch, 1991. **418**(3): p. 261-5.
100. Vivaudou, M.B., C. Arnoult, and M. Villaz, *Skeletal muscle ATP-sensitive K+ channels recorded from sarcolemmal blebs of split fibers: ATP inhibition is reduced by magnesium and ADP.* J Membr Biol, 1991. **122**(2): p. 165-75.
101. Reimann, F., F.M. Gribble, and F.M. Ashcroft, *Differential response of K(ATP) channels containing SUR2A or SUR2B subunits to nucleotides and pinacidil.* Mol Pharmacol, 2000. **58**(6): p. 1318-25.
102. Clark, R.H., et al., *Muscle dysfunction caused by a KATP channel mutation in neonatal diabetes is neuronal in origin.* Science, 2010. **329**(5990): p. 458-61.
103. Kanno, T., P. Rorsman, and S.O. Göpel, *Glucose-dependent regulation of rhythmic action potential firing in pancreatic beta-cells by K(ATP)-channel modulation.* J Physiol (Lond), 2002. **545**(Pt 2): p. 501-7.
104. Ashcroft, F.M., *ATP-sensitive potassium channelopathies: focus on insulin secretion.* J Clin Invest, 2005. **115**(8): p. 2047-58.
105. Ashcroft, F. and P. Rorsman, *Type 2 diabetes mellitus: not quite exciting enough?* Hum Mol Genet, 2004. **13 Spec No 1**: p. R21-31.
106. Ashcroft, F.M., *Adenosine 5'-triphosphate-sensitive potassium channels.* Annu Rev Neurosci, 1988. **11**: p. 97-118.
107. Seino, S. and T. Miki, *Physiological and pathophysiological roles of ATP-sensitive K+ channels.* Prog Biophys Mol Biol, 2003. **81**(2): p. 133-76.
108. Schwanstecher, C., et al., *The common single nucleotide polymorphism E23K in K(IR)6.2 sensitizes pancreatic beta-cell ATP-sensitive potassium channels toward activation through nucleoside diphosphates.* Diabetes, 2002. **51 Suppl 3**: p. S363-7.
109. Riedel, M.J., et al., *Kir6.2 polymorphisms sensitize beta-cell ATP-sensitive potassium channels to activation by acyl CoAs: a possible cellular mechanism for increased susceptibility to type 2 diabetes?* Diabetes, 2003. **52**(10): p. 2630-5.

110. Villareal, D.T., et al., *Kir6.2 variant E23K increases ATP-sensitive K+ channel activity and is associated with impaired insulin release and enhanced insulin sensitivity in adults with normal glucose tolerance.* Diabetes, 2009. **58**(8): p. 1869-78.
111. Hamming, K.S., et al., *Coexpression of the type 2 diabetes susceptibility gene variants KCNJ11 E23K and ABCC8 S1369A alter the ATP and sulfonylurea sensitivities of the ATP-sensitive K(+) channel.* Diabetes, 2009. **58**(10): p. 2419-24.
112. Nielsen, E.M., et al., *The E23K variant of Kir6.2 associates with impaired post-OGTT serum insulin response and increased risk of type 2 diabetes.* Diabetes, 2003. **52**(2): p. 573-7.
113. Florez, J.C., et al., *Haplotype structure and genotype-phenotype correlations of the sulfonylurea receptor and the islet ATP-sensitive potassium channel gene region.* Diabetes, 2004. **53**(5): p. 1360-8.
114. Chistiakov, D.A., et al., *Genetic variations in the pancreatic ATP-sensitive potassium channel, beta-cell dysfunction, and susceptibility to type 2 diabetes.* Acta Diabetol, 2009. **46**(1): p. 43-9.
115. Dunne, M.J., et al., *Hyperinsulinism in infancy: from basic science to clinical disease.* Physiol Rev, 2004. **84**(1): p. 239-75.
116. De León, D.D. and C.A. Stanley, *Mechanisms of Disease: advances in diagnosis and treatment of hyperinsulinism in neonates.* Nat Clin Pract Endocrinol Metab, 2007. **3**(1): p. 57-68.
117. Henwood, M.J., et al., *Genotype-phenotype correlations in children with congenital hyperinsulinism due to recessive mutations of the adenosine triphosphate-sensitive potassium channel genes.* J Clin Endocrinol Metab, 2005. **90**(2): p. 789-94.
118. Flanagan, S.E., et al., *Update of mutations in the genes encoding the pancreatic beta-cell K(ATP) channel subunits Kir6.2 (KCNJ11) and sulfonylurea receptor 1 (ABCC8) in diabetes mellitus and hyperinsulinism.* Hum Mutat, 2009. **30**(2): p. 170-80.
119. Sharma, N., et al., *The C terminus of SUR1 is required for trafficking of KATP channels.* J Biol Chem, 1999. **274**(29): p. 20628-32.
120. Otonkoski, T., et al., *A point mutation inactivating the sulfonylurea receptor causes the severe form of persistent hyperinsulinemic hypoglycemia of infancy in Finland.* Diabetes, 1999. **48**(2): p. 408-15.
121. Cartier, E.A., et al., *Defective trafficking and function of KATP channels caused by a sulfonylurea receptor 1 mutation associated with persistent hyperinsulinemic hypoglycemia of infancy.* Proc Natl Acad Sci USA, 2001. **98**(5): p. 2882-7.
122. Partridge, C.J., D.J. Beech, and A. Sivaprasadarao, *Identification and pharmacological correction of a membrane trafficking defect associated with a*

mutation in the sulfonylurea receptor causing familial hyperinsulinism. J Biol Chem, 2001. **276**(38): p. 35947-52.

123. Taschenberger, G., et al., *Identification of a familial hyperinsulinism-causing mutation in the sulfonylurea receptor 1 that prevents normal trafficking and function of KATP channels.* J Biol Chem, 2002. **277**(19): p. 17139-46.
124. Huopio, H., et al., *Dominantly inherited hyperinsulinism caused by a mutation in the sulfonylurea receptor type 1.* J Clin Invest, 2000. **106**(7): p. 897-906.
125. Gloyn, A.L., *Glucokinase (GCK) mutations in hyper- and hypoglycemia: maturity-onset diabetes of the young, permanent neonatal diabetes, and hyperinsulinemia of infancy.* Hum Mutat, 2003. **22**(5): p. 353-62.
126. Glaser, B., et al., *Familial hyperinsulinism caused by an activating glucokinase mutation.* N Engl J Med, 1998. **338**(4): p. 226-30.
127. Stanley, C.A., et al., *Hyperinsulinism and hyperammonemia in infants with regulatory mutations of the glutamate dehydrogenase gene.* N Engl J Med, 1998. **338**(19): p. 1352-7.
128. Molven, A., et al., *Familial hyperinsulinemic hypoglycemia caused by a defect in the SCHAD enzyme of mitochondrial fatty acid oxidation.* Diabetes, 2004. **53**(1): p. 221-7.
129. Polak, M. and J. Shield, *Neonatal and very-early-onset diabetes mellitus.* Semin Neonatol, 2004. **9**(1): p. 59-65.
130. Gloyn, A.L., et al., *Relapsing diabetes can result from moderately activating mutations in KCNJ11.* Hum Mol Genet, 2005. **14**(7): p. 925-34.
131. Temple, I.K., et al., *An imprinted gene(s) for diabetes?* Nat Genet, 1995. **9**(2): p. 110-2.
132. Flanagan, S.E., et al., *Mutations in ATP-sensitive K+ channel genes cause transient neonatal diabetes and permanent diabetes in childhood or adulthood.* Diabetes, 2007. **56**(7): p. 1930-7.
133. Girard, C.A., et al., *Functional analysis of six Kir6.2 (KCNJ11) mutations causing neonatal diabetes.* Pflugers Arch, 2006. **453**(3): p. 323-32.
134. Hattersley, A.T. and F.M. Ashcroft, *Activating mutations in Kir6.2 and neonatal diabetes: new clinical syndromes, new scientific insights, and new therapy.* Diabetes, 2005. **54**(9): p. 2503-13.
135. Gloyn, A.L., et al., *Activating mutations in the gene encoding the ATP-sensitive potassium-channel subunit Kir6.2 and permanent neonatal diabetes.* N Engl J Med, 2004. **350**(18): p. 1838-49.
136. Gloyn, A.L., et al., *KCNJ11 activating mutations are associated with developmental delay, epilepsy and neonatal diabetes syndrome and other neurological features.* Eur J Hum Genet, 2006. **14**(7): p. 824-30.

137. McTaggart, J.S., R.H. Clark, and F.M. Ashcroft, *The role of the KATP channel in glucose homeostasis in health and disease: more than meets the islet.* J Physiol (Lond), 2010. **588**(Pt 17): p. 3201-9.
138. Shimomura, K., et al., *Mutations at the same residue (R50) of Kir6.2 (KCNJ11) that cause neonatal diabetes produce different functional effects.* Diabetes, 2006. **55**(6): p. 1705-12.
139. Sagen, J.V., et al., *Permanent neonatal diabetes due to mutations in KCNJ11 encoding Kir6.2: patient characteristics and initial response to sulfonylurea therapy.* Diabetes, 2004. **53**(10): p. 2713-8.
140. Massa, O., et al., *KCNJ11 activating mutations in Italian patients with permanent neonatal diabetes.* Hum Mutat, 2005. **25**(1): p. 22-7.
141. Pearson, E.R., et al., *Switching from insulin to oral sulfonylureas in patients with diabetes due to Kir6.2 mutations.* N Engl J Med, 2006. **355**(5): p. 467-77.
142. Klupa, T., et al., *The identification of a R201H mutation in KCNJ11, which encodes Kir6.2, and successful transfer to sustained-release sulphonylurea therapy in a subject with neonatal diabetes: evidence for heterogeneity of beta cell function among carriers of the R201H mutation.* Diabetologia, 2005. **48**(5): p. 1029-31.
143. Zung, A., et al., *Glibenclamide treatment in permanent neonatal diabetes mellitus due to an activating mutation in Kir6.2.* J Clin Endocrinol Metab, 2004. **89**(11): p. 5504-7.
144. Codner, E., et al., *High-dose glibenclamide can replace insulin therapy despite transitory diarrhea in early-onset diabetes caused by a novel R201L Kir6.2 mutation.* Diabetes Care, 2005. **28**(3): p. 758-9.
145. Colombo, C., et al., *Transient neonatal diabetes mellitus is associated with a recurrent (R201H) KCNJ11 (KIR6.2) mutation.* Diabetologia, 2005. **48**(11): p. 2439-41.
146. Ashcroft, F.M., *New uses for old drugs: neonatal diabetes and sulphonylureas.* Cell Metab, 2010. **11**(3): p. 179-81.
147. Masia, R., et al., *An ATP-binding mutation (G334D) in KCNJ11 is associated with a sulfonylurea-insensitive form of developmental delay, epilepsy, and neonatal diabetes.* Diabetes, 2007. **56**(2): p. 328-36.
148. Slingerland, A.S., et al., *Improved motor development and good long-term glycaemic control with sulfonylurea treatment in a patient with the syndrome of intermediate developmental delay, early-onset generalised epilepsy and neonatal diabetes associated with the V59M mutation in the KCNJ11 gene.* Diabetologia, 2006. **49**(11): p. 2559-63.
149. Shimomura, K., et al., *A novel mutation causing DEND syndrome: a treatable channelopathy of pancreas and brain.* Neurology, 2007. **69**(13): p. 1342-9.

150. Koster, J.C., et al., *The G53D mutation in Kir6.2 (KCNJ11) is associated with neonatal diabetes and motor dysfunction in adulthood that is improved with sulfonylurea therapy.* J Clin Endocrinol Metab, 2008. **93**(3): p. 1054-61.
151. Slingerland, A.S., et al., *Sulphonylurea therapy improves cognition in a patient with the V59M KCNJ11 mutation.* Diabet Med, 2008. **25**(3): p. 277-81.
152. Mlynarski, W., et al., *Sulfonylurea improves CNS function in a case of intermediate DEND syndrome caused by a mutation in KCNJ11.* Nature clinical practice Neurology, 2007. **3**(11): p. 640-5.
153. Tonini, G., et al., *Sulfonylurea treatment outweighs insulin therapy in short-term metabolic control of patients with permanent neonatal diabetes mellitus due to activating mutations of the KCNJ11 (KIR6.2) gene.* Diabetologia, 2006. **49**(9): p. 2210-3.
154. Takanaga, H., et al., *Efflux transport of tolbutamide across the blood-brain barrier.* J Pharm Pharmacol, 1998. **50**(9): p. 1027-33.
155. Njølstad, P.R., et al., *Neonatal diabetes mellitus due to complete glucokinase deficiency.* N Engl J Med, 2001. **344**(21): p. 1588-92.
156. Njølstad, P.R., et al., *Permanent neonatal diabetes caused by glucokinase deficiency: inborn error of the glucose-insulin signaling pathway.* Diabetes, 2003. **52**(11): p. 2854-60.
157. Wildin, R.S., et al., *X-linked neonatal diabetes mellitus, enteropathy and endocrinopathy syndrome is the human equivalent of mouse scurfy.* Nat Genet, 2001. **27**(1): p. 18-20.
158. Delépine, M., et al., *EIF2AK3, encoding translation initiation factor 2-alpha kinase 3, is mutated in patients with Wolcott-Rallison syndrome.* Nat Genet, 2000. **25**(4): p. 406-9.
159. Stoffers, D.A., et al., *Early-onset type-II diabetes mellitus (MODY4) linked to IPF1.* Nat Genet, 1997. **17**(2): p. 138-9.
160. Sellick, G.S., et al., *Mutations in PTF1A cause pancreatic and cerebellar agenesis.* Nat Genet, 2004. **36**(12): p. 1301-5.
161. Babenko, A.P., et al., *Sulfonylurea receptors set the maximal open probability, ATP sensitivity and plasma membrane density of KATP channels.* FEBS Lett, 1999. **445**(1): p. 131-6.
162. Koster, J.C., Q. Sha, and C.G. Nichols, *Sulfonylurea and K(+)-channel opener sensitivity of K(ATP) channels. Functional coupling of Kir6.2 and SUR1 subunits.* J Gen Physiol, 1999. **114**(2): p. 203-13.

163. Koster, J.C., et al., *ATP inhibition of KATP channels: control of nucleotide sensitivity by the N-terminal domain of the Kir6.2 subunit.* J Physiol (Lond), 1999. **515 (Pt 1)**: p. 19-30.

164. Reimann, F., et al., *The role of lysine 185 in the kir6.2 subunit of the ATP-sensitive channel in channel inhibition by ATP.* J Physiol (Lond), 1999. **520 Pt 3**: p. 661-9.

165. Koster, J.C., et al., *Targeted overactivity of beta cell K(ATP) channels induces profound neonatal diabetes.* Cell, 2000. **100**(6): p. 645-54.

166. Koster, J.C., et al., *Expression of ATP-insensitive KATP channels in pancreatic beta-cells underlies a spectrum of diabetic phenotypes.* Diabetes, 2006. **55**(11): p. 2957-64.

167. Remedi, M.S., et al., *Secondary consequences of beta cell inexcitability: identification and prevention in a murine model of K(ATP)-induced neonatal diabetes mellitus.* Cell Metab, 2009. **9**(2): p. 140-51.

168. Girard, C.A., et al., *Expression of an activating mutation in the gene encoding the KATP channel subunit Kir6.2 in mouse pancreatic beta cells recapitulates neonatal diabetes.* J Clin Invest, 2009. **119**(1): p. 80-90.

169. Soriano, P., *Generalized lacZ expression with the ROSA26 Cre reporter strain.* Nat Genet, 1999. **21**(1): p. 70-1.

170. Clark, R.H., *Physiological studies of mutant KATP channels causing neonatal diabetes and neurological symptoms.* Thesis, (DPhil). University of Oxford., 2010.

171. Plassart, E., et al., *Paramyotonia congenita: genotype to phenotype correlations in two families and report of a new mutation in the sodium channel gene.* J Neurol Sci, 1996. **142**(1-2): p. 126-33.

172. Matthews, E., et al., *What causes paramyotonia in the United Kingdom? Common and new SCN4A mutations revealed.* Neurology, 2008. **70**(1): p. 50-3.

173. Spillane, J., D.J. Beeson, and D.M. Kullmann, *Myasthenia and related disorders of the neuromuscular junction.* J Neurol Neurosurg Psychiatr, 2010. **81**(8): p. 850-7.

174. Proks, P., et al., *A heterozygous activating mutation in the sulphonylurea receptor SUR1 (ABCC8) causes neonatal diabetes.* Hum Mol Genet, 2006. **15**(11): p. 1793-800.

175. Tronche, F., et al., *Disruption of the glucocorticoid receptor gene in the nervous system results in reduced anxiety.* Nat Genet, 1999. **23**(1): p. 99-103.

176. Proks, P., C. Girard, and F.M. Ashcroft, *Functional effects of KCNJ11 mutations causing neonatal diabetes: enhanced activation by MgATP.* Hum Mol Genet, 2005. **14**(18): p. 2717-26.

177. Ashcroft, F.M. and F.M. Gribble, *Correlating structure and function in ATP-sensitive K + channels.* Trends Neurosci, 1998. **21**(7): p. 288-94.

178. Aguilar-Bryan, L. and J. Bryan, *Molecular biology of adenosine triphosphate-sensitive potassium channels.* Endocr Rev, 1999. **20**(2): p. 101-35.
179. Seino, S., *ATP-sensitive potassium channels: a model of heteromultimeric potassium channel/receptor assemblies.* Annu Rev Physiol, 1999. **61**: p. 337-62.
180. Liss, B., et al., *K-ATP channels promote the differential degeneration of dopaminergic midbrain neurons.* Nat Neurosci, 2005. **8**(12): p. 1742-51.
181. Mourre, C., et al., *Antidiabetic sulfonylureas: localization of binding sites in the brain and effects on the hyperpolarization induced by anoxia in hippocampal slices.* Brain Res, 1989. **486**(1): p. 159-64.
182. Karschin, C., et al., *Overlapping distribution of K(ATP) channel-forming Kir6.2 subunit and the sulfonylurea receptor SUR1 in rodent brain.* FEBS Lett, 1997. **401**(1): p. 59-64.
183. Dunn-Meynell, A.A., N.E. Rawson, and B.E. Levin, *Distribution and phenotype of neurons containing the ATP-sensitive K+ channel in rat brain.* Brain Res, 1998. **814**(1-2): p. 41-54.
184. Zhou, M., et al., *Localization of pore-forming subunit of the ATP-sensitive K(+)-channel, Kir6.2, in rat brain neurons and glial cells.* Brain Res Mol Brain Res, 2002. **101**(1-2): p. 23-32.
185. Thomzig, A., et al., *Pore-forming subunits of K-ATP channels, Kir6.1 and Kir6.2, display prominent differences in regional and cellular distribution in the rat brain.* J Comp Neurol, 2005. **484**(3): p. 313-30.
186. Xia, Y., D. Eisenman, and G.G. Haddad, *Sulfonylurea receptor expression in rat brain: effect of chronic hypoxia during development.* Pediatr Res, 1993. **34**(5): p. 634-41.
187. Mourre, C., C. Widmann, and M. Lazdunski, *Sulfonylurea binding sites associated with ATP-regulated K+ channels in the central nervous system: autoradiographic analysis of their distribution and ontogenesis, and of their localization in mutant mice cerebellum.* Brain Res, 1990. **519**(1-2): p. 29-43.
188. Ohno-Shosaku, T. and C. Yamamoto, *Identification of an ATP-sensitive K+ channel in rat cultured cortical neurons.* Pflugers Arch, 1992. **422**(3): p. 260-6.
189. Fujimura, N., et al., *Contribution of ATP-sensitive potassium channels to hypoxic hyperpolarization in rat hippocampal CA1 neurons in vitro.* J Neurophysiol, 1997. **77**(1): p. 378-85.
190. Grigg, J.J. and E.G. Anderson, *Glucose and sulfonylureas modify different phases of the membrane potential change during hypoxia in rat hippocampal slices.* Brain Res, 1989. **489**(2): p. 302-10.

191. Matsumoto, N., S. Komiyama, and N. Akaike, *Pre- and postsynaptic ATP-sensitive potassium channels during metabolic inhibition of rat hippocampal CA1 neurons.* J Physiol (Lond), 2002. **541**(Pt 2): p. 511-20.
192. Spanswick, D., et al., *Leptin inhibits hypothalamic neurons by activation of ATP-sensitive potassium channels.* Nature, 1997. **390**(6659): p. 521-5.
193. Miki, T., et al., *ATP-sensitive K+ channels in the hypothalamus are essential for the maintenance of glucose homeostasis.* Nat Neurosci, 2001. **4**(5): p. 507-12.
194. Schwanstecher, C. and U. Panten, *Tolbutamide- and diazoxide-sensitive K+ channel in neurons of substantia nigra pars reticulata.* Naunyn Schmiedebergs Arch Pharmacol, 1993. **348**(1): p. 113-7.
195. Jiang, C. and G.G. Haddad, *Effect of anoxia on intracellular and extracellular potassium activity in hypoglossal neurons in vitro.* J Neurophysiol, 1991. **66**(1): p. 103-11.
196. Rothman, S.M. and J.W. Olney, *Glutamate and the pathophysiology of hypoxic--ischemic brain damage.* Ann Neurol, 1986. **19**(2): p. 105-11.
197. Ginsberg, M.D., *Neuroprotection in brain ischemia: an update (Part I).* The Neuroscientist, 1995. **1**(2): p. 95-103.
198. Katsura, K., et al., *Changes of labile metabolites during anoxia in moderately hypo- and hyperthermic rats: correlation to membrane fluxes of K+.* Brain Res, 1992. **590**(1-2): p. 6-12.
199. Amoroso, S., et al., *Glucose, sulfonylureas, and neurotransmitter release: role of ATP-sensitive K+ channels.* Science, 1990. **247**(4944): p. 852-4.
200. Yamada, K. and N. Inagaki, *Neuroprotection by KATP channels.* Journal of molecular and cellular cardiology, 2005. **38**(6): p. 945-949.
201. Yamada, K., et al., *Protective role of ATP-sensitive potassium channels in hypoxia-induced generalized seizure.* Science, 2001. **292**(5521): p. 1543-6.
202. Kasamo, K., et al., *Effects of a benzodioxan derivative MKC-242 on the firing activity of the dorsal hippocampus CA1 pyramidal neurons in awake and urethane-anaesthetized rats: in vivo electrophysiological evidence for a 5-HT 1A agonistic property.* Int J Neuropsychopharmacol, 2000. **3**(2): p. 99-108.
203. Campbell, S.L., S.S. Mathew, and J.J. Hablitz, *Pre- and postsynaptic effects of kainate on layer II/III pyramidal cells in rat neocortex.* Neuropharmacology, 2007. **53**(1): p. 37-47.
204. Häusser, M. and B.A. Clark, *Tonic synaptic inhibition modulates neuronal output pattern and spatiotemporal synaptic integration.* Neuron, 1997. **19**(3): p. 665-78.

205. Nam, S.C. and P.E. Hockberger, *Analysis of spontaneous electrical activity in cerebellar Purkinje cells acutely isolated from postnatal rats.* J Neurobiol, 1997. **33**(1): p. 18-32.

206. Zheng, S. and Z. Zuo, *Isoflurane preconditioning reduces purkinje cell death in an in vitro model of rat cerebellar ischemia.* Neuroscience, 2003. **118**(1): p. 99-106.

207. Tai, K.K., L. Pham, and D.D. Truong, *Intracisternal administration of glibenclamide or 5-hydroxydecanoate does not reverse the neuroprotective effect of ketogenic diet against ischemic brain injury-induced neurodegeneration.* Brain Inj, 2009. **23**(13-14): p. 1081-8.

208. Seharaseyon, J., et al., *Molecular composition of mitochondrial ATP-sensitive potassium channels probed by viral Kir gene transfer.* Journal of molecular and cellular cardiology, 2000. **32**(11): p. 1923-30.

209. Teshima, Y., et al., *Nicorandil prevents oxidative stress-induced apoptosis in neurons by activating mitochondrial ATP-sensitive potassium channels.* Brain Res, 2003. **990**(1-2): p. 45-50.

210. Teshima, Y., et al., *Mitochondrial ATP-sensitive potassium channel activation protects cerebellar granule neurons from apoptosis induced by oxidative stress.* Stroke, 2003. **34**(7): p. 1796-802.

211. Pocai, A., et al., *Hypothalamic K(ATP) channels control hepatic glucose production.* Nature, 2005. **434**(7036): p. 1026-31.

212. Könner, A.C., et al., *Insulin Action in AgRP-Expressing Neurons Is Required for Suppression of Hepatic Glucose Production.* Cell Metab, 2007. **5**(6): p. 438-449.

213. Gromada, J., I. Franklin, and C.B. Wollheim, *Alpha-cells of the endocrine pancreas: 35 years of research but the enigma remains.* Endocr Rev, 2007. **28**(1): p. 84-116.

214. Plum, L., et al., *Enhanced PIP3 signaling in POMC neurons causes KATP channel activation and leads to diet-sensitive obesity.* J Clin Invest, 2006. **116**(7): p. 1886-901.

215. Parton, L.E., et al., *Glucose sensing by POMC neurons regulates glucose homeostasis and is impaired in obesity.* Nature, 2007. **449**(7159): p. 228-32.

216. Röper, J. and F.M. Ashcroft, *Metabolic inhibition and low internal ATP activate K-ATP channels in rat dopaminergic substantia nigra neurones.* Pflugers Arch, 1995. **430**(1): p. 44-54.

217. Zawar, C., et al., *Cell-type specific expression of ATP-sensitive potassium channels in the rat hippocampus.* J Physiol (Lond), 1999. **514 (Pt 2)**: p. 327-41.

218. Gerken, T., et al., *The obesity-associated FTO gene encodes a 2-oxoglutarate-dependent nucleic acid demethylase.* Science, 2007. **318**(5855): p. 1469-72.

219. Sanchez-Pulido, L. and M.A. Andrade-Navarro, *The FTO (fat mass and obesity associated) gene codes for a novel member of the non-heme dioxygenase superfamily.* BMC Biochem, 2007. **8**: p. 23.

220. Jia, G., et al., *Oxidative demethylation of 3-methylthymine and 3-methyluracil in single-stranded DNA and RNA by mouse and human FTO.* FEBS Lett, 2008.

221. Clifton, I.J., et al., *Structural studies on 2-oxoglutarate oxygenases and related double-stranded beta-helix fold proteins.* J Inorg Biochem, 2006. **100**(4): p. 644-69.

222. Wu, Q., et al., *The obesity-associated Fto gene is a transcriptional coactivator.* Biochem Biophys Res Commun, 2010. **401**(3): p. 390-5.

223. Fischer, J., et al., *Inactivation of the Fto gene protects from obesity.* Nature, 2009: p. 1-6.

224. Han, Z., et al., *Crystal structure of the FTO protein reveals basis for its substrate specificity.* Nature, 2010: p. 1-6.

225. Church, C., et al., *A mouse model for the metabolic effects of the human fat mass and obesity associated FTO gene.* PLoS Genet, 2009. **5**(8): p. e1000599.

226. Morton, G.J., et al., *Central nervous system control of food intake and body weight.* Nature, 2006. **443**(7109): p. 289-95.

227. Lein, E.S., et al., *Genome-wide atlas of gene expression in the adult mouse brain.* Nature, 2007. **445**(7124): p. 168-76.

228. Fredriksson, R., et al., *The obesity gene, FTO, is of ancient origin, up-regulated during food deprivation and expressed in neurons of feeding-related nuclei of the brain.* Endocrinology, 2008. **149**(5): p. 2062-71.

229. Speakman, J.R., K.A. Rance, and A.M. Johnstone, *Polymorphisms of the FTO gene are associated with variation in energy intake, but not energy expenditure.* Obesity (Silver Spring), 2008. **16**(8): p. 1961-5.

230. Timpson, N.J., et al., *The fat mass- and obesity-associated locus and dietary intake in children.* Am J Clin Nutr, 2008. **88**(4): p. 971-8.

231. Wardle, J., et al., *The FTO gene and measured food intake in children.* International journal of obesity, 2008.

232. Haupt, A., et al., *Variation in the FTO gene influences food intake but not energy expenditure.* Exp Clin Endocrinol Diabetes, 2009. **117**(4): p. 194-7.

233. Sonestedt, E., et al., *Fat and carbohydrate intake modify the association between genetic variation in the FTO genotype and obesity.* Am J Clin Nutr, 2009. **90**(5): p. 1418-25.

234. Tanofsky-Kraff, M., et al., *The FTO gene rs9939609 obesity-risk allele and loss of control over eating.* Am J Clin Nutr, 2009. **90**(6): p. 1483-8.

235. Hakanen, M., et al., *FTO genotype is associated with body mass index after the age of seven years but not with energy intake or leisure-time physical activity.* J Clin Endocrinol Metab, 2009. **94**(4): p. 1281-7.
236. Do, R., et al., *Genetic variants of FTO influence adiposity, insulin sensitivity, leptin levels, and resting metabolic rate in the Quebec Family Study.* Diabetes, 2008. **57**(4): p. 1147-50.
237. Berentzen, T., et al., *Lack of association of fatness-related FTO gene variants with energy expenditure or physical activity.* J Clin Endocrinol Metab, 2008. **93**(7): p. 2904-8.
238. Bell, C.G., et al., *Integrated Genetic and Epigenetic Analysis Identifies Haplotype-Specific Methylation in the FTO Type 2 Diabetes and Obesity Susceptibility Locus.* PLoS ONE, 2010.
239. Meyre, D., et al., *Prevalence of loss-of-function FTO mutations in lean and obese individuals.* Diabetes, 2010. **59**(1): p. 311-8.
240. Boissel, S., et al., *Loss-of-function mutation in the dioxygenase-encoding FTO gene causes severe growth retardation and multiple malformations.* Am J Hum Genet, 2009. **85**(1): p. 106-11.
241. van der Hoeven, F., et al., *Programmed cell death is affected in the novel mouse mutant Fused toes (Ft).* Development, 1994. **120**(9): p. 2601-7.
242. Heymer, J. and U. Rüther, *Syndactyly of Ft/+ mice correlates with an imbalance in bmp4 and fgf8 expression.* Mech Dev, 1999. **88**(2): p. 173-81.
243. Anselme, I., et al., *Defects in brain patterning and head morphogenesis in the mouse mutant Fused toes.* Dev Biol, 2007. **304**(1): p. 208-20.
244. Gao, X., et al., *The Fat Mass and Obesity Associated Gene FTO Functions in the Brain to Regulate Postnatal Growth in Mice.* PLoS ONE, 2010.
245. Church, C., et al., *Overexpression of Fto leads to increased food intake and results in obesity.* Nat Genet, 2010. **42**(12): p. 1086-92.
246. Grunnet, L.G., et al., *Regulation and function of FTO mRNA expression in human skeletal muscle and subcutaneous adipose tissue.* Diabetes, 2009. **58**(10): p. 2402-8.
247. Stratigopoulos, G., et al., *Regulation of Fto/Ftm gene expression in mice and humans.* Am J Physiol Regul Integr Comp Physiol, 2008. **294**(4): p. R1185-96.
248. Wang, P., et al., *Involvement of Leptin Receptor (LepRb)-STAT3 Signaling Pathway in Brain FTO Downregulation during Energy Restriction.* Molecular medicine (Cambridge, Mass), 2011.
249. Bassols, J., et al., *Placental FTO expression relates to fetal growth.* International journal of obesity (2005), 2010. **34**(9): p. 1365-70.

250. Wåhlén, K., E. Sjölin, and J. Hoffstedt, *The common rs9939609 gene variant of the fat mass- and obesity-associated gene FTO is related to fat cell lipolysis.* J Lipid Res, 2008. **49**(3): p. 607-11.

251. Klöting, N., et al., *Inverse relationship between obesity and FTO gene expression in visceral adipose tissue in humans.* Diabetologia, 2008. **51**(4): p. 641-7.

252. Ho, A.J., et al., *A commonly carried allele of the obesity-related FTO gene is associated with reduced brain volume in the healthy elderly.* Proc Natl Acad Sci USA, 2010.

253. Dahlstrand, J., M. Lardelli, and U. Lendahl, *Nestin mRNA expression correlates with the central nervous system progenitor cell state in many, but not all, regions of developing central nervous system.* Brain Res Dev Brain Res, 1995. **84**(1): p. 109-29.

254. Hara, T., et al., *Suppression of basal autophagy in neural cells causes neurodegenerative disease in mice.* Nature, 2006. **441**(7095): p. 885-9.

255. Balthasar, N., et al., *Leptin receptor signaling in POMC neurons is required for normal body weight homeostasis.* Neuron, 2004. **42**(6): p. 983-91.

256. Novak, A., et al., *Z/EG, a double reporter mouse line that expresses enhanced green fluorescent protein upon Cre-mediated excision.* Genesis, 2000. **28**(3-4): p. 147-55.

257. Contet, C., J.N. Rawlins, and R.M. Deacon, *A comparison of 129S2/SvHsd and C57BL/6JOlaHsd mice on a test battery assessing sensorimotor, affective and cognitive behaviours: implications for the study of genetically modified mice.* Behav Brain Res, 2001. **124**(1): p. 33-46.

258. Deacon, R.M. and C.R. Gardner, *The pull-up test in rats: a simple method for evaluating muscle relaxation.* J Pharmacol Methods, 1984. **11**(2): p. 119-24.

259. Barclay, L.L., G.E. Gibson, and J.P. Blass, *The string test: an early behavioral change in thiamine deficiency.* Pharmacol Biochem Behav, 1981. **14**(2): p. 153-7.

260. Deacon, R.M., et al., *Behavioral phenotyping of mice lacking the K ATP channel subunit Kir6.2.* Physiol Behav, 2006. **87**(4): p. 723-33.

261. Guenther, K., et al., *Early behavioural changes in scrapie-affected mice and the influence of dapsone.* Eur J Neurosci, 2001. **14**(2): p. 401-9.

262. Jones, B.J. and D.J. Roberts, *The quantiative measurement of motor inco-ordination in naive mice using an accelerating rotarod.* J Pharm Pharmacol, 1968. **20**(4): p. 302-4.

263. Dunham, N.W. and T.S. Miya, *A note on a simple apparatus for detecting neurological deficit in rats and mice.* J Am Pharm Assoc Am Pharm Assoc (Baltim), 1957. **46**(3): p. 208-9.

264. Abramoff, M.D., P.J. Magalhaes, and S.J. Ram, *Image Processing with ImageJ.* Biophotonics International, 2004. **11**(7): p. 36-42.

265. Pfaffl, M.W., *A new mathematical model for relative quantification in real-time RT-PCR.* Nucleic Acids Res, 2001. **29**(9): p. e45.
266. Vandesompele, J., et al., *Accurate normalization of real-time quantitative RT-PCR data by geometric averaging of multiple internal control genes.* Genome Biol, 2002. **3**(7): p. RESEARCH0034.
267. Liu, X., et al., *Analysis of action tremor and impaired control of movement velocity in multiple sclerosis during visually guided wrist-tracking tasks.* Mov Disord, 1997. **12**(6): p. 992-9.
268. Glickstein, M., et al., *Cerebellum lesions and finger use.* Cerebellum, 2005. **4**(3): p. 189-97.
269. Annett, M., *Left, Right, Hand and Brain: The Right Shift Theory.* 1985: Lawrence Erlbaum Associates.
270. Stoodley, C.J. and J.F. Stein, *A processing speed deficit in dyslexic adults? Evidence from a peg-moving task.* Neurosci Lett, 2006. **399**(3): p. 264-7.
271. Pallant, J., *SPSS Survival Manual: A Step by Step Guide to Data Analysis Using SPSS*. 2010: Open University Press.
272. Holmes, G., *The symptoms of acute cerebellar injuries due to gunshot injuries.* Brain, 1917. **40**(4): p. 461-531.
273. Chance, P.F., et al., *Clinical nosologic and genetic aspects of Joubert and related syndromes.* J Child Neurol, 1999. **14**(10): p. 660-6; discussion 669-72.
274. Glickstein, M. and K. Doron, *Cerebellum: connections and functions.* Cerebellum, 2008. **7**(4): p. 589-94.
275. Mackie, S., et al., *Cerebellar development and clinical outcome in attention deficit hyperactivity disorder.* The American journal of psychiatry, 2007. **164**(4): p. 647-55.
276. Schmahmann, J.D., J.B. Weilburg, and J.C. Sherman, *The neuropsychiatry of the cerebellum - insights from the clinic.* Cerebellum, 2007. **6**(3): p. 254-67.
277. Allen, G., et al., *Attentional activation of the cerebellum independent of motor involvement.* Science, 1997. **275**(5308): p. 1940-3.
278. Brüning, J.C., et al., *Role of brain insulin receptor in control of body weight and reproduction.* Science, 2000. **289**(5487): p. 2122-5.
279. Proks, P., et al., *Involvement of the N-terminus of Kir6.2 in the inhibition of the KATP channel by ATP.* J Physiol (Lond), 1999. **514 (Pt 1)**: p. 19-25.
280. Purkiss, R.J., et al., *Immediate early gene expression in the rat forebrain following striatal infusion of quinolinic acid.* Eur J Neurosci, 1993. **5**(12): p. 1653-62.
281. Morgan, J.I. and T. Curran, *Stimulus-transcription coupling in the nervous system: involvement of the inducible proto-oncogenes fos and jun.* Annu Rev Neurosci, 1991. **14**: p. 421-51.

282. Konnerth, A., I. Llano, and C.M. Armstrong, *Synaptic currents in cerebellar Purkinje cells.* Proc Natl Acad Sci USA, 1990. **87**(7): p. 2662-5.

283. Zhang, C.L., A. Messing, and S.Y. Chiu, *Specific alteration of spontaneous GABAergic inhibition in cerebellar purkinje cells in mice lacking the potassium channel Kv1. 1.* J Neurosci, 1999. **19**(8): p. 2852-64.

284. Honoré, T., et al., *Quinoxalinediones: potent competitive non-NMDA glutamate receptor antagonists.* Science, 1988. **241**(4866): p. 701-3.

285. Simmonds, M.A., *A site for the potentiation of GABA-mediated responses by benzodiazepines.* Nature, 1980. **284**(5756): p. 558-60.

286. Vooijs, M., J. Jonkers, and A. Berns, *A highly efficient ligand-regulated Cre recombinase mouse line shows that LoxP recombination is position dependent.* EMBO Rep, 2001. **2**(4): p. 292-7.

287. Bean, B.P., *The action potential in mammalian central neurons.* Nat Rev Neurosci, 2007. **8**(6): p. 451-65.

288. Perkins, K.L., *Cell-attached voltage-clamp and current-clamp recording and stimulation techniques in brain slices.* J Neurosci Methods, 2006. **154**(1-2): p. 1-18.

289. Khaliq, Z.M., N.W. Gouwens, and I.M. Raman, *The contribution of resurgent sodium current to high-frequency firing in Purkinje neurons: an experimental and modeling study.* J Neurosci, 2003. **23**(12): p. 4899-912.

290. Llinás, R. and M. Sugimori, *Electrophysiological properties of in vitro Purkinje cell somata in mammalian cerebellar slices.* J Physiol (Lond), 1980. **305**: p. 171-95.

291. Martina, M., G.L. Yao, and B.P. Bean, *Properties and functional role of voltage-dependent potassium channels in dendrites of rat cerebellar Purkinje neurons.* J Neurosci, 2003. **23**(13): p. 5698-707.

292. McKay, B.E. and R.W. Turner, *Kv3 K+ channels enable burst output in rat cerebellar Purkinje cells.* Eur J Neurosci, 2004. **20**(3): p. 729-39.

293. Williams, S.R., et al., *Membrane potential bistability is controlled by the hyperpolarization-activated current I(H) in rat cerebellar Purkinje neurons in vitro.* J Physiol (Lond), 2002. **539**(Pt 2): p. 469-83.

294. Fernandez, F.R., J.D. Engbers, and R.W. Turner, *Firing dynamics of cerebellar purkinje cells.* J Neurophysiol, 2007. **98**(1): p. 278-94.

295. Routh, V.H., *Glucose-sensing neurons: are they physiologically relevant?* Physiol Behav, 2002. **76**(3): p. 403-13.

296. Silver, I.A. and M. Erecińska, *Extracellular glucose concentration in mammalian brain: continuous monitoring of changes during increased neuronal activity and upon limitation in oxygen supply in normo-, hypo-, and hyperglycemic animals.* J Neurosci, 1994. **14**(8): p. 5068-76.

297. Ballanyi, K., *Protective role of neuronal KATP channels in brain hypoxia.* J Exp Biol, 2004. **207**(Pt 18): p. 3201-12.

298. Yuan, H.B., et al., *Hypothermic preconditioning increases survival of purkinje neurons in rat cerebellar slices after an in vitro simulated ischemia.* Anesthesiology, 2004. **100**(2): p. 331-7.

299. LeMasson, G., E. Marder, and L.F. Abbott, *Activity-dependent regulation of conductances in model neurons.* Science, 1993. **259**(5103): p. 1915-7.

300. Turrigiano, G., G. LeMasson, and E. Marder, *Selective regulation of current densities underlies spontaneous changes in the activity of cultured neurons.* J Neurosci, 1995. **15**(5 Pt 1): p. 3640-52.

301. Davis, G.W. and C.S. Goodman, *Genetic analysis of synaptic development and plasticity: homeostatic regulation of synaptic efficacy.* Curr Opin Neurobiol, 1998. **8**(1): p. 149-56.

302. Davis, G.W. and I. Bezprozvanny, *Maintaining the stability of neural function: a homeostatic hypothesis.* Annu Rev Physiol, 2001. **63**: p. 847-69.

303. Hernández-Sánchez, C., T.L. Wood, and D. LeRoith, *Developmental and tissue-specific sulfonylurea receptor gene expression.* Endocrinology, 1997. **138**(2): p. 705-11.

304. Ito, M., *Mechanisms of motor learning in the cerebellum.* Brain Res, 2000. **886**(1-2): p. 237-245.

305. Harris, N.C. and A. Constanti, *Mechanism of block by ZD 7288 of the hyperpolarization-activated inward rectifying current in guinea pig substantia nigra neurons in vitro.* J Neurophysiol, 1995. **74**(6): p. 2366-78.

306. Songstad, N.T., C. Klingenberg, and P.I. Kaaresen, *Case 35-2006: a newborn boy with hypotonia.* N Engl J Med, 2007. **356**(8): p. 874; author reply 874.

307. Kobayashi, S., et al., *A case of spinal cord injury that occurred in utero.* Pediatr Neurol, 2006. **35**(5): p. 367-9.

308. Rosenthal, R.H. and T.W. Allen, *An examination of attention, arousal, and learning dysfunctions of hyperkinetic children.* Psychol Bull, 1978. **85**(4): p. 689-715.

309. Mattes, J.A., *The role of frontal lobe dysfunction in childhood hyperkinesis.* Compr Psychiatry, 1980. **21**(5): p. 358-69.

310. Slingerland, A.S., et al., *Referral rates for diagnostic testing support an incidence of permanent neonatal diabetes in three European countries of at least 1 in 260,000 live births.* Diabetologia, 2009. **52**(8): p. 1683-5.

311. Fuchs, E.C., et al., *Recruitment of parvalbumin-positive interneurons determines hippocampal function and associated behavior.* Neuron, 2007. **53**(4): p. 591-604.

312. Weiss, J.H., et al., *Cortical neurons containing somatostatin- or parvalbumin-like immunoreactivity are atypically vulnerable to excitotoxic injury in vitro.* Neurology, 1990. **40**(8): p. 1288-92.

313. Celio, M.R., *Calbindin D-28k and parvalbumin in the rat nervous system.* Neuroscience, 1990. **35**(2): p. 375-475.

314. Kawaguchi, Y., et al., *Fast spiking cells in rat hippocampus (CA1 region) contain the calcium-binding protein parvalbumin.* Brain Res, 1987. **416**(2): p. 369-74.

315. Heizmann, C.W., M.W. Berchtold, and A.M. Rowlerson, *Correlation of parvalbumin concentration with relaxation speed in mammalian muscles.* Proc Natl Acad Sci USA, 1982. **79**(23): p. 7243-7.

316. Vongvatcharanon, S., U. Vongvatcharanon, and P. Boonyoung, *Immunohistochemical localization of parvalbumin calcium-binding protein in the heart tissues of various species.* Acta Histochem, 2008. **110**(1): p. 26-33.

317. Celio, M.R. and C.W. Heizmann, *Calcium-binding protein parvalbumin as a neuronal marker.* Nature, 1981. **293**(5830): p. 300-2.

318. Celio, M.R., *Parvalbumin in most gamma-aminobutyric acid-containing neurons of the rat cerebral cortex.* Science, 1986. **231**(4741): p. 995-7.

319. Meyer, A.H., et al., *In vivo labeling of parvalbumin-positive interneurons and analysis of electrical coupling in identified neurons.* J Neurosci, 2002. **22**(16): p. 7055-64.

320. Yamamoto, T., et al., *Parvalbumin- and calbindin D28k-immunoreactive neurons in the superficial layers of the spinal cord dorsal horn of rat.* Brain Res Bull, 1989. **23**(6): p. 493-508.

321. Antal, M., T.F. Freund, and E. Polgár, *Calcium-binding proteins, parvalbumin- and calbindin-D 28k-immunoreactive neurons in the rat spinal cord and dorsal root ganglia: a light and electron microscopic study.* J Comp Neurol, 1990. **295**(3): p. 467-84.

322. Ino, H., *Immunohistochemical characterization of the orphan nuclear receptor ROR alpha in the mouse nervous system.* J Histochem Cytochem, 2004. **52**(3): p. 311-23.

323. Seto-Ohshima, A., et al., *Appearance of parvalbumin-specific immunoreactivity in the cerebral cortex and hippocampus of the developing rat and gerbil brain.* Histochemistry, 1990. **94**(6): p. 579-89.

324. Sánchez, M.P., et al., *Distribution of calbindin and parvalbumin in the developing somatosensory cortex and its primordium in the rat: an immunocytochemical study.* J Neurocytol, 1992. **21**(10): p. 717-36.

325. Alcantara, S., et al., *Transient colocalization of parvalbumin and calbindin D28k in the postnatal cerebral cortex: evidence for a phenotypic shift in developing nonpyramidal neurons.* Eur J Neurosci, 1996. **8**(7): p. 1329-39.

326. Collin, T., et al., *Developmental changes in parvalbumin regulate presynaptic Ca2+ signaling.* J Neurosci, 2005. **25**(1): p. 96-107.
327. Hippenmeyer, S., et al., *A developmental switch in the response of DRG neurons to ETS transcription factor signaling.* PLoS Biol, 2005. **3**(5): p. e159.
328. Deacon, R.M.J., et al., *Behavioral phenotyping of mice lacking the K ATP channel subunit Kir6.2.* Physiol Behav, 2006. **87**(4): p. 723-33.
329. Hanin, I. and E. Usdin, *Animal Models in Psychiatry and Neurology*. 1977: Pergamon Press.
330. Dulawa, S.C., et al., *Dopamine D4 receptor-knock-out mice exhibit reduced exploration of novel stimuli.* J Neurosci, 1999. **19**(21): p. 9550-6.
331. Bronikowski, A.M., et al., *Open-field behavior of house mice selectively bred for high voluntary wheel-running.* Behav Genet, 2001. **31**(3): p. 309-16.
332. Hovatta, I., et al., *Glyoxalase 1 and glutathione reductase 1 regulate anxiety in mice.* Nature, 2005. **438**(7068): p. 662-6.
333. Nguyen, P.V., et al., *Strain-dependent differences in LTP and hippocampus-dependent memory in inbred mice.* Learn Mem, 2000. **7**(3): p. 170-9.
334. Gerlai, R., *Gene-targeting studies of mammalian behavior: is it the mutation or the background genotype?* Trends Neurosci, 1996. **19**(5): p. 177-81.
335. Galichet, C., R. Lovell-Badge, and K. Rizzoti, *Nestin-Cre mice are affected by hypopituitarism, which is not due to significant activity of the transgene in the pituitary gland.* PLoS ONE, 2010. **5**(7): p. e11443.
336. Briancon, N., et al., *Combined neural inactivation of suppressor of cytokine signaling-3 and protein-tyrosine phosphatase-1B reveals additive, synergistic, and factor-specific roles in the regulation of body energy balance.* Diabetes, 2010. **59**(12): p. 3074-84.
337. Womack, M. and K. Khodakhah, *Active contribution of dendrites to the tonic and trimodal patterns of activity in cerebellar Purkinje neurons.* J Neurosci, 2002. **22**(24): p. 10603-12.
338. van der Vaart, T., et al., *Motor deficits in neurofibromatosis type 1 mice: the role of the cerebellum.* Genes, brain, and behavior, 2011.
339. De Zeeuw, C.I., et al., *Expression of a protein kinase C inhibitor in Purkinje cells blocks cerebellar LTD and adaptation of the vestibulo-ocular reflex.* Neuron, 1998. **20**(3): p. 495-508.
340. Schonewille, M., et al., *Reevaluating the Role of LTD in Cerebellar Motor Learning.* Neuron, 2011. **70**(1): p. 43-50.
341. Cupido, A., *Detecting cerebellar phenotypes with the Erasmus ladder.* Thesis, (PhD). Erasmus University, Rotterdam., 2009.

342. Piazza, P., J. Deminière, and S. Maccari…, *Individual reactivity to novelty predicts probability of amphetamine self-administration.* Behavioural …, 1990.
343. Larson, E.B. and M.E. Carroll, *Wheel running as a predictor of cocaine self-administration and reinstatement in female rats.* Pharmacol Biochem Behav, 2005. **82**(3): p. 590-600.
344. Uchiumi, K., et al., *Wheel-running activity increases with social stress in male DBA mice.* Physiol Behav, 2008. **93**(1-2): p. 1-7.
345. Werme, M., et al., *Delta FosB regulates wheel running.* J Neurosci, 2002. **22**(18): p. 8133-8.
346. Brené, S., et al., *Running is rewarding and antidepressive.* Physiol Behav, 2007. **92**(1-2): p. 136-40.
347. Makatsori, A., et al., *Voluntary wheel running modulates glutamate receptor subunit gene expression and stress hormone release in Lewis rats.* Psychoneuroendocrinology, 2003. **28**(5): p. 702-14.
348. Salmon, P., *Effects of physical exercise on anxiety, depression, and sensitivity to stress: a unifying theory.* Clin Psychol Rev, 2001. **21**(1): p. 33-61.
349. Duman, C.H., et al., *Voluntary exercise produces antidepressant and anxiolytic behavioral effects in mice.* Brain Res, 2008. **1199**: p. 148-58.
350. Fuss, J., et al., *Deletion of running-induced hippocampal neurogenesis by irradiation prevents development of an anxious phenotype in mice.* PLoS ONE, 2010. **5**(9).
351. Fuss, J., et al., *Voluntary exercise induces anxiety-like behavior in adult C57BL/6J mice correlating with hippocampal neurogenesis.* Hippocampus, 2010. **20**(3): p. 364-76.
352. Zhang, X.-M., et al., *Highly restricted expression of Cre recombinase in cerebellar Purkinje cells.* Genesis, 2004. **40**(1): p. 45-51.
353. Rhodes, J.S., et al., *Differential sensitivity to acute administration of cocaine, GBR 12909, and fluoxetine in mice selectively bred for hyperactive wheel-running behavior.* Psychopharmacology (Berl), 2001. **158**(2): p. 120-31.
354. Kaplan, G. and J.H. Newcorn, *Pharmacotherapy for child and adolescent attention-deficit hyperactivity disorder.* Pediatr Clin North Am, 2011. **58**(1): p. 99-120, xi.
355. Rhodes, J.S. and T. Garland, *Differential sensitivity to acute administration of Ritalin, apomorphine, SCH 23390, but not raclopride in mice selectively bred for hyperactive wheel-running behavior.* Psychopharmacology (Berl), 2003. **167**(3): p. 242-50.
356. Leigh, R.J. and D.S. Zee, *The Neurology of Eye Movements*. 3rd Edition ed. 1999: Oxford University Press.

357. Gandhi, N.J. and E.L. Keller, *Comparison of saccades perturbed by stimulation of the rostral superior colliculus, the caudal superior colliculus, and the omnipause neuron region.* J Neurophysiol, 1999. **82**(6): p. 3236-53.
358. Basso, M.A., R.J. Krauzlis, and R.H. Wurtz, *Activation and inactivation of rostral superior colliculus neurons during smooth-pursuit eye movements in monkeys.* J Neurophysiol, 2000. **84**(2): p. 892-908.
359. Chou, I.H. and S.G. Lisberger, *The role of the frontal pursuit area in learning in smooth pursuit eye movements.* J Neurosci, 2004. **24**(17): p. 4124-33.
360. Büttner, U. and A. Straube, *The effect of cerebellar midline lesions on eye-movements*, in *Neuro-Ophthalmology*. 1995. p. 75-82.
361. Zee, D.S., et al., *Effects of ablation of flocculus and paraflocculus of eye movements in primate.* J Neurophysiol, 1981. **46**(4): p. 878-99.
362. Robinson, F.R., A. Straube, and A.F. Fuchs, *Role of the caudal fastigial nucleus in saccade generation. II. Effects of muscimol inactivation.* J Neurophysiol, 1993. **70**(5): p. 1741-58.
363. Optican, L.M. and D.A. Robinson, *Cerebellar-dependent adaptive control of primate saccadic system.* J Neurophysiol, 1980. **44**(6): p. 1058-76.
364. Pierrot-Deseilligny, C., et al., *Vermal infarct with pursuit eye movement disorders.* J Neurol Neurosurg Psychiatr, 1990. **53**(6): p. 519-21.
365. Büttner, U., A. Straube, and A. Spuler, *Saccadic dysmetria and "intact" smooth pursuit eye movements after bilateral deep cerebellar nuclei lesions.* J Neurol Neurosurg Psychiatr, 1994. **57**(7): p. 832-4.
366. Bogousslavsky, J. and O. Meienberg, *Eye-movement disorders in brain-stem and cerebellar stroke.* Arch Neurol, 1987. **44**(2): p. 141-8.
367. van Donkelaar, P. and R.G. Lee, *Interactions between the eye and hand motor systems: disruptions due to cerebellar dysfunction.* J Neurophysiol, 1994. **72**(4): p. 1674-85.
368. Miall, R.C., H. Imamizu, and S. Miyauchi, *Activation of the cerebellum in co-ordinated eye and hand tracking movements: an fMRI study.* Experimental brain research Experimentelle Hirnforschung Expérimentation cérébrale, 2000. **135**(1): p. 22-33.
369. Miall, R.C., G.Z. Reckess, and H. Imamizu, *The cerebellum coordinates eye and hand tracking movements.* Nat Neurosci, 2001. **4**(6): p. 638-44.
370. Gauthier, G.M., et al., *Oculo-manual tracking of visual targets: control learning, coordination control and coordination model.* Experimental brain research Experimentelle Hirnforschung Expérimentation cérébrale, 1988. **73**(1): p. 127-37.

371. Anastasopoulos, D., et al., *Smooth pursuit eye movements and otolith-ocular responses are differently impaired in cerebellar ataxia.* Brain, 1998. **121 (Pt 8)**: p. 1497-505.

372. Lencer, R., et al., *Smooth pursuit deficits in schizophrenia, affective disorder and obsessive-compulsive disorder.* Psychol Med, 2004. **34**(3): p. 451-60.

373. Lencer, R., et al., *Cortical mechanisms of smooth pursuit eye movements with target blanking. An fMRI study.* Eur J Neurosci, 2004. **19**(5): p. 1430-6.

374. Wolpert, D.M., Z. Ghahramani, and M.I. Jordan, *An internal model for sensorimotor integration.* Science, 1995. **269**(5232): p. 1880-2.

375. Wolpert, D.M., *Computational approaches to motor control.* Trends Cogn Sci (Regul Ed), 1997. **1**(6): p. 209-16.

376. Miall, R.C., *Task-dependent changes in visual feedback control: a frequency analysis of human manual tracking.* J Mot Behav, 1996. **28**(2): p. 125-35.

377. Imamizu, H., et al., *Human cerebellar activity reflecting an acquired internal model of a new tool.* Nature, 2000. **403**(6766): p. 192-5.

378. Ding, J., D. Powell, and Y. Jiang, *Dissociable frontal controls during visible and memory-guided eye-tracking of moving targets.* Hum Brain Mapp, 2009. **30**(11): p. 3541-52.

379. Timmann, D., S. Watts, and J. Hore, *Failure of cerebellar patients to time finger opening precisely causes ball high-low inaccuracy in overarm throws.* J Neurophysiol, 1999. **82**(1): p. 103-14.

380. Gibson, A.R., et al., *Construction of a reach-to-grasp.* Novartis Found Symp, 1998. **218**: p. 233-45; discussion 245-51.

381. Van Kan, P.L., K.M. Horn, and A.R. Gibson, *The importance of hand use to discharge of interpositus neurones of the monkey.* J Physiol (Lond), 1994. **480 (Pt 1)**: p. 171-90.

382. Dhamala, M., et al., *Neural correlates of the complexity of rhythmic finger tapping.* Neuroimage, 2003. **20**(2): p. 918-26.

383. Rae, C., et al., *Cerebellar morphology in developmental dyslexia.* Neuropsychologia, 2002. **40**(8): p. 1285-92.

384. Stein, J.F., A.J. Richardson, and M.S. Fowler, *Monocular occlusion can improve binocular control and reading in dyslexics.* Brain, 2000. **123 (Pt 1)**: p. 164-70.

385. Ray, N.J., S. Fowler, and J.F. Stein, *Yellow filters can improve magnocellular function: motion sensitivity, convergence, accommodation, and reading.* Ann N Y Acad Sci, 2005. **1039**: p. 283-93.

386. Björntorp, P. and M.U. Yang, *Refeeding after fasting in the rat: effects on body composition and food efficiency.* Am J Clin Nutr, 1982. **36**(3): p. 444-9.

387. Agouni, A., et al., *In vivo differential effects of fasting, re-feeding, insulin and insulin stimulation time course on insulin signaling pathway components in peripheral tissues.* Biochem Biophys Res Commun, 2010. **401**(1): p. 104-11.

388. Irimia, J.M., et al., *Impaired glucose tolerance and predisposition to the fasted state in liver glycogen synthase knock-out mice.* J Biol Chem, 2010. **285**(17): p. 12851-61.

389. Menahan, L.A. and K.A. Sobocinski, *Comparison of carbohydrate and lipid metabolism in mice and rats during fasting.* Comp Biochem Physiol, B, 1983. **74**(4): p. 859-64.

390. Guan, H.P., et al., *Accelerated fatty acid oxidation in muscle averts fasting-induced hepatic steatosis in SJL/J mice.* J Biol Chem, 2009. **284**(36): p. 24644-52.

391. Hodge, H., et al., *Lipids of the Fasting Mouse.* Journal of Biological Chemistry, 1941. **139**(2): p. 897.

392. Jikumaru, M., et al., *Effect of starvation on the survival of male and female mice.* Physiol Chem Phys Med NMR, 2007. **39**(2): p. 247-57.

393. Jensen, P., *The Ethology of Domestic Animals: An Introductory Text*. 2nd Edition ed. 2009: CAB International.

394. Toth, L.A. and T.W. Gardiner, *Food and water restriction protocols: physiological and behavioral considerations.* Contemp Top Lab Anim Sci, 2000. **39**(6): p. 9-17.

395. Heiderstadt, K.M., et al., *The effect of chronic food and water restriction on open-field behaviour and serum corticosterone levels in rats.* Lab Anim, 2000. **34**(1): p. 20-8.

396. Bellinger, L.L., V.E. Mendel, and G.P. Moberg, *Circadian insulin, GH, prolactin, corticosterone and glucose rhythms in fed and fasted rats*, in *Horm Metab Res*. 1975. p. 132-135.

397. Malatová, Z. and I. Ahlers, *Diurnal rhythm corticosterone in fasted rats.* Endocrinol Exp, 1977. **11**(4): p. 241-7.

398. Delgado, J.M.R. and B.K. Anand, *Increase of food intake induced by electrical stimulation of the lateral hypothalamus.* Am J Physiol, 1953. **172**(1): p. 162-8.

399. Leibowitz, S.F., N.J. Hammer, and K. Chang, *Hypothalamic paraventricular nucleus lesions produce overeating and obesity in the rat.* Physiol Behav, 1981. **27**(6): p. 1031-40.

400. Zhu, J.N. and J.J. Wang, *The cerebellum in feeding control: possible function and mechanism.* Cell Mol Neurobiol, 2008. **28**(4): p. 469-78.

401. Devito, L.M. and H. Eichenbaum, *Memory for the order of events in specific sequences: contributions of the hippocampus and medial prefrontal cortex.* J Neurosci, 2011. **31**(9): p. 3169-75.

402. Wang, Y.X., et al., *Regulation of muscle fiber type and running endurance by PPARdelta.* PLoS Biol, 2004. **2**(10): p. e294.

403. Aponte, Y., D. Atasoy, and S.M. Sternson, *AGRP neurons are sufficient to orchestrate feeding behavior rapidly and without training.* Nat Neurosci, 2011. **14**(3): p. 351-5.
404. Olszewski, P.K., et al., *Hypothalamic FTO is associated with the regulation of energy intake not feeding reward.* BMC neuroscience, 2009. **10**: p. 129.
405. Bäckman, C.M., et al., *Characterization of a mouse strain expressing Cre recombinase from the 3' untranslated region of the dopamine transporter locus.* Genesis, 2006. **44**(8): p. 383-90.
406. Zhang, X.M., et al., *Highly restricted expression of Cre recombinase in cerebellar Purkinje cells.* Genesis, 2004. **40**(1): p. 45-51.
407. Koyabu, N., et al., *Uptake and efflux transport mechanisms of tolbutamide across the blood-brain barrier.* Xenobiotic Metabolism and Disposition, 1999. **14**(Supplement): p. S108-S109.
408. Zhou, W., et al., *A transgenic Cre mouse line for the study of cortical and hippocampal development.* Genesis, 2010. **48**(5): p. 343-50.
409. Simard, J.M., et al., *Endothelial sulfonylurea receptor 1-regulated NC Ca-ATP channels mediate progressive hemorrhagic necrosis following spinal cord injury.* J Clin Invest, 2007. **117**(8): p. 2105-13.
410. Stoodley, C.J. and J.F. Stein, *The cerebellum and dyslexia.* Cortex; a journal devoted to the study of the nervous system and behavior, 2009.
411. Wulff, P., et al., *Synaptic inhibition of Purkinje cells mediates consolidation of vestibulo-cerebellar motor learning.* Nat Neurosci, 2009. **12**(8): p. 1042-9.

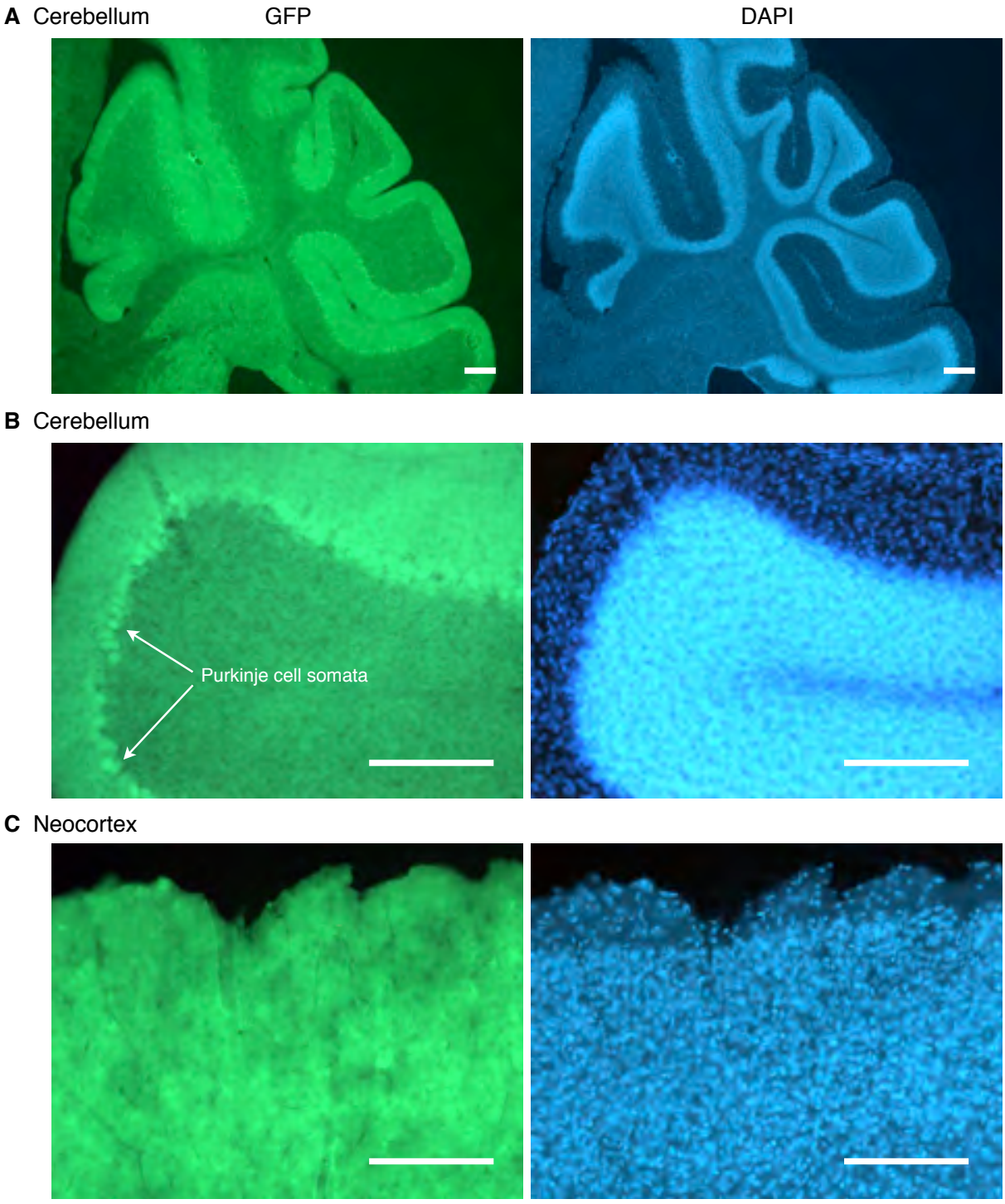

Appendix 1 GFP expression in Nes Z/EG mice

Representative images of intrinsic fluorescence in the brain from a 2-week-old Nes Z/EG mouse. GFP fluorescence is shown on the left and fluorescence from DAPI (which stains all nuclei) on the right. Cerebellum at 5x (**A**) and 20x (**B**) magnification. GFP is clearly seen in the somata of cerebellar Purkinje cells. GFP was seen throughout the brain, including the neocortex (**C**). Horizontal white bars indicate 200µm.

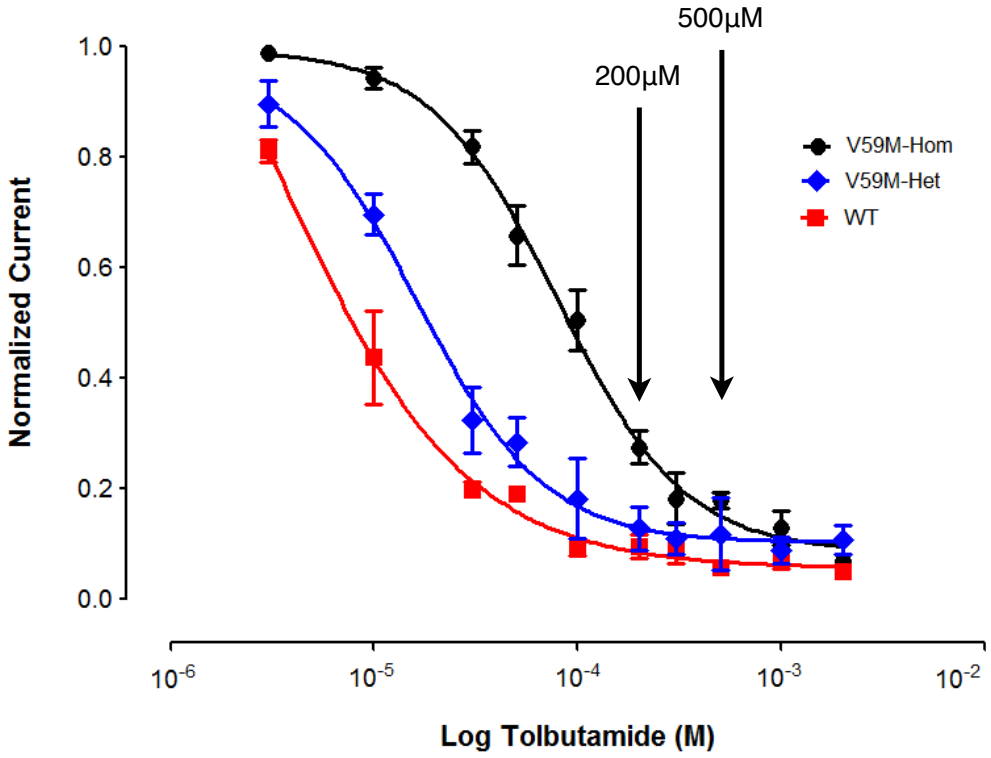

Appendix 2 Tolbutamide dose-response curves for V59M K_{ATP} channels

Xenopus oocytes were injected with SUR1 mRNA and either wild-type Kir6.2 (red line, WT), Kir6.2-V59M (black, V59M-Hom), or a 1:1 mixture of Kir6.2 and Kir6.2-V59M (blue, V59M-Het). Whole-cell currents were recorded in the absence or presence of the indicated tolbutamide concentration. The smooth curves are the best fit to the Hill equation. In 200µM tolbutamide, whole-cell currents from WT and V59M-Het oocytes were not significantly different, but currents from V59M-Hom oocytes were significantly higher than both WT and V59M-Het (t-tests). In 500µM tolbutamide, whole-cell currents from the three types of oocyte were not significantly different from each other (one-way ANOVA). Data were provided by Carolina Lahmann and are mean ± SEM.

A Water intake

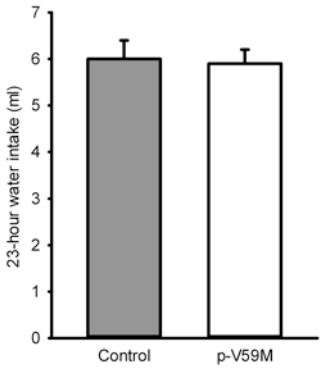

B Body weights

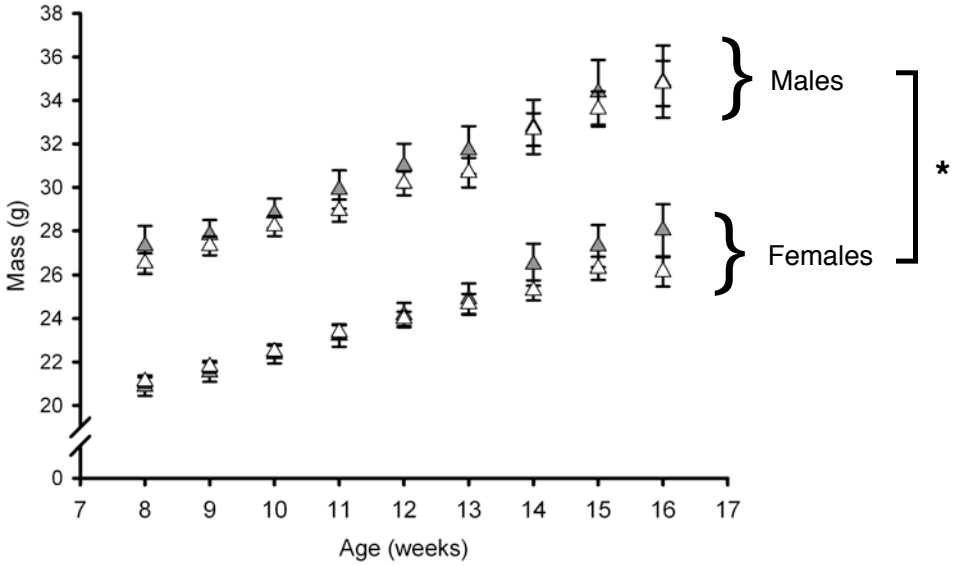

Appendix 3 Water intake and body mass of p-V59M mice and littermate controls

(**A**) Mean 23-hour water intake of control (grey bar, n = 13, 3 males, 10 females) and p-V59M (white bar, n = 10, 5 males, 5 females) mice. There were no significant differences between the mice (two-way ANOVA). (**B**) Mean body mass of male (upper two lines) and female (lower two lines) control (grey triangles) and p-V59M (white triangles) mice. n = 15-50 of each type of mouse. There were no significant differences between the mice based on genotype, but male mice were significantly heavier than females. *, $p < 0.05$, mixed between-within ANOVA. Note that there were missing data points for some mice on some weeks. For the statistical analysis, cases were excluded listwise to overcome this problem, but in the figure all data are shown. Data are mean ± SEM.

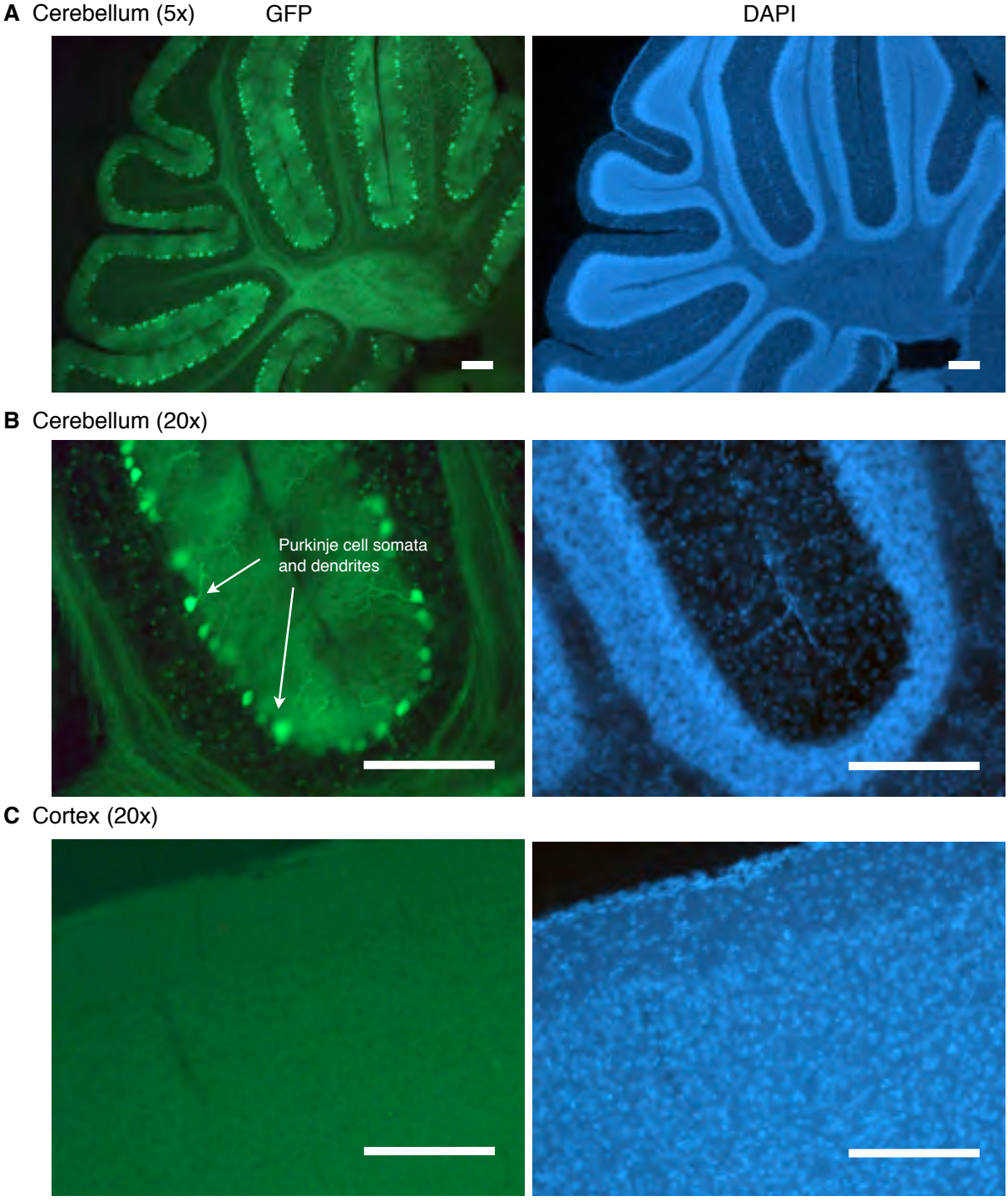

Appendix 4 GFP expression in 2-week old Pv-Z/EG mice

Representative images of intrinsic fluorescence in the brain from a 2-week-old Pv-Z/EG mouse. GFP fluorescence is shown on the left and fluorescence from DAPI (which stains all nuclei) on the right. Cerebellum at 5x (**A**) and 20x (**B**) magnification. GFP is clearly seen in the somata and dendrites of cerebellar Purkinje cells. There were very few GFP-expressing cells in the neocortex of 2-week old Pv-Z/EG mice (**C**). Horizontal white bars indicate 200µm.

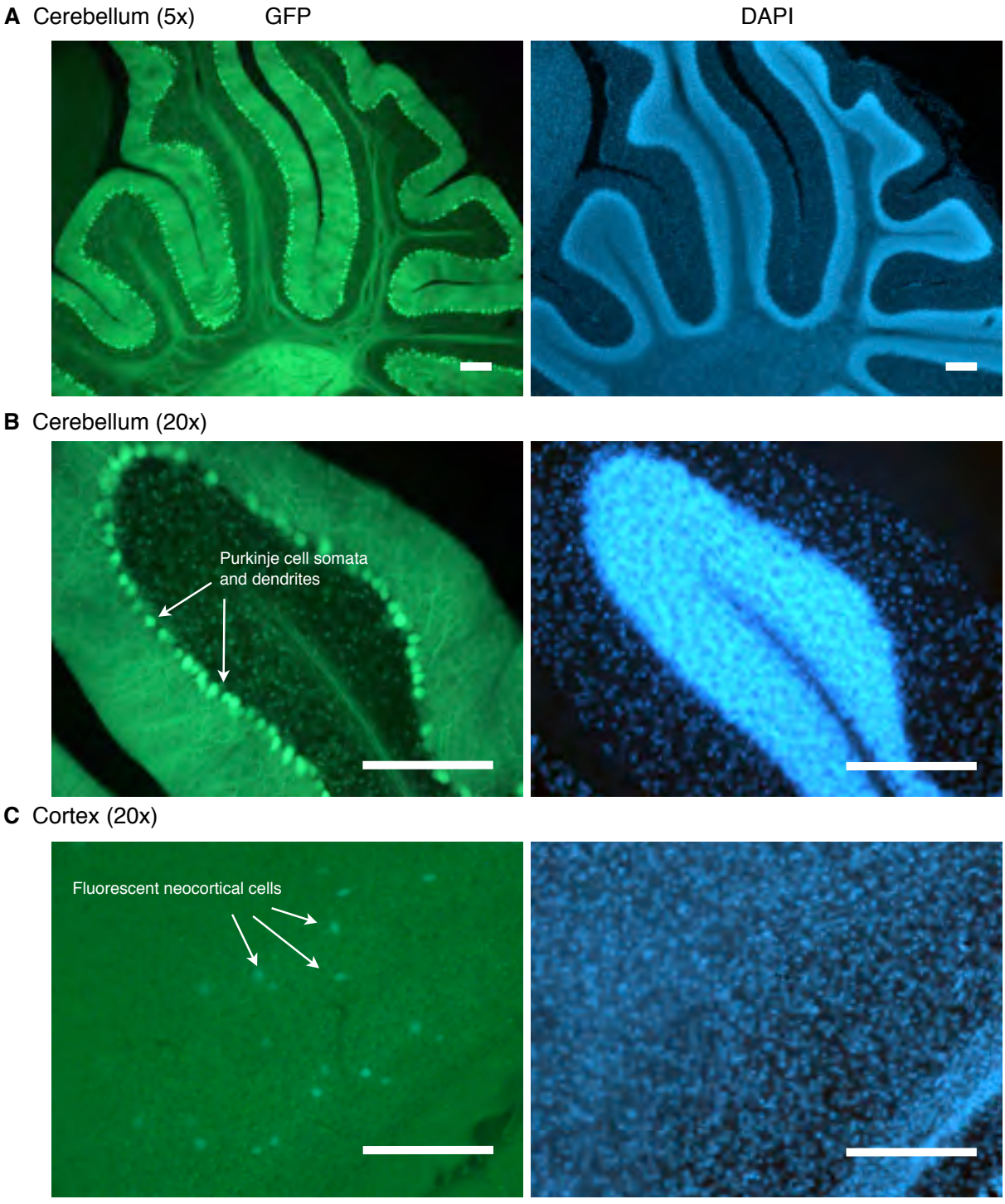

Appendix 5 GFP expression in 12-week old Pv-Z/EG mice

Representative images of intrinsic fluorescence in the brain from a 12-week-old Pv-Z/EG mouse. GFP fluorescence is shown on the left and fluorescence from DAPI (which stains all nuclei) on the right. Cerebellum at 5x (**A**) and 20x (**B**) magnification. GFP is clearly seen in the somata and dendrites of cerebellar Purkinje cells. GFP-expressing cells were distributed sparsely throughout the neocortex of 12-week old Pv-Z/EG mice (**C**). Horizontal white bars indicate 200µm.

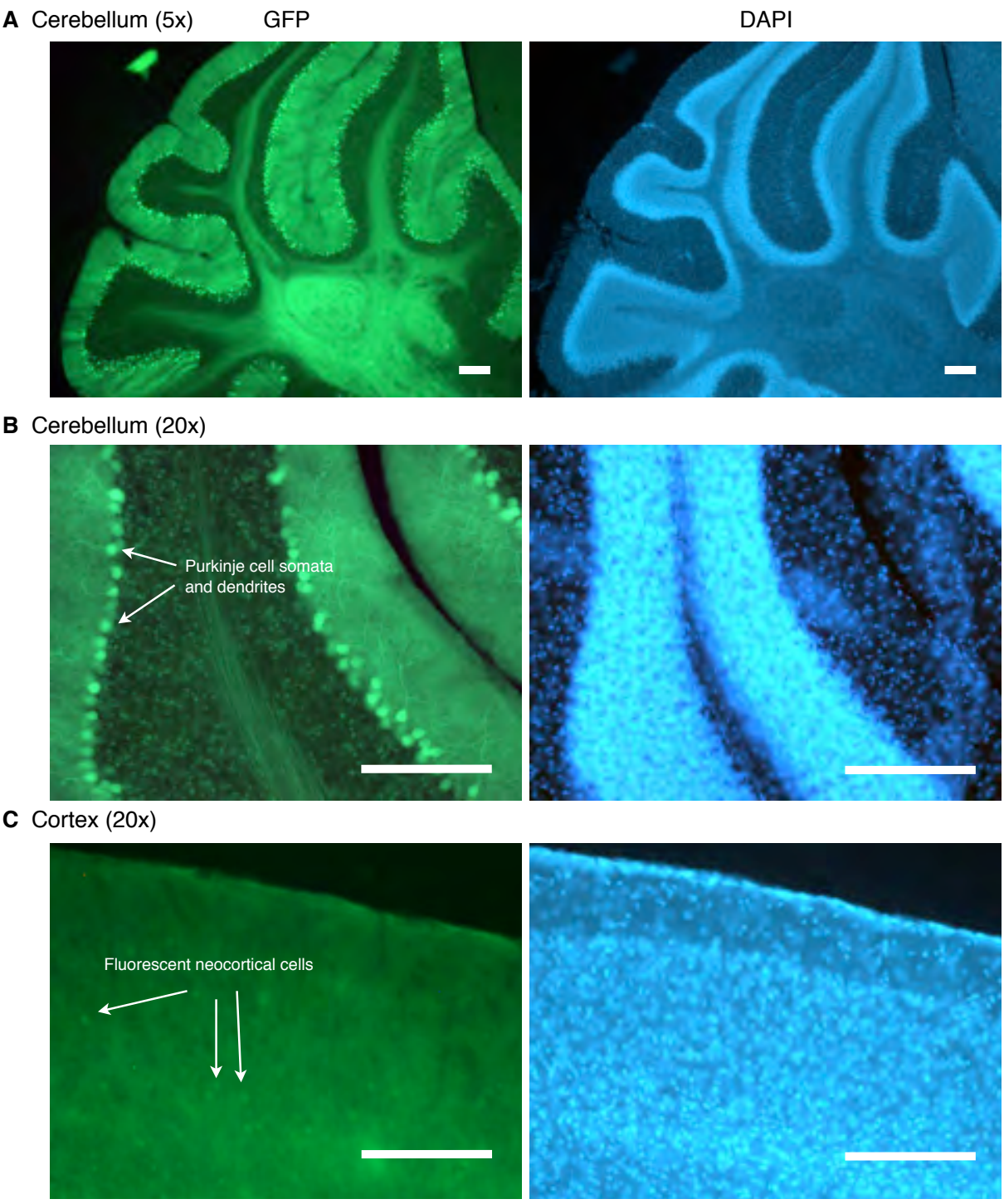

Appendix 6 GFP expression in 16-week old Pv-Z/EG mice

Representative images of intrinsic fluorescence in the brain from a 16-week-old Pv-Z/EG mouse. The pattern of GFP expression in these mice was very similar to 12-week old Pv-Z/EG mice. GFP fluorescence is shown on the left and fluorescence from DAPI (which stains all nuclei) on the right. Cerebellum at 5x (**A**) and 20x (**B**) magnification. GFP is clearly seen in the somata and dendrites of cerebellar Purkinje cells. GFP-expressing cells were distributed sparsely throughout the neocortex of 16-week old Pv-Z/EG mice (**C**). Horizontal white bars indicate 200µm.

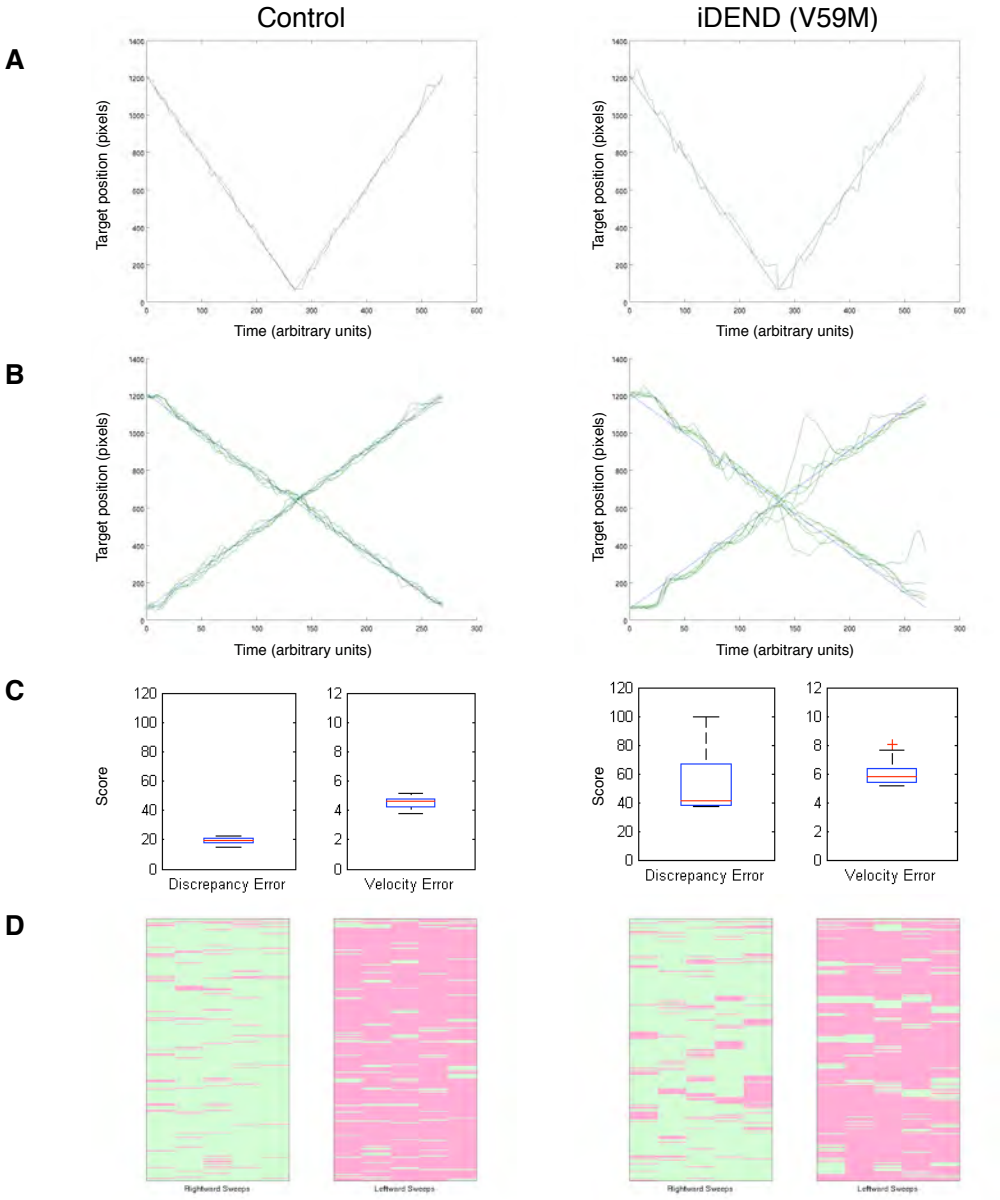

Appendix 7 Representative example of analysis of hand-eye tracking task 1.

Data are for pair 3 of control versus iDEND group. (**A**) Representative traces. Participants completed twelve sweeps in total, sweeps six and seven are shown. Negative gradient indicates leftward movement, positive gradient indicates rightward movement. Blue line indicates movement of target. The target moved at constant velocity, therefore the blue line is straight. Green line indicates movement of cursor. (**B**) Ten sweeps superimposed (sweeps one and twelve were discarded for each individual). (**C**) A discrepancy error and velocity error was calculated for each sweep. The ten error values are represented in box plots. The box is bounded by the 25th and 75th percentiles and is bisected by the median. Outliers are values beyond the 10th and 90th percentiles and are marked by a red cross. The median discrepancy and velocity errors of the iDEND patient are higher than her matched control. (**D**) Movement in the correct direction: rightward and leftward sweeps are represented in separate panels, as indicated. Each panel is composed of five columns - one column per sweep. Each column is composed of rows - each row represents a sampled point of the cursor's position (cursor position was sampled at 50Hz). Rightward movement of the cursor is indicated by a green row and leftward movement by a pink row. Thus, rightward sweeps are mainly composed of green rows, whereas leftward sweeps are composed largely of pink rows. The iDEND patient moved in the wrong direction more often than her matched control.

A Controls for PNDM patients

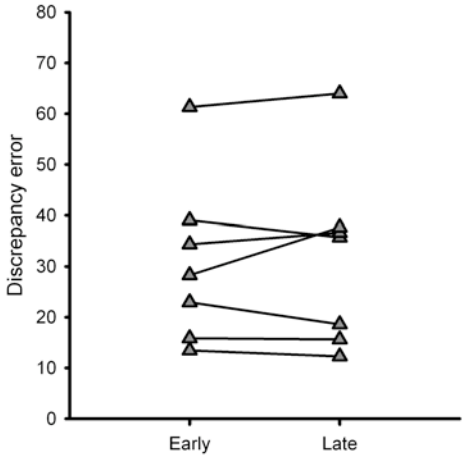

B PNDM patients

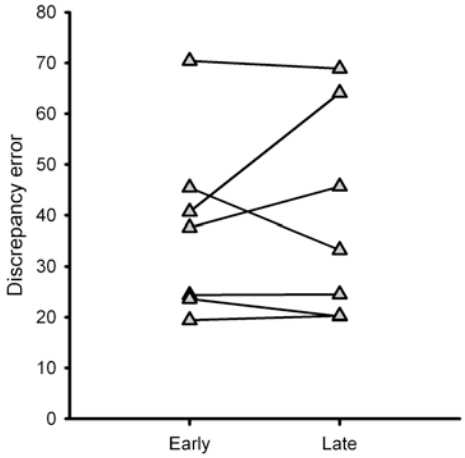

C Controls for iDEND patients

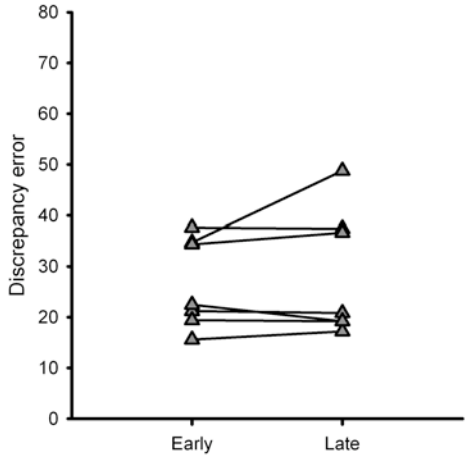

D iDEND patients

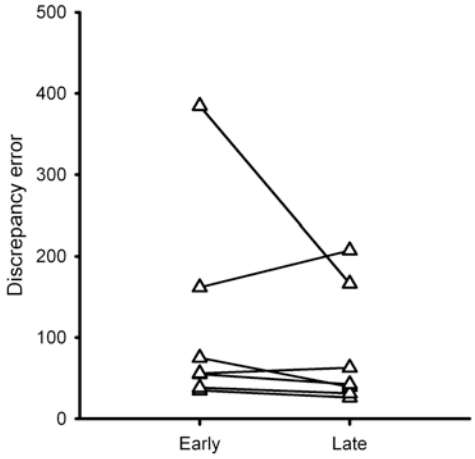

Appendix 8 Within-task effects on task 1

To see if performance was different at the start of the task compared to the end of the task (perhaps due to learning effects) the discrepancy error was calculated for the first five sweeps ('Early') and the last five sweeps ('Late') for each individual. (**A**) Matched controls for PNDM patients. 4 out of 7 individuals improved. (**B**) PNDM patients. 3 out of 7 individuals improved. (**C**) Matched controls for iDEND patients. 4 out of 7 individuals improved. (**D**) iDEND patients. 5 out of 7 individuals improved. Note the difference in scale of the y-axis.

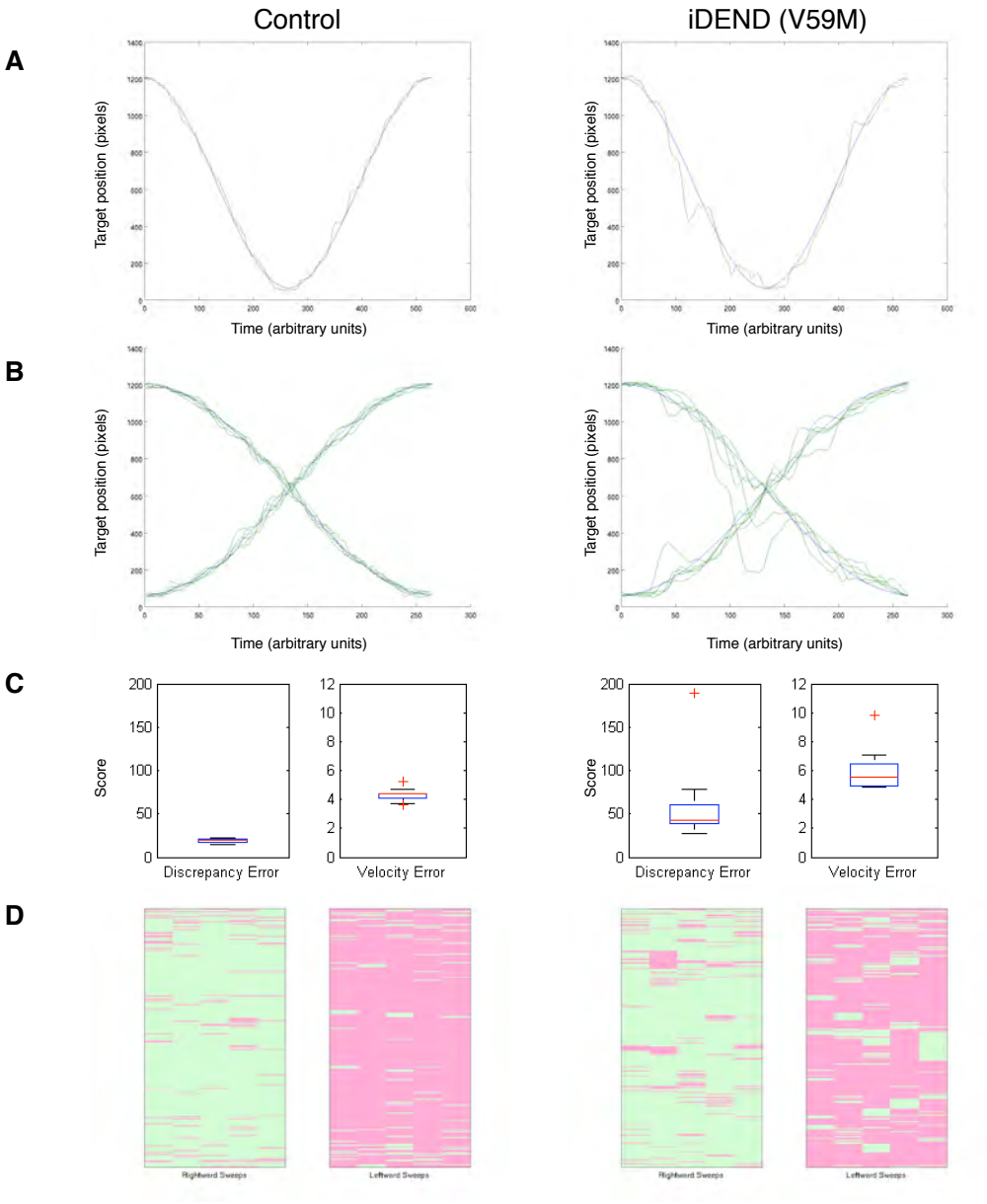

Appendix 9 Representative example of analysis of hand-eye tracking task 2.

Data are for pair 3 of control versus iDEND group. (**A**) Representative traces. Participants completed twelve sweeps in total, sweeps six and seven are shown. Negative gradient indicates leftward movement, positive gradient indicates rightward movement. Blue line indicates movement of target. The target accelerated and decelerated in a sinusoidal manner, so the blue line is curved. Green line indicates movement of cursor. (**B**) Ten sweeps superimposed (sweeps one and twelve were discarded for each individual). (**C**) A discrepancy error and velocity error was calculated for each sweep. The ten error values are represented in box plots. The box is bounded by the 25th and 75th percentiles and is bisected by the median. Outliers are values beyond the 10th and 90th percentiles and are marked by a red cross. The median discrepancy and velocity errors of the iDEND patient are higher than her matched control. (**D**) Movement in the correct direction (see Appendix 7 for a full description of this measure). The iDEND patient moved in the wrong direction more often than her matched control.

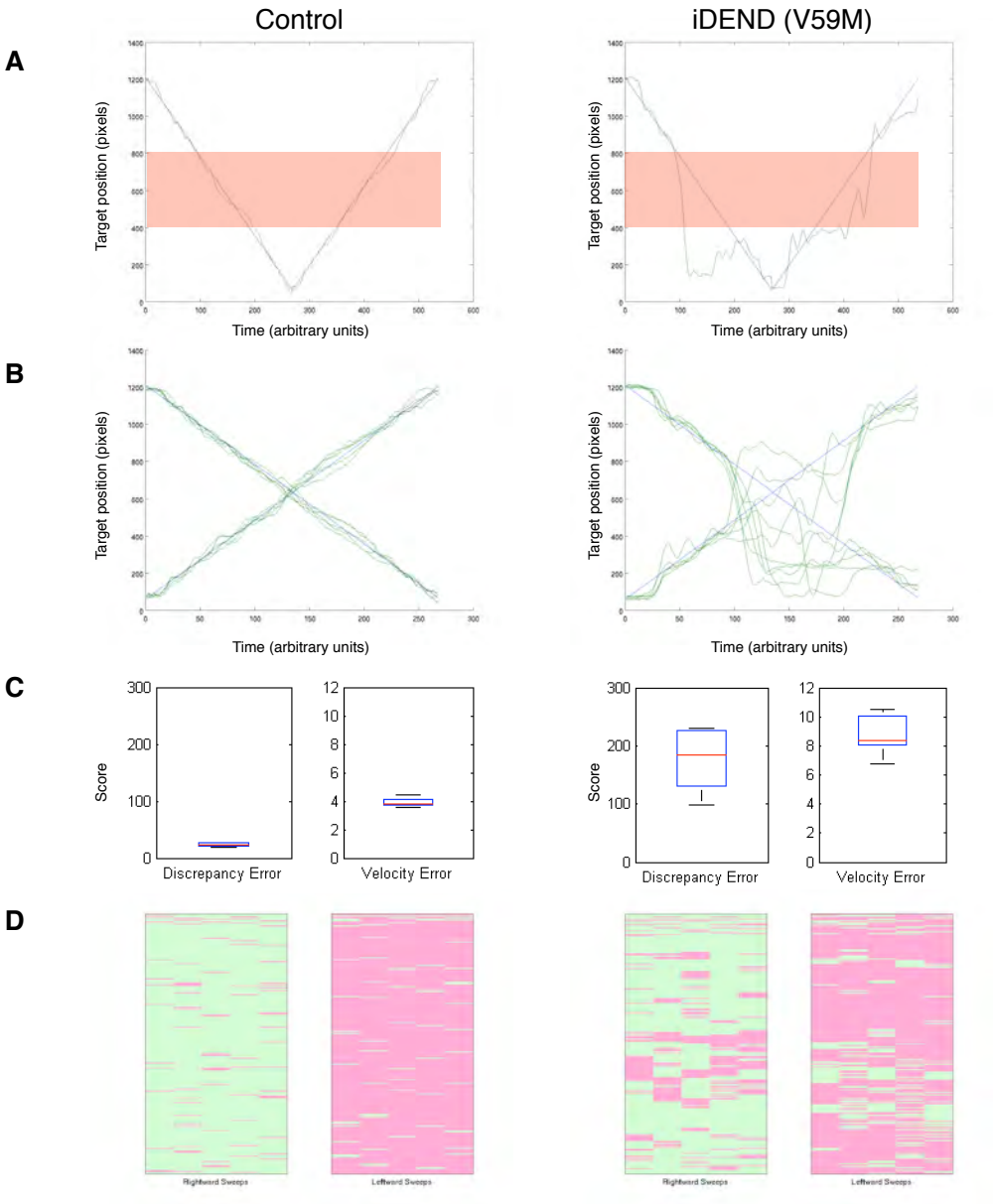

Appendix 10 Representative example of analysis of hand-eye tracking task 3.

Data are for pair 3 of control versus iDEND group. (**A**) Representative traces. Participants completed twelve sweeps in total, sweeps six and seven are shown. Negative gradient indicates leftward movement, positive gradient indicates rightward movement. Blue line indicates movement of target. The target accelerated and decelerated in a sinusoidal manner, so the blue line is curved. Green line indicates movement of cursor. The target was blanked during the middle third of each sweep, as denoted by the transparent red rectangle. Note that the inaccuracy of the iDEND patient is largely due to errors in the blanked section of the task. (**B**) Ten sweeps superimposed (sweeps one and twelve were discarded for each individual). (**C**) A discrepancy error and velocity error was calculated for each sweep. The ten error values are represented in box plots. The box is bounded by the 25th and 75th percentiles and is bisected by the median. Outliers are values beyond the 10th and 90th percentiles and are marked by a red cross. The median discrepancy and velocity errors of the iDEND patient are higher than her matched control. (**D**) Movement in the correct direction (see Appendix 7 for a full description of this measure). The iDEND patient moved in the wrong direction more often than her matched control.

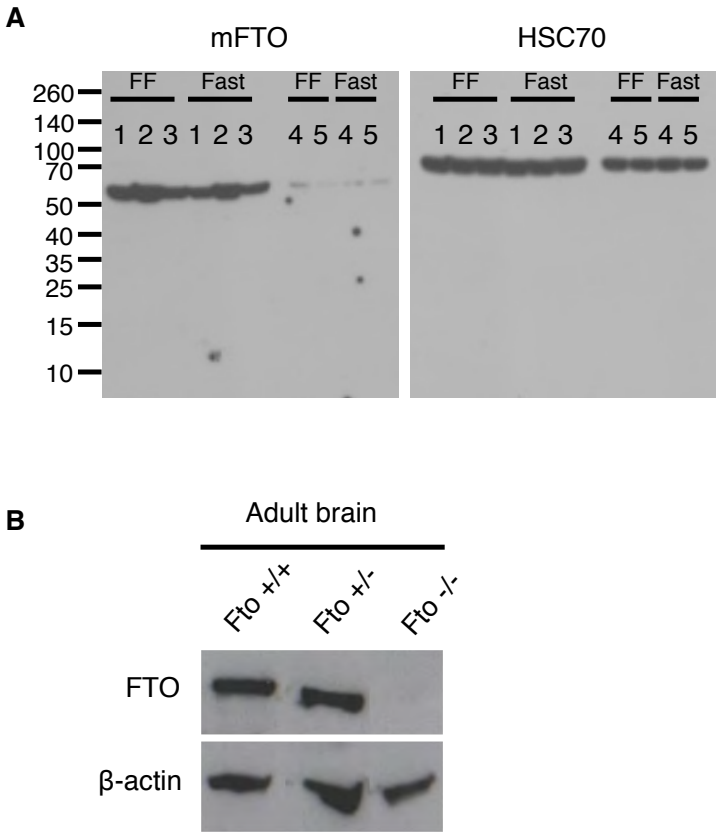

Appendix 11 Specificity of antibody raised against full-length recombinant murine FTO

(**A**) Representative Western blots. Lanes were loaded with total protein from rostral brain (1), cerebellum (2), hypothalamus (3), gastrocnemius muscle (4), extensor digitorum longus muscle (5) of free-fed (FF) and fasted (Fast) mice. The same blot was probed with anti-FTO (left) and anti-HSC70 (right) antibodies (the blot was stripped after probing with anti-FTO in order to visualise anti-HSC70 staining). Both antibodies detected a single band of the appropriate size: FTO was approximately 60kDa (predicted to be 58kDa), and HSC70 was approximately 70kDa (predicted to be 70kDa). Blots are representative of more than 8 mice. Note that the 'empty' lane that separates the brain from the muscle samples contained a pre-stained protein size ladder. This ladder did not appear on the Western blot film. (**B**) Representative Western blots, courtesy of Chris Church. Total protein from the brain was run from wild-type mice (left lane), mice lacking one copy of FTO (middle lane), and mice lacking both copies of FTO (right lane). Anti-FTO antibody detects no protein in mice lacking both copies of FTO. The blot was also probed with β-actin, which acted as a loading control.

Appendix 12a: Details of statistically significant results by chapter

Chapter 3, Section 3.4.2

Triceps Kir6.2 levels were significantly higher in females compared to males.
$F(1, 20) = 7.46$, $p = 0.013$

Brain Kir6.2 levels were significantly higher in n-V59M mice compared to pooled controls.
$F(1, 24) = 11.30$, $p = 0.003$

Chapter 3, Section 3.4.3

n-V59M Purkinje cells were significantly depolarised by the administration of 200µM tolbutamide.
$t(4) = -4.27$, $p = 0.013$

Control Purkinje cells were significantly hyperpolarised after tolbutamide was washed out compared to the basal state.
$t(5) = 3.15$, $p = 0.025$

In the basal state, the membrane potential of n-V59M Purkinje cells was significantly hyperpolarised compared to controls.
$t(9) = 5.64$, $p < 0.001$

Chapter 3, Section 3.4.4

In whole-cell patch-clamping experiments, the firing rates of n-V59M Purkinje cells were significantly lower than controls in the basal state
$t(9) = 5.41$, $p < 0.001$

and in 200µM tolbutamide
$t(9) = 3.04$, $p = 0.014$

and after tolbutamide was washed out
$t(9) = 3.65$, $p = 0.005$

Chapter 3, Section 3.4.5

In cell-attached patch-clamping experiments, n-V59M Purkinje cells fired significantly faster in 500µM tolbutamide than in the basal state
$t(4) = -4.79$, $p = 0.009$

In cell-attached patch-clamping experiments, control Purkinje cells fired significantly faster in 500µM tolbutamide & synaptic blockers than in the basal state
$t(11) = -5.73$, $p < 0.001$

In cell-attached patch-clamping experiments, n-V59M Purkinje cells also fired significantly faster in 500µM tolbutamide & synaptic blockers than in the basal state
$t(4) = -4.83$, $p = 0.008$

Appendix 12b: Details of statistically significant results by chapter

In cell-attached patch-clamping experiments, the firing rate of n-V59M Purkinje cells was significantly lower than control cells
$t(12) = 4.05$, $p = 0.002$

Chapter 3, Section 3.4.6

The basal firing rate of n-V59M Purkinje cells was higher in the cell-attached compared to the whole-cell configuration
$t(8) = 2.60$, $p = 0.032$

Chapter 4, Section 4.4

Male mice were heavier than female mice
Wilks Lambda = 0.17, $F(2, 70) = 170.96$, $p < 0.001$

Chapter 4, Section 4.4.4

In the basal state, the duration of firing of p-V59M Purkinje cells was lower than controls
$t(12) = 3.72$, $p = 0.003$

Chapter 4, Section 4.4.6

The firing rates of control Purkinje cells were significantly increased compared to the basal state when 500µM tolbutamide was added along with synaptic blockers
$t(7) = -4.09$, $p = 0.005$

The firing rates of control Purkinje cells were significantly increased in the 500µM tolbutamide condition compared to the 500µM tolbutamide & synaptic blockers condition
$t(7) = -5.18$, $p = 0.001$

The firing rates of p-V59M Purkinje cells were significantly increased compared to the basal state when 500µM tolbutamide was added along with synaptic blockers
$t(5) = -3.36$, $p = 0.020$

The firing rates of p-V59M Purkinje cells were significantly increased in the 500µM tolbutamide condition compared to the 500µM tolbutamide & synaptic blockers condition
$t(5) = -3.66$, $p = 0.015$

The firing rates of p-V59M Purkinje cells were significantly lower than controls in the basal state
$t(12) = 2.28$, $p = 0.042$

Chapter 4, Section 4.4.7

The scores of p-V59M mice on the weight-lifting task were lower than those of control mice
$F(1, 104) = 3.99$, $p = 0.048$

Appendix 12c: Details of statistically significant results by chapter

Chapter 4, Section 4.4.8

The performance of mice, regardless of their genotype or sex, differed on the three different sizes of the static rod
$F(2, 103) = 15.60$, $p < 0.001$, Wilks Lambda = 0.76

Female mice managed to stay on the accelerating rotarod for longer than males
$F(1, 104) = 4.14$, $p = 0.045$

Chapter 4, Section 4.4.9

Female mice were more spontaneously active over 23-hours than males
$F(1, 84) = 4.77$, $p = 0.032$

Chapter 4, Section 4.4.10

Female mice used the free-running wheel for longer than males during a 23-hour period
$U = 984.0$, $z = -3.68$, $p < 0.001$

p-V59M mice ran further than controls on the free-running wheel
$U = 1114.5$, $z = -2.43$, $p = 0.015$

Female mice ran further than males
$U = 995.0$, $z = -3.62$, $p < 0.001$

p-V59M mice ran with faster average speed than controls
$F(1, 111) = 7.53$, $p = 0.007$

Female mice ran with higher average speed than males
$F(1, 111) = 10.97$, $p = 0.001$

Chapter 5, Section 5.4.2

Discrepancy errors on task 2 were not equal in the four groups (iDEND, PNDM, two groups of controls)
χ^2 (3, n = 28) = 9.16, $p = 0.027$

Pairwise comparisons revealed that the discrepancy errors of iDEND patients on task 2 were significantly higher than controls.
$U = 2$, $z = -2.88$, $p = 0.002$

Appendix 12d: Details of statistically significant results by chapter

Chapter 5, Section 5.4.3

Discrepancy errors on task 3 were not equal in the four groups (iDEND, PNDM, two groups of controls)
χ^2 (3, n = 28) = 9.69, p = 0.021

Pairwise comparisons revealed that the discrepancy errors of iDEND patients on task 3 were significantly higher than controls.
U = 2, z = -2.56, p = 0.009

Velocity errors on task 3 were not equal in the four groups (iDEND, PNDM, two groups of controls)
χ^2 (3, n = 26) = 8.19, p = 0.042

Pairwise comparisons revealed that the velocity errors of iDEND patients on task 3 were significantly higher than controls
U = 2, z = -2.56, p = 0.009

Chapter 5, Section 5.4.4

Discrepancy errors on segment 2 of task 3 were not equal in the four groups (iDEND, PNDM, two groups of controls)
χ^2 (3, n = 26) = 9.22, p = 0.026

Pairwise comparisons revealed that the discrepancy errors of iDEND patients on segment 2 of task 3 were significantly higher than controls
U = 2, z = -2.56, p = 0.009

Discrepancy errors on segment 3 of task 3 were not equal in the four groups (iDEND, PNDM, two groups of controls)
χ^2 (3, n = 26) = 10.57, p = 0.014

Pairwise comparisons revealed that the discrepancy errors of iDEND patients on segment 3 of task 3 were significantly higher than controls
U = 1, z = -2.72, p = 0.004

Chapter 6, Section 6.4.1

Pooled brain FTO protein levels were significantly higher compared to pooled muscle FTO protein levels
F(1, 78) = 87.15, p < 0.001